Heterotic String Compactification and Quiver Gauge Theory on Toric Geometry

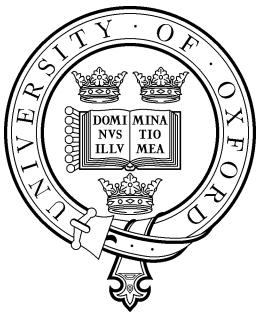

Chuang Sun

St Anne's College

University of Oxford

A thesis submitted for the degree of

Doctor of Philosophy

Trinity 2016

To Mom and Dad,
who introduced me to the world
and the beauty of invisibility,
with gratitude, admiration
and love.

Acknowledgements

I'd like to express my gratitude to my supervisor Prof. Andre Lukas, whose expertise, kindness and helpful discussion had greatly influenced my understanding of research and theoretical physics. It is not possible to present this thesis without his insight and patient guidance. I've learned so much from his work, impressed so often by his wisdom, which occasionally enlightened my paths.

Sincere thanks to my supervisor Prof. Yang-hui He, more than a good mentor, but also a dear intellectual brother, who motivated my initial interest in string theory and deeply influenced my ways of working. I treasure so much the infinite possibilities he showed me, and the experiences he shared with me.

Many thanks to my fellow students in Rudolf Peierls Centre of Theoretical Physics. I appreciate the ideas shared by Andrei Constantin, whose former work a perfect examplar for my study. Thanks to Seung-Joo Lee and Cyril Matti for collaborating on several topics. I thank Andreas Braun for enlightening discussions on toric geometry.

Besides, I must also acknowledge my dear friends: Jian Huang, Juliane Gong, Xiaofei Zhou, Yang Li, Yichen Li, Yiu Siu, Yanis Houpas, David Kraljic.

Abstract

This thesis is composed of papers in two areas: heterotic string model building on Calabi-Yau manifolds, and bipartite field theory with applications to brane tilings. However, the two streams share a common topic – string model building on toric geometry. Toric variety appears as both the ambient space for constructing Calabi-Yau hyper-surface, and the moduli space of D-brane configurations.

We study heterotic model building on 16 specific Calabi-Yau (CY) manifolds as hypersurfaces in toric four-folds. These 16 manifolds are the only ones among the more than half a billion manifolds in the Kreuzer-Skarke (KS) list with a non-trivial fundamental group. We classify the line bundle models on these manifolds, both for SU(5) and SO(10) Grand Unified Theories (GUT), which lead to consistent supersymmetric string vacua and they have three chiral families. In order to apply the model building to the whole KS list, we then systematically classify the freely-acting symmetries. For this purpose we develop a method of classifying all freely acting discrete groups of CY on toric spaces, and generate its weighted projective representations. A few new discrete symmetries are found and presented. This is the first step towards heterotic string model building on CYs constructed by reflexive polytopes of KS list.

The second part of this thesis emphasises the applications of quiver gauge theory and dimer models. We generalise the results for quiver theories with low block numbers, revealing an new intriguing algebraic structure underlying a class of possible superconformal fixed points. After explicitly computing the Diophantine equation of five block cases, we use this structure to re-organize the result in a form that can be applied to arbitrary block numbers. We argue that these theories can be thought of as vectors in the root system of the corresponding quiver. In addition to exploring the block quiver theory, we also compute the large area toric models and their associated dimer models. We compute the Kasteleyn matrix of the conifolds and its orbifolds, then turn on the vacuum expectation value (vev.) for massless fields. New dimer models with large triangulation areas are classified and presented.

Contents

Chapter 1

Introduction

1.1 String Theory

Quantum field theory (QFT) provides us with a combined view of quantum mechanics and special relativity and it forms the basis of our current understanding of particle physics, in the form of the standard model of particle physics (SM). On the other hand, general relativity (GR) gives us a beautiful geometrical view of the universe, where, on the one hand, massive objects move according to the curvature of space-time and, on the other hand, this curvature is controlled by the distribution of mass. It would be desirable to unify these two main theories which are underpinning our current understanding of fundamental physics. However, it turns out that attempts to quantise gravity using the methods applied in QFTs run into serious problems. Over the years, string theory has developed into a theory that allows for a unification of QFT and GR at the quantum level. It turns out that string theory might also resolve some of the other problems which arise within the SM, such as the hierarchy problem, the origin of three families of quarks and leptons and their pattern of masses.

String theory is a theory of quantised, relativistic strings which contains only one free parameter – the string tension T which is often expressed in terms of the Regge slope α' as $T = (2\pi\alpha')^{-1}$. Note that this is the only free parameter in string theory compared to roughly twenty in the SM (coupling constants, fine structure constant, Weinberg angle etc.) The string can either be open or closed, where closed strings are vibrating 'cycles' and open strings are line intervals with two endpoints. Let us have a brief look at the bosonic string theory in d-dimensional Minkowski space-time, which is controlled by the Nambu-Goto action

$$S_{NG} = \frac{1}{2\pi\alpha'} \int_{\Sigma} d\sigma d\tau \sqrt{|\det\, G(X)|}\ .$$

The world-sheet Σ is swept out by the string, parametrised by (σ, τ), where σ and τ are the spatial and time parameters, respectively. The integral is the area of Σ measured with

the induced metric $G_{\alpha\beta} = \partial_\alpha X^\mu \partial_\beta X^\nu \eta_{\mu\nu}$, where $X^\mu(\sigma,\tau)$ is the embedding of Σ into the d-dimensional space-time with the Minkowski-metric $\eta_{\mu\nu}$, where $\mu,\nu = 0,1,...,d-1$. The equation of motion for this action turns out to be the wave equation $\partial_\alpha \partial^\alpha X^\mu = 0$, which implies that the string wave function is a summation of different vibration modes. Then by bringing in the *light cone coordinates*, we can split the general solutions of X into the left mover and right mover:

$$X^\mu(\sigma,\tau) = X^\mu_R(\tau-\sigma) + X^\mu_L(\tau+\sigma) \ ,$$

which greatly simplifies the string mode expansion. The first quantisation of strings leads to a spectrum of vibrations which is, schematically, of the form $\alpha' m^2 = n \in \mathbb{Z}^{\geq 0}$. The relation between string theory and particle physics involves identifying these vibrational modes of the string with individual particles. It turns out that, for all consistent string theories, the zero modes of the closed string spectrum (that is, the modes for $n = 0$) always contains a mode which can be identified with the graviton (a spin two field $g_{\mu\nu}$). Moreover, scattering of these gravitons within string theory leads to finite answers and, hence, does not have the same problem that arises for a quantisation of gravity following the rules of QFT. It is in this sense that string theory is said to provide a quantum theory of gravity. For open strings, one can impose either Dirichlet (D) or Neumann (N) boundary condition for each end of the string. The physical meaning of Neumann boundary condition is that the string momentum does not flow off. However, the Dirichlet boundary condition sets the end of the string fixed, hence the momentum on the open string is not conserved. Meanwhile, Poincaré invariance demands that the total space-time momentum of string theory must be conserved. This implies that the hyper-surfaces swept by the string ends are physical objects, which have been called 'D-branes'. The two ends of the open string carry charges in the fundamental representations of the gauge group (Chan-Paton factors) [1], such that the open string has the quantum numbers of a gauge field which can be thought of as being localised on the D-brane.

In a theory with only bosonic strings, a tachyon would appear which indicates an instability of this theory. This can be avoided by involving supersymmetry (SUSY). Supersymmetry, in a word, is a conjectured symmetry of spacetime which relates bosons (integer valued spin) and their super-partners, fermions (half integer spin). In the context of string theory, it means bringing in the superpartners $\psi^\mu_\pm(\sigma,\tau)$ of $X^\mu(\sigma,\tau)$ by space-time supersymmetry. The fermions $\psi^\mu_\pm$ on the world-sheet of a closed string can be periodic (Ramond) or anti-periodic (Neveu-Schwarz) for each chirality. This leads to four different sectors, with the (NS,NS) and (R,R) sectors leading to bosons and the (NS,R) and (R,NS) sectors leading to fermions in a target space. For the open strings, however, the two chiralities are coupled, which leads to only two sectors: the NS sector for bosons and R sector for fermions. Quantisation of string theory is only

possible in the critical dimension d_{crit}, where $d_{crit} = 10$ for the super-string by anomaly cancellation. In addition, the spectrum must be truncated by the Gliozzi-Scherk-Olive (GSO) [2] projection to make sure that the tachyon is projected out and the remaining spectrum provides equal numbers of bosons and fermions. Combining these features with open or closed strings, it turns out that five consistent string theories can be constructed, which we now summarise.

The type I string theory is a $\mathcal{N} = 1$ theory with 16 super-charges, where both open and closed strings are involved. The open strings are assigned charges by the Chan-Paton method, giving rise to gauge theories at the zero mode level. At the quantum level, the consistency condition, namely the cancellation of quantum anomalies, requires the gauge group to be $SO(32)$. If we then consider theories with only closed strings, there are two type II theories and heterotic string theory. The theory with two conserved supercharges of opposite chirality is called type IIA, and it is left-right symmetric. The type IIB theory involves oriented closed strings and it is, therefore, a chiral theory. They both have 32 supercharges. The heterotic string theory is composed of closed strings, but it comes with only 16 super-charges and is a chiral theory. Due to the fact that left movers and right movers are decoupled, the right-moving modes are the same as in type II, but the left-moving modes are changed to include a current algebra which gives rise to gauge fields. From anomaly cancellation, this gauge theory can be either $SO(32)$ or $E_8 \times E_8$.

The five types of strings are linked by a web of dualities [3]. For example, the T-duality implies that two different geometries are physically equivalent under the transformation $R \to l_s^2/R$, where one of the dimensions is a circle of radius R and $l_s = \sqrt{\alpha'}$ is the string length. T-duality relates the two type II theories to each other and the two heterotic theories to each other. On the other hand, S-duality relates the strong coupling regime of one theory with the weak coupling regime of another by means of the transformation $g_s \to 1/g_s$, where g_s is the string coupling. It relates the type I theory to the $SO(32)$ heterotic string and the type IIB to itself. We can then ask what happens with the two remaining theories, type IIA and heterotic $E_8 \times E_8$, when g_s becomes large. In this case, an additional, eleventh dimension of size $g_s l_s$ appears. This leads to a new 11-dimensional theory called M-theory [4].

String theory is still far from fully developed. It has yet to prove that it can make unique, flawless predictions. The idea of *string compactification* arises naturally to resolve the discrepancy between the critical dimension $D = 10$ of the five type discussed above and the number of observed dimensions $d = 4$. An "internal" six-dimensional space K with length scales far below current limits of measurement is introduced such that the total 10-dimensional space time is of

the form $M_4 \times K$, with four-dimensional Minkovski space M_4. In the simplest cases, the metric on this space needs to satisfy the 10-dimensional Einstein equation subject to vanishing stress energy. To generate the right amount of supersymmetry, K must allow for a Ricci-flat metric and is, hence, a Calabi-Yau (CY) manifold [5]. Alternatively, CY manifolds can also be defined as complex Kähler manifolds with vanishing first Chern class. There are many approaches to the construction of CY manifolds, yet the largest class remains the CYs constructed over toric varieties [6]. This type of toric variety could be identified with the weighted projective space, parametrised by reflexive polygons in lattice space. The CY manifolds of this kind are the first central objects of this thesis. In the following subsection we will have a detailed discussion of heterotic string compactification on CY manifolds.

On the other hand, D-branes encode a deep connection between algebra and geometry, where *quiver gauge theory* is brought in and of central importance. By placing the D-branes on a singularity of type $\mathbb{C}^2/\Gamma$ (where Γ is a subgroup of $SU(2)$) [7], the gauge theory living on them is encoded by an affine Dynkin diagram. In this picture, fractional branes are mapped to nodes in the Dynkin diagram while strings stretching between the fractional branes are mapped to lines in the Dynkin diagram. This connection between the Lie algebras of affine Dynkin diagrams and the geometry of ALE spaces is known as McKay correspondence [8]. The McKay correspondence can also be realised in other ways. For instance, the Hanany-Witten setup [9] containing the configuration of NS5-branes with D-branes stretching between them. Here the NS5-branes are mapped to lines while D-branes stretching between NS5-branes are mapped to nodes, where lines and nodes are gathered into a graph called a *quiver graph*. For these objects, nodes represent gauge groups, oriented arrows between two nodes represent bifundamental chiral multiplets, and certain closed paths in the quiver (which represent gauge-invariant operators) represent terms in the superpotential. More importantly, since the branes are breaking the original supersymmetry (32 supercharges) to 8 supercharges, we then have a four dimensional $\mathcal{N} = 2$ super-symmetric string theory. Meanwhile, many attempts have been made to generalise the McKay correspondence from a two-dimensional complex space to a three-dimensional complex space [10–13]. One option, for example, is to place the D-branes on a three-dimensional singular Calabi-Yau manifold, for example the conifold and its quotient space of a finite abelian group. The supersymmetry of the gauge theory living on the D-branes is now reduced to 4 supercharges ($\mathcal{N} = 1$ supersymmetry). This will be the second central object of the thesis. In the subsection 1.4 and appendix B, we have a detailed introduction of brane tilings.

This thesis focuses on two topics in the context of string and M-theory: heterotic string compactification and quiver gauge theory on $\mathcal{N} = 1$ super-symmetric string theory. However they all share one common topic – the model building on toric geometry. Toric geometry provides us with a powerful and intuitive toolbox for string model building. The simple underlying idea of toric geometry is to parametrise algebraic varieties by integral lattices and this idea has many applications in a wide range of contexts. In the first part (Chapters 2 and 3) of the thesis, we explore the string model building on CY manifolds constructed over the toric ambient space, and develop a method of systematically classifying discrete symmetries. In the second part (Chapters 4 and 5), we generalise the expression of Diophantine equations for quiver gauge theory with large number of gauge factors, and classify dimer models with large triangulation areas. Before that, in the following subsections of Chapter 1, we will summarise the relevant building blocks in string compactification, as well as the reasons for bringing in Calabi-Yau manifold and toric geometry. We also introduce the framework of quiver gauge theory, and its relations to bipartite field theory (BFT) and toric geometry. This will complete the background for the main Chapters.

1.2 String Compactification

As mentioned earlier, the aim of string phenomenology is to bridge the gap between abstract algebraic geometrical theories and measurable physics, which requires a careful study of the low energy effective string action, the corresponding field contents as well as their interactions. String compactification comes in as a necessary step towards computing effective action and scattering amplitudes. This procedure usually involves integrating out the internal manifold and reducing the fields into a lower dimensional spacetime. Recall that the particle spectrum of a string theory consists of a finite number of massless states and an infinite tower of massive excitations, and understanding the ground states is the key to understanding low energy excitations.

Kaluza and Klein first proposed a framework [14,15] where only one extra dimension (S^1 space) is reduced. Let us have a quick look at the field contents of $\mathcal{N} = 1$ supergravity in ten dimension, which appears in the heterotic string theory with gauge group $E_8 \times E_8$ or $SO(32)$. The massless sector consists of Yang-Mills supermultiplets (A^a_M, χ^a) in the adjoint representations of the gauge group, and the supergravity multiplets consist of a graviton as the vielbein e^A_M, an antisymmetric tensor B_{MN}, a scalar ϕ, a gravitino ψ_M and a spinor λ. The spinors are all Majorana-Weyl with ψ_M left-handed and λ right-handed. Capital letters $M, N, ...$ denote ten-dimensional space-time coordinates, whereas $A, B, ...$ are local Lorentz indices. The Dirac

matrices for ten-dimensional space-time are represented by $\Gamma^M = e^M_A \Gamma^A$. One way to derive the action in 10 dimensions is to first formulate 11-dimensional supergravity and then perform a truncation to 10 dimensions. We know from [16] that the 11-dimensional supergravity theory only involves three different fields: the vielbein e^A_M, a Majorana gravitino ψ_M and a three-form potential A_{MNP}, where now the indices are 11-valued. In this reduction, the 11D vielbein decomposes into the 10D vielbein, a vector and a scalar; A_{MNP} decomposes into a threeform A_{MNP} and a two form B_{MN} i.e. A_{MN11}; The gravitino decomposes into a pair of Majorana-Weyl gravitinos $\psi^i_M \ \ (i = 1, 2)$ and a pair of Majorana-Weyl spinors λ^i in 10D. The detailed effective action can be seen in [17], for now we only need to make sure of the field contents.

In the context of the heterotic string, we assume the vacuum to be of the form $M_4 \times K$, where M_4 is a 4D Minkowski space and K is a compact 6D manifold. Regarding the geometry of the internal space, the unbroken $\mathcal{N} = 1$ super-symmetry implies the Hermitian-Yang-Mills equations, which has a solution on a Ricci-flat Kähler manifold, or equivalently, the Calabi-Yau manifold with $SU(3)$ holonomy. The existence of spaces with $SU(3)$ holonomy was conjectured by Calabi [18] and proved by Yau [19]. In addition, the existence of a non-zero covariant spinor implies that K has $SU(3)$ holonomy. Very importantly, if K is Kähler, this will imply that the line element can be expressed locally in terms of a real scalar function $K(z, \bar{z})$ known as the Kähler potential : $ds^2 = \frac{\partial^2 K}{\partial z^i \partial \bar{z^j}} dz^i d\bar{z^j}$, which means every Kähler metric can be expressed locally in this form. Therefore the classification of Kähler manifolds becomes a topological problem.

As for the particle spectrum, the standard embedding (identifying the gauge connection with spin connection) leads to a four-dimensional theory with E_6 gauge group. In the context of $E_8 \times E_8$ heterotic string theory, the spin connection of K could be embedded into one of the E_8 factors, and the E_6 unifying group will emerge with chiral superfields arising as fundamental representations. All known particle interactions are assumed to be unified in the maximal subgroup H of $E_8 \otimes E_8$ which commutes with Γ, the structure group. It is usual to embed Γ in E_8 and to assume that the maximal subgroup within E_8 commuting with Γ is the unifying group. In this context, the other E_8 is the hidden sector communicating only gravitationally with the world of everyday experience and may be the source of supersymmetry breaking via gaugino condensation. In some sense, the coefficient vector bundles for the holomorphic forms representing superfields are the associated vector bundles built on the representation of Γ, arising when the adjoint $E_8 \otimes E_8$ is broken under $\Gamma \otimes H$, with H the unifying group. For example, we can use the natural $SU(3)$ principal bundle over the Calabi-Yau manifold, essentially equating the spin connection of CY with the vacuum Yang-Mills connection of an $SU(3)$

subgroup of E_8. This gives us an E_6 unifying group along with the other E_8 hidden sector. Under $SU(3) \times E_6 \subset E_8$, the representations split as $\underline{\mathbf{248}} = (\underline{\mathbf{8}}, \underline{\mathbf{1}}) \oplus (\underline{\mathbf{3}}, \underline{\mathbf{27}}) \oplus (\underline{\overline{\mathbf{3}}}, \underline{\overline{\mathbf{27}}}) \oplus (\underline{\mathbf{1}}, \underline{\mathbf{78}})$. The topological properties of K is crucial in determining the other low-energy properties of the model. In particular, the Hodge numbers of the manifold determine the number of light chiral supermultiplets transforming as $\underline{\mathbf{27}}$ and $\underline{\overline{\mathbf{27}}}$, and the vacuum structure of the manifold determines the discrete symmetries of the theory which restrict the allowed Yukawa couplings of the chiral supermultiplets. More importantly, the number of generations for such a model is one half of the Euler characteristic of K. If K admits a freely acting discrete symmetry G, we might also make the compactification on $K' = K/G$, as long as K' has Euler characteristic $\chi = -6$ [5].

The unification in addition to the matter contents of the standard model implies that there is a unified group structure at high energies. There is a simple Lie group $G \supset SU(3) \times SU(2) \times U(1)$ called a GUT group, named after the corresponding high energy theory the Grand Unified Theory (GUT). The E_6 we mentioned above is one option, along others such as $SU(5)$ and $SO(10)$. For example, by breaking $SU(5)$ into the Standard Model gauge group $(SU(3)_C \times SU(2)_L \times U(1)_Y)$, the gauge bosons decompose into standard model representations as $\mathbf{24} \to (\mathbf{8}, \mathbf{1})_0 \oplus (\mathbf{1}, \mathbf{3})_0 \oplus (\mathbf{1}, \mathbf{1})_0 \oplus (\mathbf{3}, \mathbf{2})_{-5} \oplus (\bar{\mathbf{3}}, \mathbf{2})_5$, where the first three terms are the standard model gauge bosons, and the latter two are exotic gauge bosons. And the matter in the anti-fundamental representations decomposes as $\bar{\mathbf{5}} \to (\bar{\mathbf{3}}, \mathbf{1})_2 \oplus (\mathbf{1}, \mathbf{2})_{-3}$ and $\mathbf{10} \to (\mathbf{3}, \mathbf{2})_1 \oplus (\bar{\mathbf{3}}, \mathbf{1})_{-4} \oplus (\mathbf{1}, \mathbf{1})_6$. Note that the $U(1)$ charge is normalized to be six times the usual hypercharge $Y \in \mathbb{Z}/6$. These representations form exactly a single generation of the standard model. More details of the work on $SU(4)$ and $SU(5)$ unifying groups will be summarised in Chapter 2, where we study line bundle model building on toric four-folds. More work and details of model building with monad bundles and line bundles can be found in [20–29].

1.3 Toric Geometry

In this section we introduce the applications of toric geometry in string phenomenology, and the basic construction of toric varieties. The detailed construction and examples of the Batyrev construction of toric varieties can be found in 2.2.1 and appendix A.

Toric varieties are geometric objects defined by combinatorial information. In algebraic geometry, a toric variety or torus embedding is an algebraic variety containing an algebraic torus T (affine variety isomorphic to $(\mathbb{C}^*)^n, n \geq 1$) as an open dense subset, such that the action of the torus on itself extends to the whole variety. A nice property of toric varieties is that, the geometry is fully determined by the combinatorics of the associated fan, which makes computations

very tractable.

There are many methods of defining a toric variety. The original motivation is to study the torus embedding. Given an algebraic torus T, the group of characters $Hom(T, \mathbb{C}^*)$ forms a lattice. If we have a collection of points A as a subset of this lattice, then each point would give us a map to $\mathbb{C}$, hence the whole collection determines a map to $\mathbb{C}^{|A|}$. By taking the Zariski closure of the image of this map, one obtains an affine variety and the variety is a torus embedding. In a similar way one can also produce a projective toric variety by taking the projective closure of the map.

Another point of view is the following: first define N as a finite ranked lattice of a free abelian group. Then we define a specific type of cone called a "strongly convex rational polyhedral cone" in N, with its apex at the origin, generated by a finite number of vectors in N which contains no line through the origin. For each cone σ, its affine toric variety U_σ is the spectrum of the semigroup algebra of the dual cone. If further we have a fan as the collection of cones, then the toric variety of this fan is just the patched variety of all different stratifications of the corresponding cones. The type of fan studied in this thesis is called a reflexive polytope, where there is no inner point except the origin inside the fan. The toric varieties defined by a reflexive polygon and its dual fan are the "mirror partners" in the context of mirror symmetry.

For example, the complex projective plane $\mathbb{CP}^2$ is represented by three complex homogeneous coordinates s.t. $|z_1|^2 + |z_2|^2 + |z_3|^2 = 1$. The scaling of the coordinates implies a $U(1)$ action as $(z_1, z_2, z_3) \backsimeq e^{i\phi}(z_1, z_2, z_3)$. The toric description of $\mathbb{CP}^2$ can be understood as the following: There are three vertices $v_1 = (1, 0), v_2 = (0, 1), v_3 = (-1, -1)$ correspondent to the three divisors $\{z_i = 0\}, i = 1, 2, 3$. In Batyrev construction [30], the toric variety is defined as

$$X := (\mathbb{C}^r - \mathcal{Z})/(\mathbb{C}^*)^{r-n} ,$$

where r is the number of homogeneous coordinates, n is the number of $\mathbb{C}^*$ actions and $\mathcal{Z}$ is the zero set of the Stanley-Reisner (SR) ideal. In this case, the zero set is $\mathcal{Z} = \{z_1 = z_2 = z_3 = 0\}$, thus we have $\mathbb{CP}^2 := (\mathbb{C}^3 - \{z_1 = z_2 = z_3 = 0\})/(z_1, z_2, z_3) \backsim \lambda(z_1, z_2, z_3)$, which recovers the usual definition of a projective space. In Chapter 2 we have detailed examples of Batyrev construction, and interested readers can refer to [31–33] for more examples on toric geometry.

What is the motivation for constructing toric geometry in string theory? The first reason would be the construction of Calabi-Yau manifolds in string model building. Over the years people

have managed to construct CY manifolds using different methods, such as complete intersection Calabi-Yaus (CICYs) in products of projective spaces [34], the elliptic fibred [35] and the hypersurfaces in toric four-folds [6]. These Calabi-Yau datasets provide a vast number of candidate internal three-folds for a realistic model, although many of them may be ruled out even on the grounds of basic phenomenology. The most impressive list, of course, is the last one due to Kreuzer-Skarke (KS) [6]. There are in total 473,800,776 ambient toric four-folds, each coming from a reflexive polytope in 4-dimensions. At least an equal number of CY manifolds can then be constructed.

On the other hand, toric geometry plays an important role in mirror symmetry [32]. In general, mirror symmetry refers to a correspondence that maps objects of a certain type – manifolds, varieties or schemes – to objects of a different type in such a way that the "A-model" of the original object is exchanged with the "B-model" or the mirrored object. For the CY manifold, as an example, its A-model encodes deformations of the Kähler structure and its B-model encodes deformations of its complex structure. On the other hand, one version of mirror symmetry, called Batyrev-Borisov [36, 37], interchanges the A-model of CY with its B-model. For now mirror symmetry still remains a conjecture, but in many cases it is known to hold. In particular, CY mirror symmetry has been proven whenever the CY is a complete intersection in a toric variety.

The third reason for us to study the toric construction is due to bipartite field theory (BFT), where toric varieties arise as the moduli space of D-brane configuration at singularities in type IIB string theory. In recent progress on AdS/CFT correspondence, people have tried to investigate theories of fewer supersymmetries than the celebrated $AdS_5 \times S^5/\mathcal{N} = 4$ Yang-Mills duality by Maldacena [38]. One approach is to break supersymmetry by changing the geometry of the string background, i.e. replacing the $AdS_5 \times S^5$ geometry with a different manifold $AdS_5 \times X_5$, where X_5 is a Sasaki-Einstein (SE) manifold in order to preserve $\mathcal{N} = 1$ super-symmetry. Among the possible choices of X_5, toric SE manifolds have proven to be very tractable. They can provide an infinite number of $\mathcal{N} = 1$ super-symmetric gauge theories admitting non-trivial infrared superconformal fixed points. In the coming section we will have a brief introduction to D-brane configurations at toric singularities.

1.4 Brane Tilings

We now discuss string model building in type II theory, where a toric variety appears as the moduli space of the D-brane configuration. As a general feature, D3-branes located at singu-

lar points of a toric Calabi-Yau cone possess a vacuum space as a toric variety parametrised by a 2-D diagram. For these models, their gauge group factors and the field contents can be summarised in a bipartite graph called *dimer graph*, where black nodes and white nodes are evenly distributed. The so called bipartite field theory (BFT) refers to the model building work on toric singularities, and toolboxes such as quiver gauge theory, brane tilings and dimer technology. In this subsection we will summarise the crucial components of BFT, while the detailed theory of brane tilings can be found in appendix B.

When the D-branes in type II string theory are placed on an ALE singularity of ADE type [7], the corresponding gauge theory can be encoded by the Dynkin diagram where strings stretching between the fractional branes are mapped to lines in the Dynkin diagram. Since the ALE singularity breaks one half of the supersymmetry and the D-branes break the further half, this type of gauge theory has eight supercharges, hence a $\mathcal{N} = 2$ supersymmetry. In such a supersymmetric theory it is enough to specify the gauge group and the matter content in order to fix the superpotential. Therefore, we have a picture of a Dynkin diagram mapped to the moduli space of vacua which has the singularity of ADE type. This connection between the Lie algebras of affine Dynkin diagrams and the geometry of ALE spaces is called McKay correspondence [8], which has become an important object in string theory.

In addition, McKay correspondence can also be realized under other contexts in string theory. For example, the Hanany-Witten configuration results in a gauge theory on D-branes encoded by an A_{N-1} Dynkin diagram. This is where the *quiver graph* is introduced. Further, one can apply S and T duality onto the path algebra of a quiver diagram, resulting in different D-brane configurations [39,40]. Many attempts have been made to generalise the McKay correspondence from the two complex dimensional space to three, resulting in $\mathcal{N} = 1$ super-symmetric theories. For example, one can extend the 2-dimensional correspondence stated above from D-branes probing 2-dimensional singular manifold to D-branes probing 3-dimensional singular Calabi-Yau manifold [41]. It turns out that, in a quiver graph, nodes represent gauge groups, oriented arrows between two nodes represent bifundamental chiral multiplets, and certain closed paths in the quiver represent the gauge invariant operators, forming the superpotential. There has been an industry to construct even more classes of such quiver gauge theories, ranging from orbifolds [42–44], toric singularities [41, 45–47] to brane tilings [48–52].

The natural question then arises as whether one could classify the $\mathcal{N} = 1$ quiver gauge theories in a schematic way. One way of organising the quivers is called "blocks", where several nodes in a quiver are grouped in a block, yet unlinked between themselves. This method originated

in the study of del Pezzo surfaces [53], and was further applied to other super-conformal theories [54–57]. It turns out that many known quiver theories, which often appear with geometries such as orbifold singularities and del Pezzo surfaces, can have their quiver diagrams contracted to a succinct block diagram. Moreover, the necessary conditions for such a theory, i.e. vanishing beta and gamma functions, would translate to an integer equation system called Diophantine equations. Chapter 4 is aimed at a conjecture of the general properties of Diophantine equations of a generalised "blocked" quiver.

Brane tilings and dimer models are the other important building blocks of bipartite field theory. They reflect type IIB configurations of NS5 and D5-branes that are dual to gauge theories on D3-branes transverse to arbitrary singularities on toric three-folds. In our construction, the NS5-branes extend in the 0123 directions and wraps a holomorphic curve embedded in the 4567 directions, where the 46 directions are taken to be compact. The D5-branes span the 012346 directions and stretch between the NS5 skeleton, giving rise to a $\mathcal{N} = 1$ four dimensional theory. The field content is now captured by drawing the brane tiling in the 46 plane. It is *bipartite* due to the fact that all its nodes can be coloured in white or black, such that edges only connect black nodes and white nodes. The following table 1.1 contains a dictionary explaining the relation between objects in bipartite field theory:

Gauge theory	String theory	Quiver graph	Brane tiling
$SU(N)/U(N)$ gauge group	D-branes	Node	Polygonal face
Chiral multiplet	String stretched between branes	Arrow	Edge
Superpotential term	Region where k strings locally interact	Closed path correspondents to gauge invariant term	k-valent Vertex

Table 1.1: The quiver/brane tiling dictionary

To obtain $\mathcal{N} = 1$ super-symmetries in the AdS/CFT picture, one option is to modify the topology of the string theory background, for instance replacing the S^5 space with another manifold X_5, leaving us with less field contents and a moduli space with more singularities. Due to the constraints of $\mathcal{N} = 1$ supersymmetry, X_5 must be a Sasaki-Einstein manifold, the simplest definition of which is that metric cone is a Calabi-Yau 3-fold. Hence the metric should be of the form: $ds^2 = dr^2 + r^2 dX_5^2$. Usually the Sasaki-Einstein manifold only needs a single $U(1)$ isometry, for the purpose of R-symmetry. However in our work we mainly focus on the toric Sasaki-Einsten manifolds (its Calabi-Yau cone admit $U(1)^3$ isometries), which are even more tractable. In addition, the toric moduli space provides us with an infinite number of $\mathcal{N} = 1$ super-symmetry gauge theories admitting non-trivial infrared super-conformal fixed

points, which is essential for our study on brane tilings. Some other classes of geometries we can use to replace the S^5 space are: Abelian orbifolds S^5/Γ, where $\Gamma \simeq \mathbb{Z}_n$ or $\mathbb{Z}_n \times \mathbb{Z}_m$; the conifold and its orbifolds; the $Y^{p,q}$ and $L^{a,b,c}$ manifolds. Chapter 5 contains a systematic classification of dimer models on toric singularities of conifolds, and the interested reader can refer to appendix B for a detailed introduction of quiver theory and brane tilings.

1.5 Outline of Thesis

So far, the former subsections have briefly mentioned the knowledge background relevant to the work in this thesis. The rest of the thesis will be focused on the concrete discussion of string compactification on toric geometry as well as the topics in quiver gauge theory.

The systematic overview of the physical and mathematical tools are distributed as follows: in Chapter 2 and appendix A, we provide the definitions and examples of the Batyrev construction of a toric variety, as well as Calabi-Yau hyper-surfaces in toric ambient spaces. Then in appendix B, we introduce definitions and examples in quiver gauge theory and brane tilings. Interested readers could firstly refer to these Chapters for some preparation.

In Chapter 2 we study heterotic model building on 16 specific Calabi-Yau manifolds as hypersurfaces in toric four-folds. These 16 manifolds are the only ones among the more than half a billion manifolds in the Kreuzer-Skarke (KS) list with a non-trivial fundamental group. We classify the line bundle models on these manifolds, both for SU(5) and SO(10) Grand Unified Theories (GUT), which lead to consistent supersymmetric string vacua and have three chiral families. A total of about 29,000 models is found, which constitutes a starting point for detailed heterotic model building on Calabi-Yau manifolds based on the KS list. In order to apply the model building to the whole KS list, we then systematically classify the freely-acting symmetries in Chapter 3. For this purpose we have developed a method of classifying all freely acting discrete groups of CY on toric spaces, and generating its weighted projective representations. The mathematical construction of freely acting symmetries of toric Calabi-Yau is throughly discussed, as well as the algorithm related to the fixed point set and the smoothness of discrete actions. We have implemented this algorithm of classifying the discrete symmetry for the KS list, and found computationally a few new examples of discrete symmetries beyond the known ones of the 16 special families. This is the first step towards heterotic string model building on CYs constructed by reflexive polytopes of KS list.

The second part of this thesis emphasises the applications of quiver gauge theory and dimer models to $\mathcal{N} = 1$ super-conformal theory. Chapter 4 is a generalisation of super-conformal block quiver gauge theories. We re-derive results for quiver gauge theories with low block numbers revealing a new intriguing algebraic structure underlying a class of possible superconformal fixed points of such theories. After explicitly computing the Diophantine equations of five block cases, we use this structure to re-organize the result in a form that can be applied to arbitrary block numbers. We argue that these theories can be thought of as vectors in the root system of the corresponding quiver. And superconformality conditions are shown to be associated with certain subsets of imaginary roots, which also allows for an interpretation of Seiberg duality as the action of the affine Weyl group on the root lattice. In addition to exploring the block quiver theory, we also compute the large area toric models and their associated dimer models. Chapter 5 represents new results of dimer models with number of triangulation areas larger than six. We applied the recently developed dimer technology, namely computing the Kasteleyn matrix of the conifolds and its quotient spaces, then turn on the vacuum expectation values (vev.) for certain fields to approach the expected toric models. We establish and implement this method, and discover many more intriguing new dimer models. These new dimer models have never been discussed before and can potentially shed light on string phenomenology for a large class of toric models.

Chapter 2

Heterotic Model Building: 16 Special Manifolds

2.1 Introduction

Over the past few years, a programme of *algorithmic string compactification* has been established where a combination of the latest developments in computer algebra and algebraic geometry have been utilized to study the compactification of the heterotic string on smooth Calabi-Yau three-folds with holomorphic vector bundles satsifying the Hermitian Yang-Mills equations [58, 59]. This is very much in the spirit of the recent advances in applications of algorithmic geometry to string and particle phenomenology [60–63]. Earlier model building programmes which have paved the way for the current systematic approach have led to a relatively small number of models [64–67] which have the particle content of the minimally supersymmetric standard model (MSSM). In contrast, in the latest scan [59] over 10^{40} candidate models on complete intersection Calabi-Yau manifolds (CICYs), around 10^5 heterotic standard models were produced.

Of the databases of Calabi-Yau three-folds created over the last three decades in attempting to answer the original question of [34] whether superstring theory can indeed give the real world of particle physics, the increasingly numerous - and also chronological - sets are the complete intersections (CICY) in products of projective spaces [34], the elliptically fibred [35] and the hypersurfaces in toric four-folds [6] (cf. [68] for a brief review). Such Calabi-Yau datasets provide a vast number of candidate internal three-folds for a realistic model, although many of them may be ruled out even on the grounds of basic phenomenology.

The most impressive list, of course, is the last, due to Kreuzer-Skarke (KS). These total 473,800,776 ambient toric four-folds, each coming from a reflexive polytope in 4-dimensions.

Thus there are at least this many Calabi-Yau three-folds. However, since the majority of the toric ambient spaces are singular and need to be resolved the expected number of Calabi-Yau three-folds from this set is even higher. The Hodge numbers are invariant under this resolution and thus have been extracted to produce the famous plot (which we will exhibit later in the text) of a total of 30,108 distinct Hodge number pairs. To establish stable vector bundles over this largest known set of Calabi-Yau three-folds is of obvious importance. To truly probe the "heterotic landscape" of compactifications which give rise to universes with particle physics akin to ours, one must systematically go beyond the set thus far probed, which had been focused on the CICYs [20–25, 58, 59, 67] and the elliptic [26, 27] sets.

The study of bundles for model building on the KS dataset was initiated in [28] where the Calabi-Yau manifolds with smooth ambient toric four-folds were isolated and studied in detail. Interestingly, of the some half-billion manifolds, only 124 have smooth ambient spaces. Bundles which give 3 net generations upon quotienting some potential discrete symmetry and which satisfy all constraints including, notably, Green-Schwarz anomaly cancellation, were classified.

Subsequently, a bench-mark study was performed by going up in $h^{1,1}$ of the KS list [29]. Now, the largest Hodge pairs of any smooth Calabi-Yau three-fold is $(h^{1,1}, h^{2,1}) = (491, 11)$ (with the mirror having $(h^{1,1}, h^{2,1}) = (11, 491)$), giving the experimental bound of 960 on the absolute value of the Euler number. In [29], they studied the manifolds up to $h^{1,1} = 3$, which already has some 300 manifolds. The space of positive bundles of monad type were constructed on these spaces.

In any event, the procedure of heterotic compactification is well understood. Given a generically simply connected Calabi-Yau three-fold $\widetilde{X}$, we need to find a freely-acting discrete symmetry group Γ, so that $\widetilde{X}/\Gamma$ is a smooth quotient. We then need to construct stable Γ-equivariant bundles $\widetilde{V}$ on the cover $\widetilde{X}$ so that on the quotient $X = \widetilde{X}/\Gamma$, $\widetilde{V}$ descends to a bona fide bundle V. It is the cohomology of V, coupled with Wilson lines valued in the group Γ, that gives us the particle content which we need to compute. In other words, we need to find Calabi-Yau manifolds X with non-trivial fundamental group $\pi_1(X) \simeq \Gamma$. Often, the manifolds $\widetilde{X}$ and X are referred to as "upstairs" and the "downstairs" manifolds, to emphasize their quotienting relation.

The simplest set of vector bundles to construct and analyze is that of line bundle sums [24, 59]. Hence, an important step is to classify heterotic line bundle models on Calabi-Yau manifolds in the KS list and extract the ones capable of leading to realistic particle physics. Of course, the

existence of freely acting groups Γ on the Calabi-Yau manifolds is crucial in order to complete this programme. Unfortunately, these freely-acting symmetries are not systematically known for the KS manifolds. Indeed, even for the CICY dataset, which had been in existence since the early 1990s, the symmetry groups were only recently classified using the latest computer algebra [69]. Are there any manifolds in the KS list with known discrete symmetries? A related but simpler question is the following: Are there any manifolds in the KS list already possessing a non-trivial fundamental group? This latter question was already addressed in Ref. [30] and the answer is remarkable:

> *Of the some 500 million manifolds in the KS list, only 16 have non-trivial fundamental group.*

In fact, the 16 covering spaces for these are also in the KS list, and the discrete symmetries Γ thereof are known; in particular, their order $|\Gamma|$ is simply the ratio of the Euler numbers of the "upstairs" and the "downstairs" manifolds. On these 16 special "downstairs" manifolds one can then directly build stable bundles or, equivalently, stable equivariant bundles can be built on the corresponding 16 "upstairs" manifolds. This is the undertaking of our present chapter and constitutes an important scan over a distinguished subset of the KS database.

We emphasize that we expect many more than the aforementioned 16 manifolds in the KS list to have freely acting symmetries. However, the quotients of those manifolds do not have a description as a hypersurface in a toric four-fold and can, therefore, not be found by searching for non-trivial first fundamental groups in the KS list. Systematic heterotic model building on this full set of KS manifolds with freely-acting symmetries is the challenging task ahead but this will have to await a full classification of freely-acting symmetries.

The chapter is organized as follows. We start in Section 3.2 by describing the 16 special base three-folds in detail. In Section 3.3, we consider heterotic line bundle models subject to some phenomenological constraints on these manifolds and the algorithm for a systematic scan over all such models is laid out. The result of this scan follows in Section 2.4 and we conclude with discussion and prospects in Section 2.5.

Nomenclature Unless stated otherwise, we adhere to the following notations in this chapter:

N	The 4-dimensional lattice space of Δ
M	The dual lattice space of Δ°
Δ	Polytope in an auxiliary four-dimensional lattice

Δ°	Dual polytope of Δ
$\mathcal{A}_\Delta$	"Downstairs" ambient toric variety constructed from the polytope Δ
X_Δ	Calabi-Yau hypersurface three-fold naturally embedded in $\mathcal{A}_\Delta$
$\mathrm{Pic}(M)$	Picard group of holomorphic line bundles on a manifold M
n	Number of vertices in the polytope Δ
$x_{\rho=1,\cdots,n}$	Homogeneous coordinates of an ambient toric variety $\mathcal{A}$
$D_{\rho=1,\cdots,n}$	Divisors defined as the vanishing loci of x_ρ
k	Dimension of Picard group
$J_{r=1,\cdots,k}$	Harmonic (1,1)-form basis elements of $H^{1,1}(X,\mathbb{Z})$
$\widetilde{\mathcal{A}_\Delta}$	"Upstairs" ambient toric variety associated with $\mathcal{A}_\Delta$
$\widetilde{X_\Delta}$	Calabi-Yau hypersurface three-fold naturally embedded in $\widetilde{\mathcal{A}_\Delta}$
$\mathrm{ch}(V)$	Chern character of bundle V
$c(V)$	Chern class of bundle V
$\mu(V)$	Mu-slope of bundle V
$\mathrm{ind}(V)$	Index of the Dirac operator twisted by bundle V
K	Kähler cone matrix of a projective variety

2.2 The base manifolds: sixteen Calabi-Yau three-folds

As mentioned above, the largest known class to date of smooth, compact Calabi-Yau three-folds is constructed as hypersurfaces in a toric ambient four-fold and is often called Kreuzer-Skarke (KS) data set [6, 70]. The huge database cosists of the toric ambient varieties $\mathcal{A}_\Delta$ as well as the Calabi-Yau hypersurfaces X_Δ therein, both of which are combinatorially described by a "reflexive" polytope Δ living in an auxiliary four-dimensional lattice. The classification of reflexive four-polytopes had been undertaken and resulted in the data set of $473,800,766$ polytopes, each of which gives rise to one or more Calabi-Yau three-fold geometries. Only 16 spaces in KS data set carry non-trivial first fundamental groups, which are all of the cyclic form, $\pi_1 \cong \mathbb{Z}/p\,\mathbb{Z}$, for $p = 2, 3, 5$ [30]. For the heterotic model-building purposes, one is in need of Wilson lines,

so these 16 Calabi-Yau three-folds form a natural starting point.

More common in heterotic model building is to start from a simply-connected Calabi-Yau three-fold $\widetilde{X}$ with freely-acting discrete symmetry group Γ and then form the quotient $X = \widetilde{X}/\Gamma$ which represents a Calabi-Yau manifold with first fundamental group equal to Γ. Indeed, for the CICY data set [34], all the 7890 Calabi-Yau three-folds turn out to be simply-connected and a heavy computer search had to be performed to classify the freely-acting discrete symmetries [69]. Typical heterotic models have thus been built firstly on the upstairs CICY $\widetilde{X}$ and have then been descended to the downstairs Calabi-Yau X. A similar approach has also been taken for the model building based on the KS list carried out in Ref. [29].

In this chapter, we attempt to construct heterotic models outright from the downstairs geometry. We shall start in this section by describing some basic geometry of the sixteen toric Calabi-Yau three-folds X with $\pi_1(X) \neq \emptyset$. This includes Hodge numbers, Chern classes, intersection rings and Kähler cones. The precise quotient relationship with the corresponding upstairs three-folds $\widetilde{X}$, as well as the full list of relevant geometries, can be found in Appendix C.2.

2.2.1 The construction

Let us label the sixteen Calabi-Yau three-folds and their ambient toric four-folds by $X_{i=1,\cdots,16}$ and $\mathcal{A}_{i=1,\cdots,16}$, respectively. They come from the corresponding (reflexive) polytopes Δ_i in an auxiliary rank-four lattice N, whose vertex information [30] is summarised in Appendix C.1. Before describing their geometry in section 2.2.2, partly to set the scene up, we illustrate the general procedure for the toric construction of Calabi-Yau three-fold, by the explicit example, $X_3 \subset \mathcal{A}_3$ and Δ_3. For a more detailed introduction, interested readers are kindly referred, e.g., to Ref. [28] and references therein.

Let us first extract the lattice polytope Δ_3 from Appendix C.1:

$$\left(\begin{array}{cccccccc} x_1 & x_2 & x_3 & x_4 & x_5 & x_6 & x_7 & x_8 \\ \hline 2 & 0 & 0 & 0 & 0 & 0 & 0 & -2 \\ 0 & -1 & 0 & 1 & -1 & 0 & 1 & 0 \\ 0 & 0 & -1 & 1 & -1 & 1 & 0 & 0 \\ 1 & 0 & 0 & 1 & -1 & 0 & 0 & -1 \end{array}\right) .$$

It has $n = 8$ vertices in $N \simeq \mathbb{Z}^4$ leading to 8 homogeneous coordinates $x_{\rho=1,\cdots,8}$ for the ambient toric four-fold $\mathcal{A}_3$; the 4 rows of the above matrix describe the 4 projectivisations that reduce

the complex dimension from 8 down to 4. Next, the dual polytope Δ_3° in the dual lattice M is constructed as

$$\Delta_3^\circ := \{m \in M \mid \langle m, v\rangle \geqslant -1 \ , \ \forall v \in \Delta_3\} \ ,$$

and one can easily check that Δ_3° is also a lattice polytope. Then it so turns out that each of the lattice points in Δ_3° is mapped to a global section of the normal bundle for the embedding, $X_3 \subset \mathcal{A}_3$, of the Calabi-Yau three-fold (see Eq. (45) of Ref. [28] for the explicit map). Here, Δ_3° has 41 lattice points and the corresponding 41 sections are obtained as:

$$\begin{gathered}
x_2^2x_3^2x_4^2x_8^2 \ , \ x_2^2x_3^2x_5^2x_8^2 \ , \ x_1x_2^2x_3^2x_4x_5x_8 \ , \ x_1^2x_2^2x_3^2x_4^2 \ , \ x_2^2x_3x_4x_5x_6x_8^2 \ , \ x_1x_2^2x_3x_4^2x_6x_8 \ , \\
x_2^2x_4^2x_6^2x_8^2 \ , \ x_2x_3^2x_4x_5x_7x_8^2 \ , \ x_1x_2x_3^2x_4^2x_7x_8 \ , \ x_2x_3x_4^2x_6x_7x_8^2 \ , \ x_3^2x_4^2x_7^2x_8^2 \ , \ x_1^2x_2^2x_3^2x_5^2 \ , \\
x_1x_2^2x_3x_5^2x_6x_8 \ , \ x_1^2x_2^2x_3x_4x_5x_6 \ , \ x_2^2x_5^2x_6^2x_8^2 \ , \ x_1x_2^2x_4x_5x_6^2x_8 \ , \ x_1^2x_2^2x_4^2x_6^2 \ , \ x_1x_2x_3^2x_5^2x_7x_8 \ , \\
x_1^2x_2x_3^2x_4x_5x_7 \ , \ x_2x_3x_5^2x_6x_7x_8^2 \ , \ x_1x_2x_3x_4x_5x_6x_7x_8 \ , \ x_1^2x_2x_3x_4^2x_6x_7 \ , \ x_2x_4x_5x_6^2x_7x_8^2 \ , \\
x_1x_2x_4^2x_6^2x_7x_8 \ , \ x_3^2x_5^2x_7^2x_8^2 \ , \ x_1x_3^2x_4x_5x_7^2x_8 \ , \ x_1^2x_3^2x_4^2x_7^2 \ , \ x_3x_4x_5x_6x_7^2x_8^2 \ , \ x_1x_3x_4^2x_6x_7^2x_8 \ , \\
x_4^2x_6^2x_7^2x_8^2 \ , \ x_1^2x_2^2x_5^2x_6^2 \ , \ x_1^2x_2x_3x_5^2x_6x_7 \ , \ x_1x_2x_5^2x_6^2x_7x_8 \ , \ x_1^2x_2x_4x_5x_6^2x_7 \ , \ x_1^2x_3^2x_5^2x_7^2 \ , \\
x_1x_3x_5^2x_6x_7^2x_8 \ , \ x_1^2x_3x_4x_5x_6x_7^2 \ , \ x_5^2x_6^2x_7^2x_8^2 \ , \ x_1x_4x_5x_6^2x_7^2x_8 \ , \ x_1^2x_4^2x_6^2x_7^2 \ , \ x_1^2x_5^2x_6^2x_7^2 \ .
\end{gathered} \tag{2.1}$$

which, when linearly combined, give the defining equation for X_3.

Note that as the non-trivial fundamental group is a toric morphism, it is natural to expect that the KS list also contains the sixteen upstairs geometries, which we denote by $\widetilde{X_i} \subset \widetilde{\mathcal{A}_i}$. By construction, the upstairs three-folds $\widetilde{X_i}$ should admit a freely-acting discrete symmetry Γ_i so that $X_i = \widetilde{X_i}/\Gamma_i$ with $\pi_1(X_i) = \Gamma_i$. We have indeed found the corresponding upstairs polytopes $\widetilde{\Delta_i}$ associated with the sixteen downstairs (see Appendix C.1 for their vertex lists). It turns out that three of the sixteen upstairs Calabi-Yau three-folds $\widetilde{X_i} \subset \widetilde{\mathcal{A}_i}$ belong to the CICY list [34]: $\widetilde{X_1}$ is the quintic three-fold in $\mathbb{P}^4$, $\widetilde{X_2}$ the bi-cubic in $\mathbb{P}^2 \times \mathbb{P}^2$ and $\widetilde{X_3}$ the tetra-quadric in $\mathbb{P}^{1\times 4}$. Although the models in this chapter are constructed over the downstairs manifolds, one can compare, as a cross-check, the models over X_1, X_2 and X_3 with the known results over the CICYs [22, 23].

We finally remark that the ambient toric varieties $\mathcal{A}_\Delta$ constructed by the standard toric procedure might in general involve singularities. In order to obtain smooth Calabi-Yau hypersurfaces X, one must resolve the singularities of the ambient space to a point-like level via "triangulation" of the polytope Δ in a certain manner [31]. The triangulation splits Δ maximally and leads to a partial desingularisation of the toric variety $\mathcal{A}_\Delta$. In principle, there may arise several different desingularisations for a single toric variety $\mathcal{A}_\Delta$, in which case the number of geometries increases. Indeed, X_6 and X_{14} turn out to have two and three desingularisations, respectively, while the other fourteen Calabi-Yau manifolds only have one each.

2.2.2 Some geometrical properties

Having constructed the Calabi-Yau three-folds in the previous subsection, we now move on to study their geometrical properties relevant to the heterotic model-building. Instead of describing all the details in an abstract manner, we continue with the example X_3; the $\mathbb{Z}_2$-quotient of the tetra-quadric $\widetilde{X}_3$ in $\mathbb{P}^{1\times 4}$. The detailed prescription for computing the geometric properties can be found from Appendix B of [28]. Alternatively, one could also make use of the computer package [71] to extract all the information. The resulting geometry can be summarised as follows.

Firstly, we have $k \equiv \text{rk}(\text{Pic}(\mathcal{A}_3)) = 4$ and hence, the Picard group is generated by four elements $J_{r=1,\cdots,4}$. One can then choose the basis elements appropriately so that the toric divisors $D_{\rho=1,\cdots,8}$ defined as the vanishing locus of the homogeneous coordinate x_ρ have the following expressions:

$$D_1 = J_4,\ D_2 = J_3,\ D_3 = J_2,\ D_4 = J_1,\ D_5 = J_1,\ D_6 = J_2,\ D_7 = J_3,\ D_8 = J_4\ , \tag{2.2}$$

where, by abuse of notation, the harmonic $(1,1)$-forms J_r are also used to denote the basis of Picard group. Furthermore, unless ambiguities arise, we shall not attempt to carefully distinguish the harmonic forms of the ambient space from their pullbacks to the hypersurface. Next, the intersection polynomial of X_3 is:

$$J_1\,J_2\,J_3 + J_1\,J_2\,J_4 + J_1\,J_3\,J_4 + J_2\,J_3\,J_4\ ,$$

which means that the only non-vanishing triple intersections are

$$d_{123}(X_3) = d_{124}(X_3) = d_{134}(X_3) = d_{234}(X_3) = 1$$

and those obtained by the permutations of the indices above. The Hodge numbers can also be easily computed:

$$h^{1,1}(X_3) = 4,\quad h^{1,2}(X_3) = 36\ ,$$

leading to the Euler character $\chi(X_3) = -64$. The second Chern character for the tangent bundle, which is crucial for the anomaly check, is given by

$$\text{ch}_2(TX) = \{12,12,12,12\} = \sum_{r=1}^{4} 12\ \nu^r\ , \tag{2.3}$$

in the dual 4-form basis $\nu^{r=1,\cdots,4}$ defined such that $\int_{X_3} J_r \wedge \nu^s = \delta_r^s$. Finally, the Kähler cone matrix $K = [K_{rs}]$, describing the Kähler cone as the set of all Kähler parameters t^r satysfying

$K_{rs}t^s \geq 0$ for all $r = 1, \ldots, h^{1,1}(X)$, takes the form

$$K = \begin{pmatrix} 1 & 0 & 0 & 0 \\ 0 & 1 & 0 & 0 \\ 0 & 0 & 1 & 0 \\ 0 & 0 & 0 & 1 \end{pmatrix} , \tag{2.4}$$

thus representing the part of $\mathbf{t}$ space with $t^{r=1,\cdots,4} > 0$.

The reader might have notice that $h^{1,1}(X_3) = 4 = h^{1,1}(\mathcal{A}_3)$ in this example. In general, however, $h^{1,1}(X)$ can be larger than $h^{1,1}(\mathcal{A})$ and a hypersurface of this type is called "non-favourable," as we do not have a complete control over all the Kähler forms of X through the simple toric description of the ambient space $\mathcal{A}$. The notion of favourability means that the Kähler structure of the Calabi-Yau hypersurface is entirely descended down from that of the ambient space; namely, the integral cohomology group of the hypersurface can be realised by a toric morphism from the ambient space. Amongst the sixteen downstairs geometries X_i, only the two, X_{15} and X_{16}, turn out to be non-favourable. As we do not completely understand their Kähler structure, we will not attempt to build models on either of these two manifolds.

In Appendix C.2.2, the geometrical properties summarised so far for $X_3 \subset \mathcal{A}_3$ are tabulated for all the downstairs manifolds $X_i \subset \mathcal{A}_i$, as well as their upstairs covers $\widetilde{X_i} \subset \widetilde{\mathcal{A}_i}$, $i = 1, \ldots, 16$. Another illustration for how to read off the geometry from the table is given in Appendix C.2.1 for $X_1 \subset \mathcal{A}_1$ and $\widetilde{X_1} \subset \widetilde{\mathcal{A}_1}$.

Let us close this subsection by touching upon an issue with multiple triangulations. As mentioned in section 2.2.1, the Calabi-Yau three-folds X_6 and X_{14} turn out to admit two and three triangulations, respectively. Here we take the former as an example. Its toric data is encoded in the polytope Δ_6:

$$\left(\begin{array}{ccccccc} x_1 & x_2 & x_3 & x_4 & x_5 & x_6 & x_7 \\ \hline -4 & 0 & 0 & 0 & 2 & 0 & -2 \\ -3 & 1 & 0 & -1 & 0 & -2 & -2 \\ 1 & 0 & 1 & -1 & 0 & -1 & 0 \\ -1 & 0 & 0 & -1 & 1 & 0 & -1 \end{array}\right) ;$$

this polytope turns out to admit the following two different star triangulations [1],

$$\begin{aligned}\mathcal{T}_1 &= \{\{1,2,5,6\},\{2,3,4,5\},\{1,2,3,5\},\{2,4,5,6\},\{2,4,6,7\},\{1,2,6,7\},\\ &\quad \{2,3,4,7\},\{1,2,3,7\},\{3,4,6,7\},\{1,3,6,7\},\{3,4,5,6\},\{1,3,5,6\}\}\\ \mathcal{T}_2 &= \{\{1,2,5,6\},\{2,3,4,5\},\{1,2,3,5\},\{2,4,5,6\},\{2,4,6,7\},\{1,2,6,7\},\\ &\quad \{2,3,4,7\},\{1,2,3,7\},\{4,5,6,7\},\{1,5,6,7\},\{3,4,5,7\},\{1,3,5,7\}\}\end{aligned}$$

where triangulations of the polytope Δ_6 are described as a list of four-dimensional cones. For instance, the first element $\{1,2,5,6\} \in \mathcal{T}_1$ represents the four-dimensional cone spanned by the corresponding four vertices:

$$(-4,-3,1,-1),\ (0,1,0,0),\ (2,0,0,1),\ (0,-2,-1,0).$$

It also turns out that the two smooth hypersurfaces, associated with the two triangulations $\mathcal{T}_1$ and $\mathcal{T}_2$, have the same intersection structure and the same second Chern class. It is expected in such a case that the two Calabi-Yau hypersurfaces are connected in the Kähler moduli space. In other words, the two Kähler cones adjoin along a common facet. Thus, the pair can be thought of as leading to a single Calabi-Yau three-fold X_6, whose Kähler cone is the union of the two sub-cones,

$$K(X_6) = \bigcup_{j=1}^{2} K_j \ ,$$

where K_1 and K_2 are the Kähler cones of the two hypersurfaces associated with $\mathcal{T}_1$ and $\mathcal{T}_2$, respectively (see Ref. [29] for the details). The Kähler cone matrices for the two sub-cones turn out to be

$$K_1 = \begin{pmatrix} 0 & 1 & 0 \\ 1 & 0 & -2 \\ 0 & -1 & 1 \end{pmatrix} \quad \text{and} \quad K_2 = \begin{pmatrix} 0 & 0 & 1 \\ 1 & 0 & -2 \\ 0 & 1 & -1 \end{pmatrix} \ ,$$

and therefore, the Kähler cone matrix for the union can be computed as:

$$K(X_6) = \begin{pmatrix} 1 & 0 & 0 \\ 0 & 1 & 0 \\ 0 & 0 & 1 \end{pmatrix} \ .$$

One can similarly play with Δ_{14}. For this geometry as well it turns out that the three triangulations lead to a single Calabi-Yau three-fold, X_{14}. As for the Kähler cone, the three sub-cones are

$$K_1 = \begin{pmatrix} 0 & 1 & 0 \\ 1 & -1 & 0 \\ 0 & -1 & 1 \end{pmatrix} \quad K_2 = \begin{pmatrix} 0 & 0 & 1 \\ 0 & 1 & -1 \\ 1 & 0 & -1 \end{pmatrix} \quad K_3 = \begin{pmatrix} 1 & 0 & 0 \\ -1 & 0 & -1 \\ -1 & 1 & 0 \end{pmatrix} \ , \tag{2.5}$$

[1] A triangulation is star if all maximal simplices contain a common point, in this case reduced to be cones expanded by four vertices and the origin point. In our notation the origin point is omitted, leaving only the four indices labeling the vertices.

and via the simple joining one obtains the Kähler cone of X_{14}:

$$K(X_{14}) = \begin{pmatrix} 1 & 0 & 0 \\ 0 & 1 & 0 \\ 0 & 0 & 1 \end{pmatrix} . \tag{2.6}$$

In summary, although there are different triangulations for Δ_6 and Δ_{14}, one ends up obtaining a single geometry each, X_6 and X_{14}, respectively.

2.2.3 Location in the Calabi-Yau landscape

Since a very special corner in the landscape of Calabi-Yau three-folds has been chosen, it might be interesting to see the location of these sixteen, say, in the famous Hodge number plot [72]. Figure 2.1 shows the Hodge number plot of all the Calabi-Yau three-folds known to date, together with that of the sixteen manifolds X_i and of their mirrors. Some basic topological data for both downstairs X_i and upstairs $\widetilde{X_i}$ is also summarized in Table 2.1 for reference.

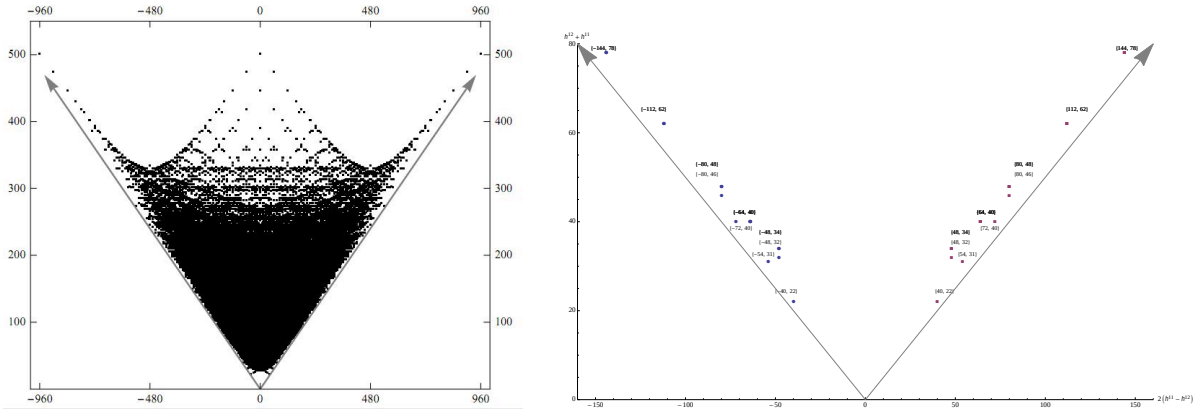

Figure 2.1: *The Hodge number plot:* $\{2(h^{1,1} - h^{2,1}), h^{1,1} + h^{2,1}\}$. *The left figure is for all the Calabi-Yau three-folds known to date and the right is for the sixteen non-simply-connected Calabi-Yau three-folds* X_i *as well as their mirrors; the blue round dots are for the original sixteen and the purple squares are for the mirrors.*

2.3 Physical constraints and search algorithm

As indicated in Table 2.1, of the sixteen downstairs three-folds, the first fourteen, $X_{i=1,\cdots,14}$, turn out to be favourable and, in this chapter, we shall take the initial step towards the construction of heterotic line bundle standard models on them. The main difficulty with the two non-favourable geometries arises from the Kähler forms which do not descend from the ambient space; the corresponding components of the Kähler matrix and the triple intersection numbers are difficult to obtain from the ambient toric data, since the line bundles could be safely

i	1	2	3	4	5	6	7	8	9	10	11	12	13	14	15	16
$h^{1,1}(\widetilde{X_i})$	1	2	4	4_{nf}	3	3	4_{nf}	4_{nf}	4	4	4	5_{nf}	5_{nf}	3	7_{nf}	7_{nf}
$h^{1,1}(X_i)$	1	2	4	2	3	3	3	3	4	4	4	4	4	3	5_{nf}	5_{nf}
$-\chi(\widetilde{X_i})$	200	162	128	216	160	224	288	288	96	128	128	160	160	224	96	96
$-\chi(X_i)$	40	54	64	72	80	112	144	144	48	64	64	80	80	112	48	48
$\pi_1(X_i)$	$\mathbb{Z}_5$	$\mathbb{Z}_3$	$\mathbb{Z}_2$	$\mathbb{Z}_3$	$\mathbb{Z}_2$	$\mathbb{Z}_2$	$\mathbb{Z}_2$	$\mathbb{Z}_2$	$\mathbb{Z}_2$	$\mathbb{Z}_2$	$\mathbb{Z}_2$	$\mathbb{Z}_2$	$\mathbb{Z}_2$	$\mathbb{Z}_2$	$\mathbb{Z}_2$	$\mathbb{Z}_2$

Table 2.1: *Picard numbers and Euler characters of the downstairs Calabi-Yau three-folds X_i and their upstairs covers $\widetilde{X_i}$, for $i = 1, \ldots, 16$. In the last row is also shown the π_1 of the downstairs manifolds X_i. The subscript "nf" for Picard number indicates that the geometry is non-favourable.*

descended down to CY manifolds are coming only from toric divisors, with a smaller number than the dimension of CY manifold. While for the extra line bundles of CY manifolds, it is not straight forward to write them out and not possible to compute the triple intersection numbers since the calculation is essentially done over the toric variety. Therefore, the missing info makes it impossible to fully check certain consistency conditions of the bundle, notably the poly-stability condition discussed below.

2.3.1 Choice of bundles and gauge group

Let us begin by discussing the choice of gauge bundle and the resulting four-dimensional gauge group. First of all, we need to choose a bundle V with structure group G which embeds into the visible E_8 gauge group. The resulting low-energy gauge group, H, is the commutant of G within E_8. As discussed earlier, for V we would like to consider Whitney sums of line bundles of the form

$$V = \bigoplus_{a=1}^{n} L_a \ , \quad L_a = \mathcal{O}_X(\mathbf{k}_a) \ , \tag{2.7}$$

where the line bundles are labeled by integer vectors $\mathbf{k}_a$ with $h^{1,1}(X)$ components k_a^r such that their first Chern classes can be written as $c_1(L_a) = k_a^r J_r$. The structure group of this line bundle sum should have an embedding into E_8. For this reason, we will demand that $c_1(V) = 0$ or, equivalently,

$$\sum_{a=1}^{n} \mathbf{k}_a = 0 \ , \tag{2.8}$$

which leads, generically, to the structure group $G = S(U(1)^n)$. For $n = 4, 5$ this structure group embeds into E_8 via the subgroup chains $S(U(1)^4) \subset SU(4) \subset E_8$ and $S(U(1)^5) \subset SU(5) \subset E_8$, respectively. This results in the commutants $H = SO(10) \times U(1)^3$ for $n = 4$ and

$H = SU(5) \times U(1)^4$ for $n = 5$. Both, $SU(5)$ and $SO(10)$, are attractive grand unification groups and they can be further broken to the standard model group after the inclusion of Wilson lines. Hence, constructing such $SU(5)$ and $SO(10)$ models, subject to further constraints discussed below, is the first step in the standard heterotic model building programme. The additional $U(1)$ symmetries turn out to be typically Green-Schwarz anomalous. Hence, the associated gauge bosons are super massive and of no phenomenological concern.

2.3.2 Anomaly cancelation

In general, anomaly cancelation can be expressed as the topological condition

$$\mathrm{ch}_2(V) + \mathrm{ch}_2(\hat{V}) - \mathrm{ch}_2(TX) = [C] \ , \tag{2.9}$$

where V is the bundle in the observable E_8 sector, as discussed, $\tilde{V}$ is its hidden counterpart and $[C]$ is the homology class of a holomorphic curve, C, wrapped by a five-brane. A simple way to guarantee that this condition can be satisfied is to require that

$$\mathrm{c}_2(TX) - \mathrm{c}_2(V) \in \mathrm{Mori}(X) \ , \tag{2.10}$$

where $\mathrm{Mori}(X)$ is the cone of effective classes of X. Here, we have used that $\mathrm{ch}_2(TX) = -\mathrm{c}_2(TX)$ and that $\mathrm{ch}_2(V) = -c_2(V)$ for bundles V with $c_1(V) = 0$. Provided condition (2.10) holds the model can indeed always be completed in an anomaly-free way so that Eq. (2.9) is satisfied. Concretely, Eq. (2.10) guarantees that there exists a complex curve C with $[C] = \mathrm{c}_2(TX) - \mathrm{c}_2(V)$, so that wrapping a five brane on this curve and choosing the hidden bundle to be trivial will do the job (although other choices involving a non-trivial hidden bundle are usually possible as well).

To compute the the second Chern class $c_2(V) = c_{2r}(V)\nu^r$ of line bundle sums (2.7) we can use the result

$$c_{2r}(V) = -\frac{1}{2} d_{rst} \sum_{a=1}^{n} k_a^s k_a^t \ , \tag{2.11}$$

where d_{rst} are the triple intersection numbers. For the 16 manifolds under consideration these numbers, as well as the second Chern classes, $c_2(TX)$, of the tangent bundle are provided in Appendix C.2.

2.3.3 Poly-stability

The Donaldson-Uhlenbeck-Yau theorem states that for a "poly-stable" holomorphic vector bundle V over a Kähler manifold X, there exists a unique connection satisfying the Hermitian

Yang-Mills equations. Thus, in order to make the models consistent with supersymmetry, we need to verify that the sum of holomorphic line bundles is poly-stable.
Poly-stability of a bundle (coherent sheaf) $\mathcal{F}$ is defined by means of the *slope*

$$\mu(\mathcal{F}) \equiv \frac{1}{\mathrm{rk}(\mathcal{F})} \int_X c_1(\mathcal{F}) \wedge J \wedge J \ , \tag{2.12}$$

where J is the Kähler form of the Calabi-Yau three-fold X. The bundle $\mathcal{F}$ is called *poly-stable* if it decomposes as a direct sum of stable pieces,

$$\mathcal{F} = \bigoplus_{a=1}^{m} \mathcal{F}_a \ , \tag{2.13}$$

of equal slope $\mu(\mathcal{F}_a) = \mu(\mathcal{F})$, for $a = 1, \cdots, m$. In our case, the bundle V splits into the line bundles L_a as in Eq. (2.7). Line bundles, however, are trivially stable as they do not have a proper subsheaf. This feature is one of the reasons why heterotic line bundle models are technically much easier to deal with than models with non-Abelian structure groups. All that remains from poly-stability is the conditions on the slopes. Since $c_1(V) = 0$, we have $\mu(V) = 0$ and, hence, the slopes of all constituent line bundles L_a must vanish. This translates into the conditions

$$\mu(L_a) = k_a^r \kappa_r = 0 \quad \text{where} \quad \kappa_r = d_{rst} t^s t^t \ , \tag{2.14}$$

for $a = 1, \ldots, n$ which must be satisfied simultaneously for Kähler parameters t^r in the interior of the Kähler cone. The intersection numbers and the data describing the Kähler cone for our 16 manifolds is provided in Appendix C.2.

2.3.4 $SU(5)$ GUT theory

A model with a (rank four or five) line bundle sum (2.7) in the observable sector that satisfies the constraints (2.8), (2.10) and (2.14) can be completed to a consistent supersymmetric heterotic string compactification leading to a four-dimensional $N = 1$ supergravity with gauge group $SU(5)$ or $SO(10)$ (times anomalous $U(1)$ factors). Subsequent conditions, which we will impose shortly, are physical in nature and are intended to single out models with a phenomenologically attractive particle spectrum. The details of how this is done somewhat depend on the grand unified group under consideration and we will discuss the two cases in turn, starting with $SU(5)$. In this case we start with a line bundle sum (2.7) of rank five ($n = 5$) and associated structure group $G = S(U(1)^5)$. This leads to a four-dimensional gauge group $H = SU(5) \times S(U(1)^5)$. The four-dimensional spectrum consists of the following $SU(5) \times S(U(1)^5)$ multiplets:

$$\mathbf{10}_a \ , \quad \overline{\mathbf{10}}_a \ , \quad \overline{\mathbf{5}}_{a,b} \ , \quad \mathbf{5}_{a,b} \ , \quad \mathbf{1}_{a,b} \ . \tag{2.15}$$

Here, the subscripts $a, b, \cdots = 1, \ldots, 5$ indicate which of the additional $U(1)$ factors in $S(U(1)^5)$ the multiplet is charged under. A $\mathbf{10}_a$ ($\overline{\mathbf{10}}_a$) multiplet carries charge 1 (-1) under the a^{th} $U(1)$ and is uncharged under the others. A $\overline{\mathbf{5}}_{a,b}$ ($\mathbf{5}_{a,b}$), where $a < b$, carries charge 1 (-1) only under the a^{th} and b^{th} $U(1)$ while the only charges of a singlet $\mathbf{1}_{a,b}$, where $a \neq b$, are 1 under the a^{th} $U(1)$ and -1 under the b^{th} $U(1)$.

The multiplicity of these various multiplets is computed by the dimension of associated cohomology groups as given in Table 2.2. The most basic phenomenological constraint to impose

$SU(5) \times S(U(1)^5)$ repr.	associated cohomology	contained in
$\mathbf{10}_a$	$H^1(X, L_a)$	$H^1(X, V)$
$\overline{\mathbf{10}}_a$	$H^1(X, L_a^*)$	$H^1(X, V^*)$
$\overline{\mathbf{5}}_{a,b}$	$H^1(X, L_a \otimes L_b)$	$H^1(X, \wedge^2 V)$
$\mathbf{5}_{a,b}$	$H^1(X, L_a^* \otimes L_b^*)$	$H^1(X, \wedge^2 V^*)$
$\mathbf{1}_{a,b}$	$H^1(X, L_a \otimes L_b^*)$	$H^1(X, V \otimes V^*)$

Table 2.2: *The spectrum of $SU(5)$ models and associated cohomology groups.*

on this spectrum is chiral asymmetry of three in the $\mathbf{10}$–$\overline{\mathbf{10}}$ sector. This translates into the condition

$$\text{ind}(V) = -3 \ ,$$

on the index of V which can be explicitly computed from

$$\text{ind}(V) = \frac{1}{6} d_{rst} \sum_{a=1}^{n} k_a^r k_a^s k_a^t \ . \tag{2.16}$$

Of course, a similar constraint on the chiral asymmetry should hold in the $\overline{\mathbf{5}}$–$\mathbf{5}$ sector. In general, for a rank m bundle V, we have the relation

$$\text{ind}(\wedge^2 V) = (m-4)\text{ind}(V) \tag{2.17}$$

So for the rank five bundles presently considered it follows that $\text{ind}(\wedge^2 V) = \text{ind}(V)$. Hence the requirement (2.16) on the chiral asymmetry in the $\mathbf{10}$–$\overline{\mathbf{10}}$ sector already implies the correct chiral asymmetry for the $\overline{\mathbf{5}}$–$\mathbf{5}$ multiplets, $\text{ind}(\wedge^2 V) = -3$, and no additional constraint is required.

The index constraints imposed so far are necessary but of course not sufficient for a realistic spectrum. For example, one obvious additional phenomenological requirement would be the

absence of $\overline{\mathbf{10}}$ multiplets which amounts to the vanishing of the associated cohomology group, that is, $h^1(X, V^*) = 0$. However, cohomology calculations are much more involved than index calculations and currently there is no complete algorithm for calculating line bundle cohomology on Calabi-Yau hypersurfaces in toric four-folds. For this reason, we will not impose cohomology constraints on our models in the present chapter, although this will have to be done at a later stage.

However, working with line bundle sums allows us to impose slightly stronger constraints which are based on the indices of the individual line bundles. Of course we can express the indices of V and $\wedge^2 V$ in terms of the indices of their constituent line bundles as

$$\text{ind}(V) = \sum_{a=1}^{n} \text{ind}(L_a) \ , \quad \text{ind}(\wedge^2 V) = \sum_{a<b} \text{ind}(L_a \otimes L_b) \ , \tag{2.18}$$

where, by the index theorem, the index of an individual line bundle $L = \mathcal{O}_X(\mathbf{k})$ is given by

$$\text{ind}(L) = d_{rst} \left(\frac{1}{6} k^r k^s k^t + \frac{1}{12} k^r c_2^{st}(TX) \right) \ . \tag{2.19}$$

Suppose that $\text{ind}(L_a) > 0$ for one of the line bundles L_a. Then, in this sector, there is a chiral net-surplus of $\overline{\mathbf{10}}$ multiplets which is protected by the index and will survive the inclusion of a Wilson line. Since such $\overline{\mathbf{10}}$ multiplets and their standard-model descendants are phenomenologically unwanted we should impose [2] that $\text{ind}(L_a) \leq 0$ for all a. Combining this with the overall constraint (2.16) on the chiral asymmetry and Eq. (2.18) this implies that

$$-3 \leqslant \text{ind}(L_a) \leqslant 0 \tag{2.20}$$

for all $a = 1, \ldots, 5$. A similar argument can be made for the $\overline{\mathbf{5}}$–$\mathbf{5}$ multiplets. A positive index, $\text{ind}(L_a \otimes L_b) > 0$, would imply chiral $\mathbf{5}$ multiplets in this sector. They would survive the Wilson line breaking and lead to unwanted Higgs triplets. Hence, we should require that $\text{ind}(L_a \otimes L_b) \leq 0$ for all $a < b$ which implies that

$$-3 \leqslant \text{ind}(L_a \otimes L_b) \leqslant 0 \ , \tag{2.21}$$

for all $a < b$.

Table 2.3 summarizes both the consistency constraints explained earlier and the phenomenological constraints discussed in this subsection. This set of constraints will be used to classify rank five line bundle models on our 16 Calabi-Yau manifolds.

[2] The caveat is that line bundle models frequently represent special loci in a larger moduli space of non-Abelian bundles. Line bundle models with exotic states – vector-like under the GUT group/standard model group but chiral under the $U(1)$ symmetries – may become realistic when continued into the non-Abelian part of the moduli space where some or all of the $U(1)$ symmetries are broken. In this case, the exotic states may become fully vector-like, acquire a mass and are removed from the low-energy spectrum. While this is an entirely plausible model building route, here we prefer a "cleaner" approach where the spectrum at the Abelian locus can already lead to a realistic spectrum.

Physics	Background geometry
Gauge group	$c_1(V) = 0$
Anomaly	$c_2(TX) - c_2(V) \in \text{ Mori}(X)$
Supersymmetry	$\mu(L_a) = 0, \text{ for } 1 \leq a \leq 5$
Three generations	$\text{ind}(V) = -3$
No exotics	$-3 \leq \text{ind}(L_a) \leq 0, \quad \text{for } 1 \leq a \leq 5\,;$ $-3 \leq \text{ind}(L_a \otimes L_b) \leq 0, \quad \text{for } 1 \leq a < b \leq 5$

Table 2.3: *Consistency and phenomenological constraints imposed on rank five line bundle sums of the form* (2.7).

2.3.5 $SO(10)$ GUT theory

In this case, we start with a line bundle sum (2.7) of rank four ($n = 4$) with a structure group $G = S(U(1)^4)$. The resulting four-dimensional gauge group is $H = SO(10) \times S(U(1)^4)$ and the multiplets under this gauge group which arise are

$$\mathbf{16}_a \ , \ \ \overline{\mathbf{16}}_a \ , \ \ \mathbf{10}_{a,b} \ , \ \ \mathbf{1}_{a,b} \ . \tag{2.22}$$

In analogy to the $SU(5)$ case, the subscripts $a, b, \cdots = 1, \ldots, 4$ indicate which of the four $U(1)$ symmetries the multiplet is charged under. A $\mathbf{16}_a$ ($\overline{\mathbf{16}}_a$) multiplet carries charge 1 (-1) under the a^{th} $U(1)$ symmetry and is uncharged under the others. A $\mathbf{10}_{a,b}$ multiplet, where $a < b$, carries charge 1 under the a^{th} and b^{th} $U(1)$ symmetry and is otherwise uncharged while a singlet $\mathbf{1}_{a,b}$, where $a \neq b$, has charge 1 under the a^{th} $U(1)$ and charge -1 under the b^{th} $U(1)$.
The multiplicity of each of the above multiplets is computed from associate cohomology groups as indicated in Table 2.4. The three generation condition on the $\mathbf{16}$–$\overline{\mathbf{16}}$ multiplets remains the

$SO(10) \times S(U(1)^4)$ repr.	associated cohomology	contained in
$\mathbf{16}_a$	$H^1(X, L_a)$	$H^1(X, V)$
$\overline{\mathbf{16}}_a$	$H^1(X, L_a^*)$	$H^1(X, V^*)$
$\mathbf{10}_{a,b}$	$H^1(X, L_a \otimes L_b)$	$H^1(X, \wedge^2 V)$
$\mathbf{1}_{a,b}$	$H^1(X, L_a \otimes L_b^*)$	$H^1(X, V \otimes V^*)$

Table 2.4: *The spectrum of $SO(10)$ models and associated cohomology groups.*

same:

$$\text{ind}(V) = -3\ . \tag{2.23}$$

For rank four bundles Eq. (2.17) implies that $\text{ind}(\wedge^2 V) = 0$ so no further constraint needs to be imposed. In analogy with the $SU(5)$ case, in order to avoid $\overline{\mathbf{16}}$ exotics, we should impose that

$$-3 \leq \text{ind}(L_a) \leq 0 \tag{2.24}$$

for all $a = 1, \ldots, 4$. The line bundle indices can be explicitly computed from Eq. (2.19). The **10** sector is automatically vector-like so no further constraint analogous to Eq. (2.21) is required. Table 2.5 summarizes the consistency constraints explained earlier and the phenomenological constraints discussed above. These constraints will be used to classify rank four line bundle sums on our 16 manifolds.

Physics	Background geometry
Gauge group	$c_1(V) = 0$
Anomaly	$\text{ch}_2(TX) - \text{ch}_2(V) \in \text{Mori}(X)$
Supersymmetry	$\mu(L_a) = 0,\ \text{for } 1 \leq a \leq 4$
Three generations	$\text{ind}(V) = -3$
No exotics	$-3 \leq \text{ind}(L_a) \leq 0,\ \ \text{for } 1 \leq a \leq 4$

Table 2.5: *Consistency and phenomenological constraints on rank four line bundles of the form* (2.7).

2.3.6 Search algorithm

In principle, the scanning procedure is straight-forward now. We firstly generate all the single line bundles, $L = \mathcal{O}_X(\mathbf{k})$ with entries k^r in a certain range and with their index between -3 and 0. Then we compose these line bundles into rank four or five sums imposing the constraints detailed in Table 2.3 and 2.5, respectively, as we go along and at the earliest possible stage.
Which range of line bundle entries k_a^r should we consider in this process? Unfortunately, we are not aware of a finiteness proof for line bundle sums which satisfy the constraints in Table 2.3 and 2.5, nor do we know how to derive a concrete theoretical bound on the maximal size of the entries k_a^r from those constraints. Lacking such a bound we proceed computationally. For a given positive integer k_{max} we can find all line bundle models with $k_a^r \in [-k_{\text{max}}, k_{\text{max}}]$. We do this for increasing values $k_{\text{max}} = 1, 2, 3, \ldots$ and find the viable models for each value. If

the number of these models does not increase for three consecutive $k_{\max}$ values, the search is considered complete. In this way, we are able to verify finiteness and find the complete set of viable models for rank five bundles. For rank four, we find the complete set for some of the manifolds but are limited by computational power for the others.
Finally, there is a practical step for simplifying the bundle search. If the Kähler cone, in the form given by the original toric data, does not coincide with the positive region where all $t^r > 0$ it is useful to arrange this by a suitable basis transformation. This makes checking certain properties, such as the effectiveness of a given curve class, easier. We refer to Ref. [28] for details.

2.4 Results

In this section, we describe the results of our scans for phenomenologically attractive $SU(5)$ and $SO(10)$ line bundle GUT models on the 14 favourable Calabi-Yau three-folds out of our 16 special ones.

2.4.1 $SU(5)$ GUT theory

For the rank five line bundle sums we are able to verify finiteness computationally for each manifold, using the method based on scanning over entries k_a^r with $-k_{\max} \leq k_a^r \leq k_{\max}$ for increasing $k_{\max}$, as explained above. As an illustration, we have plotted the number of viable models on X_9 as a function of $k_{\max}$ in Fig. 2.2. As is evident from the figure, the number saturates at $k_{\max} = 4$ and stays constant thereafter. A similar behaviour is observed for all other spaces.

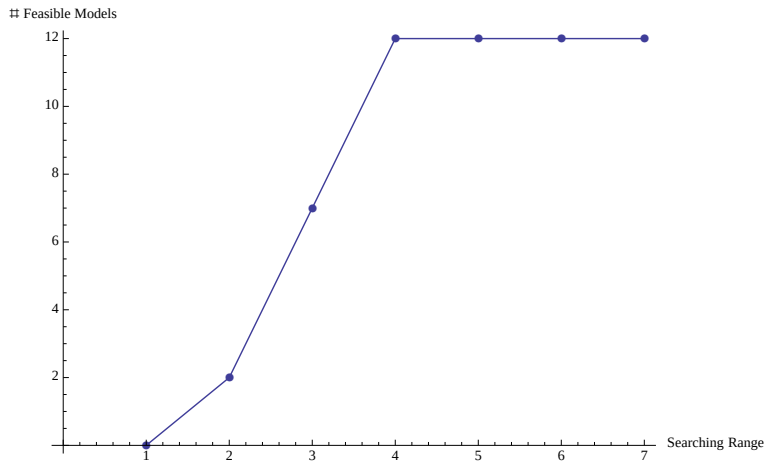

Figure 2.2: *The number of viable line-bundle models on X_9 as a function of $k_{\max}$.*

Recall from Table 2.1 that amongst the favourable base manifolds $X_{i=1,\cdots,14}$, only X_1 has Picard number 1, X_2 and X_4 have Picard number 2, X_5, X_6, X_7, X_8, X_{14} have Picard number 3, and X_3, X_9, X_{10}, X_{11}, X_{12}, X_{13} have Picard number 4. It turns out that viable models arise on all the six manifolds with Picard number 4 and on two out of the five manifolds with Picard number 3, namely X_6 and X_{14}, in total 122 models. The number of models for each manifold is summarized in Table 2.6 and the explicit line bundle sums are given in Appendix C.3. A line bundle data set can be downloaded from Ref. [73].

	X_1	X_2	X_3	X_4	X_5	X_6	X_7	X_8	X_9	X_{10}	X_{11}	X_{12}	X_{13}	X_{14}	total
# $SU(5)$	0	0	10	0	0	2	0	0	12	25	54	1	17	1	122
max. $\lvert k_a^r\rvert$	-	-	4	-	-	4	-	-	4	5	5	4	5	4	
# $SO(10)$	0	0	7017 *	0	5	13	0	9	2207	4416 *	8783 *	1109 *	5283 *	28	28870
max. $\lvert k_a^r\rvert$	-	-	17	-	6	7	-	4	15	20	19	21	21	7	

Table 2.6: *Numbers of viable rank five ($SU(5)$) and rank four ($SO(10)$) line bundle models and maximal value of $|k_a^r|$ for each base manifold. For the $SO(10)$ cases marked with a star numbers are converging but have not quite saturated despite the large entries.*

2.4.2 $SO(10)$ GUT theory

As in the $SU(5)$ cases, viable models only arise on base manifolds with Picard number greater than 2. It turns out that amongst the five Picard number 3 manifolds, X_7 does not admit any viable models, and the other four, X_5, X_6, X_8, X_{14} admit 5, 13, 9, 28 bundles, respectively. For all those cases, the scan has saturated according to our criterion and the complete set of viable models has been found. In total this is 55 models which are listed in Appendix C.3. For the other six manifolds X_3, X_9, X_{10}, X_{11}, X_{12}, X_{13}, all with Picard number four, only X_9 is complete and admits 2207 bundles. For the others, the number of viable bundles is converging but still growing slowly despite the large range of integer entries. The number of models found in each case is summarized in Table 2.6 and the complete data sets can be downloaded from Ref. [73].

2.4.3 An $SU(5)$ example

To illustrate our results we would like to present explicitly one example from our data set, a three generation $SU(5)$ GUT theory on the Calabi-Yau manifold X_9. We recall that X_9 is a Picard number four manifold, constructed from eight homogeneous coordinates (see Appendix C.1 for details). From Table 2.6 we can see that there are 12 viable $SU(5)$ models on this manifold, with line bundle entries in the range $-4 \leq k_a^r \leq 4$.

Let us consider the first of these models from the table in Appendix C.3 which is specified by a line bundle sum V of the five line bundles

$$L_1 = \mathcal{O}_X(-4,0,1,1), \quad L_2 = \mathcal{O}_X(1,3,-1,-1), \quad L_3 = L_4 = L_5 = \mathcal{O}_X(1,-1,0,0)\ . \tag{2.25}$$

Evidently, $c_1(V) = 0$ and, since three of the line bundles are the same, only two slope-zero conditions (2.14) have to be satisfied in the four-dimensional Kähler cone. With the intersection numbers and Kähler cone given in Appendix C.2, we find that this can indeed be achieved. Further, $c_2(TX) = (12,12,12,4)$ and, from Eq. (2.11), $c_2(V) = (3,5,9,-7)$ so that $c_2(TX) - c_2(V) = (9,7,3,11)$ which represents a class in the Mori cone. Hence, the model can be completed to an anomaly-free model. By construction we have, of course, $\mathrm{ind}(V) = \mathrm{ind}(\wedge^2 V) = -3$ but, in general, the distribution of this chiral asymmetry over the various line bundle sector depends on the model. For our example, the only non-zero line bundle cohomologies are $\mathrm{ind}(L_1) = -3$ and $\mathrm{ind}(L_2 \otimes L_3) = \mathrm{ind}(L_2 \otimes L_4) = \mathrm{ind}(L_2 \otimes L_5) = -1$ which implies a chiral spectrum

$$\mathbf{10}_1,\ \mathbf{10}_1,\ \mathbf{10}_1,\ \overline{\mathbf{5}}_{2,3},\ \overline{\mathbf{5}}_{2,4},\ \overline{\mathbf{5}}_{2,5}\ . \tag{2.26}$$

Hence, the all three chiral $\mathbf{10}$ multiplets are charged under the first $U(1)$ symmetry and uncharged under the others. Although, at this stage, we do not know the charge of the Higgs multiplet $\mathbf{5}^{\bar{H}}$ it is clear that all up Yukawa couplings $\mathbf{5}^{\bar{H}}\mathbf{10}\,\mathbf{10}$ are forbidden (perturbatively and at the Abelian locus). Indeed, for those terms to be $S(U(1)^5)$ invariant we require a Higgs multiplet with charge -2 under the first $U(1)$ and uncharged otherwise, a charge pattern which is not available at the Abelian locus.

We also note from Eq. (2.25) that the matrix (k_a^r) of line bundle entries has rank two. This means that two of the four $U(1)$ symmetries are Green-Schwarz anomalous with corresponding super heavy gauge bosons while the other two are non-anomalous with massless gauge bosons. Those latter two $U(1)$ symmetries can be spontaneously broken, and their gauge bosons removed from the low-energy spectrum, by moving away from the line bundle locus (see Ref. [23] for details).

2.5 Conclusion and outlook

In this chapter, we have studied heterotic model building on the sixteen families of torically generated Calabi-Yau three-folds with non-trivial first fundamental group [30]. From those 16 manifolds, we have selected the 14 favourable three-folds and we have classified phenomenologically attractive $SU(5)$ and $SO(10)$ line bundle GUT models thereon. Concretely, we have searched for $SU(5)$ and $SO(10)$ GUT models which are supersymmetric, anomaly free and have the correct values of the chiral asymmetries to produce a three-family standard model spectrum

(after subsequent inclusion of a Wilson line). For $SU(5)$ we have succeeded in finding all such line bundle models on the 14 base spaces, thereby proving finiteness of the class computationally. The result is a total of 122 $SU(5)$ GUT models.

For $SO(10)$ we have obtained a complete classification for all spaces up to Picard number three, resulting in a total of 55 $SO(10)$ GUT models. For the other six manifolds, all with Picard number four, only one (X_9) was amenable to a complete classification. For the other five manifolds, although the number of models were converging with increasing line bundle entries, they had not quite saturated even at fairly high values of about $k_{\max} = 20$. We expect that we have found the vast majority of models on these manifolds with a small fraction containing some large line bundle entries still missing. Altogether we find 28870 viable $SO(10)$ models. All models, both for $SU(5)$ and $SO(10)$, can be download from the website [73].

The main technical obstacle to determine the full spectrum of these models – before and after Wilson line breaking – is the computation of line bundle cohomology on torically defined Calabi-Yau manifolds. We hope to address this problem in the future.

We consider the present work as the first step in a programme of classifying all line bundle standard models on the Calabi-Yau manifolds in the Kreuzer-Skarke list. A number of technical challenges have to be overcome in order to complete this programme, including a classification of freely-acting symmetries for these Calabi-Yau manifolds and the aforementioned computation of line bundle cohomology.

Chapter 3

Discrete Symmetries of toric Calabi-Yau manifolds

3.1 Introduction

Discrete symmetries of Calabi-Yau (CY) manifolds are important for a number of reasons. Freely-acting symmetries can be used to form quotient CY manifolds, leading to new CY manifolds with smaller Hodge numbers. Such quotient CY manifolds have been used to fill out the previous fairly sparse tip of the Hodge number plot [26] and, due to their relatively small moduli spaces, they are useful for string compactifications. Further, most standard constructions lead to CY manifolds with a trivial first fundamental group. And the freely-acting symmetries of these manifolds are built from CYs with non-trivial first fundamental groups. Moreover, the presence of a non-trivial first fundamental group is required for a string compactification whenever gauge field Wilson lines need to be included. In particular, for CY compactifications of the heterotic string the inclusion of Wilson lines [74–76] appears to be the only viable way to arrive at phenomenologically promising models. It is for such compactifications, therefore, especially important to know about freely-acting discrete symmetries and this is, in fact, one of the current "bottlenecks" in the attempt to systematically construct heterotic CY vacua.

The oldest and conceptually simplest set of CY three-folds is the complete intersection of projective spaces (CICYs), some 7890 manifolds classified in [34]. Over the years, considerable progress has been made in finding freely-acting symmetries of CICYs, culminating in [69] which provides a classification of such symmetries which descend from linear actions on the ambient spaces for the entire CICY dataset. It was found that only 195 of the 7890 manifolds have freely-acting symmetries of this kind, although many of these 195 manifolds allow for multiple symmetries. These results have been used to construct new CY quotients with small Hodge

numbers and to systematically search for physically viable heterotic models on CICYs.

Much less is known about discrete symmetries for the largest known set of CY three-folds, defined as hypersurfaces in four-dimensional toric varieties (TCY), as classified by Kreuzer and Skarke in [6]. The main purpose of this chapter is to take a first step towards a classification of discrete symmetries for these CY three-folds. The Kreuzer-Skarke list consists of about half a billion reflexive polytopes leading to an even larger number of associated CY manifolds obtained by triangulation. In [77], this process of triangulation has been carried out for all cases with Picard number $h^{1,1}(X) \leq 7$ and we will be relying on this dataset.

What is currently known about symmetries of TCY manifolds? Batyrev and Kreuzer [30] have classified all cases with freely-acting symmetries such that the quotient can again be described as a hypersurface in a toric variety. Surprisingly, among the half a billion reflexive polytopes, there are only 16 freely-acting symmetries of this kind, associated to 16 of these reflexive polytopes. However, in general, the quotient manifold associated to a freely-acting symmetry of a TCY manifold does not have to be a TCY manifold itself and there is no expectation that these 16 cases provide a complete list of freely-acting symmetries. In fact, this is already clear from the overlap between the two sets of CICY and TCY three-folds. It is well-known that the quintic in $\mathbb{P}^4$, which appears in both data sets, has a freely-acting $\mathbb{Z}_5 \times \mathbb{Z}_5$ symmetry. The quintic is also among the 16 cases identified by Batyrev and Kreuzer, who identify a freely-acting $\mathbb{Z}_5$ symmetry. In other words, only a single $\mathbb{Z}_5$ symmetry is "toric" and appears in the classification of Batyrev and Kreuzer, while the full $\mathbb{Z}_5 \times \mathbb{Z}_5$ symmetry is not toric and is, hence, not seen in this way. Further examples of this kind are provided by the bi-cubic in $\mathbb{P}^2 \times \mathbb{P}^2$ (with a toric $\mathbb{Z}_3$ symmetry among the 16 cases and a non-toric $\mathbb{Z}_3 \times \mathbb{Z}_3$ symmetry group) and the tetra-quadric in $\mathbb{P}^1 \times \mathbb{P}^1 \times \mathbb{P}^1 \times \mathbb{P}^1$ (with a toric $\mathbb{Z}_2$ symmetry among the 16 and various larger, non-toric symmetry groups). These examples certainly show that the 16 spaces identified by Batyrev and Kreuzer can have larger symmetry groups than the toric ones identified in their paper. It is also likely that there are more TCY manifolds with freely-acting (but non-toric) symmetries. As for non-freely acting symmetries, we are not aware of examples for TCY manifolds which are not CICY manifolds at the same time.

Our first step will be to set up an algorithm for classifying symmetries, Γ, of CY three-folds X which are hyper-surfaces $X \subset A$ in a four-dimensional toric ambient space A, defined as the zero set of a polynomial p. More precisely, we will focus on groups Γ which can be embedded into the symmetry group G_A of A. We proceed in the following steps:

- Find the ambient space symmetry group G_A from the toric data for A.

- For a given finite group Γ, study all injective group monomorphisms $\Gamma \to G_A$.
- For each such group monomorphism, find the most general invariant polynomial p.
- Check if the hyper-surface defined by such p is generically smooth.
- If freely-acting symmetries are desired, check if the symmetry action is fixed point free.

For constructing the freely-acting symmetries, the Euler number, $\eta(X)$ of the CY manifolds needs to be divisible by the group order $|\Gamma|$. A given TCY manifolds X (with $\eta(X) \neq 0$), therefore, has a finite list of candidate symmetry groups Γ, each of which can be analysed as described above. In this way, a complete list of freely-acting symmetry groups (embedded into G_A) can be found for each TCY manifold.

For non freely-acting groups there is no a priori constraint on the group order. The only information we can use is that the group order must divide the several geometrical invariants of the CY, hence at least we have an upper bound on the finite groups. Then we apply the above algorithm (dropping the last step of checking fixed points) for the finite number of groups at any given group order, starting with group order two and successively increasing up to a desired maximum. In this way, we can find all symmetries (embedded into G_A), freely-acting or not, until we enumerated all groups within the upper bound. In practice, since symmetry groups of CY manifolds tend to be small, this can amount to a complete classification provided the group order can be pushed sufficiently high.

In the present chapter, we undertake first steps towards a classification of symmetries based on the above algorithm by applying it to all TCY manifolds with $h^{1,1}(X) \leq 3$, some 350 manifolds. In this way, we find all freely-acting discrete symmetries (which can be embedded into G_A) of these manifolds. We reproduce all symmetries among these manifolds known from the Batyrev-Kreuzer classification, as well as those known from the overlap with CICY manifolds. We also find one new, non-toric symmetry group, $\mathbb{Z}_2 \times \mathbb{Z}_2$, on one of the 16 manifolds, where one of the $\mathbb{Z}_2$ sub-groups is the toric symmetry identified by Batyrev-Kreuzer. For the resulting five TCY manifolds with $h^{1,1}(X) \leq 3$ and with freely-acting symmetries we also search for additional, non freely-acting symmetries. Our result for discrete symmetries is summarised in Section 3.5.

We also use our algorithm to construct a freely-acting $\mathbb{Z}_2$ for a TCY with $h^{1,1}(X) = 6$. This particular TCY is not among the 16 cases identified by Batyrev and Kreuzer, which shows that there are indeed more manifolds with freely-acting symmetries.

The outline of the Chapter is as follows. In the next section, we describe the mathematical background for our algorithm in some detail but at a relatively informal level. Technical details and proofs can be found in the Appendix A. Section 3.3 sets out the classification algorithm which is applied to two specific examples in Section 3.4. Our results from the systematic search of all TCY for $h^{1,1}(X) \leq 3$ are given in Table 3.1.

3.2 Construction of discrete symmetries

First we review the detailed construction of toric Calabi-Yau in subsection 3.2.1, where the Calabi-Yau hyper-surface is defined as a co-dimension one sub-variety of a toric four-fold. Then the discrete symmetries are identified as symmetry actions which keep the downstairs CY a smooth and non-simply connected manifold. However, before we generate the symmetry actions, we must decide which finite groups are promising for constructing their representations. There is no specific result on the general requirements of a discrete symmetry, we hence need to at least find an upper bound on the group order, and only check the smaller order groups. To solve this problem, we refer to the original papers on vacuum of superstrings [5, 78, 79], which states that the order of discrete symmetry group must divide the Euler characteristics and Hirzebruch signatures of the twisted bundle (the product of tangent bundle and normal bundle $TM^l \otimes NM^k$). The computation of these geometrical indices was well developed and in fact we only need to require that the order of discrete symmetry group divides the greatest common divisor (GCD) of the signatures up to a certain order. Therefore, the computation of GCD of the twisted bundles is the first calculation which helps us to generate a list of finite groups for further check.

Further, a discrete symmetry of CY is also a symmetry of the toric ambient space, because the CY is defined by any linear combination of a set of homogeneous monomials on the toric ambient space. Therefore we could firstly figure out the symmetry group of toric ambient space, which covers the discrete symmetries of CY hyper-surfaces as subgroups. Then the toric symmetry group are used to generate a large amount of projective representations, which we further check to be discrete symmetries or not.

Along the way of establishing the structure of discrete symmetries, we brought in many new definitions and theorems, which turned out to be rigorous yet tedious, therefore we write the whole theory in appendix A. Here we only summarise the most crucial steps of the algorithm. It turns out that the algorithms could be split into three steps: The computation of symmetry

group of toric variety; the construction of symmetry actions; the calculation of fixed point set and smoothness of the symmetry action.

3.2.1 Convention

The Calabi-Yau manifold is defined as a hyper-surface in a toric four-fold as ambient space, in another word the toric variety constructed from reflexive polytopes. We start out with a pair of reflexive polytopes denoted by Δ°, Δ. The polytope Δ gives the monomials defining a Calabi-Yau hypersurface X and is in the M lattice, whereas Δ° sits in the N-lattice which also contains the fan of our ambient space. We denote k-dimensional faces of Δ by $\Theta^{[k]}$ and k-dimensional faces of Δ° by $\Theta^{\circ[k]}$. The pairing between vectors in $N \otimes \mathbb{R}$ and $M \otimes \mathbb{R}$ is written as $\langle n, m \rangle$. We now have n d-dimensional vectors v_i in the N lattice space defining the generators of the normal fan $\Sigma \subset N$, namely $\Sigma^{(1)} = \{\mathbf{v}_1, \ldots, \mathbf{v}_n\}$. Choosing the 'global definition' of a toric variety which best suits our purpose, we assign coordinates $\mathbf{x} = (x_1, \ldots, x_n) \in \mathbb{C}^n$ to the generators $\mathbf{v}_i$.

The associated toric variety $\mathbb{P}_\Sigma$ and the Calabi-Yau hypersurface X will be singular for most reflexive polytopes, and we need to find a (crepant) resolution. In the case of Calabi-Yau threefolds, such a resolution can always be found by refining the fan $\Sigma' \to \Sigma$, where Σ' is a fan over the simplices (on the boundary of Δ°) of a maximal fine regular star triangulation of Δ° (the corresponding resolution on X is called MPCP in [31]). In the following discussion, we will refer to maximal fine regular star triangulations simply as triangulations. We denote a triangulation of a polytope Δ in terms of its cones of maximal dimension by $tr(\Delta)$. In such a triangulation, we can discard everything happening inside of faces of co-dimension one of Δ°, as the corresponding strata will not meet X. This is precisely the approach taken in [77], where we read out polygons for the toric ambient space.

To actually define the toric variety, we need to gather the information of the triangulation to define an "invariant set" called zero sets of $(\mathbb{C}^*)^n$ space. $Z(I)$ is a zero set formed by generators which do not form a cone:

$$Z(I) = \{\mathbf{x} \in \mathbb{C}^n \,|\, x_i = 0 \;\; \forall\, i \in I\} \subset \mathbb{C}^n \tag{3.1}$$

where I is the index set $I = \{i_1, \ldots, i_p\} \subset \{1, \ldots, n\}$.

Another important recipe of the weighted projective space is the charge matrix, which also characterises the toric action $\mathcal{G} \subset (\mathbb{C}^*)^n$. If $\mathcal{G}$ is the set of all $\mathbf{t} = (t_1, \ldots, t_n) \in (\mathbb{C}^*)^n$ satisfying

$$\prod_{i=1}^{n} t_i^{v_{ir}} = 1 \quad \text{for all} \quad r = 1, \ldots, d \,,$$

we can then write out the linear relations of the vertices

$$\sum_{i=1}^{n} q_i^r \mathbf{v}_i = 0 \,,$$

where $(q^r{}_i)$ form the Charge matrix Q. Hence, the continuous part, $\mathcal{G}_{\text{cont}}$ of $\mathcal{G}$ is given by

$$\mathcal{G}_{\text{cont}} = \{\text{diag}(\mathbf{s}^{\mathbf{q}_i}) \,|\, \mathbf{s} \in (\mathbb{C}^*)^{n-d}\} \cong (\mathbb{C}^*)^{n-d} \,. \tag{3.2}$$

Given the zero sets and toric action, we can express the toric variety as the quotient of an upstairs space by the toric action.

$$A := \frac{B}{\mathcal{G}} := \frac{\mathbb{C}^n - Z(\Sigma)}{\mathcal{G}} \tag{3.3}$$

The monomials that defines the CY is then associated with lattice point in the dual lattice polytope defined as:

$$\triangle^\circ := \{m \in M | \langle m, v\rangle \geqslant -1, \forall v \in \triangle\} \tag{3.4}$$

The monomials are then in one to one correspondence with the points in m as:

$$CY(m) = \prod_{i=1,..,d} x_i^{\langle m, v_i\rangle + 1} \tag{3.5}$$

To explain the Batyrev construction described above, let us have a look at the $\mathbb{CP}^2$ space. Following our convention, the three vertices $\Sigma^{(1)} = \{(0,1), (1,0), (-1,-1)\}$ form the reflexive polytope, for which the dual polygon contains three vertices $(2,-1), (-1,2), (-1,-1)$ and all the points within. The only linear relation between the vertices gives us the Charge matrix as $(1,1,1)$, which then translate into the torus action as $(x,y,z) \sim \lambda\ (x,y,z), \lambda \in \mathbb{C}^*$. Since there are 10 points in the dual polygon, we then have 10 monomials forming the CY family, containing abc, ab^2, a^2b and a^3, where $a, b, c \in \{x, y, z\}$.

Example 1. We now have a look at an example toric space of $h^{1,1} = 2$. The normal fan is composed of 6 vertices as

$$\mathbf{v}_1 = (-1,0,0,1), \mathbf{v}_2 = (-1,0,2,0), \mathbf{v}_3 = (-1,0,3,-1), \mathbf{v}_4 = (-1,2,0,0),$$
$$\mathbf{v}_5 = (-1,3,0,0), \mathbf{v}_6 = (1,-1,-1,0)$$

The Charge matrix, encoding the linear relations between the vectors, is summarising the weighted projective structure:

$$(q_r{}^i) = \begin{pmatrix} 0 & 1 & 0 & 1 & 0 & 2 \\ 1 & 0 & 1 & 0 & 1 & 3 \end{pmatrix}$$

We hence have the continuous part as $\mathcal{G}_{cont} = \{s_2, s_1, s_2, s_1, s_2, s_1^2 s_2^3\} \cong \mathbb{C}^{*2}$. One triangulation of the polytope is:

$$tr(\Delta) = \{conv[\{v_1, v_2, v_3, v_4\}], conv[\{v_1, v_2, v_3, v_6\}], conv[\{v_1, v_2, v_4, v_5\}], conv[\{v_1, v_2, v_5, v_6\}],$$
$$conv[\{v_1, v_3, v_4, v_6\}], conv[\{v_1, v_4, v_5, v_6\}], conv[\{v_2, v_3, v_4, v_5\}], conv[\{v_2, v_3, v_5, v_6\}], conv[\{v_3, v_4, v_5, v_6\}]\},$$

where *conv* means the convex cone formed by the four vertices. Then by counting the incidence information from triangulation data, we have the zero sets $Z(I) = \{x_1 = x_3 = x_5 = 0\} \cup \{x_2 = x_4 = x_6 = 0\}$.

Example 2. Another $h^{1,1} = 2$ example. The six vertices are:

$$\mathbf{v}_1 = (-1, 0, 0, 0), \mathbf{v}_2 = (-1, 0, 0, 1), \mathbf{v}_3 = (-1, 0, 1, 0), \mathbf{v}_4 = (-1, 0, 1, 1),$$
$$\mathbf{v}_5 = (-1, 1, 0, 0), \mathbf{v}_6 = (3, -1, -1, -1)$$

we have the Charge matrix

$$(q_r{}^i) = \begin{pmatrix} 0 & 1 & 1 & 0 & 1 & 1 \\ 1 & 0 & 0 & 1 & 1 & 1 \end{pmatrix}$$

giving us the fibered $\mathbb{P}^1 \times \mathbb{P}^1$ space. The continuous part of toric action is $\mathcal{G}_{cont} = \{s_2, s_1, s_1, s_2, s_1 s_2, s_1 s_2\}$. We then triangulate the polygon as

$$tr(\Delta) = \{conv[\{v_1, v_2, v_4, v_5\}], conv[\{v_1, v_2, v_4, v_6\}], conv[\{v_1, v_2, v_5, v_6\}], conv[\{v_1, v_3, v_4, v_5\}],$$
$$conv[\{v_1, v_3, v_4, v_6\}], conv[\{v_1, v_3, v_5, v_6\}], conv[\{v_2, v_4, v_5, v_6\}], conv[\{v_3, v_4, v_5, v_6\}]\}$$

which gives us the zero set as $Z(I) = \{x_2 = x_3 = 0\} \cup \{x_1 = x_4 = x_5 = x_6 = 0\}$.

3.2.2 Symmetry group of the toric ambient space

Recall that the toric fourfold as the ambient space is defined as $A = B/\mathcal{G} = \{\mathbb{C}^n - Z(\Sigma)\}/\mathcal{G}$. Our algorithm, intuitively, is sequentially considering the symmetries of zero set Z, the upstairs space B, then finally the toric action $\mathcal{G}$. Naturally one would think that the symmetry group of A must combine these three objects, and indeed it is.

Let us first think of the symmetry structure of the zero set Z. We denote the collection of all such index sets and corresponding zero sets by

$$\mathcal{I} = \{I \subset \{1, \ldots, n\} \,|\, \{\mathbf{v}_i \,|\, i \in I\} \text{ do not form a cone}\}\,, \quad \mathcal{Z} = \{Z(I) \,|\, I \in \mathcal{I}\} \tag{3.6}$$

Our zero set of toric variety is then

$$Z = \bigcup_{I \in \mathcal{I}} Z(I) \tag{3.7}$$

To avoid redundancies, we drop all zero sets $Z(I)$ from $\mathcal{Z}$ which are already contained in larger zero sets and, correspondingly, all index sets I which contain smaller index sets are dropped from $\mathcal{I}$.

Now we claim that, the symmetry group of the zero set P, could be characterised as R/S, where R is the permutation group which mapped any $I \in \mathcal{I}$ to any index set within $\mathcal{I}$, S the permutation group mapped each $I \in \mathcal{I}$ to itself. In another word we define $S = \{\sigma \in S_n \,|\, \sigma(I) = I,\ \forall\, I \in \mathcal{I}\} \subset S_n$, and $R = \{\sigma \in S_n \,|\, \sigma(I) \in \mathcal{I},\ \forall I \in \mathcal{I}\}$. In fact the following sequence splits: $1 \to S \xrightarrow{\imath} R \xrightarrow{[\cdot]} P \to 1$, where $\imath$ is the inclusion map and $[\cdot]$ denotes taking the equivalence class. Hence the equivalent classes in R define the symmetry group P. For detailed proof of P as order-preserving permutations, see A.1.1 and A.1.2..

Example 1. By counting the incidence information, we know that $\mathcal{I} = \{\{1, 3, 5\}, \{2, 4, 6\}\}$. From the definition of S, we know that it contains all the permutations which send the index set $\{1, 3, 5\}$ to either itself or $\{2, 4, 6\}$, and vice versa. Meanwhile $R = S_3 \times S_3$, with two S_3 for both index sets $\{1, 3, 5\}$ and $\{2, 4, 6\}$. Therefore $P = S_2$ which exchanges the two index sets.

Example 2. For this example, both S and R are only containing permutations within $\{2, 3\}$ and $\{1, 4, 5, 6\}$, resulting in P being the identity group.

We now define index sets $\mathcal{J}$ and $\mathcal{K}$, which covers all the information we need to compute the symmetry group of toric ambient space: The index set $\mathcal{J}$ is defined as the overlaps of all the $I \in \mathcal{I}$, namely $\mathcal{J} = \{1, \ldots, n\}/\sim$, where $\sim$ means i, j are in the same I. We also need to group the homogeneous coordinates of $\mathcal{G}$, such that we have the index sets $\mathcal{K}$ to collect the same columns in the Charge matrix. Therefore the toric action $\mathcal{G}$ could be written as $\mathcal{G} = \bigotimes_{K \in \mathcal{K}} \mathcal{G}_{\mathbf{q}_K}(K)$. Given the symmetry group of Z, we state that the symmetry group of G_B is $G_B \cong P_B \ltimes H_B$, where H_B is the continuous part that mapped each zero set to itself, defined as $H_B = \{g \in G_B \,|\, g(Z(I)) = Z(I),\ \forall I \in \mathcal{I}\} \subset G_B$. By further discussion, one realised that

$C_{\mathrm{Gl}(n,\mathbb{C})}(\mathcal{G}) = \bigotimes_{K\in\mathcal{K}} \mathrm{Gl}(K,\mathbb{C})$. Then P_B is defined as R_B/S_B, with R_B, S_B, P_B defined as the isomorphic images of R, S, P into $\mathrm{GL}(n,\mathbb{C})$.

Example 1. By combining the incidence information of all the triangulation cones, we realise $\mathcal{J} = \mathcal{K} = \{\{6\},\{2,4\},\{1,3,5\}\}$. Then $H_B = \mathrm{GL}(\{1,3,5\},\mathbb{C}) \times \mathrm{GL}(\{2,4,6\},\mathbb{C}) \cong \mathrm{GL}(3,\mathbb{C})^2$, and $P_B \cong S_2$ as the image of P in $\mathrm{GL}(n,\mathbb{C})$.

Example 2. We have $\mathcal{J} = \mathcal{K} = \{\{1,4\},\{2,3\},\{5,6\}\}$, and $H_B = \mathrm{GL}(\{2,3\},\mathbb{C})\times\mathrm{GL}(\{1,4,5,6\},\mathbb{C})$. P_B for this example is trivial.

The next calculation reflects how does the quotient of B by $\mathcal{G}$ constrain the symmetry group of toric space. From general group theory, we need to compute the normaliser of the toric group $\mathcal{G}$ within the symmetry group G_B. However, it is not straight forward to compute them directly in G_B, we then firstly try to calculate the normaliser of $\mathcal{G}$ in $GL(n,\mathbb{C})$, then intersect G_B. For the former step, we define the other two permutation groups as $\mathcal{R} = S_n \cap N_{\mathrm{Gl}(n,\mathbb{C})}(\mathcal{G})$, $\mathcal{S} = S_n \cap C_{\mathrm{Gl}(n,\mathbb{C})}(\mathcal{G})$, to have $\mathcal{R} = \mathcal{P} \ltimes \mathcal{S}$, where $N_{\mathrm{Gl}(n,\mathbb{C})}(\mathcal{G})$ is the normaliser of $\mathcal{G}$ in $\mathrm{Gl}(n,\mathbb{C})$ and $C_{\mathrm{Gl}(n,\mathbb{C})}(\mathcal{G})$ the commutant. Then in order to intersect G_B, we compute

$$R_A = R \cap \mathcal{R}\ , \quad S_A = S \cap \mathcal{S}\ , \quad P_A = R_A/S_A\ , \quad R_A = P_A \ltimes S_A\ .$$

Finally it turns out that the symmetry group of G_A could be expressed as:

$$G_A = P_A \ltimes (H_A/\mathcal{G})\ . \tag{3.8}$$

where $H_A = H_B \cap C_{\mathrm{Gl}(n,\mathbb{C})}(\mathcal{G}) = \bigotimes_{J\in\mathcal{J}} \mathrm{Gl}(J,\mathbb{C})$.

Above is the method of computing G_A. Following the two examples in former section, we have:

Example 1. $\mathcal{I} = \{\{1,3,5\},\{2,4,6\}\}$, $\mathcal{J} = \mathcal{K} = \{\{6\},\{2,4\},\{1,3,5\}\}$.
Therefore $H_A = GL(\{6\},\mathbb{C}) \times GL(\{2,4\},\mathbb{C}) \times GL(\{1,3,5\},\mathbb{C})/\mathcal{G}$.

Example 2. $\mathcal{I} = \{\{2,3\},\{1,4,5,6\}\}$, $\mathcal{J} = \mathcal{K} = \{\{1,4\},\{2,3\},\{5,6\}\}$.
Therefore $H_A = GL(\{1,4\},\mathbb{C}) \times GL(\{2,3\},\mathbb{C}) \times GL(\{5,6\},\mathbb{C})/\mathcal{G}$.
One can refer to the section 3.4 for more detailed discussions.

3.2.3 Construction of representations of symmetry action

We now think about the embedding of the symmetry action Γ into the toric symmetry group G_A as a group homomorphism. We can write $R(\gamma) = (\pi(\gamma), r(\gamma))$, where $\pi : \Gamma \to P_A$ and $r : \Gamma \to H_A/\mathcal{G}$. What are the properties of π and r, given that R is a homomorphism? From the multiplication rule $(p, h)(\tilde{p}, \tilde{h}) = (p\tilde{p}, \tilde{p}^1 h \tilde{p} \tilde{h})$ in G_A it follows that

$$\pi(\gamma\tilde{\gamma}) = \pi(\gamma)\pi(\tilde{\gamma}) \tag{3.9}$$

$$r(\gamma\tilde{\gamma}) = \pi(\tilde{\gamma})^{-1} r(\gamma)\pi(\tilde{\gamma}) r(\tilde{\gamma}) \,, \tag{3.10}$$

so that $\pi : \Gamma \to P_A$ is a homomorphism and $r : \Gamma \to H_A/\mathcal{G}$ is a π-homomorphism. Therefore our task would be to firstly generate the permutation representations of the finite symmetry group, then the corresponding twisted projective representations.

The permutation part $\pi : \Gamma_A \to P_A \subset S(\mathcal{K})$ can be viewed as purely permutations and could be decomposed into its transitive constituents π_i, each of which is a transitive permutation representation on a subset $\mathcal{K}_i \subset \mathcal{K}$. This is equivalent to some representation of P_A by right multiplication on the cosets of $P_A/\mathcal{H}_i$ for some sub-group $\mathcal{H}_i$. More precisely, choosing some $x \in \mathcal{K}_i$, the group $\mathcal{H}_i$ is the stabiliser of x and the permutation representations on $P_A/\mathcal{H}_i$ and $\mathcal{K}_i$ are equivalent via $\mathcal{H}_i\gamma \to \gamma x$. So, in essence, constructing the permutation representations of Γ_A amounts to understanding its sub-group structure. Hence for a certain finite group $G := \langle g_1, ..., g_n \rangle$, we only need to permute all its subgroups, the concrete representation for each g_i would just be the index change of $g_i \to g_i H_j$, where H_j are chosen from all the subgroups.

A more difficult task is to compute the projective π-twisted representations for a toric variety as weighted projective spaces. Let's firstly recall the method in the ordinary projective space. Assume that we have found a, not necessarily injective, group homomorphism $\pi : G \to P_A$. If the ambient space is a product of several projective spaces, we then know that $\pi(\gamma)$ acts transitively on a number of 'blocks' B_i with the same size and leaves everything else unchanged. Also the restriction of $r(\gamma)$ for $\gamma \in G_i$ to B_i defines a representation of G_i. We now claim that it is enough to fix a single r_1 to recover the whole π-representation.

Let us hence consider G_1, the stabiliser of the first block, and fix the representation $r_1 : G_1 \mapsto \mathrm{GL}(B_1, \mathbb{C})$. To reconstruct the whole action of G we pick a set of group elements γ_i such that $\pi(\gamma_i)(1) = i$. We can make the choice $\gamma_1 = 1$ in G. We can then write any group element as

$$\gamma = \gamma_{\pi(\gamma)(i)} h \gamma_i^{-1} \,, \tag{3.11}$$

with h in G_1, for any i. We can hence think of h to depend on γ and i. To see this, note that h is given by

$$h = \gamma^{-1}_{\pi(\gamma)(i)}\gamma\gamma_i\,. \tag{3.12}$$

This is in G_1 as

$$\begin{aligned}\pi(h)(1) &= \pi(\gamma_{\pi(\gamma)(i)})^{-1}\pi(\gamma)\pi(\gamma_i)(1)\\ &= \pi(\gamma_{\pi(\gamma)(i)})^{-1}\pi(\gamma)(i)\\ &= 1\end{aligned} \tag{3.13}$$

We may hence write

$$R(\gamma) = R(\gamma_{\pi(\gamma)(i)})R(h)R(\gamma_i^{-1}) \tag{3.14}$$

for any i and γ using an appropriate h. Going through the definitions this means that we can write

$$r_i(\gamma) = r_1(h) \tag{3.15}$$

This allows us to recover all of the matrices $r_i(\gamma)$ and hence the entire π-twisted representation. As we may construct h for any γ and i, the above relation holds for any π-twisted representation and we only need to find all group homomorphisms $\pi : G \to P_A$ and all linear representations of $r_i : G_1 \to GL(K, \mathbb{C})$ to construct all π-twisted representations.

However, it is not always true that the general $\pi : G \to P_A$ acts transitively on the blocks and there may be several orbits. In this case, we can repeat the above construction separately for each orbit O_k and then combine all of the data to find a linear representation $R : G \to P_A \ltimes H_A$. Here, the representation matrix (3.11) becomes block diagonal with each block acting on the elements $\{B_k\}$ forming the k-th orbit O_k. Note that neither all of the representations π nor all of the representations $r_1^k : G_1^k \to GL(B_k, \mathbb{C})$ need to be faithful to find a faithful representation R.

In short, given an action of $\pi : G \to P_A$ and in aim of finding all π-twisted representations $r(\gamma)$, we hence need to

- Find all representations $\pi : G \to P_A$, not necessarily faithful.
- Find all orbits of the blocks under this action.
- For each orbit, pick out a block and call it B_1. This defines the group G_1.
- Choose the group elements g_i.
- Study all linear representations r_1 (not necessarily faithful) of G_1 on $GL(B_1, \mathbb{C})$.

- For each such linear representation r_1, we may find the corresponding h for each i and γ using (3.12). Using this h, we can determine all $r_i(\gamma)$ using (3.15). This completely fixes the representation R regarding the orbit under consideration.

- By choosing a linear representation for each orbit, we completely fix the representation R.

As for the weighted projective space, we claim that the similar method works. See the detailed discussions in the appendix A.

3.2.4 Smoothness and fixed points

By definition, we want to check whether the matrix representations generated act freely on the upstairs CY hyper-surface. The smoothness means that, by gathering the invariant monomials after the symmetry action, the downstairs family is still forming a smooth hyper-surface. Meanwhile the freely symmetry action must have an empty fixed point set.

For checking the smoothness, a slightly different situation is that we now have toric ambient space as patches of cones. Recall that for a hyper-surface defined on a single projective space by polynomial P, we only need to compute its Jacobi ideal as $I_s^\sigma = \{P^\sigma = \frac{\partial P^\sigma}{\partial x_1^\sigma} = \cdots = \frac{\partial P^\sigma}{\partial x_4^\sigma} = 0\}$. In the toric case, we need to check for each patch whether there is a singular point.

Intuitively we assign the singular points into two different types, with the first type preserving the singular point of the cone itself, the other coming from the polynomial defining the hyper-surface. More specifically, the first type for each cone $\sigma \in \Sigma$ is just the point where all the coordinate x_i corresponding to v_i vanish. And for this type we only need to compute the determinant of the vertices forming the cone. The smooth cone must have determinant as ± 1, otherwise we could just stop the algorithm.

For the second type, where the cone σ itself is smooth, the singular points must be checked via defining polynomial of the CY. The issue now is that we need to project the CY defined via the global coordinates into a certain cone. After some discussion, we know that the singularities arise through fixed points of the group action of G on $\mathbb{C}^4$ would turn it into $V(\sigma) = \mathbb{C}^4/G$. And we can lift $X \subset V(\sigma)$ to a (different) hypersurface $\tilde{X}$ in $\mathbb{C}^4$ which descends to X via a free group action of G. Smoothness of the covering space is then equivalent to smoothness of the quotient. After re-writing the coordinates into the cone, we realise that the same method for a general projective space still works. Therefore our method for checking the smoothness could be summarised as follows:

- Determine the most general invariant family of hypersurface equations (polynomials P) We denote a generic member of this family by X.

- Loop over all four-dimensional cones σ of Σ' (this is the fan given to us by [77]). Let us denote the four[1] generators of the rays of σ by $v_i^\sigma, i = 1, ..., 4$.

  - find out if the cone is smooth (the determinant of the matrix formed by the v_i is ± 1). If this is not the case, there is a singularity located at the point of $\mathbb{P}_{\Sigma'}$ where all of the coordinates x_i^σ associated to the v_i^σ vanish. Check if this point meets X, i.e. if $x_i^\sigma = 0, \forall i = 1..4$ automatically solves $P = 0$. If that is the case $\rightarrow$ BREAK and dump $r(G)$
  - define P^σ by setting to unity all coordinates whose corresponding rays are not contained in σ. Then check if the ideal

    $$I_s^\sigma = \{P^\sigma = \frac{\partial P^\sigma}{\partial x_1^\sigma} = \cdots = \frac{\partial P^\sigma}{\partial x_4^\sigma} = 0\} \tag{3.16}$$

    is empty ('method 1'). If not $\rightarrow$ BREAK and dump $r(G)$

- If all of the I_s^σ are empty, we have a smooth manifold symmetric under the action $r(G)$

We then move on to the method of calculating the fixed point set. Denote by $\Pi : \hat{\Gamma} \rightarrow \Gamma$ the group projection, by $\nu : \hat{G}_A \rightarrow G_A$ the projection for the ambient space symmetry groups and by $q : \hat{A} \rightarrow A$ the ambient space projection. Evidently, if $\Pi(\hat{\gamma}) = \gamma$ and $R(\gamma) = \nu \circ \hat{R}(\hat{\gamma})$ then

$$q \circ \hat{R}(\hat{\gamma}) = R(\gamma) \circ q \ . \tag{3.17}$$

For a $\gamma \in \Gamma$ define the associated downstairs fixed point set by

$$F_\gamma = \{a \in A \mid R(\gamma)a = a\} \ , \tag{3.18}$$

and its upstairs counterpart by

$$\hat{F}_{\hat{\gamma}} = \{\hat{a} \in \hat{A} \mid \hat{R}(\hat{\gamma})(\hat{a}) \in \hat{a}\mathcal{G}\} \ . \tag{3.19}$$

Then Eq. (3.17) implies that

$$q(\hat{F}_{\hat{\gamma}}) = F_{\Pi(\hat{\gamma})} \ . \tag{3.20}$$

We can also define the Calabi-Yau manifolds $X \subset A$ and its upstairs counterpart $\hat{X} \subset \hat{A}$ such that $q(\hat{X}) = X$. What we are actually interested in is the intersection of the fixed point sets

[1] By construction, all cones in question are simplicial.

with the Calabi-Yau hyper surface, that is $\mathcal{F}_\gamma := F_\gamma \cap X$. Their upstairs counterparts are $\hat{\mathcal{F}}_{\hat{\gamma}} = \hat{F}_{\hat{\gamma}} \cap \hat{X}$. Then

$$q(\hat{\mathcal{F}}_{\hat{\gamma}}) = \mathcal{F}_\gamma \ . \tag{3.21}$$

What we want is for the Calabi-Yau manifold not to intersect the fixed point set, that is, we need $\mathcal{F}_\gamma$ to be empty. From the previous equation this is the same as saying that $\hat{\mathcal{F}}_{\hat{\gamma}}$ is empty. Let us denote by $\hat{R}_K$ the block of the representation $\hat{K}$ corresponding to the set of coordinates $K \in \mathcal{K}$ and by $\mathbf{z}_K$ the corresponding the upstairs coordinates in this block. On these coordinates the topic group $\mathcal{G}$ acts as $\mathbf{z}_K \to \mathbf{s}^{\mathbf{q}_K}\mathbf{z}_K$ and, hence, the upstairs fixed point condition in Eq. (3.19) can be written as

$$\hat{R}_K(\hat{\gamma})\mathbf{z}_K = \mathbf{s}^{\mathbf{q}_K}\mathbf{z}_K \tag{3.22}$$

for all $K \in \mathcal{K}$. These equations can be described by an ideal I in the ring $\mathbb{C}[\mathbf{z}, \mathbf{s}]$ (one may have to multiply with powers of some parameters s_r if the corresponding charges q_r^i are negative, in order to achieve polynomial form).

Intuitively it is quite apparent that we only have to compute the intersection of zero sets defined by equation.(3.22) and the Calabi-Yau hyper-surfaces. However two subtleties come as the following. First of all the Calabi-Yau hyper-surface is not unique, but varies within a huge family whose defining ideal is linear combination of invariant monomials. In practice it is never possible to check each Calabi-Yau to confirm the fixed point free property, and it turns out we could only randomly pick up several CYs and repeat the computation, until there is one or more Calabi-Yau which doesn't intersect the ambient fixed point set.

The second subtlety is that, we must exclude the variety defined by the Stanley-Reisner (SR) ideal from the fixed point set. This is due to the construction of the toric variety as a weighted projective space, the same reason why we do not consider zero of $\mathbb{C}^{n+1}$ in $\mathbb{P}^n$ space. There are two SR ideals appearing in our computation: one is used to define the zero set Z of the toric ambient space, while the other is the zero set correspond to $\mathcal{G}$, and we had to remove both. As for the practical computation, it is not a good choice to simply compute the saturation of fixed point equations by the SR ideals, because the variety hence defined does not necessarily exclude all the points in SR ideal. The reason is that a saturation of different ideals only gives the topological closure, whereas the saturation of fixed points set and SR varieties are open sets. Therefore in practice we must compare the two radical ideals of the fixed point equations with or without the SR ideals, to know exactly whether we have the discrete symmetry as required.

3.3 Algorithm of classification

We now summarise the whole algorithm classifying the freely acting symmetry for toric Calabi-yau hyper-surfaces.

I. **Prepare the toric four-fold lists.** Start with a Hodge number $h^{1,1}$, define the list $T_{h^{1,1}}$ as all the toric varieties with the chosen $h^{1,1}$.

II. **Compute the geometry of TCYs.** For each ambient space A in $T_{h^{1,1}}$, compute the GCD of third Chern class and signature of twisted bundles, which gives us the candidate finite groups as discrete symmetries. In addition, compute the monomials P_i defining the Calabi-Yau hyper-surfaces.

III. **Compute the symmetries of ambient space.** Compute the toric symmetry group G_A as sequentially figuring out $\mathcal{I}$,$\mathcal{J}$,$\mathcal{K}$,$\mathcal{L}$. Combining the Charge matrix, we have the semi-direct product as $G_A = P_A \ltimes (H_A/\mathcal{G})$

IV. **Generate the representations.** For each group G as the candidate, generate the matrix representations $R_G = \{r_1, ..., r_{|R_G|}\}$ following the method in 3.2.3.

V. **Check the discrete symmetry actions.** For each representation r in R_G, generate a few random hyper-surfaces using P_i, and compute the list P_i^{inv} as invariant combinations of monomials after the symmetry action. Check the smoothness and fixed point set for r.

The detailed implementation is quite lengthy and referred to the appendix A. As the geometry of KS list, we are using the database [77], and we use GAP [80] for the group data of constructing the projective representations. The computation system is composed of *Mathematica* modules and the AG computation is finished in *Singular*. The CY hyper-surfaces are generated with random coefficients of each monomial ranging from 0 to 100. If the computation in Singular is too complicated over Complex fields, we then alternatively use quite a few finite prime fields as the base field, to make sure we had the consistent result.

3.4 Examples

We now list a few examples to explain the algorithm and following the steps as in section (3.3).

3.4.1 A $\mathbb{Z}_2$ symmetry of tetra-quadric

The tetra-quadric ambient space falls in the class of CICY, yet it could also be constructed as a toric 4-fold. We start with tetra-quadric to explain the details of the geometrical data and how is the algorithm progressed. The Hodge numbers of the tetra-quadric are $h^{1,1} = 4,\ h^{1,2} = 68$, which we assumed is already prepared in **Step I**.

Step II: The ambient space is constructed by a reflexive polygon of 8 vertices in the 4-dim lattice space:

$$\begin{aligned} \mathbf{v}_1 = (-1,0,0,0), \mathbf{v}_2 = (-1,0,0,1), \mathbf{v}_3 = (-1,0,1,0), \mathbf{v}_4 = (-1,1,0,0), \\ \mathbf{v}_5 = (1,-1,0,0), \mathbf{v}_6 = (1,0,-1,0), \mathbf{v}_7 = (1,0,0,-1), \mathbf{v}_8 = (1,0,0,0) \end{aligned} \tag{3.23}$$

The zero set is then characterised by $\mathcal{I}$ as:

$$\begin{aligned} \mathcal{I} = \{\{1,8\},\{2,7\},\{3,6\},\{4,5\}\}, \\ Z = \{x_1 = x_8 = 0\} \cup \{x_2 = x_7 = 0\} \cup \{x_3 = x_6 = 0\} \cup \{x_4 = x_5 = 0\} \end{aligned} \tag{3.24}$$

Its Charge matrix

$$(q_r{}^i) = \begin{pmatrix} 0 & 0 & 0 & 1 & 1 & 0 & 0 & 0 \\ 0 & 0 & 1 & 0 & 0 & 1 & 0 & 0 \\ 0 & 1 & 0 & 0 & 0 & 0 & 1 & 0 \\ 1 & 0 & 0 & 0 & 0 & 0 & 0 & 1 \end{pmatrix} \tag{3.25}$$

gives us the toric action:

$$\mathcal{G} = \{\{s_4, s_4, s_3, s_3, s_2, s_2, s_1, s_1\} \,|s_i \in \mathbb{C}^*\} \tag{3.26}$$

In general, we cannot expect there to be only one geometry for a certain polytope, because different triangulations might give rise to different geometries with varied Chow groups and intersection numbers. Therefore in practice we need to distinguish different triangulations, even if they might turns out to have equivalent geometries.

We could further compute the Chern classes and Euler number etc. given the intersection numbers. Since the Hodge number $h^{1,1} = 4$, we expect there to be 4 basis elements in the Chow group and write as $J_i, i = \{1,2,3,4\}$. Now the intersection number is:

$$J_i \wedge J_j \wedge J_k = 2\ \epsilon_{i,j,k}, i,j,k = 1,...,4 \tag{3.27}$$

Further computations tell us that the second Chern class expressed in this base is $C_2 = 4(J_1J_2 + J_1J_3 + J_2J_3 + J_1J_4 + J_2J_4 + J_3J_4)$, while the Euler Characteristic is -128. In addition, the GCD of Euler number and Hirzebruch signatures of twisted bundles is 16, we hence need to consider

all the finite groups with order less or equal to 16, such as $\mathbb{Z}_2, \mathbb{Z}_4, \mathbb{Z}_2 \ltimes \mathbb{Z}_2$, $\mathbb{Z}_8$, $\mathbb{Z}_2 \ltimes \mathbb{Z}_4$ and $\mathbb{Z}_2 \ltimes (\mathbb{Z}_2 \ltimes \mathbb{Z}_2)$ etc. For each of them we need to generate all the π-representations using the method in former sections.
As for the monomials defining the TCY family, we simply use the formula (3.4), which gives us 81 homogeneous monomials.

Step III. The other piece of information for generating the π-representations is the symmetry group of toric ambient space. We have

$$\mathcal{J} = \mathcal{K} = \mathcal{I} = \{\{1,8\},\{2,7\},\{3,6\},\{4,5\}\} \tag{3.28}$$

which implies that $S = S(\{1,8\}) \times S(\{2,7\}) \times S(\{3,6\}) \times S(\{4,5\}) \cong (S_2)^4$. Therefore P is interchanging the four equal length blocks, $P \cong S_4$.

Following the information of $\mathcal{K}$ and $\mathcal{J}$, the P_A is now defined as the quotient of

$$R_A = \text{permutations of blocks} \times S_A,$$

where S_A is just $S(\{1,8\}) \times S(\{2,7\}) \times S(\{3,6\}) \times S(\{4,5\}) \cong (S_2)^4$. Hence $P_A = S_4$, interchanging the 4 blocks as the permutation part of the ambient symmetry group. On the continuous part, we have

$$H_A = GL(\{1,8\},\mathbb{C}) \times GL(\{3,7\},\mathbb{C}) \times GL(\{3,6\},\mathbb{C}) \times GL(\{4,5\},\mathbb{C})/\mathcal{G}, \tag{3.29}$$

which still allows the permutations of variable within each blocks.

Analysing the structure of H_A, we can see that the symmetry action of the CY could be interchanging the 4 blocks, while remains the action within each block the same. Actually the symmetry action had already been systematically analysed in the paper [69]. In **Step IV.** we generally construct all the matrix representations. For example we can now choose $\mathbb{Z}_4$ group generated by g_1 as

$$r(Id) = \mathbb{I} \qquad r(g_1^2) = \begin{pmatrix} & \sigma_3 & & \\ 1 & & & \\ & & & \sigma_3 \\ & & 1 & \end{pmatrix}$$

$$r(g_1^2) = \begin{pmatrix} \sigma_3 & & & \\ & \sigma_3 & & \\ & & \sigma_3 & \\ & & & \sigma_3 \end{pmatrix} \qquad r(g_1^3) = \begin{pmatrix} & 1 & & \\ \sigma_3 & & & \\ & & & 1 \\ & & \sigma_3 & \end{pmatrix}, \tag{3.30}$$

where we use Pauli matrices as $\sigma_1 = \left(\begin{smallmatrix} 0 & 1 \\ 1 & 0 \end{smallmatrix}\right)$, $\sigma_2 = \left(\begin{smallmatrix} 0 & -i \\ i & 0 \end{smallmatrix}\right)$ and $\sigma_3 = \left(\begin{smallmatrix} 1 & 0 \\ 0 & -1 \end{smallmatrix}\right)$.
The matrix representations were acting onto the homogeneous variables following the order $\mathcal{K} = \{x_1, x_8, x_2, x_7, x_3, x_6, x_4, x_5\}$.

To see whether the above representation acts freely on the CY hyper-surface, we need to use the Reynolds Operator to pick up the invariant family as consists of 41 invariant monomials defining the downstairs CY hyper-surface such as $x_1^2x_2^2x_3^2x_4^2, x_1x_2x_3x_4x_5x_6x_7x_8, ..., x_3x_4x_5x_6x_7^2x_8^2$.
Let's now pick up $r(g_1)$, and write out the fixed point equations:

$$\begin{gathered} s_4x_1 - x_1 = 0, s_4x_8 + x_8 = 0, s_3x_2 - x_2 = 0, s_3x_7 + x_7 = 0, \\ s_2x_3 - x_3 = 0, s_2x_6 + x_6 = 0, s_1x_4 - x_4 = 0, s_1x_5 + x_5 = 0 \end{gathered} \tag{3.31}$$

By excluding the zero set

$$\{x_1 = x_8 = 0\} \cup \{x_2 = x_7 = 0\} \cup \{x_3 = x_6 = 0\} \cup \{x_4 = x_5 = 0\} \cup \{s_i = 0\}, i = 1, ..., 4,$$

we see that there is no fixed point for the CY family.

3.4.2 A $\mathbb{Z}_2$ symmetry of bundled tetra-quadric

Another new $\mathbb{Z}_2$ discrete symmetry that we have found is the Calabi-Yau constructed of 10 homogeneous coordinates/vertices:

$$\begin{gathered} \mathbf{v}_1 = (-1,-1,-1,-1), \mathbf{v}_2 = (-1,0,0,0), \mathbf{v}_3 = (0,-1,0,0), \mathbf{v}_4 = (0,0,-1,0), \mathbf{v}_5 = (0,0,0,-1), \\ \mathbf{v}_6 = (0,0,0,1), \mathbf{v}_7 = (0,0,1,0), \mathbf{v}_8 = (0,1,0,0), \mathbf{v}_9 = (1,0,0,0), \mathbf{v}_{10} = (1,1,1,1) \end{gathered}$$

The Charge matrix is:

$$\mathcal{Q} = \begin{pmatrix} 0 & 1 & 0 & 0 & 0 & 0 & 0 & 0 & 1 & 0 \\ 0 & 0 & 1 & 0 & 0 & 0 & 0 & 1 & 0 & 0 \\ 0 & 0 & 0 & 1 & 0 & 0 & 1 & 0 & 0 & 0 \\ 0 & 0 & 0 & 0 & 1 & 1 & 0 & 0 & 0 & 0 \\ 0 & 1 & 1 & 1 & 1 & 0 & 0 & 0 & 0 & 1 \\ 1 & 0 & 0 & 0 & 0 & 1 & 1 & 1 & 1 & 0 \end{pmatrix} \tag{3.32}$$

The zero set Z is now characterised by $\mathcal{I}$ as:

$$
\begin{aligned}
x_1 = x_{10} = 0 \cup x_2 = x_9 = 0 \cup x_3 = x_8 = 0 \cup x_4 = x_7 = 0 \cup x_5 = x_6 = 0 \cup \\
x_1 = x_6 = x_7 = 0 \cup x_1 = x_6 = x_8 = 0 \cup x_1 = x_6 = x_9 = 0 \cup x_1 = x_7 = x_8 = 0 \cup \\
x_1 = x_7 = x_9 = 0 \cup x_1 = x_8 = x_9 = 0 \cup x_2 = x_3 = x_4 = 0 \cup x_2 = x_3 = x_5 = 0 \cup \\
x_2 = x_3 = x_{10} = 0 \cup x_2 = x_4 = x_5 = 0 \cup x_2 = x_4 = x_{10} = 0 \cup x_2 = x_5 = x_{10} = 0 \cup \\
x_3 = x_4 = x_5 = 0 \cup x_3 = x_4 = x_{10} = 0 \cup x_3 = x_5 = x_{10} = 0 \cup x_4 = x_5 = x_{10} = 0 \cup \\
x_6 = x_7 = x_8 = 0 \cup x_6 = x_7 = x_9 = 0 \cup x_6 = x_8 = x_9 = 0 \cup x_7 = x_8 = x_9 = 0
\end{aligned}
\tag{3.33}
$$

thus giving us $\mathcal{J} = \mathcal{K} = \{\{1\}, \{2\}, \{3\}, \{4\}, \{5\}, \{6\}, \{7\}, \{8\}, \{9\}, \{10\}\}$
with its toric action:

$$
\mathcal{G} = \{(s_6, s_1 s_5, s_2 s_5, s_3 s_5, s_4 s_5, s_4 s_6, s_3 s_6, s_2 s_6, s_1 s_6, s_5) | s_i \in \mathbb{C}^*\} \tag{3.34}
$$

The $\mathbb{Z}_2$ discrete symmetry action is with generator:

$$
r(g_1) = \{x_1 \leftrightarrow x_{10}, x_2 \leftrightarrow x_9, x_3 \leftrightarrow x_8, x_4 \leftrightarrow x_7, x_5 \leftrightarrow x_6\} \tag{3.35}
$$

One can check that this is actually a fixed point free action and leaves the quotient CY a smooth hyper-surface.

3.5 Scan results

The complete search of the KS list is so far not reachable, we hence start from toric CYs with lower Hodge numbers to more complicated geometries. What's more the existing 16 CY families with fundamental groups as discrete symmetries fall into the range $h^{1,1} = \{2, 3, 4, 5\}$, where we also expect the new discrete symmetries to arise. One computational difficulty is that the algebraic geometrical check of fixed points set is very time consuming, and not easy for timing. Possible solutions, as mentioned before, would be using a few finite base fields and random Calabi-Yau surfaces, yet this might go wild during the actual *Singular* calculations. Another consideration is, as the group order becomes larger, it caused more resource and time to generate the representations as well as their Schur covers. Statistically since all the discrete symmetries known are in the simple form as $\mathbb{Z}_2, \mathbb{Z}_3, \mathbb{Z}_5, ..$, we might first try out the finite groups of orders less or equal to 4.

We therefore plan to run the systematic scan in the following spirit:

The geometry data on the Database [77] is including all the triangulations & toric informations up to $h^{1,1} = 6$. The number of inequivalent geometries are $39, 306, 2014, 13635, 85679...$ We firstly test out the 16 families and their known discrete symmetries, which includes the famous bicubic and tetra-quadric shared by CICY. Then we start with each $h^{1,1}$ and the finite groups with order ≤ 4. Meanwhile we run the fixed point test before the smoothness test because statistically it is harder for a concrete representation to come with an empty fixed point set. Once the small ordered groups are finished, we then run the higher ordered groups.

After testing and running the complicated system for months, we can now make some important statements on the discrete symmetries with $h^{1,1} = \{2, 3, 4\}$, and we do actually find out a few new discrete symmetries except the known ones. We realises that it is a truly difficult situation to run into any discrete symmetries if it is not the fundamental group of a toric CY. We hereby firstly mentioned the new examples we've found out, then describe the details of our scan. Finally we want to point out a new interesting idea of non-freely acting symmetries and the possible realisations.

3.5.1 Discrete Symmetries

The 3.4.2 example in the former section gives us a new discrete symmetry of $h^{1,1} = 6$.

The scan of all the $h^{1,1} = 2, 3$ geometries of finite groups of order less or equal to 4 gives us only one new freely acting symmetry except the known cases in paper [81] of the 16 families.

3.5.1.1 A $\mathbb{Z}_2 \ltimes \mathbb{Z}_2$ discrete symmetry

Consider the reflexive polytope formed by the following vertices:

$$\begin{gathered}\mathbf{v}_1 = (-1, 0, 0, 0), \mathbf{v}_2 = (-1, 0, 0, 2), \mathbf{v}_3 = (-1, 0, 1, 1), \mathbf{v}_4 = (-1, 2, -1, -1), \\ \mathbf{v}_5 = (-1, 2, 0, -1), \mathbf{v}_6 = (1, -1, 0, 0), \mathbf{v}_7 = (-1, 0, 0, 1)\end{gathered} \tag{3.36}$$

The zero set is then characterised by $\mathcal{I}$ as:

$$\mathcal{I} = \{\{1, 2\}, \{5, 7\}, \{3, 4, 6\}\}, \quad Z = \{x_1 = x_2 = 0\} \cup \{x_5 = x_7 = 0\} \cup \{x_3 = x_4 = x_6 = 0\} \tag{3.37}$$

The Charge matrix is

$$(q_r{}^i) = \begin{pmatrix} 0 & 0 & 0 & 0 & 1 & 2 & 1 \\ 0 & 0 & 1 & 1 & 0 & 2 & 0 \\ 1 & 1 & 0 & 0 & 2 & 4 & 0 \end{pmatrix}, \tag{3.38}$$

which gives us the toric action

$$\mathcal{G} = \{(s_1 s_3^2, s_1^2 s_2^2 s_3^4, s_1, s_3, s_3, s_2, s_2) | s_1, s_2, s_3 \in \mathbb{C}^*\} \tag{3.39}$$

The toric ambient space have Hodge numbers as $h^{1,1} = 3, h^{2,1} = 115$.

As for this polytope, we choose the following triangulation:

$$\begin{gathered}[v_1, v_3, v_4, v_5], [v_1, v_3, v_4, v_7], [v_1, v_3, v_5, v_6], [v_1, v_3, v_6, v_7], [v_1, v_4, v_5, v_6], [v_1, v_4, v_6, v_7], \\ [v_2, v_3, v_4, v_5], [v_2, v_3, v_4, v_7], [v_2, v_3, v_5, v_6], [v_2, v_3, v_6, v_7], [v_2, v_4, v_5, v_6], [v_2, v_4, v_6, v_7]\end{gathered} \tag{3.40}$$

which has twelve 4-dim cones. We could compute the Chern classes and Euler number etc. given the intersection numbers. Since the Hodge number $h^{1,1} = 3$, we expect there to be 3 basis elements in the Chow group and denote them as $J_i, i = \{1, 2, 3\}$. Now the intersection numbers are:

$$\begin{gathered}J_1 \wedge J_2 \wedge J_3 = 2, J_1 \wedge J_3 \wedge J_2 = 2, J_2 \wedge J_1 \wedge J_3 = 2, J_2 \wedge J_3 \wedge J_1 = 2, \\ J_2 \wedge J_3 \wedge J_3 = -4, J_3 \wedge J_1 \wedge J_2 = 2, J_3 \wedge J_2 \wedge J_1 = 2, \\ J_3 \wedge J_2 \wedge J_3 = -4, J_3 \wedge J_3 \wedge J_2 = -4\end{gathered} \tag{3.41}$$

and the remaining terms vanish. Further computations tell us that the second Chern class expressed in this base is $C_2 = 5J_2^2 + 24J_1J_2 + 12J_3J_2 - 6J_3^2$, while the Euler Characteristic is -224. In addition, the GCD of Euler number and Hirzebruch signatures of twisted bundles is 8, hence the following groups need to be checked: $\mathbb{Z}_2, \mathbb{Z}_4, \mathbb{Z}_2 \ltimes \mathbb{Z}_2, \mathbb{Z}_8, \mathbb{Z}_2 \ltimes \mathbb{Z}_4$ and $\mathbb{Z}_2 \ltimes (\mathbb{Z}_2 \ltimes \mathbb{Z}_2)$. For each of them we need to generate all the π-representations using the method in former sections.

The other piece of information for generating the π-representations is the symmetry group of toric ambient space. We have

$$\begin{aligned}\mathcal{J} &= \{\{1, 2\}, \{5, 7\}, \{3, 4, 6\}\}, \\ \mathcal{K} &= \{\{1, 2\}, \{3, 4\}, \{5\}, \{6\}, \{7\}\},\end{aligned} \tag{3.42}$$

which implies that $S = S(\{1, 2\}) \times S(\{5, 7\}) \times S(\{3, 4, 6\}) \cong S_2 \times S_2 \times S_3$. We also have P as interchanging the two blocks $\{1, 2\}$ and $\{5, 7\}$ of $\mathcal{J}$, hence $P \cong S_2$. One might notice that without the interference from the toric action, the symmetry group is a rather straight forward

list involving only the triangulation information. However later we could see the changes of ambient symmetry group contributed from the Charge matrix.

Following the information of $\mathcal{K}$ and $\mathcal{J}$, the P_A is not defined as the quotient of

$$R_A = S(\{1,2\}) \times S(\{3,4\}) \tag{3.43}$$

by

$$S_A = S(\{1,2\}) \times S(\{3,4\}), \tag{3.44}$$

hence we have the trivial P_A. However one does notice that H_A is now

$$H_A = GL(\{1,2\},\mathbb{C}) \times GL(\{5,7\},\mathbb{C}) \times GL(\{3,4,6\},\mathbb{C})/\mathcal{G}, \tag{3.45}$$

which still allows the permutations of homogeneous variables to appear into the discrete symmetry action. The question that remains is just how to construct the explicit matrix representations of all the possible symmetry groups.

There is only one orbit with two blocks $\{1,2\},\{3,4\}$ in $\mathcal{G}$, which means the best chance we can get permutation representations inside $H_A/\mathcal{G}$ is the interchanging of $\{1,2\}$ and $\{3,4\}$ blocks. Take $\mathbb{Z}_2 \ltimes \mathbb{Z}_2$ for example, the following generator of $\mathbb{Z}_2$ as matrix representations could be:

$$r(g_1) = \begin{pmatrix} \mathbb{I}_3 & & \\ & \sigma_1 & \\ & & \mathbb{I}_2 \end{pmatrix} \tag{3.46}$$

The matrix representations were acting onto the homogeneous variables following the order $\mathcal{K} = \{x_5, x_6, x_7, x_1, x_2, x_3, x_4\}$.

The CY hyper-surface upstairs is defined by linear combination of 153 monomials correspondent to each point in the polar polytope, in the form of $x_1^8x_4^4x_7^4$, $x_1^8x_3x_4^3x_7^4$, $x_1^8x_3^2x_4^2x_7^4$,...,$x_2^4x_3^4x_5^2x_7^2$,$x_3^3x_4x_5^4$,$x_2^2x_3^4x_5^3x_7$,$x_3^4x_5^4$... If we calculate the invariant ones after the discrete symmetry action, we would realise that they form a base of the Calabi-Yau family composed of 50 polynomials such as $x_1^2x_2^2x_3^2x_4^2x_5^2x_7^2$, $x_1^2x_5x_6x_7x_4^2$, ..., $x_4^4x_7^4x_1^8$, for which we check the smoothness and fixed point set.

We now claim that the following matrix representation of $\mathbb{Z}_2 \ltimes \mathbb{Z}_2 = \{1, g_1, g_2, g_1g_2\}$ is one discrete symmetry of a generic Calabi-Yau hyper-surface:

$$r(Id) = \left(\mathbb{I}_7\right) \qquad r(g_1) = \begin{pmatrix} 1 & & & \\ & -\mathbb{I}_2 & & \\ & & \sigma_1 & \\ & & & \sigma_1 \end{pmatrix}$$
$$r(g_1 g_2) = \begin{pmatrix} \mathbb{I}_3 & & \\ & \sigma_1\sigma_3 & \\ & & \sigma_1\sigma_3 \end{pmatrix} \qquad r(g_2) = \begin{pmatrix} 1 & & & \\ & -\mathbb{I}_2 & & \\ & & \sigma_3 & \\ & & & \sigma_3 \end{pmatrix} \tag{3.47}$$

The matrix are acting accordingly on variables $\{x_5, x_6, x_7, x_1, x_2, x_3, x_4\}$.
Note that this is not a linear representation but a projective representation, namely the direct multiplication will not only has 4 elements but 8, however some of them will be reduced by $\mathcal{G}$ action, reflecting the fact that we are working on projective spaces.
Let's now pick up for example $r(g_1)$, and write out the fixed point equations for it.

$$\begin{aligned} &s_1 s_3^2 x_5 - x_5 = 0, s_1^2 s_2^2 s_3^4 x_6 + x_6 = 0, s_1 x_7 + x_7 = 0, \\ &s_3 x_1 - x_2 = 0, s_3 x_2 - x_1 = 0, s_2 x_3 - x_4 = 0, s_2 x_4 - x_3 = 0 \end{aligned} \tag{3.48}$$

By excluding the zero sets

$$\{x_1 = x_2 = 0\} \cup \{x_5 = x_7 = 0\} \cup \{x_3 = x_4 = x_6 = 0\} \cup \{s_1 = 0\} \cup \{s_2 = 0\} \cup \{s_3 = 0\}$$

One can check that there is no fixed point set intersecting the generic Calabi-Yau.
Note that this Calabi-Yau actually resides in the 16 families, however the fundamental group for it is $\mathbb{Z}_2$ rather than $\mathbb{Z}_2 \ltimes \mathbb{Z}_2$, whose matrix representation is:

$$r(Id) = \mathbb{I}_7 \qquad r(g_1) = \begin{pmatrix} 1 & & & \\ & -\mathbb{I}_2 & & \\ & & \sigma_3 & \\ & & & \sigma_3 \end{pmatrix} \tag{3.49}$$

This symmetry action is sharing one generator with the new symmetry action that we have found out, which suggests that even for the 16 families, one can recombine the known discrete symmetries to get new ones.

3.5.1.2 Scan results

We now summarise all the discrete symmetries with toric CY of $h^{1,1} \leq 3$ into the following table 3.1:

# of geometry	Hodge number	polytope	charge matrix (transposed)	discrete symmetry	matrix representation
#1 quintic	$h^{1,1}=1$ $h^{1,2}=101$	$\begin{pmatrix} -1 & 0 & 0 & 0 \\ -1 & 0 & 0 & 1 \\ -1 & 0 & 1 & 0 \\ -1 & 1 & 0 & 0 \\ 4 & -1 & -1 & -1 \end{pmatrix}$	$\begin{pmatrix} 1 \\ 1 \\ 1 \\ 1 \\ 1 \end{pmatrix}$	$\mathbb{Z}_5 := \langle g_1 \rangle$	$r(g_1) = \begin{pmatrix} 1 & & & & \\ & e^{\frac{2i\pi}{5}} & & & \\ & & e^{\frac{4i\pi}{5}} & & \\ & & & e^{-\frac{4i\pi}{5}} & \\ & & & & e^{-\frac{2i\pi}{5}} \end{pmatrix}$
				$\mathbb{Z}_5 \times \mathbb{Z}_5 := \langle g_1, g_2 \rangle$	$\alpha = \begin{pmatrix} 1 & & & & \\ & e^{\frac{2i\pi}{5}} & & & \\ & & e^{\frac{4i\pi}{5}} & & \\ & & & e^{-\frac{4i\pi}{5}} & \\ & & & & e^{-\frac{2i\pi}{5}} \end{pmatrix}$, $r(g_1,g_2) = \{\alpha, \left[\begin{smallmatrix} 1 & 2 & 3 & 4 & 5 \\ 1 & 2 & 3 & 4 & 5 \end{smallmatrix}\right]\}$ $r(g_1,g_2) = \{\alpha, \left[\begin{smallmatrix} 1 & 2 & 3 & 4 & 5 \\ 5 & 1 & 2 & 3 & 4 \end{smallmatrix}\right]\}$ $r(g_1,g_2) = \{\alpha, \left[\begin{smallmatrix} 1 & 2 & 3 & 4 & 5 \\ 4 & 5 & 1 & 2 & 3 \end{smallmatrix}\right]\}$ $r(g_1,g_2) = \{\alpha, \left[\begin{smallmatrix} 1 & 2 & 3 & 4 & 5 \\ 3 & 4 & 5 & 1 & 2 \end{smallmatrix}\right]\}$ $r(g_1,g_2) = \{\alpha, \left[\begin{smallmatrix} 1 & 2 & 3 & 4 & 5 \\ 2 & 3 & 4 & 5 & 1 \end{smallmatrix}\right]\}$
#2 bi-cubic	$h^{1,1}=2$ $h^{1,2}=83$	$\begin{pmatrix} -1 & 0 & 0 & 0 \\ -1 & 0 & 0 & 1 \\ -1 & 0 & 1 & 0 \\ -1 & 1 & 0 & 0 \\ 2 & -1 & -1 & 0 \\ 2 & 0 & 0 & -1 \end{pmatrix}$	$\begin{pmatrix} 0 & 1 \\ 0 & 1 \\ 1 & 0 \\ 1 & 0 \\ 1 & 0 \\ 0 & 1 \end{pmatrix}$	$\mathbb{Z}_3 := \langle g_1 \rangle$	$\beta = \begin{pmatrix} 1 & & \\ & e^{\frac{2i\pi}{3}} & \\ & & e^{-\frac{2i\pi}{3}} \end{pmatrix}$, $r(g_1) := \begin{pmatrix} \beta & \\ & \beta \end{pmatrix}$
				$\mathbb{Z}_3 \times \mathbb{Z}_3 := \langle g_1, g_2 \rangle$	$\alpha = \begin{pmatrix} 1 & & \\ & e^{\frac{2i\pi}{3}} & \\ & & e^{-\frac{2i\pi}{3}} \end{pmatrix}$ $\beta = \begin{pmatrix} 1 & & \\ & e^{\frac{2i\pi}{3}} & \\ & & e^{-\frac{2i\pi}{3}} \end{pmatrix}$, $\gamma = \left[\begin{smallmatrix} 1 & 2 & 3 \\ 3 & 1 & 2 \end{smallmatrix}\right]$ $r(g_1,g_2) = \{\begin{pmatrix} \alpha & \\ & \alpha \end{pmatrix}, \gamma\}$, $r(g_1,g_2) = \{\begin{pmatrix} \beta & \\ & \beta \end{pmatrix}, \gamma\}$, $r(g_1,g_2) = \{\begin{pmatrix} \beta & \\ & \beta \end{pmatrix}, \gamma\}$, $r(g_1,g_2) = \{\begin{pmatrix} \beta & \\ & \beta \end{pmatrix}, \gamma\}$
#3	$h^{1,1}=3$ $h^{1,2}=83$	$\begin{pmatrix} -1 & 0 & 0 & 0 \\ -1 & 0 & 0 & 1 \\ -1 & 0 & 2 & 0 \\ -1 & 4 & -2 & -1 \\ 1 & -1 & 0 & 0 \\ -1 & 0 & 1 & 0 \\ -1 & 2 & -1 & 0 \end{pmatrix}$	$\begin{pmatrix} 0 & 0 & 1 \\ 0 & 1 & 1 \\ 0 & 0 & 1 \\ 0 & 1 & 1 \\ 2 & 4 & 4 \\ 1 & 2 & 0 \\ 1 & 0 & 0 \end{pmatrix}$	$\mathbb{Z}_2 := \langle g_1 \rangle$	$r(g_1) = \begin{pmatrix} \mathbb{I}_3 & \\ & -\mathbb{I}_4 \end{pmatrix}$
#4	$h^{1,1}=3$ $h^{1,2}=115$	$\begin{pmatrix} -1 & 0 & 0 & 0 \\ -1 & 0 & 0 & 2 \\ -1 & 0 & 1 & 1 \\ -1 & 2 & -1 & -1 \\ -1 & 2 & 0 & -1 \\ 1 & -1 & 0 & 0 \\ -1 & 0 & 0 & 1 \end{pmatrix}$	$\begin{pmatrix} 0 & 0 & 1 \\ 0 & 0 & 1 \\ 0 & 1 & 0 \\ 0 & 1 & 0 \\ 1 & 0 & 2 \\ 2 & 2 & 4 \\ 1 & 0 & 0 \end{pmatrix}$	$\mathbb{Z}_2 := \langle g_1 \rangle$	$r(g_1) = \begin{pmatrix} 1 & & & \\ & -\mathbb{I}_2 & & \\ & & \sigma_3 & \\ & & & \sigma_3 \end{pmatrix}$
				$\mathbb{Z}_2 \ltimes \mathbb{Z}_2 := \langle g_1, g_2 \rangle$	the one in formula (3.47)
#5	$h^{1,1}=3$ $h^{1,2}=115$	$\begin{pmatrix} -1 & 0 & 0 & 0 \\ -1 & 0 & 1 & 0 \\ -1 & 0 & 1 & 1 \\ -1 & 2 & -1 & -1 \\ -1 & 2 & -1 & 0 \\ -1 & 2 & 0 & 0 \\ 1 & -1 & 0 & 0 \end{pmatrix}$	$\begin{pmatrix} 0 & 0 & 1 \\ 0 & 1 & 0 \\ 1 & 0 & 0 \\ 1 & 0 & 0 \\ 0 & 1 & 0 \\ 0 & 0 & 1 \\ 2 & 2 & 2 \end{pmatrix}$	$\mathbb{Z}_2 := \langle g_1 \rangle$	$r(g_1) = \begin{pmatrix} -1 & & & \\ & \sigma_3 & & \\ & & \sigma_3 & \\ & & & \sigma_3 \end{pmatrix}$

Table 3.1: discrete symmetries

3.5.2 Non-freely Acting Examples

Non-freely acting symmetries are of importance because of the following reason:

Let's assume that the upstairs CY manifold is denoted by X and the discrete symmetry group $\mathcal{G}$ is not necessarily freely-acting. However the symmetry group has a freely-acting subgroup, $\Gamma_f \in \mathcal{G}$, and we have the downstairs CY manifold defined by the quotient $\hat{X} = X/\Gamma_f$ with the projection $p : X \to \hat{X}$. We also define the normaliser of the freely acting subgroup Γ_f in $\mathcal{G}$ as $\Gamma := N_{\mathcal{G}}(\Gamma_f)$.

The phenomenological considerations would be that vector bundles V living on X descends down to a bundle $\hat{V} \to \hat{X}$, s.t. $V = p^*\hat{V}$. If we further assume that $\hat{V}$ has a $\hat{\mathcal{G}}$ equivariant structure s.t. downstairs symmetry group lifts to the downstairs bundle, and the upstairs bundle V has a Γ equivariant structure.

Recall that for the vector bundle with structure group H, we have that the effective GUT group G is the commutant of H within E_8. Under the above assumptions, the low-energy GUT group G is further broken to the standard model group G_{SM} by the Γ_f Wilson line bundle W. Now the complete downstairs bundle is $\hat{V} \oplus W$ and the adjoint representation of E_8 is now decomposed under $H \times G_{SM} \times \Gamma_f$ as:

$$\mathbf{248} \to \bigoplus i(R_i, r_i, w_i) + c.c. \ . \tag{3.50}$$

These i-th multiplet type in this decomposition resides in

$$[H^1(X, V_i) \otimes w_i^*]_0, \quad [H^1(X, V_i^*) \otimes w_i]_0 \tag{3.51}$$

where V_i is the induced bundle corresponding to H representation R_i and the subscript 0 denotes the Γ_f singlets. It appears that the Γ_f representation content of the relevant cohomologies is

$$H^1(X, V_i) \cong \rho^{\oplus k_i} \oplus \nu_i, \quad H^1(X, V_i^*) \cong \nu_i^* \tag{3.52}$$

where ρ is the regular representation of Γ_f and ν_i are arbitrary Γ_f representation. Therefore given the Γ_f as subgroup of Γ, we could have a refined version of the particle contents. We now share a few non-freely acting symmetries, giving us the smooth downstairs CY hyper-surface, but not necessarily fixed point free.

3.5.2.1 $h^{1,1} = 3,\ h^{2,1} = 115$

Let us now look at a few smooth action for the example 3.5.1.1. Given the $\mathbb{Z}_2$ action defined in 3.5.1.1, there are plenty of smooth actions including the $\mathbb{Z}_2$ as a subgroup (#4 in the table).

For example the following $\mathbb{Z}_2 \times \mathbb{Z}_2$ representation:

$$
\begin{aligned}
r(Id) &= \mathbb{I}_7 & r(g_1) &= \begin{pmatrix} 1 & & & & \\ & -\mathbb{I}_2 & & & \\ & & \sigma_3 & & \\ & & & \sigma_3 \end{pmatrix} \\
r(g_2) &= \begin{pmatrix} \mathbb{I}_5 & \\ & -\mathbb{I}_2 \end{pmatrix} & r(g_1 g_2) &= \begin{pmatrix} 1 & & & & \\ & -\mathbb{I}_2 & & & \\ & & \sigma_3 & & \\ & & & \sigma_1\sigma_3\sigma_1 \end{pmatrix}
\end{aligned}
\tag{3.53}
$$

of which the invariant Calabi-Yau family is the same as the $\mathbb{Z}_2$ symmetry.

and the following $\mathbb{Z}_2 \times \mathbb{Z}_2$ symmetry:

$$
\begin{aligned}
r(Id) &= \mathbb{I}_7 & r(g_1) &= \begin{pmatrix} 1 & & & & \\ & -\mathbb{I}_2 & & & \\ & & \sigma_3 & & \\ & & & \sigma_3 \end{pmatrix} \\
r(g_2) &= \begin{pmatrix} 1 & & & & \\ & -\mathbb{I}_2 & & & \\ & & \sigma_3 & & \\ & & & \sigma_1\sigma_3\sigma_1 \end{pmatrix} & r(g_1 g_2) &= \begin{pmatrix} \mathbb{I}_5 & \\ & -\mathbb{I}_2 \end{pmatrix}
\end{aligned}
\tag{3.54}
$$

3.6 Conclusion

In this chapter we brought about the method of systematically constructing the discrete symmetry actions as well as computing its fixed point set and checking the smoothness. This is a rather complicated topic involving toric geometry, representation theory and algebraic geometry computations. The recent progress in [69, 77, 81] made this possible and we found a few new discrete symmetries, which will be the first step towards string model building on the vast class of KS list beyond the 16 special families. It is desirable to further apply this method to ambient spaces of larger Hodge numbers as well as large order finite groups as the candidates of discrete symmetries.

Chapter 4

Superconformal Block Quivers, Duality Trees and Diophantine Equations

4.1 Introduction

Over the last few decades, the study of quiver theories has occupied a prominent position both in pure mathematics, especially in algebraic geometry and representation theory (cf. e.g., [82–86]), and in theoretical physics, especially in the AdS/CFT correspondence and in the phenomenology of Standard-like models (cf. e.g., [42, 44, 87–89]). One salient feature is that gauge theories arising as world-volume quantum field theories living on stacks of branes probing Calabi-Yau singularities naturally have a product structure for the gauge group as well as bi-fundamental and adjoint fields realized by open-strings; such generically supersymmetric gauge theories are thus encoded by quivers.

The dialogue between the world-volume physics and the geometry of the Calabi-Yau singularity has given us a wealth of new physics and mathematics over the last score of years. There is a variety of such theories one can construct, or "geometrically engineer", in this way depending on the type of branes and the choice of the Calabi-Yau space. Of main interest has been the construction of $(3+1)$-dimensional gauge theories preserving $\mathcal{N}=1$ or $\mathcal{N}=2$ supersymmetries, which feature centrally to the AdS_5/CFT_4 correspondence [38] and which, of course, are of some phenomenological concern. There has been an industry to construct even more classes of such quiver gauge theories with an underlying geometry, ranging from orbifolds [42–44], to toric singularities [41, 45–47], as well as their avatars as brane tilings [48–52], to more generic spaces [90–92]. A myriad of theories have been established and countless successes, recounted.

Let us focus on $\mathcal{N}=1$ theories. Indeed, whereas the $\mathcal{N}=2$ Lagrangian is fixed once the matter content is specified, whereby limiting the possibilities for interaction, the $\mathcal{N}=1$ superpotential

is an additional ingredient to the matter specified by the quiver. In fact, the F-terms prescribe formal algebraic relations to the arrows in the quiver, giving rise to so-called labelled quivers with relations, which has been recently intensely investigated by mathematicians. Furthermore, a key advantage of $\mathcal{N} = 1$ is chirality - a desired phenomenological property; in terms of the quiver, this is reflected by the fact that not every arrow between two nodes has a counter-part going in the opposite direction. Finally, because of the inherent holographic nature of certain classes of our gauge theories, they have superconformal fixed points in the infra-red. This is, of course, reflected by the archetypal example of AdS/CFT, the $\mathcal{N} = 4$ super-Yang-Mills theory in $(3 + 1)$-dimensions from which all our quiver theories geometrically descend.

The natural question thus arises as to whether one could march toward a classification scheme of the plethora of superconformal $\mathcal{N} = 1$ quiver gauge theories which have bedecked the literature. This is, of course, an ambitious goal, especially given the unclassified nature of Calabi-Yau threefold singularities. Note though that the quivers studied here are more general since they are not necessarily Calabi-Yau threefolds. In the toric subclass of Calabi-Yau manifolds, due to the combinatorial nature of the geometry, attempts are under way towards an enumeration [52, 93–96].

The organization of quivers by grouping nodes which are unlinked into so-called "blocks" has emerged in the study of sheaves over del Pezzo surfaces [53]. This was also applied to the superconformal context over the years [54–57], culminating in a systematic investigation in [87]. Such seemingly innocuous procedure turns out to be very powerful. As demonstrated in [87], many of the known theories, often corresponding to such complicated geometries as cones over Hirzebruch surfaces or pseudo del Pezzo surfaces, can have their quiver diagrams contracted to ones with only a few blocks.

Now, it had been realized that Seiberg duality is a very particular transformation on quiver theories [46,47,97] and various geometrical interpretations ranging from Picard-Lefschetz transformations [56] and Weyl group action on the quiver root system [98, 99], to mutations in exceptional collections of coherent sheaves [55] and to tiltings in the derived category [100, 101] have been studied. Such a duality is well adapted to the block structure. In addition, the ranks of the nodes obey Diophantine equations [56, 102] which generalize the Markov equation. The possible values after a blossoming "tree" of duality transformations all satisfy a Diophantine equation determined by the geometry.

Our motivation is clear: First, we wish to continue the study of the taxonomy of $\mathcal{N} = 1$ quiver theories, organized by blocks. In [87], the situation up to four-blocks was detailed. The reason the case study stopped there is because starting from five-blocks, a qualitative difference arises: it is not clear which cycles enter in the superpotential, and it is not completely clear if an arbitrary number of Seiberg Dualities leave the quiver chiral. Our first challenge is to address this issue in a completely algorithmic and exhaustive way. Indeed, in Sec. 4.3 we will see that Seiberg duality leaves the models chiral.

This possibility to continue to a higher number of block is only the tip of the iceberg. We shall see how the representation theory of quivers comes to our aid and offers us a unifying light under which we could examine the quiver block structure, the assignment of ranks and arrows, as well as the general form which the Diophantine equations must assume. Thus representation theory, algebraic geometry and number theory come into full interplay with the physics.

The chapter is organized as follows: We begin in Section 4.2 by setting the notation of our problem of classifying block-quivers by illustrating with the known examples of three and four-blocks. Using the representation theory of quivers, especially a certain bi-linear form called the Tits form, we show how the Diophantine equation for the three-block model can be retrieved exactly and what Seiberg duality means in this context, while in the four-block quiver we unravel a structure that leads to the Diophantine equation which is also present in the three-block models. Then, in Section 4.3 we study the first highly non-trivial case of five-block quivers, which have eluded much of the physics and mathematics literature. We show, despite the extremely complicated combinatorics, that we can still use the Tits form to organise the Diophantine equation and shed light into Seiberg duality. We conclude with outlooks in Section 4.4. Of use will be Appendix D.1 which is an enlightening but self-contained review of the rudiments of quiver representation theory which will be used in the chapter.

4.2 Block Quivers

In this section we begin with a brief reminder for the reader of the concept of block quivers, how Diophantine equations arise from the requirement of existence of superconformal fixed points, as well as the emergence of representation-theoretic quantities in relation to physical constraints. We will illustrate with the well-known example of the three-block quivers, under a new and unifying light. For short, self-contained exposition to some relevant terminology of quivers, especially from a mathematical perspective, we refer the reader to Appendix D.1.

The central object of our concern is the *chiral quiver*, by which we mean any quiver diagram which has no bi-directional arrows (including, in particular, self-adjoining loops which connect a node to itself). The reason for this restriction will soon be clear; essentially it is because we will only be dealing with anti-symmetrized adjacency matrices which do not capture the information of bi-directional arrows. Chirality is a general feature of $\mathcal{N} = 1$ quivers which have risen over the last decade of the AdS/CFT Correspondence belongs to this category. Following [87] we recall that a *block* in a chiral quiver diagram is as follows:

Definition A block is a set of nodes among which there are no arrows, such that all nodes in a block are either heads or tails of arrows connecting them to other blocks. Furthermore, all nodes within the block have the same rank.

Physically, this simply means that we have organised a set of gauge group factors, all of which are of equal rank and which have no bi-fundamental fields charged amongst them, into a "block". The whole set can then be described as a single node with a multiplicity denoting the cardinality of the set, and single arrows with multiplicities connecting this block to others. We see, indeed, that we are dis-allowing arrows which join nodes to themselves. With this convention any chiral quiver diagram has a block structure with all blocks trivially having multiplicity one. We sketch these notions with an example in Fig. 4.1, where blocks 1, 2 and 3 respectively consist of the nodes $\{1, 4, 7\}$, $\{2, 5\}$ and $\{3, 6\}$. A block quiver can therefore be presented by the following

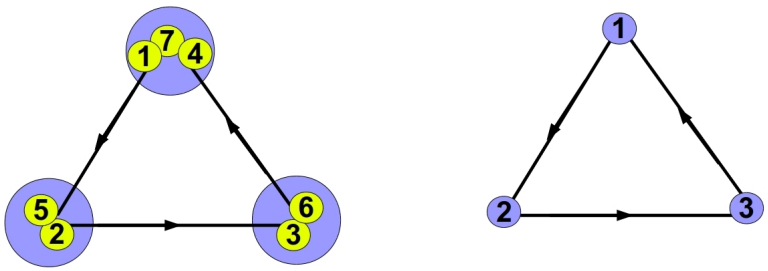

Figure 4.1: A three-block structured quiver diagram. Quiver nodes in yellow are gathered in block nodes in violet. The arrows in both pictures denote collectively all possible arrows among the indicated yellow nodes.

data:

- the number of blocks,
- the number of nodes in each block, and
- the number of arrows connecting any pair of blocks.

Bearing this in mind, let us set the notation to be adopted in this work:

> **Notation** Blocks are indexed by integers $i \in \{1, 2, \dots n\}$. We denote the number of nodes in block i by α_i and the number of bi-fundamentals between blocks i and j with a_{ij}. The orientation of the arrows is taken into account by demanding $a_{ij} = -a_{ji}$; this is the usual anti-symmetric adjacency matrix (and thus does not encode bi-directional arrows). Because within each block the nodes are not connected, we can shrink the adjacency matrix a_{ij} into a block-adjacency matrix which we denote by q_n; clearly q_n is a $n \times n$ antisymmetric matrix over $\mathbb{Z}$. Moreover, we let the R-charge of the bi-fundamental field a_{ij} be r_{ij}. Lastly, we write $N_i = Nx_i$ for the rank of the gauge group of block i, with N representing any common divisor of the ranks of all the blocks.

Now, the main problem of our interest is the following,

> Problem: *Among all possible data (N_i, α_i, q_n) for block quivers, classify those which admit a consistent, superconformal quiver gauge theory in (3+1)-dimensions.*

The answer to this question, for $n = 3$, has been given in both the mathematics and the physics literature [53–56, 87].

4.2.1 Three-Block Quivers

We begin by reviewing the physics approach of [87] for $n = 3$. Given a chiral quiver, like the right one in Fig. 4.1, we must first clarify the physical constraints that should be imposed in order to have a sensible superconformal gauge theory.

Anomaly Cancellation: First, one has to make sure that the gauge (triangle ABJ) anomalies are cancelled. This is equivalent to the condition that the block-reduced rank vector $d = \{\alpha_i x_i\}$ of the quiver, lies in the kernel of the anti-symmetrized reduced quiver matrix q_n:

$$q_3 \cdot d = 0 \,, \qquad q_3 = \begin{pmatrix} 0 & a_{12} & -a_{31} \\ -a_{12} & 0 & a_{23} \\ a_{31} & -a_{23} & 0 \end{pmatrix} \,, \quad d := \begin{pmatrix} \alpha_1 x_1 \\ \alpha_2 x_2 \\ \alpha_3 x_3 \end{pmatrix} \,, \tag{4.1}$$

where the indices indicate the tail and the head of each arrow respectively. When the matrix indices are not in agreement with the arrow indices we write a minus sign. Moreover, the quiver diagram must be free of *source* and *sink* configurations where source (sink) is a node with all incident arrows outgoing (incoming); this fixes an overall orientation of the quiver which we

choose as counter-clockwise. Now, the kernel of a 3×3 antisymmetric matrix is always one dimensional, and for the given case the basis vector of $\ker(q_3)$ is simply

$$d = \begin{pmatrix} a_{23} \\ a_{31} \\ a_{12} \end{pmatrix} \ . \tag{4.2}$$

Beta functions: Next, we require the beta functions for each coupling present in the theory must vanish. The numerators of the beta functions are given by the $SU(N)$ NSVZ formula [103], which for the ith block reads

$$\beta_i = N_i + \sum_{A \in \text{adj}[i]} N_i(r_{A,i} - 1) + \frac{1}{2} \sum_{B \in \text{bifund}[i,j]} N_j(r_{B,ij} - 1) \ , \tag{4.3}$$

where r is the R-charge of the fields, which are adjoints (adj) or bi-fundamentals (bifund). Of course, we only have bi-fundamentals here. Note that for our purpose, considering the numerators of the beta functions is enough, since the vanishing of the numerators is equivalent to the vanishing of the whole fraction, given that the denominator is finite.
Furthermore, in [104], it was shown that in a $(3+1)$-dimensional conformal field theory the gravitational central charges c and a are equal in the large N limit, a result which was further generalized in [87] to any superconformal quiver gauge theory. There, the authors used this fact to show that there is an extra condition on the beta functions

$$\lim_{N \to \infty} \text{tr}R = \sum_i N_i \beta_i = c - a = 0 \ . \tag{4.4}$$

Gamma functions (marginality): Conformality also requires the gamma functions to vanish. Our last physical input thus is the requirement that all the operators in the superpotential are marginal at the interacting superconformal fixed point, namely that they have R-charge equal to 2. The possible operators present in the superpotential for the three-block quiver on the right of Fig. 4.1 are its cyclic paths and correspond to cubic operators collectively represented as

$$\hat{X}_{12}\hat{X}_{23}\hat{X}_{31} \ ,$$

with $\hat{X}_{ij}$ an arrow from block i to block j. The marginality condition then translates to

$$r_{12} + r_{23} + r_{31} = 2. \tag{4.5}$$

Putting together the requirement (4.5) and the vanishing of the beta functions (4.3) for the three couplings results in a system of three unknown R-charges which satisfy four equations. Condition (4.4) imposes the linear relation among the three beta functions that allows for a

solution to the system. Substituting (4.2),(4.5) in (4.4) results in an equation in terms of the quiver data:

$$\frac{a_{23}^2}{\alpha_1} + \frac{a_{31}^2}{\alpha_2} + \frac{a_{12}^2}{\alpha_3} = a_{12}a_{23}a_{31} \ . \tag{4.6}$$

This is a *Diophantine equation* in the variables a_{ij} and α_i, which are by definition integers. For $\alpha_1 = \alpha_2 = \alpha_3 = \alpha$, (4.6) reduces to the well-studied *Markov equation*. This equation has solutions over $\mathbb{Z}$ which can be organized in a *tree* (cf. [102]). This also holds for generic values of $\alpha_1, \alpha_2, \alpha_3$. More specifically, given a solution (a_{23}, a_{31}, a_{12}) one can construct an infinite set of solutions by the following operations:

$$(a_{23}, a_{31}, a_{12}) \to \begin{cases} (\alpha_1 a_{12}a_{31} - a_{23}, a_{31}, a_{12}) \\ (a_{23}, \alpha_2 a_{12}a_{23} - a_{31}, a_{12}) \\ (a_{23}, a_{31}, \alpha_3 a_{23}a_{31} - a_{12}) \end{cases} . \tag{4.7}$$

In [46, 47, 102] it was shown how Seiberg duality can be represented as a quiver duality which can be described as follows: Pick a node to dualize, say node k; define three sets of arrows, $Q_{\text{in}}, Q_{\text{out}}$ and $Q_{\bar{k}}$ containing incoming, outgoing and non incident arrows with respect to the duality vertex; change the orientation of all arrows in $Q_{\text{in}} \cup Q_{\text{out}}$; change the arrows in $Q_{\bar{k}}$ as $a_{ij} \mapsto a_{ij} - a_{ik}a_{kj}$. Now recall that anomaly cancellation forces the rank of each node to be proportional to the number of its non incident arrows. This condition in combination with the operations described above, correctly reproduce the rank of the dualized node as $N_C^{\text{dual}} = N_F - N_C$, where the number of flavors of the vertex k is defined as

$$N_F = \sum_{a_{jk} \in Q_{\text{in}}} a_{jk}x_j = \sum_{a_{kj} \in Q_{\text{out}}} a_{kj}x_j. \tag{4.8}$$

Note that the transformation (4.7) exactly matches the operations induced by Seiberg duality. Thus, the latter can be described as the action of the automorphism group on the Markov tree; we will return to this point on Seiberg duality in the next section. In [87] the solutions corresponding to the "roots" of the duality trees for generic values of the node multiplicities were found to be corresponding to all the three-block del Pezzo and pseudo del Pezzo quivers, as well as two new non-del Pezzo quivers which were dubbed "shrunk", for it was shown that they arise from a specific operation (shrinking) on the block quiver.

4.2.2 The Markov Equation and the Adjacency Matrix

Let us now put the Diophantine equation in a form that will be relevant for our investigations later. Recall that the $\{i, j\}$-th first minor M_{ij} of an $n \times n$ matrix, is the determinant of the submatrix with row i and column j deleted while the $\{i, j\}$-th cofactor is given by $C_{ij} =$

$(-)^{i+j}M_{ij}$. Because of the anti-symmetry of q_3, given in (4.1), one can see that its minors are quadratic in the edge multiplicities and the matrix of minors assumes the following simple form:

$$M = \{M_{ij}\} = \begin{pmatrix} a_{23}^2 & -a_{31}a_{23} & a_{12}a_{23} \\ -a_{31}a_{23} & a_{31}^2 & -a_{12}a_{31} \\ a_{12}a_{23} & -a_{12}a_{31} & a_{12}^2 \end{pmatrix} . \tag{4.9}$$

Now, the Diophantine equation (4.6) can be written as a sum over the cofactors of the adjacency matrix, weighted by the respective elements of the quiver matrix and the block multiplicities α_i. That is, equation (4.6) can be represented as

$$\sum_i C_{ii} \prod_{n \neq i} \alpha_n - \sum_{i<j} q_3(i,j) C_{ij} \prod_n \alpha_n = 0 \ , \tag{4.10}$$

where the indices run in $\{1, 2, 3\}$. The reason for writing the Markov equation in this form will become evident in the next subsection where we clarify its origin using representation theoretic concepts, while in Section 4.3 we show that it is a general formula that applies for an arbitrary odd number of blocks and derive an analogous one for even numbers.

Note that this construction, surprisingly suggests that all the physical input of superconformality is somehow hidden in the adjacency matrix. For example, this formula does not require either the superpotential to be marginal or the beta function for every coupling to vanish. The summation over minors automatically ensures these features!

4.2.3 The Markov Equation and the Tits Form

Equation (4.6) has been derived in different contexts and via different routes. In the mathematics literature, using complete exceptional collections of coherent sheaves over del Pezzo surfaces [53], it was derived as a Diophantine equation which the ranks of the exceptional sheaves should satisfy. In [54, 55, 105, 106] these results were independently re-derived and linked with quiver gauge theories and Seiberg duality thereof, while in [107] this equation was derived using monodromy.

In this subsection we will show how the generalized Markov equation is related to the Tits form of the quiver. For the sake of completeness we begin by briefly reviewing the basic facts about bilinear forms associated with quivers. A nice place where the interested reader can look for further background material on bilinear forms and the Tits form is [108] and references therein.

Bilinear Forms on Quivers Given a quiver $\mathbf{Q} = (\mathbf{Q_0}, \mathbf{Q_1})$, where $\mathbf{Q_0}$ denotes the set of vertices and $\mathbf{Q_1}$ the set of arrows, one can define a *representation* of $\mathbf{Q}$ as the assignment of a vector space V_i to each vertex $i \in \mathbf{Q}_0$ and a linear map $V_\rho : \ V_{t_{(\rho)}} \mapsto V_{h_{(\rho)}}$ to each arrow $\rho \in \mathbf{Q}_1$, with the subscripts t and h denoting the tail and the head of an arrow respectively. We call the vector $\{\mathrm{dim}V_i\}$ the *representation vector* of the quiver. A *path algebra*, with the product operation given by concatenation of arrows, can be associated to a quiver. In the cases that we consider here there is also a set of algebraic relations $\mathcal{F}$, that the arrows obey, which come from the F-terms (superpotential) of the gauge theory. Quivers with such relations are called *bounded*. The quotient of the path algebra by $\mathcal{F}$ yields the so-called $\mathcal{F}$*-flat* or *Jacobian algebra* A of $\mathbf{Q}$.

On the modules of A, we can define the *Euler form* as the alternating bilinear form given by

$$\langle \mathrm{dim}M, \mathrm{dim}N \rangle = \sum_{i=0}^{\infty} (-)^i \mathrm{dimExt}^i(M, N) \ , \tag{4.11}$$

where M, N are A-modules.

In the case of an unbounded quiver, that is, one with no superpotential, the only non zero Ext groups are those for $i = 0, 1$. Hence the Euler form can be reduced to the bilinear form, $\langle -, - \rangle : \mathbb{Z}\mathbf{Q_0} \times \mathbb{Z}\mathbf{Q_0} \mapsto \mathbb{Z}$, presented as

$$\langle \mathbf{x}, \mathbf{y} \rangle = \sum_{i \in \mathbf{Q_0}} x_i y_i - \sum_{\rho \in \mathbf{Q_1}} x_{t(\rho)} y_{h(\rho)} \ , \tag{4.12}$$

where $\mathbf{x} \equiv \{\mathrm{dim}V_i\}$. The symmetrization of (4.12), referred to as the *Cartan form*, can be written as

$$(\mathbf{x}, \mathbf{y}) = \langle \mathbf{x}, \mathbf{y} \rangle + \langle \mathbf{y}, \mathbf{x} \rangle = \mathbf{x}^T C_Q \mathbf{y} \ , \tag{4.13}$$

where $C_Q = (c_{i,j})_{i,j \in \mathbf{Q_0}}$ is a symmetric $|\mathbf{Q_0}| \times |\mathbf{Q_0}|$ generalized Cartan matrix with $\mathbb{Z}$ valued entries, given by

$$c_{i,j} = \begin{cases} 2 - 2\#(\text{loops at } i), & \text{if} \quad i = j \\ -\#\text{arrows between } i \text{ and } j, & \text{if} \quad i \neq j \end{cases} \tag{4.14}$$

Last, we define the *Tits form* which is the quadratic form associated with the Euler form,

$$q_{\mathbf{Q}}(\mathbf{x}) \equiv (\mathbf{x}, \mathbf{x}) = \sum_{i \in \mathbf{Q_0}} x_i^2 - \sum_{\rho \in \mathbf{Q_1}} x_{t(\rho)} x_{h(\rho)} = \frac{1}{2} \mathbf{x}^T C_Q \mathbf{x} \tag{4.15}$$

We are now in a position to relate these concepts to the block quivers. In order to make use of the Tits form for our case, we first have to ensure that the higher Ext groups do indeed vanish. In [53, 54], it was shown that the three-block quivers studied here can be represented by exceptional collections of sheaves over del Pezzo surfaces, which by definition have all the

higher Ext groups vanishing, as desired. Therefore, the Tits form for the three-block case of Fig. 4.1 using the adjacency matrix (4.1) reads:

$$\begin{aligned} q_Q(\mathbf{x}) = q_Q(x_1, x_2, x_3) &\equiv \sum_{i \in \mathbf{Q}_0} x_i^2 - \sum_{i<j} |q_3(i,j)| x_i x_j \\ &= \alpha_1 x_1^2 + \alpha_2 x_2^2 + \alpha_3 x_3^2 - a_{12} x_1 x_2 \alpha_1 \alpha_2 - a_{23} x_2 x_3 \alpha_2 \alpha_3 - a_{31} x_1 x_3 \alpha_1 \alpha_3 \end{aligned} \tag{4.16}$$

The Markov equation though is given by a slightly modified form. For that, let us consider an orientation dependent version of (4.16), which we call q_{Q_s} (s for "signed"), without the absolute value in the adjacency matrix elements. As we immediately show this form yields the desired Diophantine equation whose roots label superconformal gauge theories. We then connect q_{Q_s} with the Tits form q_Q. For the three-block case it reads:

$$\begin{aligned} q_{Q_s}(\mathbf{x}) = q_Q(x_1, x_2, x_3) &\equiv \sum_{i \in \mathbf{Q}_0} x_i^2 - \sum_{i<j} q_3(i,j) x_i x_j \\ &= \alpha_1 x_1^2 + \alpha_2 x_2^2 + \alpha_3 x_3^2 - a_{12} x_1 x_2 \alpha_1 \alpha_2 - a_{23} x_2 x_3 \alpha_2 \alpha_3 + a_{31} x_1 x_3 \alpha_1 \alpha_3 . \end{aligned} \tag{4.17}$$

After setting

$$x_1 = \sqrt{\frac{\alpha_2 \alpha_3}{\alpha_1 K^2}} a_{23} \ , \ x_2 = \sqrt{\frac{\alpha_1 \alpha_3}{\alpha_2 K^2}} a_{31} \ , \ x_3 = \sqrt{\frac{\alpha_1 \alpha_2}{\alpha_3 K^2}} a_{12}, \tag{4.18}$$

where $K^2 = 12(9) - (\alpha_1 + \alpha_2 + \alpha_3)$ for a del Pezzo(non del Pezzo) quiver [53, 87] ensures that $x_i \in \mathbb{Z}$, we are left precisely with the Markov equation (4.6)! These conditions are exactly those found in [53] (cf. Sec 3) in the context of exceptional collections of sheaves and coincide with the anomaly cancellation (4.2). Going back to the matrix of minors (4.9), we immediately see that setting $q_{Q_s} = 0$ yields the minor summation formula (4.10) with $C_{ij} = x_i x_j$.

Now, by adding and subtracting the term $a_{31} x_1 x_3 \alpha_1 \alpha_3$ to (4.16), we obtain $q_Q = q_{Q_s} - 2a_{31} x_1 x_3 \alpha_1 \alpha_3$. Using the fact that we are looking for solutions of the Markov equation, i.e. $q_{Q_s} = 0$, we see that the dimension vector of a superconformal quiver gauge theory satisfies

$$q_Q(x_1, x_2, x_3) = -2|q(3,1)| \alpha_1 \alpha_3 x_1 x_3 \ . \tag{4.19}$$

Using the relations (4.18) this equation can be rewritten as

$$q_Q(x_1, x_2, x_3) = -2\sqrt{\alpha_1 \alpha_2 \alpha_3 K^2} x_1 x_2 x_3 \ . \tag{4.20}$$

with $\sqrt{\alpha_1 \alpha_2 \alpha_3 K^2} \in \mathbb{Z}$. Thus, we arrive at the conclusion that *the dimension vectors of superconformal gauge theories have a negative Tits form*[1].

The Tits form is important because it defines the *type* of a quiver: positive definite, positive semi-definite and indefinite correspond respectively to finite, tame and wild types (cf. [84]).

[1] See [109] for the appearance of the Tits form in $\mathcal{N} = 2$ quivers.

Moreover, together with its extension given by Kac, the Tits form provides the link between quiver representations and root systems.

We can associate the dimension vector (i.e., the vector whose entries are the ranks of the gauge group factors) to a root of the root system of the underlying quiver and the Cartan form (4.13) to the inner product on the root space. The Tits form is therefore the norm-squared of a root vector. It is a celebrated theorem of Kac (see App. D.1.1) that real roots correspond to quivers with exactly one indecomposable representation and the norm-squared of the dimension vector is equal to 1; in contrast, imaginary roots correspond to the case where there are families of indecomposable representations and the norm-squared is less than or equal to 0.

In light of Kac's theorem the fact that we have a negative norm means that our choices of dimension vectors, imposed by superconformality, correspond to imaginary roots of the root system associated with the quiver. The ranks of superconformal gauge theories form the subset of such dimension vectors that satisfy (4.19). It would be very interesting to see if these physically special quiver representations also have special algebraic properties[2] which could shed some light in the study of wild quivers. Since very little is known on that subject we will not try to address this question here, but will leave it as an interesting comment.

4.2.4 Seiberg Duality and the Affine Weyl Group

In [98] Seiberg duality was interpreted as the action of the affine Weyl group on the root system of an (affine) A-D-E type quiver diagram. As we now show, in our construction this result can be generalized to arbitrary three-block quivers. We will later see that this statement actually holds for any odd block number. Before discussing that let us briefly remind the reader how one defines the *Weyl group* of the root system associated to a quiver $\mathbf{Q}$ and connects it with the classification scheme of finite-tame-wild. The idea behind this construction is to think of the vector space spanned by the dimension vectors of the quiver as a root space of the algebra associated with the quiver.

For simplicity we write the vertex set as $\mathbf{Q}_0 = \{1, 2, ..., n\}$ and denote the corresponding basis of $\mathbb{Z}\mathbf{Q_0}$ as $\mathbf{e_1}, ..., \mathbf{e_n}$. For each vertex $i \in \mathbf{Q_0}$ define an element $r_i \in \mathrm{Aut}(\mathbb{Z}\mathbf{Q_0})$ whose action on a dimension vector $\mathbf{x} \in \mathbb{Z}\mathbf{Q_0}$ reads

$$r_i[\mathbf{x}] = \mathbf{x} - 2\frac{(\mathbf{x}, \mathbf{e_i})}{(\mathbf{e_i}, \mathbf{e_i})}\mathbf{e_i} = \mathbf{x} - (\mathbf{x}, \mathbf{e_i})\mathbf{e_i} \tag{4.21}$$

[2] An example of a root with a special property is a so called *Schur* root, which corresponds to a dimension vector of an indecomposable representation [83].

where the inner product $(-,-)$ is given by the Cartan form (4.13). If there are no loops at vertex i then we call r_i a simple reflection and $\mathbf{e_i}$ a simple root. One can easily check that a simple reflection leaves the Tits form (4.15) invariant. The Weyl group $W(Q)$ of the quiver is defined as the subgroup of $\mathrm{Aut}(\mathbb{Z}\mathbf{Q_0})$ generated by the simple reflections r_i.

Let us now adapt this discussion in the three-block quivers depicted in Fig. 4.1 and see how Seiberg duality arises in this context. Note that since we allow for arbitrary number of arrows between two nodes, we are not restricted to an A-D-E quiver diagram. To illustrate the idea with a simple example, we first focus in the case where all block multiplicities α_i are set to one, and we will then generalize to arbitrary numbers. By writing the Tits form (4.16) as

$$(\mathbf{x},\mathbf{x}) = \frac{1}{2}\mathbf{x}^T C_Q \mathbf{x}$$

one can read off the Cartan matrix of a three-block quiver. That is:

$$C_Q = \begin{pmatrix} 2 & -a_{12} & -a_{31} \\ -a_{12} & 2 & -a_{23} \\ -a_{31} & -a_{23} & 2 \end{pmatrix} \tag{4.22}$$

In general, one can define a Cartan matrix as $C = 2\mathbb{I} - q$, where q is the adjacency matrix defined irrespectively of the orientation of the arrows. In our case we have defined q_3 as the antisymmetrized adjacency matrix (4.1), hence this relation does not hold. The Cartan matrix is symmetric, so it is associated to a simply-laced algebra, and it can be easily shown that it is indefinite. That is it has both positive and negative principal minors. It thus describes some Kac-Moody algebra of *indefinite* type, in accordance with the fact that we are dealing with wild quivers.

To proceed, consider the reflection of a vector $\mathbf{x} = (x_1, x_2, x_3)^{\mathrm{T}}$ with respect to the simple root $\mathbf{e_1} = (1,0,0)^{\mathrm{T}}$. We have

$$r_1[\mathbf{x}] = \mathbf{x} - (2x_1 - a_{12}x_2 - a_{31}x_3)\mathbf{e_1} = \begin{pmatrix} a_{12}x_2 + a_{31}x_3 - x_1 \\ x_2 \\ x_3 \end{pmatrix}. \tag{4.23}$$

Recall that $\mathbf{x}$ is the dimension vector representing a superconformal gauge theory and Seiberg duality is described as the transformation (4.7) and the operations outlined in the paragraph right below it. In addition, the rank of the node with label "1" is $x_1 = N_{C_1}$, the number of flavors is given by (4.8) as $N_{F_1} = a_{12}x_2 = a_{31}x_3$ while the rank of the dualized node reads $N_C^{dual} = N_F - N_C$. We thus see that the top component of the right hand side of (4.23) is the

rank of the first node when Seiberg dualized, plus a shift. Therefore, we arrive at the following realization of Seiberg duality in terms of roots:

$$S_i[\mathbf{x}] = r_i[\mathbf{x}] - N_{F_i}\mathbf{e_i}, \tag{4.24}$$

where $S_i[\mathbf{x}]$ denotes Seiberg duality of the quiver gauge theory $\mathbf{x}$ with respect to node "i". Such an operation is known as an *affine reflection*. As we now show, affine reflections leave the Markov equation invariant. Let us demonstrate that by computing the Diophantine equation for the dualized quiver with block multiplicities equal to one. Recall that the Markov equation can be written (cf. (4.19)) in the form

$$(\mathbf{x}, \mathbf{x}) = -2\sqrt{K^2}\prod_j x_j.$$

Using (4.24) we find that the norm-squared of a vector dualized with respect to block "i" reads

$$(S_i[\mathbf{x}], S_i[\mathbf{x}]) = -2\sqrt{K^2}x_i'\prod_{j\neq i} x_j, \tag{4.25}$$

where $x_i' = a_{ij}x_j - x_i = N_{F_i} - N_{C_i}$. This nicely demonstrates that the subset of roots that correspond to superconformal gauge theories is closed under Seiberg duality. In other words, this results asserts that superconformal gauge theories are special roots of the quiver algebra and Seiberg duality corresponds to the action of the affine Weyl group on the root system.
We now repeat the discussion for generic three-block quivers. Had we followed the same method as right above we would have ended up with a Cartan matrix of the form

$$C_Q = \begin{pmatrix} 2\alpha_1 & -\alpha_1\alpha_2 a_{12} & -\alpha_1\alpha_3 a_{31} \\ -\alpha_1\alpha_2 a_{12} & 2\alpha_2 & -\alpha_2\alpha_3 a_{23} \\ -\alpha_1\alpha_3 a_{31} & -\alpha_2\alpha_3 a_{23} & 2\alpha_3 \end{pmatrix}. \tag{4.26}$$

Recall that a Cartan matrix should have 2's in the diagonal. The α_i factors in (4.26) are due to the block reduction of the quiver. In order to construct the correct C_Q, we should instead consider the nodes in each block as independent entries in the adjacency matrix. By doing that we obtain a matrix of dimension $\sum_i \alpha_i \times \sum_i \alpha_i$ with the desired property. In other words we consider the Tits form as $(\sum \alpha_i)$-ary quadratic form, where the first α_1 variables degenerate to x_1, the second α_2 to x_2 and the last α_3 to x_3. We therefore have

$$C_Q = \left(\begin{array}{ccc|ccc|ccc} & & & -a_{12} & \dots & -a_{12} & -a_{13} & \dots & -a_{13} \\ & 2\mathbb{I}_{\alpha_1} & & \vdots & \ddots & \vdots & \vdots & \ddots & \vdots \\ & & & -a_{12} & \dots & -a_{12} & -a_{13} & \dots & -a_{13} \\ \hline -a_{12} & \dots & -a_{12} & & & & -a_{23} & \dots & -a_{23} \\ \vdots & \ddots & \vdots & & 2\mathbb{I}_{\alpha_2} & & \vdots & \ddots & \vdots \\ -a_{12} & \dots & -a_{12} & & & & -a_{23} & \dots & -a_{23} \\ \hline -a_{13} & \dots & -a_{13} & -a_{23} & \dots & -a_{23} & & & \\ \vdots & \ddots & \vdots & \vdots & \ddots & \vdots & & 2\mathbb{I}_{\alpha_3} & \\ -a_{13} & \dots & -a_{13} & -a_{23} & \dots & -a_{23} & & & \end{array}\right), \tag{4.27}$$

The basis vector, with respect to which we are going to reflect, is $\mathbf{a} = (0, \dots, 0, \underbrace{1, \dots, 1}_{\alpha_i}, 0, \dots, 0)$ with ones in the i-th α_i entries and zeros in the rest. This corresponds to duality of block i. The norm of this root is given by $(\mathbf{a}, \mathbf{a}) = 2\alpha_i$. The inner product of a generic vector $\mathbf{x} = (\underbrace{x_1, \dots, x_1}_{\alpha_1}, \underbrace{x_2, \dots, x_2}_{\alpha_2}, \underbrace{x_3, \dots, x_3}_{\alpha_3})$ with $\mathbf{a}$ is given by

$$(\mathbf{x}, \mathbf{a}) = \alpha_i(2x_i - a_{ij}\alpha_j x_j - a_{ik}\alpha_k x_k)$$

where j, k index the other two blocks. Using the definition of the flavour number, this expression reads

$$(\mathbf{x}, \mathbf{a}) = 2\alpha_i(N_{C_i} - N_{F_i}) \tag{4.28}$$

Using the reflection formula (4.21) we see that (4.24) generalizes to

$$S_i[\mathbf{x}] = r_i[\mathbf{x}] - N_{F_i}\mathbf{a}, \tag{4.29}$$

and computing the norm of the dualized vector, we find that it obeys the relation

$$(S_i[\mathbf{x}], S_i[\mathbf{x}]) = (\mathbf{x}, \mathbf{x}) - 2\alpha_i N_{F_i}(N_{C_i} - N'_{C_i}). \tag{4.30}$$

Using (4.20) we arrive at the following result

$$(S_i[\mathbf{x}], S_i[\mathbf{x}]) = -2\sqrt{\alpha_1\alpha_2\alpha_3 K^2}\, x'_i \prod_{j\neq i} x_n. \tag{4.31}$$

That is, Seiberg duality corresponds to an affine Weyl reflection for any three-block quiver, where duality with respect to block "i" maps to reflection with respect to the vector $\mathbf{a}$ with ones in the i-th α_i entries and zeros in the rest.

Summary: In this section we reviewed the concept of block quivers and re-derived results well-known in both the mathematics and the physics literature for the case of three-block quivers. We have shown that conformality of the gauge theory, which the quiver encodes, and anomaly cancellation place constraints on the adjacency and rank data of the quiver, in the form of a Diophantine equation. For three-blocks, this is a (generalized) Markov equation.
We then recalled standard techniques of representation theory of quivers. In particular, we used the Tits bilinear form defined on the space of dimension vectors - or root space - of the quiver. We showed that a signed version of the Tits form is precisely the aforementioned Diophantine equation. This allowed for a correspondence between superconformal gauge theories and root vectors of the quiver's root system. In the ensuing section, we will see that our results persist for an arbitrary quiver.

Finally, on quiver theories in our context, there is the famous Seiberg duality action. We saw that this translates to an affine Weyl reflection on the root space and the Diophantine equation remains invariant. This is in accord with the fact the duality tree of Seiberg-dual theories are classified by solutions of our Diophantine equation [102].

4.3 New Results for Higher Block Number

Having reviewed the three-block case under a new perspective, one naturally wonders how to proceed to higher number of blocks. In this section we will generalize our previous discussion to four- and five-block quivers and then conjecture the form of the superconformality conditions for any number of blocks.

4.3.1 Four-Block Models

Now, the four-block situation was also addressed in [87] and we refer the reader to the classification therein. We remark that because for $n = 4$, there is a unique choice to draw a quiver with no sink or source configurations. Furthermore, since we have an antisymmetric matrix of even dimension as the reduced adjacency matrix, the determinant does not vanish automatically and the situation is a little more difficult to regard it fully in terms of our quadratic form analysis. We are able though to unravel a similar structure as a sum of minors for the four block case as well. The adjacency matrix that we will consider is

$$q_4 = \begin{pmatrix} 0 & a_{12} & -a_{13} & -a_{14} \\ -a_{12} & 0 & a_{23} & -a_{24} \\ a_{13} & -a_{23} & 0 & a_{34} \\ a_{14} & a_{24} & -a_{34} & 0 \end{pmatrix}, \tag{4.32}$$

such that

$$\det q_4 = a_{41}a_{23} + a_{31}a_{42} - a_{12}a_{34} = 0, \tag{4.33}$$

as required for anomaly cancellation. The 3×3 first minors of the adjacency matrix vanish since they are proportional to $\det q_4$. Therefore let us consider the 2×2 second minors of (4.32) where a second minor $M_{ij,kl}$ is defined as the determinant of the submatrix that results if one removes the i, j rows and the k, l columns of the original matrix. The relevant minor matrix for our case is

$$M_{q_4} = \begin{array}{c} \\ 12 \\ 13 \\ 14 \\ 23 \\ 24 \\ 34 \end{array} \begin{array}{c} \begin{array}{cccccc} 12 & 13 & 14 & 23 & 24 & 34 \end{array} \\ \begin{pmatrix} a_{34}^2 & -a_{24}a_{34} & a_{23}a_{34} & -a_{14}a_{34} & -a_{13}a_{34} & a_{12}a_{34} \\ -a_{24}a_{34} & a_{24}^2 & -a_{23}a_{24} & a_{14}a_{24} & a_{13}a_{24} & -a_{12}a_{24} \\ a_{23}a_{34} & -a_{23}a_{24} & a_{23}^2 & -a_{14}a_{23} & -a_{13}a_{23} & a_{12}a_{23} \\ -a_{14}a_{34} & a_{14}a_{24} & -a_{14}a_{23} & a_{14}^2 & a_{13}a_{14} & -a_{12}a_{14} \\ -a_{13}a_{34} & a_{13}a_{24} & -a_{13}a_{23} & a_{13}a_{14} & a_{13}^2 & -a_{12}a_{13} \\ a_{12}a_{34} & -a_{12}a_{24} & a_{12}a_{23} & -a_{12}a_{14} & -a_{12}a_{13} & a_{12}^2 \end{pmatrix} \end{array}, \tag{4.34}$$

where the outer column and row indicate the set of rows and columns of the adjacency matrix that are deleted in order to obtain the corresponding element of the minor matrix, e.g. $M_{q_4}(2,3) \equiv M_{13,14} = -a_{23}a_{24}$. The Diophantine equation whose solutions are in one to one correspondence with the superconformal four-block quivers can be written as

$$\sum_{i<j} M_{ij,ij} \prod_{m\neq i,j} \alpha_m - \sum_{i\neq j<k} (-)^{j+k} q_4(j,k) M_{ij,ik} \prod_{m\neq i} \alpha_m + \sum_{i<j<k<l} q_4(i,j) q_4(i,l) M_{ij,il} \prod_m \alpha_m = 0 \tag{4.35}$$

supplemented by (4.33), where α_i denotes the multiplicity of the i-th block and the indices run in $\{1,2,3,4\}$. By substituting the minors one recovers the Diophantine equation reported in [87],

$$\begin{aligned} \frac{a_{12}^2}{\alpha_3\alpha_4} + \frac{a_{13}^2}{\alpha_2\alpha_4} + \frac{a_{14}^2}{\alpha_2\alpha_3} + \frac{a_{23}^2}{\alpha_1\alpha_4} + \frac{a_{24}^2}{\alpha_1\alpha_3} + \frac{a_{34}^2}{\alpha_1\alpha_2} + \frac{a_{12}a_{24}a_{14}}{\alpha_3} - \frac{a_{12}a_{23}a_{13}}{\alpha_4} \\ + \frac{a_{13}a_{34}a_{14}}{\alpha_2} - \frac{a_{23}a_{34}a_{24}}{\alpha_1} - a_{12}a_{23}a_{34}a_{14} = 0 \end{aligned} \tag{4.36}$$

Although this formula seems somehow arbitrarily written there is a check for its validity and that is the way it reduces to the three-block equation. Let us see what happens when we remove the block with label one for example. This corresponds to the deletion of the first column and first row of the adjacency matrix q_4, leaving us with a three-block model adjacency matrix identical to q_3 in (4.1), while we also set α_1 to zero. From the sum (4.35) we see that the only terms remaining are the ones that are not multiplied by α_1. These are,

$$\begin{aligned} M_{12,12}\alpha_3\alpha_4 \;&+\; M_{13,13}\alpha_2\alpha_4 + M_{14,14}\alpha_2\alpha_3 \\ &+\; \Big(q_4(2,3)M_{12,13} - q_4(2,4)M_{12,14} + q_4(3,4)M_{13,14}\Big)\alpha_2\alpha_3\alpha_4 = 0 \end{aligned} \tag{4.37}$$

Now the remaining elements of q_4 become entries of q_3 as $q_4(i,j) \mapsto q_3(i-1,j-1)$ while the 2×2 minors of q_4 become the first minors of q_3 and together with the sign $(-)^{j+k}$ yield the cofactors of q_3 as $(-)^{j+k}M^{(q_4)}_{ij,ik} \mapsto C^{(q_3)}_{j-1,k-1}$. Having this relation in mind one can immediately see that the formula (4.35) correctly reduces to (4.10)! In the next paragraph we will see that the five-block Diophantine equation is identical to the three-block one. This statement, in combination with the fact that the reduction from four to three blocks can be demonstrated using the minor sum, implies that the formula (4.35) holds also for six-block quivers where again a summation of second minors should classify conformal theories. Thus, one can justifiably extrapolate this claim to any even number of blocks.

In this case though the relation with a bilinear form on the quiver is not clear. Since the summation over minors suggests a continuation from the three blocks, it is natural to think that an analogous perspective would be valid for the four blocks too. We leave this investigation for future work.

4.3.2 Five-Block Models

Let us move on to the next case of $n = 5$. We are looking for quivers with five blocks where there are no sink or source configurations. We will readily see that we now encounter a new situation. For $n = 3, 4$, the possible topologies of such graphs were unique, but this is not the case for order five and higher. Hence one has to count all such connected sinkless-sourceless graphs and mod out by topological equivalence, where we consider two graphs equivalent if they are related by a permutation of the edges and nodes.

4.3.2.1 The Inequivalent Graphs

We find six equivalence classes, the representatives of which we refer to as Type I to VI. We draw them in Fig. 4.2 and we also list the oriented cycles which correspond to operators in the superpotential. The cycle structure of the six types is summarized as follows (outdegree refers to the number of arrows going out of the node):

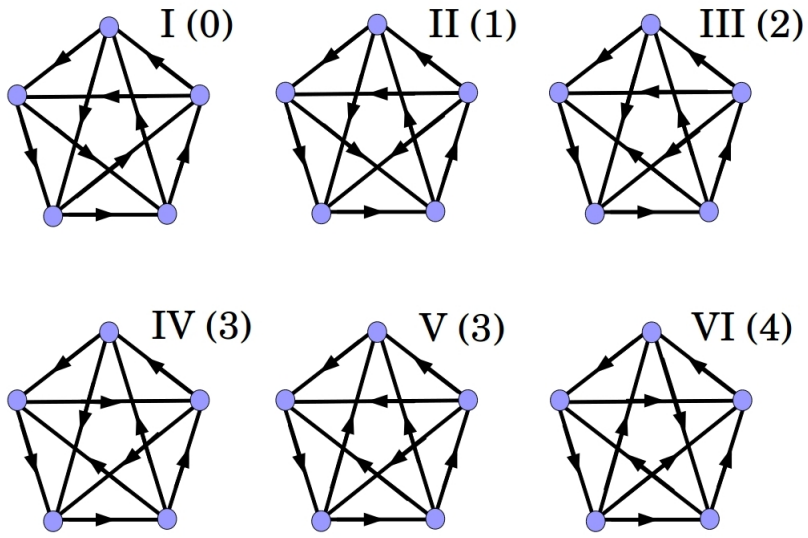

Figure 4.2: The six inequivalent chiral five-block quivers. The numbers in brackets indicate the number of clockwise internal (the ones not in the perimeter of the pentagon) arrows.

Cycle counting

- Type I: clockwise outdegrees (starting from mid top) $(2, 2, 2, 2, 2)$; 12 cycles; 2 quintics, 5 quartics, 5 cubics
- Type II: clockwise outdegrees $(2, 3, 2, 1, 2)$; 9 cycles; 1 quintic, 4 quartics, 4 cubics
- Type III: clockwise outdegrees $(2, 3, 3, 1, 1)$; 7 cycles; 1 quintic, 3 quartics, 3 cubics
- Type IV: clockwise outdegrees $(2, 2, 3, 1, 2)$; 10 cycles; 3 quintics, 3 quartics, 4 cubics
- Type V: clockwise outdegrees $(1, 3, 3, 2, 1)$; 6 cycles; 1 quintic, 2 quartics, 3 cubics
- Type VI: clockwise outdegrees $(2, 1, 2, 3, 2)$; 9 cycles; 2 quintics, 3 quartics, 4 cubics

4.3.2.2 Detailed Analysis of Type I

Let us begin with a detailed analysis of Type I, whose block quiver is given in Figure 4.3. As in the three-block case we are going to impose the following conditions:

1. anomaly cancellation: the dimension vector lies in the kernel of the quiver reduced adjacency matrix q_5;
2. beta functions: the weighted sum of the beta functions vanish;
3. gamma functions: R-charge of each cycle sums to 2.

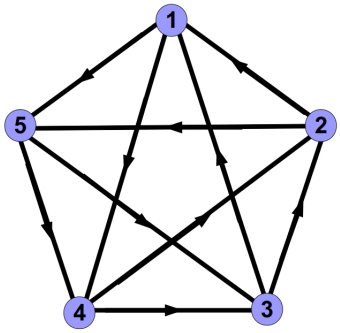

Figure 4.3: The quiver for Type I of the five-block theory.

Now, following our previous notation, the adjacency matrix is

$$q_5 = \begin{pmatrix} 0 & a_{12} & a_{13} & -a_{41} & -a_{51} \\ -a_{12} & 0 & a_{23} & a_{24} & -a_{52} \\ -a_{13} & -a_{23} & 0 & a_{34} & a_{35} \\ a_{41} & -a_{24} & -a_{34} & 0 & a_{45} \\ a_{51} & a_{52} & -a_{35} & -a_{45} & 0 \end{pmatrix} . \tag{4.38}$$

The first condition then reads (recall that the rank is $N_i = Nx_i$):

$$q_5 \cdot (\alpha_1 x_1, \alpha_2 x_2, \alpha_3 x_3, \alpha_4 x_4, \alpha_5 x_5)^\top = \mathbf{0} \ , \tag{4.39}$$

which translates to

$$\begin{aligned} \alpha_1 x_1 &\propto a_{45}a_{23} - a_{35}a_{24} - a_{52}a_{34} \equiv A_1 \\ \alpha_2 x_2 &\propto a_{51}a_{34} - a_{45}a_{13} - a_{41}a_{35} \equiv A_2 \\ \alpha_3 x_3 &\propto a_{45}a_{12} - a_{51}a_{24} - a_{41}a_{52} \equiv A_3 \\ \alpha_4 x_4 &\propto a_{23}a_{51} - a_{35}a_{12} - a_{13}a_{52} \equiv A_4 \\ \alpha_5 x_5 &\propto a_{34}a_{12} - a_{41}a_{23} - a_{13}a_{24} \equiv A_5. \end{aligned} \tag{4.40}$$

Note that these equations can be nicely summarized in the following form

$$A_{i_1} = \frac{1}{8}\epsilon_{i_1 i_2 i_3 i_4 i_5} a_{i_2 i_3} a_{i_4 i_5}. \tag{4.41}$$

Next, using the NSVZ numerators for the beta functions, we find

$$\begin{aligned}
\beta_1 &= Nx_1+\frac{N}{2}\Big(A_5a_{51}(r_{51}-1)+A_4a_{41}(r_{41}-1)+A_3a_{13}(r_{13}-1)+A_2a_{12}(r_{12}-1)\Big)\\
\beta_2 &= Nx_2+\frac{N}{2}\Big(A_1a_{12}(r_{12}-1)+A_5a_{52}(r_{52}-1)+A_4a_{24}(r_{24}-1)+A_3a_{23}(r_{23}-1)\Big)\\
\beta_3 &= Nx_3+\frac{N}{2}\Big(A_2a_{23}(r_{23}-1)+A_1a_{13}(r_{13}-1)+A_5a_{35}(r_{35}-1)+A_4a_{34}(r_{34}-1)\Big)\\
\beta_4 &= Nx_4+\frac{N}{2}\Big(A_3a_{34}(r_{34}-1)+A_2a_{24}(r_{24}-1)+A_1a_{41}(r_{41}-1)+A_5a_{45}(r_{45}-1)\Big)\\
\beta_5 &= Nx_5+\frac{N}{2}\Big(A_1a_{51}(r_{51}-1)+A_2a_{52}(r_{52}-1)+A_3a_{35}(r_{35}-1)+A_4a_{45}(r_{45}-1)\Big).
\end{aligned} \tag{4.42}$$

Finally, since our graph has twelve oriented cycles which could contribute to the superpotential, we have twelve equations that the R-charges of the various operators should satisfy in order to have total R-charge equal to two for each cycle. These are:

$$r_{12}+r_{23}+r_{34}+r_{45}+r_{15} = 2 \tag{4.43}$$
$$r_{13}+r_{14}+r_{24}+r_{25}+r_{35} = 2 \tag{4.44}$$
$$r_{15}+r_{35}+r_{23}+r_{12} = 2 \tag{4.45}$$
$$r_{15}+r_{45}+r_{34}+r_{13} = 2 \tag{4.46}$$
$$r_{15}+r_{45}+r_{24}+r_{12} = 2 \tag{4.47}$$
$$r_{14}+r_{34}+r_{23}+r_{12} = 2 \tag{4.48}$$
$$r_{45}+r_{34}+r_{23}+r_{25} = 2 \tag{4.49}$$
$$r_{15}+r_{35}+r_{13} = 2 \tag{4.50}$$
$$r_{45}+r_{24}+r_{25} = 2 \tag{4.51}$$
$$r_{14}+r_{34}+r_{13} = 2 \tag{4.52}$$
$$r_{25}+r_{35}+r_{23} = 2 \tag{4.53}$$
$$r_{14}+r_{24}+r_{12} = 2 \tag{4.54}$$

At this point we are in a situation where we have ten unknown R-charges and seventeen equations to satisfy, the five beta functions and the twelve R-charge equations. The vanishing of the beta functions imposes a linear dependence on them reducing the total number of equations to sixteen while some of the R-charge conditions are linearly dependent on others. In order for the system to have a solution, one has to choose subsets of R-charge relations of rank six.
Therefore, for Type I five-block quivers one has to make a choice of subsets of gauge invariant operators to contribute to the superpotential. The choice can be made by suitably adjusting the couplings of the rest of the operators to zero. In other words, in the five block case superconformality imposes some form of hierarchy among the couplings of the theory. Mathematically,

this is reflected by the fact that not all of the equations (4.43) are linearly independent and they cannot all be satisfied simultaneously.

In total, there are 33 choices of subsets of rank six, each of which can be solved consistently. We list these sets in Appendix D.8. Note that each subset is required to have cardinality at least, but not exactly, six since some of the relations may be linearly dependent on others. For example the set of R-charge relations number (33) of the collection (D.8) picks out the relations (4.43),(4.45),(4.46),(4.47),(4.48),(4.49). The cubic relations are linearly dependent on these so for this choice one has to set to zero only the coupling of the quintic operator[3] (4.44).

$$y_{13524}\hat{a}_{13}\hat{a}_{35}\hat{a}_{52}\hat{a}_{24}\hat{a}_{41} \ . \tag{4.55}$$

That is,

$$y_{13524} = 0. \tag{4.56}$$

Doing this enables one to bypass the marginality condition (4.44) because this quintic term decouples from the system which now admits a solution. Putting together the requirement of the vanishing of the weighted sum of the beta functions $\sum N_i\beta_i = 0$, the anomaly cancellation (4.40) and the chosen set of marginal operators, we obtain a Diophantine equation in terms of the quiver data. We will take advantage of the discussions above and cast the equation into a quadratic form:

$$\frac{A_1^2}{\alpha_1} + \frac{A_2^2}{\alpha_2} + \frac{A_3^2}{\alpha_3} + \frac{A_4^2}{\alpha_4} + \frac{A_5^2}{\alpha_5} = a_{12}A_1A_2 + a_{34}A_3A_4 + a_{51}A_1A_5 + a_{52}A_2A_5 \ , \tag{4.57}$$

where we recall A_i from (4.40) and, in fact, $A_iA_j = C_{ij} \equiv (-)^{i+j}M_{ij}$, where C_{ij} is a cofactor and M_{ij} is the $\{i,j\}$ minor of the reduced quiver matrix q_5. The RHS of the above equation can be written in 5 ways,

$$\begin{aligned}
&a_{34}A_3A_4 + a_{51}A_1A_5 + a_{12}A_1A_2 + a_{52}A_2A_5 \\
&a_{45}A_4A_5 + a_{51}A_1A_5 + a_{23}A_2A_3 + a_{41}A_1A_4 \\
&a_{34}A_3A_4 + a_{45}A_4A_5 + a_{12}A_1A_2 + a_{35}A_3A_5 \\
&a_{34}A_3A_4 + a_{51}A_1A_5 + a_{23}A_2A_3 + a_{24}A_2A_4 \\
&a_{45}A_4A_5 + a_{12}A_1A_2 + a_{23}A_2A_3 + a_{13}A_1A_3 \ .
\end{aligned} \tag{4.58}$$

Re-organizing, as before in the three-block case, we can rewrite (4.57) as a sum over minors M_{ij} of q_5:

$$\sum_i C_{ii}\prod_{j\neq i}\alpha_j - \sum_{i<j} q_5(i,j)C_{ij}\prod_k \alpha_k = 0 \ , \tag{4.59}$$

[3]Note that a term like (4.55) represents a collection of operators in the superpotential since there are more than one node in each block.

where the indices run in $\{1,2,3,4,5\}$. Upon considering the fact that the determinant of q_5 (being an antisymmetric matrix of odd dimension) is zero and that the determinant can be expressed as an alternating sum of minors along any line or column weighted by the respective matrix elements, eq. (4.59) reduces to (4.57) with the RHS being any of (4.58). Written in this way, this five-block equation is a straightforward generalization of the one found for the three-block case.

However, this formula is correct only for this specific subset of operators and the ones that are related to it by permutations and arrow reversals as we will see in subsection 4.3.2.4. This subset is special in the sense that it is the one with maximal cardinality. In other words it is the one that requires the lowest number of couplings to be set to zero. As we previously saw, the only such coupling for this choice of simultaneously marginal operators is (4.56).
In this case, one can write the Diophantine equation as the "signed" Tits form of the quiver in complete analogy with the three-blocks:

$$q_{Q_s}(x_1,x_2,x_3,x_4,x_5) = \sum_i \alpha_i x_i^2 - \sum_{i<j} q_5(i,j)\alpha_i\alpha_j x_i x_j \ . \tag{4.60}$$

In other words the dimension vectors for which the resulting gauge theory is superconformal satisfy

$$q_Q(x_1,x_2,x_3,x_4,x_5) = -2 \sum_{i<j \mid q_5(i,j)<0} |q_5(i,j)|\alpha_i\alpha_j x_i x_j \ , \tag{4.61}$$

where q_Q is the actual Tits form (4.15) of the representation. Upon setting $x_j \propto \sqrt{\frac{\prod_{i\neq j}\alpha_i}{\alpha_j}} A_j$ one arrives at equation (4.59). The observation that the equation can be written as a sum of minors now stems from the Tits form construction. The robustness of our results for the low block numbers implies that they hold for any block quiver. Before formalizing this conjecture let us dwell more on this specific case.

Furthermore, one can go on and solve for the R-charges. Solving for the 4 out of 5 beta-functions in addition to the R-charge marginality conditions we have 10 equations and 10 unknowns. The fifth beta-function will vanish by construction since we have also imposed the

Diophantine equation. We find the following rational functions:

$$\begin{aligned}
r_{12} &= \frac{2}{A_1A_2}\Big(a_{45}\frac{A_3}{\alpha_3} - (\alpha_4 a_{34}a_{45} + a_{35})\frac{A_4}{\alpha_4} + a_{34}\frac{A_5}{\alpha_5}\Big) \\
r_{13} &= \frac{2}{A_1A_3}\Big(-a_{45}\frac{A_2}{\alpha_2} + a_{23}a_{45}A_3 + (\alpha_4 a_{24}a_{45} - a_{52})\frac{A_4}{\alpha_4} - a_{24}\frac{A_5}{\alpha_5}\Big) \\
r_{14} &= \frac{2}{A_1A_4}\Big(-a_{35}\frac{A_2}{\alpha_2} + (\alpha_3 a_{23}a_{35} - a_{52})\frac{A_3}{\alpha_3} + a_{23}a_{45}A_4 - a_{23}\frac{A_5}{\alpha_5}\Big) \\
r_{15} &= \frac{2}{A_1A_5}\Big(a_{34}\frac{A_2}{\alpha_2} - (a_{24} + \alpha_3 a_{23}a_{34})\frac{A_3}{\alpha_3} + a_{23}\frac{A_4}{\alpha_4}\Big) \\
r_{23} &= \frac{2}{A_2A_3}\Big(a_{45}\frac{A_1}{\alpha_1} + a_{51}\frac{A_4}{\alpha_4} - (\alpha_5 a_{45}a_{51} + a_{41})\frac{A_5}{\alpha_5}\Big) \\
r_{24} &= \frac{2}{A_2A_4}\Big(-a_{35}\frac{A_1}{\alpha_1} + a_{51}\frac{\alpha_3 a_{34}A_4 + \alpha_3 a_{35}A_5 - A_3}{\alpha_3} - a_{13}\frac{A_5}{\alpha_5}\Big) \\
r_{35} &= \frac{2}{A_3A_5}\Big(-a_{24}\frac{A_1}{\alpha_1} - a_{41}\frac{A_2}{\alpha_2} + a_{12}\frac{\alpha_4 a_{24}A_2 + \alpha_4 a_{34}A_3 - A_4}{\alpha_4}\Big) \\
r_{45} &= \frac{2}{A_4A_5}\Big(a_{23}\frac{A_1}{\alpha_1} - (\alpha_2 a_{23}a_{12} + a_{13})\frac{A_2}{\alpha_2} + a_{12}\frac{A_3}{\alpha_3}\Big),
\end{aligned} \tag{4.62}$$

with the remaining 2 given by the marginality conditions (4.43) and (4.45)-(4.49).

4.3.2.3 Reproducing Known Theories

Now, since we are doing a classification of consistent superconformal quivers, we need to check whether theories known in the AdS/CFT literature are special cases. In this subsection we verify that the toric quiver gauge theories constructed in [52, 94] are indeed a subclass of solutions of the Diophantine equation presented here. These models, being toric, have the same rank N in all blocks.

The requirement of equal ranks translates into setting $x = \frac{A_1}{\alpha_1} = \frac{A_2}{\alpha_2} = \frac{A_3}{\alpha_3} = \frac{A_4}{\alpha_4} = \frac{A_5}{\alpha_5}$. Then the rank of the blocks decouples from the equations as a free parameter and the anomaly cancellation condition (4.40) becomes

$$q_5 \cdot (\alpha_1, \alpha_2, \alpha_3, \alpha_4, \alpha_5)^\top = \mathbf{0} \ .$$

Since the block multiplicities should lie in the kernel of the adjacency matrix, we must require that $\alpha_i = A_i$. Then equation (4.59) reads

$$\sum_{i=1}^{5}\alpha_i - \alpha_1\alpha_2 a_{12} - \alpha_1\alpha_3 a_{13} + \alpha_1\alpha_4 a_{41} - \alpha_2\alpha_3 a_{23} - \alpha_2\alpha_4 a_{24} - \alpha_3\alpha_4 a_{34} = 0 \ , \tag{4.63}$$

with the rest of the arrows given by the relations

$$\begin{aligned} a_{51} &= \frac{\alpha_2 a_{12} + \alpha_3 a_{13} - \alpha_4 a_{41}}{\alpha_5} \quad , \quad a_{52} = \frac{\alpha_3 a_{23} + \alpha_4 a_{24} - \alpha_1 a_{12}}{\alpha_5} \\ a_{35} &= \frac{\alpha_1 a_{13} + \alpha_2 a_{23} - \alpha_4 a_{34}}{\alpha_5} \quad , \quad a_{45} = \frac{\alpha_2 a_{24} + \alpha_3 a_{34} - \alpha_1 a_{41}}{\alpha_5}. \end{aligned} \tag{4.64}$$

As can be seen from the quiver diagram these relations are nothing but the requirement of having equal number of incoming and outgoing arrows for each block. The conditions (4.64) where chosen randomly on block five since they fix all its incident arrows in terms of the others. Given these substitutions, all the cofactors of the new adjacency matrix equal the cofactor C_{55} of the initial one. This cofactor is the determinant of the four-block matrix that is obtained by deleting the fifth row and column of q_5, or in other words it represents the four-block model that arises from the five-block one when we remove the fifth node. For consistency we should therefore demand this determinant to vanish in order to descent to an anomaly free $4b$-theory if we remove a block from a $5b$-quiver. The equality of all the cofactors ensures that this will then be valid for all the 4×4 sub-determinants representing all the $4b$-models that can arise by the removal of a node.

The requirement of having $A_i = 0$ does not imply that the block multiplicities are zero as well. Indeed when deriving this relation right above, we assumed that all the minors of the adjacency matrix are non zero, meaning that its rank is $r[q_5] = 4$. By imposing the anomaly cancellation for the sub-quivers we essentially further reduce the rank of the matrix to $r[q_5] = 2$ since we impose relations for every sub-determinant to vanish. The kernel space of such a matrix is therefore 3 dimensional and an arbitrary vector reads

$$\begin{pmatrix} \alpha_1 \\ \alpha_2 \\ \alpha_3 \\ \alpha_4 \\ \alpha_5 \end{pmatrix} = \alpha \begin{pmatrix} -a_{52} \\ a_{51} \\ 0 \\ 0 \\ a_{12} \end{pmatrix} + \beta \begin{pmatrix} a_{24} \\ a_{41} \\ 0 \\ a_{12} \\ 0 \end{pmatrix} + \gamma \begin{pmatrix} a_{23} \\ -a_{13} \\ a_{12} \\ 0 \\ 0 \end{pmatrix}, \tag{4.65}$$

where α, β, γ are arbitrary positive integers. Given these substitutions for the block multiplicities the Diophantine equation finally reads

$$\begin{aligned} &\alpha\Big[- a_{52}(\alpha a_{12} a_{51} - 1) + a_{51}(\beta a_{12} a_{24} - 1) + a_{12}(\gamma a_{51} a_{23} - 1)\Big] + \\ &\beta\Big[a_{12}(\alpha a_{51} a_{24} - 1) + a_{24}(\beta a_{12} a_{41} - 1) + a_{41}(\gamma a_{12} a_{23} - 1)\Big] + \\ &\gamma\Big[a_{23}(\alpha a_{51} a_{12} - 1) + a_{12}(\beta a_{23} a_{41} - 1) - a_{13}(\gamma a_{12} a_{23} - 1)\Big] = 0, \end{aligned} \tag{4.66}$$

with the rest of the arrows given by

$$a_{34} = \frac{a_{24} a_{13} + a_{23} a_{41}}{a_{12}}, \quad a_{35} = \frac{a_{23} a_{51} - a_{13} a_{52}}{a_{12}}, \quad a_{45} = \frac{a_{24} a_{51} + a_{41} a_{52}}{a_{12}}. \tag{4.67}$$

The known del Pezzo quivers PdP_2 , dP_2^{II} , dP_3^{II} , PdP_{3b}^{II} , PdP_4 are solutions of equations (4.65),(4.66),(4.67) with $(\alpha, \beta, \gamma) = (1, 1, 1)$. For example denoting the solution vector of a model as

$$(\alpha_1, \alpha_2, \alpha_3, \alpha_4, \alpha_5; a_{12}, a_{13}, a_{41}, a_{51}, a_{23}, a_{24}, a_{52}, a_{34}, a_{35}, a_{45})$$

the quiver of the second toric phase of the dP_3 theory (see Fig. 4.4) corresponds to

$$\mathbf{v}_{dP_3}^{II} = (2, 1, 1, 1, 1; 1, 1, 1, 1, 1, 1, 0, 2, 1, 1).$$

For the sake of completeness we present the other solutions of the known superconformal del

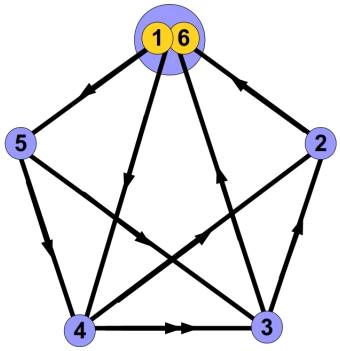

Figure 4.4: The quiver of the second toric phase of the del Pezzo 3 theory.

Pezzo quivers.

$$\begin{aligned}
\mathbf{v}_{PdP_2} &= (1, 1, 1, 1, 1; 2, 0, 1, 1, 2, 1, 1, 1, 1, 1) \\
\mathbf{v}_{dP_2}^{II} &= (1, 1, 1, 1, 1; 1, 1, 1, 1, 2, 0, 1, 2, 1, 1) \\
\mathbf{v}_{PdP_{3b}}^{II} &= (2, 1, 1, 1, 1; 1, 1, 1, 1, 1, 1, 0, 2, 1, 1) \\
\mathbf{v}_{PdP_4} &= (1, 1, 2, 2, 1; 1, 1, 1, 1, 1, 0, 1, 1, 0, 1)
\end{aligned}$$

4.3.2.4 Equivalence Classes for Type I

As previously mentioned, the five-block case is the first where one has to make a choice of simultaneously marginal operators in the superpotential. For Type I there are 33 such subsets of six linearly independent R-charge relations, listed in the Appendix (D.8), which lead to 33 Diophantine equations. Are any of these equivalent to each other? The answer is positive but unfortunately not for all. Before discussing that let us clarify what is the equivalence relation. A n-ary quadratic form can be represented by a symmetric $n \times n$ matrix as

$$q(\mathbf{x}) = \sum_{i,j=1}^{n} a_{ij} x_i x_j \equiv \frac{1}{2} \mathbf{x}^T C_q \mathbf{x} \tag{4.68}$$

where $\mathbf{x}$ is a column vector with entries $x_1 \dots x_n$ and C_q is the symmetric matrix with elements

$$C_q(i,j) = (a_{ij} + a_{ji})$$

Two forms are equivalent if their corresponding symmetric matrices are related by a similarity transformation. This is because if $C_q = S^T \cdot C_{q'} \cdot S$ then all the values of q' are determined from the values of q as $q(\mathbf{x}) = q'(S \cdot \mathbf{x})$. All the Diophantine equations can be written as quadratic forms over the variables $A_1, \dots, A_5$ defined in (4.40). We thus consider as equivalent two Diophantine equations, corresponding to two different choices of R-charge conditions, if they are equivalent as quadratic forms. This means that if one solution $\mathbf{x}_0$ of the former equation is known then a solution of the latter can be immediately written as $\mathbf{y}_0 = S \cdot \mathbf{x}_0$.

We find that there are 6 equivalence classes. Although the Diophantine equations are written as quadratic forms, the do not obey the nice structure of summation over minors, neither are their Tits forms negative definite. Since this analysis does not give any further insight into what we have already seen, we list all our results in Appendix D.2.2. In there the reader can find the Diophantine equations for each representative choice of R-charge relations for the Type I quivers. For each choice we also identify which couplings of the superpotential must be set to zero.

4.3.2.5 Enumeration of Other Types

We recall from the beginning of the section that there are 6 distinct, topologically inequivalent, types of five-block quivers and we discussed Type I in detail above. Fortunately, all the other five Types of quiver diagrams and their equivalence classes, are related to Type I by permutations and orientation reversal operations on the arrows. In other words, all the Diophantine equations obtained from the various subsets of R-charge marginality conditions for each Type are equivalent to those of Type I.

We find that Type II, III and V lead to a unique set of simultaneously marginal operators and are equivalent with Class 4 of Type I, represented by the set (33) of R-charge conditions, which we discussed in detail in the previous subsections. Types IV and VI have 22 and 11 sets of simultaneously marginal operators which lead to the same numbers of equations, again related to the various classes of Type I. The cycle structure of these quivers are listed in Appendix D.2.3.

4.3.2.6 Duality Tree for Five-Block Models

Let us now comment on Seiberg duality and see that indeed it leaves our Diophantine equation invariant. As we saw in section 4.3.2.2 the five-block Diophantine equation is a straightforward generalization of the three-block one, and thus Seiberg duality is easily seen to correspond to affine Weyl reflections for the five-block models as well. Let us here focus on the duality as the set of operations reported in [47] and reviewed in Section 4.2.1. As a bi-product we will find out that the duality exchanges equations among the six quiver Types that we have.

So let us analyze a specific example for the Type I quiver drawn in Fig. 4.3 where, for simplicity, all the block multiplicities are set to one. Suppose we want to dualize with respect to node "1" in the quiver. This amounts to the following operations

$$\begin{aligned} &a_{51} \to -a_{51},\ a_{41} \to -a_{41},\ a_{13} \to -a_{13},\ a_{12} \to -a_{12} \\ &a_{24} \to a_{24} - a_{12}a_{41},\ a_{52} \to a_{52} + a_{12}a_{51},\ a_{34} \to a_{34} - a_{13}a_{41},\ a_{35} \to a_{35} - a_{13}a_{51} \end{aligned} \tag{4.69}$$

Let us assume that

$$a_{24} > a_{12}a_{41},\ a_{52} > a_{12}a_{51},\ a_{34} > a_{13}a_{41},\ a_{35} > a_{13}a_{51}, \tag{4.70}$$

so that the "dual" arrows do not change direction. Then Seiberg duality leads to the quiver in the middle quiver of Fig. 4.5. Note that the reversal of the arrows incident to node "1"

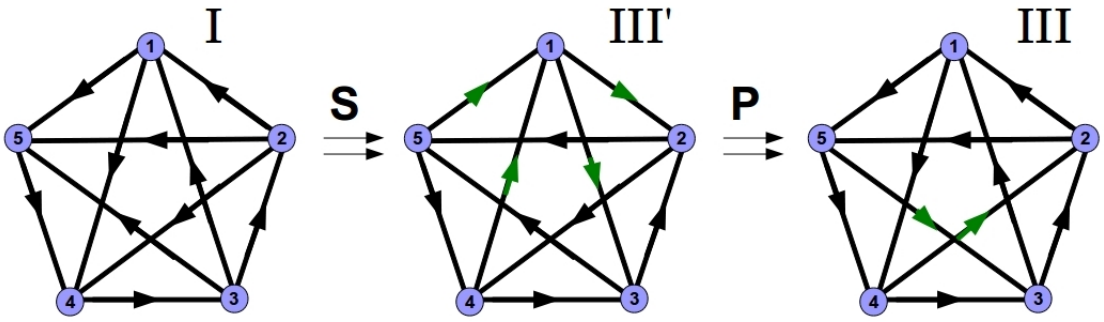

Figure 4.5: Seiberg duality acting on a quiver of type I. Green arrows are the ones that change direction. **P** corresponds to the permutation that brings the middle quiver to its canonical form as it is defined in Fig. 4.2. The top right labels denote the type of each diagram.

changes the cycle structure of the quiver. In order to see of what Type is the dualized graph, one has to count its oriented cycles. By doing so we find that it is of Type III. The permutation $P = (1)(24)(35)$ brings the dualized diagram to its canonical form as defined in Fig. 4.2, that is with a clear counter-clockwise orientation of the "outer" pentagon (the perimeter). Note that had we violated one of (4.70) we would have an outcome of another type. Recall that from

the analysis in section 4.3.2.2 the rank of the node "i" is proportional to A_i as in (4.40). The transformations (4.69) act on the A's as follows

$$A_1 \to A_1 - a_{41}A_4 - a_{51}A_5,\ A_2 \to -A_2,\ A_3 \to -A_3,\ A_4 \to -A_4,\ A_5 \to -A_5. \tag{4.71}$$

The minus signs in front of the dual ranks are notational artifacts since they arise due to the fact that we consider the arrows to change sign when reversed. The anomaly cancellation forces the dimension vector to be in the kernel of the quiver matrix. The overall minus in the dual ranks is due to the fact that the duality as we define it on the quiver data reflects this vector through the origin of the null space of q_5. This is also evident in the three-block case where the rank vector is proportional to the vector with entries the non incident arrow of each node (cf. (4.2)). Had we ended up with a minus sign in the rank of some blocks and positive in the others, then we would face a real problem, which is certainly not the case for us.
It is straightforward to verify that the transformation $A_1 \to \alpha_1 a_{41}A_4 + \alpha_1 a_{51}A_5 - A_1$ leaves the five-block Diophantine equation invariant! The best way to see this is to use the last line of (4.58) as the RHS of (4.57) since it involves only arrows that remain unaffected from the operations (4.69). This corresponds exactly to $N_{C_1} \mapsto N_{F_1} - N_{C_1}$. The fact that the determinant vanishes ensures that the number of flavours is uniquely defined, that is $a_{41}A_4 + a_{51}A_5 = a_{12}A_2 + a_{13}A_3$.

4.3.3 Summary and Generalization to n-Blocks

In this section we have presented our results for block models up to five nodes, including the known five-block theories on del-Pezzo surfaces. We saw that they are underlined by an identical algebraic structure as the three-block ones while for four-blocks the situation is slightly altered. Even though there exists a formula which admits a similar structure as in the odd cases the connection with representation theoretic concepts is blurry.

Moreover, we illustrated a method for constructing toric five-block theories from lower ones. The existence of a composition chain $3b \rightleftarrows 4b \to 5b$ (b for blocks), together with the unified way that superconformality conditions appear suggests that for any n there are subsets of theories that can be reconstructed from lower ones. Finally, we saw how Seiberg duality can be realized as an action on the $5b$-quiver that leaves the Diophantine equation invariant.

Unfortunately, due to the exponential increase in complexity we cannot explicitly verify higher-block quivers but the persistence of the summation over minors formula strongly recommends a continuation to any quiver. Our highly non-trivial analysis and the robustness of our results for

the low numbers of blocks leads us to conjecture a generic classification of chiral superconformal $\mathcal{N}=1$ quiver gauge theories:

CONJECTURE 1 *Given a quiver with $n=2l+1$ blocks and the maximal set of simultaneously marginal operators, the resulting theory admits an interacting superconformal fixed point in the IR if the quiver data, in the notation of Sec.4.2 (cf. p.6), satisfy the following Diophantine equation:*

$$\sum_i C_{ii}\prod_{j\neq i}\alpha_j - \sum_{i<j} q_n(i,j)C_{ij}\prod_k \alpha_k = 0\ , \tag{4.72}$$

where C_{ij} is the (i,j) cofactor of the anti-symmetrized adjacency matrix q_n and the indices run in $\{1,\ldots,n\}$.
The dimension vector corresponding to the gauge theory satisfies

$$q_Q(x_1,...,x_n) = -2\sum_{i<j\ |\ q_n(i,j)<0} |q_n(i,j)|\alpha_i\alpha_j x_i x_j, \tag{4.73}$$

where q_Q is the Tits form of the quiver. The rank of block i is given by

$$x_i \propto \sqrt{\frac{M_{ii}\prod_{j\neq i}\alpha_j}{\alpha_i}}, \tag{4.74}$$

with M_{ij} being the (i,j), $(n-1)\times(n-1)$ first minor of q_n. The proportionality constant is fixed so that $x_i\in\mathbb{Z}$. Therefore, superconformal gauge theories correspond to imaginary roots of the quiver's root system. The affine Weyl group that permutes these roots offers a realization of Seiberg duality in this context.

CONJECTURE 2 *Given a quiver with $n=2l$ blocks and the maximal set of simultaneously marginal operators, the resulting theory admits an interacting superconformal fixed point in the IR if the quiver data, satisfy the following Diophantine equation:*

$$\sum_{i_1<i_2} M_{i_1 i_2, i_1 i_2}\prod_{m\neq i_1,i_2}\alpha_m \ - \sum_{i_1\neq i_2<i_3}(-)^{i_2+i_3}q_n(i_2,i_3)M_{i_1 i_2, i_1 i_3}\prod_{m\neq i_1}\alpha_m + \\ + \sum_{i_1<\ldots<i_n} q_n(i_1,i_2)q_n(i_1,i_n)M_{i_1 i_2, i_1 i_n}\prod_m \alpha_m = 0 \tag{4.75}$$

where $M_{ij,kl}$ is the $(ij;kl)$ second minor of the anti-symmetrized adjacency matrix q_n and the indices run in $\{1,\ldots,n\}$.
Having a superconformal $2l$-block model the operation of removing one block leads to a superconformal $(2l-1)$-block model. But the same operation on a $(2l+1)$-block quiver results only in an anomaly free $2l$-block theory.

Even though we have calculated explicitly one even-block quiver the way that $4b$ reduces to $3b$ through the minor formula is suggestive for the $6b$ construction as well. Note that although the last term in (4.75) does not participate in the $2l-1$ quiver since it is weighted by all the node multiplicities α_m, including the one we set to zero in order to descent to $2l-1$-blocks, the way it is written it reproduces a $2l$-order term in the arrow multiplicities which is the order $2l$ operator in the perimeter of the polygon. That is for example the analogue of the term $a_{12}a_{23}a_{34}a_{14}$ in (4.36). This is because the second minor of a $2l \times 2l$ matrix is of order $2l-2$ in the arrow multiplicities and together with the quadratic piece yields the term of order $2l$.

4.4 Conclusions and Outlook

In this chapter we have organized superconformal chiral quiver theories into block structure whilst exploring a unified perspective using the representation theory of quivers. The pigeonholing of the plethora of quiver theories into block-quivers each block of which contains non-adjacent nodes dramatically reduces the complexity of the problem and gives a handle on a step-wise catalogue of the superconformal gauge theories. Many of the complicated geometries which ordinarily give rise to many product gauge groups, especially Calabi-Yau manifolds as cones over higher del Pezzo surfaces, now simply belong to the class of 3-, 4- or 5-block models. Importantly, we have incorporated physical conditions of anomaly-cancellation, conformality as well as marginality by enforcing all superpotential terms to have R-charge 2, directly into our scheme; these strong constraints translate to combinatorics. We envision that with further computer work, we can efficiently classify more and more of quivers with superpotential.

A powerful invariant for a block-quiver is an underlying Diophantine equation which the adjacency matrix and the ranks of the nodes must obey. Interpreting the ranks as the dimension vector of the representation of the quiver, and using the so-call Tits quadratic form thereon, we have shown how the Diophantine equation arises upto 5-blocks and conjectured a general form. The exponential increase in complexity of our problem as the number of blocks rises, forbids us to further support our results by direct computation, but we find it highly non trivial and suggestive that the first three cases can be attacked in a unified way. The complication of having to enumerate the inequivalent graphs for higher block number is one more computational obstacle. The first few terms in the sequence that counts inequivalent graphs up to seven blocks are $(0, 0, 1, 1, 6, 36, 356, ...)$.
For each geometry, there is a tree of Seiberg-dual theories arising by consecutive action on the various nodes (blocks). The ranks and subsequent adjacency matrices of these dual theories are,

surprisingly, controlled by this Diophantine equation by precisely being its solutions. Therefore understanding of this equation is of great significance.
Taking advantage of the presentation of the Diophantine equation as the Tits form of the quiver, Seiberg duality is seen as Weyl reflections in the space of roots, giving a representation-theoretic approach, which is not restricted in the A-D-E cases - complementing the usual geometric ones such as mutation and Picard-Lefshetz monodromy - to the tree of dualities. Indeed, the Diophantine equation is invariant under such Weyl reflections.

Furthermore, we draw a connection between the representation theory of quivers, their Tits form and $\mathcal{N} = 1$, 4-d superconformal gauge theories for quivers with odd number of blocks. In the case of tame quivers, a type under which many of our models fall into, the zeros of the Tits form control the indecomposable representations which are in correspondence with the imaginary roots of the underlying root system. In the notorious case of wild quivers though, the correspondence between roots and indecomposable representations is not any more a bijection. We demonstrated that there is a connection between the zeros of the Tits form for any case and superconformal gauge theories. For the quivers with an even number of blocks the situation is more blur. We could not identify a clear connection with a bilinear form but we managed to show that the in that case as well, the polynomial invariant that controls superconformal fixed points, can be presented as a sum over minors of the adjacency matrix. We leave further investigation of these cases for future work.

In addition to fitting further known theories into our context, which also includes a huge class of known examples, there is much left to do. Given the conjectural forms of the Diophantine equations and block structures, we can reverse engineer the subsequent quivers with superpotential. We can do this by finding the explicit moduli space of vacua from the quiver data and find Calabi-Yau geometries, the world-volume theories of the D-branes probing which are not yet known. Within the toric sub-class, which comprises most of the known examples to AdS/CFT, there is an interpretation in terms of brane-tilings where the ranks of all nodes are equal, our classification frame-work thus also gets simplified. It would be interesting to investigate this class in further detail as well as to further explore, understand and develop our representation theoretic approach to the problem of enumerating superconformal theories and their relation to the underlying root system of the quiver diagram.

Chapter 5

A New Compendium of Brane-Tilings

5.1 Introduction

One of the most fertile testing-grounds for the physics of the AdS/CFT Correspondence and the mathematics of singularity resolutions and quiver representation theory has been the study of 4-dimensional supersymmetric gauge theories whose moduli space of vacua is an affine toric Calabi-Yau threefold $\mathcal{M}$, which has a conical singularity over a Sasaki-Einstein manifold of one less real dimension. In this setup, one can think of the gauge theory as being geometrically engineered by a setup of type IIB branes "probing" the singularity $\mathcal{M}$, or, T-duality-wise, as being furnished by a Hanany-Witten configuration of type IIA branes.

More than a decade has passed since the first systematic treatment of the question "what is the gauge theory given an arbitrary toric diagram?" [46], and a tremendous number of enlightening lessons have been learnt. These have included, in the physics community, the understanding that toric duality is Seiberg duality [47, 97] as well as subsequently relations to cluster mutation [110], the manifestation in mirror symmetry and tropical geometry [51], the connection with Grothendieck's dessins d'enfants and certain isogenies of elliptic curves [111–113], the proposition of specular duality [114] and the advent of bipartite field theories [115–117].

In parallel, in the pure mathematics community, this dialogue between the gauge theory and the geometry and combinatorics of $\mathcal{M}$ has engendered such new directions in Calabi-Yau algebras and quiver representations [118–124], the non-commutative crepant resolutions of toric singularities [125–129], geometric perspective on cluster algebras [130–132].

The high-light of this long development and indeed the inspiration for most of the above story is, of course, the realisation that *the quiver representation, with superpotential, of the gauge theory whose vacuum moduli space is an affine toric Calabi-Yau threefold is graph dual to a*

bipartite graph on a torus, known as a dimer model or a brane-tiling of the doubly period plane [49–51]. This will thus be the motivation of our story.

From a computational perspective, one would like a useful catalogue of quiver gauge theories and associated Calabi-Yau geometries, namely a database of pairs (Q, D) where Q is a quiver with superpotential expressed as a bipartite graph on the torus and D is the toric diagram of the CY3 which is a convex integer polygon. Ideally, we would like further properties such as R-charges, j-invariants for the dessins, etc. and these will be added in due course. It should be emphasized that Q and D are not in bijection, and many different, consistent Qs have the same D; the set of such Q are Seiberg duals.

Indeed, to have this catalogue was the old desire of [46] and the so-called *Inverse Algorithm* was devised to extract the quiver and superpotential via partial resolution of the orbifold $\mathcal{C}/\mathbb{Z}_m \times \mathbb{Z}_n$ to D. The chief bottle-neck to that method was the exponential-running time of find dual cones needed for the partial resolutions. The recently developed dimer technology leads to the advantage that the quiver and superpotential are combined into a single object [133]. And the first catalogue of this kind, based on the number of superpotential terms, i.e., the number of black-white pairs was implemented in [94].

Although illustrative and helpful, the existing data is still limited: only up to 3 dimer pairs, meaning 6 terms in the superpotential, could be reached. Moreover, since the mapping from Q to D is many to one, it is perhaps more natural to proceed with the classification from the geometry side. Bearing these in mind and with the advances in computational algebra and combinatorial geometry tailored for gauge theories [134], a clear path is strewn before us. It is the purpose of this chapter to push the boundaries of computation and to provide as comprehensive database as possible. We will march forward, in increasing area of the toric diagram D, and use a combination of dimer methodology and Higgsing in field theory, to obtain the various dual phases of gauge theories flowing to the Calabi-Yau geometry associated to D.

5.2 Dimer Technology

In this section we present a lighting review of brane tiling technology. In order to set up the stage for our computations, we also review the basics of the connection between brane tilings and geometry and the implementation of partial resolution in terms of them.

5.2.1 D3-Branes Probing Toric CY 3-Folds and Brane Tilings

It is by now well-established that the world-volume gauge theories of a stack of D3-branes probing an affine toric Calabi-Yau 3-fold is described by so-called brane tilings. This is by far the largest class of examples studied in the AdS/CFT correspondence: the world-volume theory is a 3+1-dimensional CFT and the transverse Calabi-Yau directions are cones over Sasaki-Einstein 5-manifolds such as S^5. The physics of the gauge theory is encoded by a bipartite graph drawn on T^2, equivalently, by a tiling of the doubly periodic plane; the mathematics of the non-compact Calabi-Yau 3-fold is captured by a toric diagram, which is a convex lattice polygon. [1]

The key relation is that given the gauge theory, which generically is a quiver theory with superpotential, one can compute its vacuum moduli space (defined by F-flatness and D-flatness) as the Calabi-Yau 3-fold $\mathcal{M}$ with toric diagram $\mathcal{D}$, this has traditionally been called the *Forward Algorithm*; and vice versa, the *Inverse Algorithm* [46] is when once given a toric diagram $\mathcal{D}$, one attempts to construct a gauge theory which is the world-volume gauge theory of D-branes probing $\mathcal{M}$.

The gauge theory can be readily extracted from the bipartite tiling as follows. Consider the fundamental domain (the unit cell of a torus),

1. Each inequivalent polygonal face (say labeled by i) corresponds to a $U(N_i)$ gauge group factor in a product gauge group structure;

2. Choose an orientation, say black/white nodes corresponds to clockwise/counterclockwise respectively;

3. Each inequivalent edge corresponds to a bifundamental field X_{ij} of $U(N_i) \times U(N_j)$ if it neighbours faces i and j along our direction chosen (i could equal to j whereupon X_{ii} is an adjoint field of $U(N_i)$);

4. Each black/white node corresponds to a monomial term in the polynomial superpotential W by multiplying the edges adjacent to the nodes, the overall sign in front of the monomial is +/- according to our orientation;

[1] An affine toric variety of complex dimension n is usually described by a convex polyhedral cone in $\mathbb{R}^n$ but the Calabi-Yau condition imposes the extra condition that the end-points of the vector generators of the cone are co-hyperplanar. Thus for threefolds, the toric diagram can be taken to be a convex lattice polygon in the plane.

5. The graph dual of the bipartite graph is the periodic version of the quiver diagram of the gauge theory.

The archetypal example is given by the so-called $\mathbb{F}_0(I)$ theory, whose vacuum moduli space is $\mathbb{F}_0$, the complex Calabi-Yau cone over $\mathbb{P}^1 \times \mathbb{P}^1$; we present the brane-tiling and the equivalent quiver/superpotential data as follows:

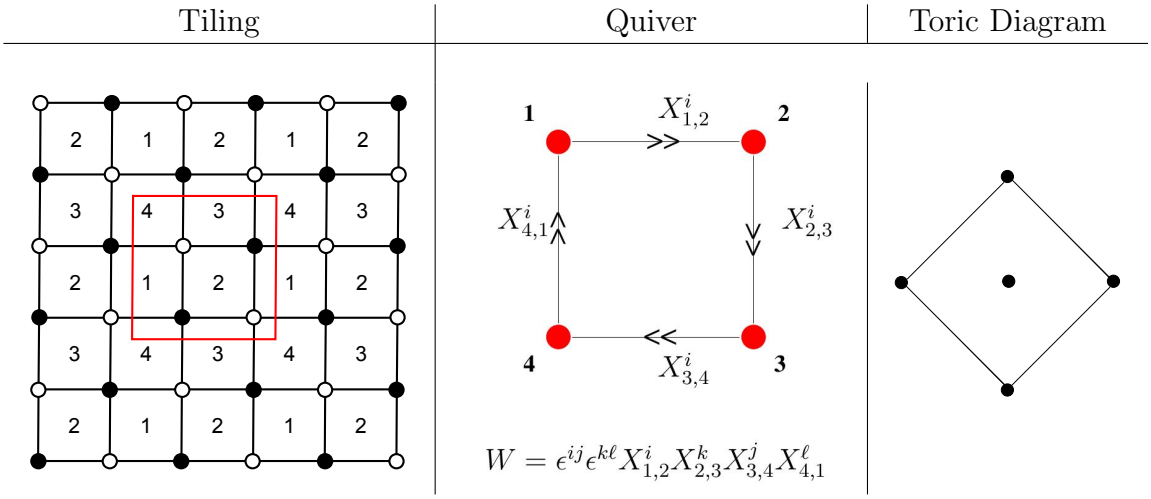

We see that there are 4 gauge group factors and for convenience we take all $N_i = 1$, we have an $U(1)^4$ theory. There are 8 edges, denoting the 8 fields $X^a_{i,i+1}$ for $a = 1, 2$ and $i = 1, 2, 3, 4$ modulo 4. Finally, expanding out the Levi-Civita symbols, there are 4 monomial terms in the superpotential, 2 each of +/- signs.

5.2.2 Geometry and Perfect Matchings

Perfect matchings are combinatorial objects that play a central role in the study of bipartite graphs. A perfect matching p is defined as a collection of edges in the brane tiling such that every node is the endpoint of exactly one edge in p.

Perfect matching substantially simplify the connection between brane tilings and geometry. Let us consider the following map between chiral fields in the quiver X_i, equivalently edges in the brane tiling, and perfect matchings p_μ

$$X_i = \prod_{\mu=1}^{c} p_\mu^{P_{i\mu}} \,, \tag{5.1}$$

with c as the total number of perfect matchings [49]. The P-matrix summarize the edge content of perfect matchings and is defined as follows

$$P_{i\mu} = \begin{cases} 1 & \text{if} \quad X_i \in p_\mu \\ 0 & \text{if} \quad X_i \notin p_\mu \end{cases} \tag{5.2}$$

A remarkable feature of the map in (5.1) is that when chiral fields are expressed in terms of perfect matching variables in this way, all F-terms automatically vanish. Perfect matchings are thus in correspondence with fields in the GLSM description of the toric CY 3-fold, namely points in its toric diagram.

Perfect matchings and the toric diagram can be efficiently determined using the *Kasteleyn matrix* K. We define K as the adjacency matrix of the graph in which rows are indexed by black nodes and columns are indexed by white nodes, i.e. for every edge X_i in the bipartite graph between nodes $\mathbf{b}_\mu$ and $\mathbf{w}_\nu$, we introduce a contribution X_i to the $K_{\mu\nu}$ entry. In addition, whenever an edge crosses the boundary of the unit cell in the x and/or y directions, we add $x^{\pm 1}$ and $y^{\pm 1}$ weights, respectively. The exponents are positive or negative depending on whether the crossing occurs in the positive or negative direction, which is determined by orienting edges from white to black nodes.

Let us illustrate these ideas with an example. 5.1 shows the quiver diagram for the suspended pinch point (SPP). The superpotential is

$$W = X_{12}X_{21}X_{22} - X_{22}X_{23}X_{32} + X_{13}X_{23}X_{31}X_{32} - X_{12}X_{13}X_{21}X_{31}\,. \tag{5.3}$$

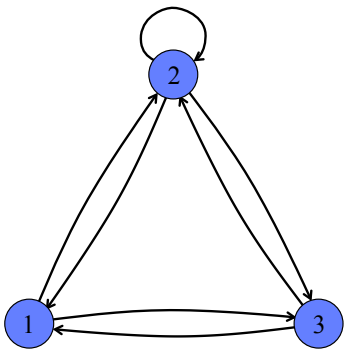

Figure 5.1: Quiver diagram for SPP.

All this information is encoded in the brane tiling shown in 5.2.

The superpotential has four terms, which are represented in the brane tiling by two white and two black nodes. We have labeled the nodes in blue to facilitate the construction of the Kasteleyn matrix. It is given by

$$K = \left(\begin{array}{c|c|c} & w[1] & w[2] \\ \hline b[1] & X_{22}\,x & X_{23} + X_{32}\,x \\ \hline b[2] & X_{12} + X_{21}\,x & X_{31}\,y + X_{13}\,xy \end{array}\right) \tag{5.4}$$

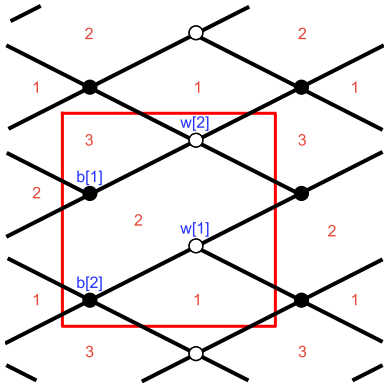

Figure 5.2: Brane tiling for SPP.

The determinant of the Kasteleyn matrix generates the perfect matchings. In this case, we get

$$\det K = -X_{12}X_{23} - (X_{21}X_{23} + X_{12}X_{32})\, x - X_{21}X_{32}\, x^2 + X_{22}X_{31}\, xy + X_{13}X_{22}\, x^2 y\,. \tag{5.5}$$

Every monomial in this expression corresponds to a perfect matching. Furthermore, the powers of x and y indicate their position in the toric diagram, as shown in 5.5. The perfect matching can be summarized in the P-matrix as follows

$$P = \left(\begin{array}{c|cccccc} & p_1 & p_2 & p_3 & p_4 & p_5 & p_6 \\ \hline X_{22} & 0 & 0 & 0 & 0 & 1 & 1 \\ X_{12} & 1 & 0 & 1 & 0 & 0 & 0 \\ X_{21} & 0 & 1 & 0 & 1 & 0 & 0 \\ X_{23} & 1 & 1 & 0 & 0 & 0 & 0 \\ X_{32} & 0 & 0 & 1 & 1 & 0 & 0 \\ X_{31} & 0 & 0 & 0 & 0 & 1 & 0 \\ X_{13} & 0 & 0 & 0 & 0 & 0 & 1 \end{array}\right) \tag{5.6}$$

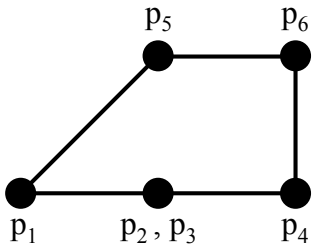

Figure 5.3: Toric diagram for SPP. We indicate the perfect matching associated to each point.

5.2.3 Partial Resolution and Dimers

Brane tilings completely solved the problem of finding the gauge theory associated to a generic toric CY 3-fold and vice versa. There are well established procedures for going from brane

tilings to geometry and in the opposite direction, the *fast forward* [49] and *fast inverse algorithms* [51], respectively. One of the main goals to this chapter is to develop a practical approach to determine the brane tiling associated to a general toric diagram. While the fast inverse algorithm provides an answer to this question, its automation is challenging. We thus opt for an alternative approach, which admits a rather simple computer implementation.

Our strategy will be to perform partial resolution, which translates to higgsing in the gauge theory. In terms of brane tilings, it corresponds to removing the edges associated to the fields acquiring non-zero vevs. We will exploit the map between perfect matchings and fields in the gauge theory to systematically identify the vevs that are turned on when certain points in the toric diagram are deleted.

Any geometry for which the brane tiling is known can be used as the starting point for partial resolution. In this work we always denote the conifold as $\mathcal{C}$. There are two canonical classes of initial theories that have been broadly used in the literature. The first one is $\mathbb{C}^3/(\mathbb{Z}_N \times \mathbb{Z}_M)$ orbifolds, with the two generators of the orbifold group acting on $\mathbb{C}^3$ as: $(X, Y, Z) \equiv (e^{i2\pi/N}X, e^{-i2\pi/N}Y, Z)$ and $(X, Y, Z) \equiv (X, e^{i2\pi/M}Y, e^{-i2\pi/M}Z)$. The resulting toric diagram is shown in 5.4.a, and the corresponding brane tiling is an hexagonal lattice with an $N \times M$ unit cell. Partial resolutions from $\mathcal{C}/(\mathbb{Z}_N \times \mathbb{Z}_M)$ have been considered in e.g. [48]. The second standard class of starting points are $\mathbb{Z}_N \times \mathbb{Z}_M$ orbifolds of the conifold $\mathcal{C}$. Given the defining equation for the conifold $xy = uv$, the two generators of the orbifold group act as follows: $(x, y, u, v) \equiv (e^{i2\pi/N}x, e^{-i2\pi/N}y, u, v)$ and $(x, y, u, v) \equiv (x, y, e^{i2\pi/M}u, e^{-i2\pi/M}v)$. The toric diagram for this class of geometries is shown in 5.4.b and the brane tiling is a square lattice with an $N \times M$ unit cell. We will adopt the orbifolds of the conifold as our initial theories.

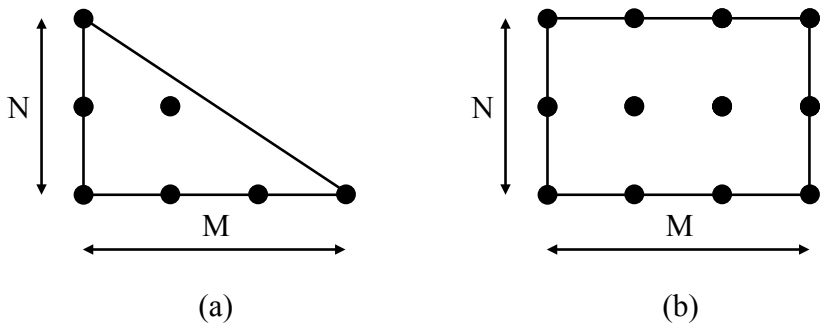

Figure 5.4: Toric diagrams for: a) $\mathbb{C}^3/(\mathbb{Z}_N \times \mathbb{Z}_M)$ and b) $\mathcal{C}/(\mathbb{Z}_N \times \mathbb{Z}_M)$. We will use the second class of geometries as the starting points of partial resolution.

We now illustrate the dimer implementation of partial resolution with an explicit example. Let us derive the brane tiling for the SPP from a $\mathcal{C}/(\mathbb{Z}_N \times \mathbb{Z}_M)$ orbifold. Considering the toric diagrams, it is clear that it would be sufficient to start from $\mathcal{C}/\mathbb{Z}_2$. However, in order to demonstrate the methods in a more involved partial resolutions, let us use $\mathcal{C}/(\mathbb{Z}_2 \times \mathbb{Z}_2)$ as the initial theory. The brane tiling for $\mathcal{C}/(\mathbb{Z}_2 \times \mathbb{Z}_2)$ is shown in 5.5.[2]

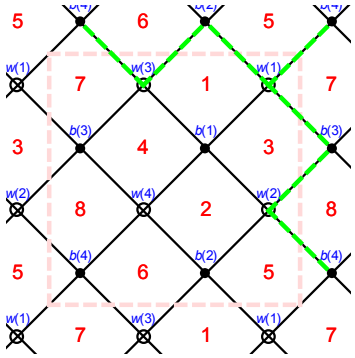

Figure 5.5: Brane tiling for $\mathcal{C}/(\mathbb{Z}_2 \times \mathbb{Z}_2)$.

The Kasteleyn matrix is given by

$$K = \left(\begin{array}{c|cccc} & w[1] & w[2] & w[3] & w[4] \\ \hline b[1] & X_{13} & X_{32} & X_{41} & X_{24} \\ b[2] & X_{51}\, y & X_{25} & X_{16}\, y & X_{62} \\ b[3] & X_{37}\, x & X_{83}\, x & X_{74} & X_{48} \\ b[4] & X_{75}\, xy & X_{58}\, x & X_{67}\, y & X_{86} \end{array}\right) . \tag{5.7}$$

We obtain the perfect matchings by computing its determinant. They are summarized in the following P-matrix:

	$(0,0)$	$(1,0)$		$(2,0)$	$(1,1)$		$(2,1)$												$(2,2)$		$(0,2)$	$(1,2)$		$(2,2)$
	p_1	p_2	p_3	p_4	p_5	p_6	p_7	p_8	p_9	p_{10}	p_{11}	p_{12}	p_{13}	p_{14}	p_{15}	p_{16}	p_{17}	p_{18}	p_{19}	p_{20}	p_{21}	p_{22}	p_{23}	p_{24}
X_{13}	1	1	0	0	1	0	1	0	0	0	0	0	0	0	1	0	1	0	0	0	0	0	0	0
X_{16}	0	0	0	0	0	0	1	0	0	0	0	0	0	0	0	1	1	0	1	0	0	1	0	1
X_{24}	0	0	0	0	0	0	0	0	1	0	1	0	1	0	0	0	0	0	1	0	0	0	1	1
X_{25}	1	0	1	0	1	0	0	0	1	0	0	1	1	0	0	0	0	0	0	0	0	0	0	0
X_{32}	0	0	0	0	0	1	0	0	0	1	0	0	0	1	0	1	0	0	0	0	1	1	0	0
X_{37}	0	0	1	1	0	0	0	0	1	1	0	0	0	0	0	1	0	0	1	0	0	0	0	0
X_{41}	0	0	1	1	0	0	0	1	0	0	0	1	0	0	0	0	0	1	0	1	0	0	0	0
X_{48}	0	0	0	0	1	0	1	1	0	0	0	1	0	0	0	0	0	0	0	0	1	1	0	0
X_{51}	0	0	0	0	0	1	0	1	0	0	1	0	0	0	0	0	0	1	0	0	1	0	1	0
X_{58}	0	1	0	1	0	0	1	1	0	0	1	0	0	0	0	0	0	0	1	0	0	0	0	0
X_{62}	0	1	0	1	0	0	0	0	0	1	0	0	0	1	1	0	0	0	0	1	0	0	0	0
X_{67}	0	0	0	0	1	0	0	0	1	1	0	0	0	0	1	0	0	0	0	0	1	0	1	0
X_{74}	1	1	0	0	0	1	0	0	0	0	1	0	1	1	0	0	0	0	0	0	0	0	0	0
X_{75}	0	0	0	0	0	0	0	0	0	0	0	1	1	1	0	0	0	0	0	1	0	1	0	1
X_{83}	0	0	0	0	0	0	0	0	0	0	0	0	0	0	1	0	1	1	0	1	0	0	1	1
X_{86}	1	0	1	0	0	1	0	0	0	0	0	0	0	0	0	1	1	1	0	0	0	0	0	0

(5.8)

[2]There are other brane tilings for $\mathcal{C}/(\mathbb{Z}_2 \times \mathbb{Z}_2)$, which correspond to additional toric phases obtained from this one by Seiberg duality.

where in the top row we have indicated the corresponding point in the toric diagram, which is shown in figure. 5.6. The significance of the rows that are highlighted in blue will be discussed soon.

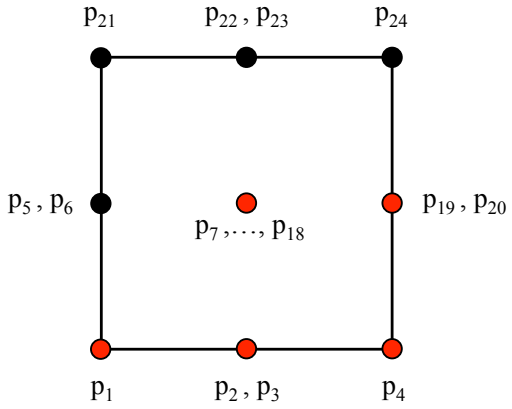

Figure 5.6: Toric diagram for $\mathcal{C}/(\mathbb{Z}_2 \times \mathbb{Z}_2)$. We indicate the perfect matching associated to each point and a possible embedding of the SPP toric diagram (in red).

According to (5.1), we should regard chiral fields as products of perfect matchings. The vev of a chiral field is the product of the vevs of its perfect matching constituents. Then, a chiral field gets a vev and is removed from the brane tiling only when all the perfect matchings that contain it get a vev. Therefore, what we want here is to remove certain fields contained in the perfect matchings $p_5, p_6, p_{21}, p_{22}, p_{23}, p_{24}$, while keeping the five red toric points in figure. 5.6. If we delete the five fields marked by blue bars in P matrix, the SPP dimer will be recovered. And the superpotential is written out by counting only the terms containing the remained fields:

$$W = -X_{12}X_{13}X_{21}X_{31} + X_{12}X_{21}X_{22} + X_{13}X_{23}X_{31}X_{32} - X_{22}X_{23}X_{32} \tag{5.9}$$

5.2.4 Existing Classifications

A plethora of explicit brane tilings have been constructed in the literature. Below we summarize the existing systematic classifications of *classes* of models. Several additional scattered examples exist.

- Del Pezzo surfaces. The brane tilings for all toric phases for toric del Pezzo surfaces dP_n, $n = 0, \ldots 3$, have been classified.
- Abelian orbifolds of the conifold. More generally, it is straightforward to construct the brane tilings for abelian orbifolds of arbitrary geometries by appropriately enlarging the

unit cell. The geometric action of the orbifold group is encoded in the periodicity conditions. However, a systematic classification of the orbifold possibilities of geometries beyond conifold does not currently exist.

- The $Y^{p,q}$ and $L^{a,b,c}$ infinite families [135]. In fact the $Y^{p,q}$ theories are fully contained within the $L^{a,b,c}$ class. The toric diagram for these geometries have four external edges. Explicit metrics for the $Y^{p,q}$ and $L^{a,b,c}$ Sasaki-Einstein manifolds can be constructed, and the gauge theories for these geometries had a substantial impact in the $\mathrm{AdS}_5/\mathrm{CFT}_4$ correspondence with $\mathcal{N}=1$ supersymmetry. It allowed for refined tests of the correspondence for the infinite classes of dual pairs.

- The $X^{p,q}$ family. The toric diagram for these geometries have five external edges. While the classification in [136] was not performed in the language of brane tilings, it is straightforward to translate it.

5.3 Algorithm and Classification Scheme

5.3.1 Algorithm of classification

Having reviewed the problem to some detail as well as presented the available databases, it is clear that a much more comprehensive catalogue of brane-tiling/dimer models is needed. Given that our method of Higgsing will produce consistent models, it is expedient to start to identify the relevant toric geometries, order by order, and construct the gauge theory corresponding to the geometry. Specifically, our strategy is as follows

1. First classify all the toric diagrams (convex polygons) up to $\mathrm{SL}(2;\mathbb{Z})$ transformation, against the number of triangulation area N. In this chapter we focus on cases with $N=6,7,8$.

2. For each toric diagram, construct the rectangular dimer model as our starting point.

   (a) Place the toric diagram into a lattice space (2-dimensional), such that it is minimally covered by a $m\times n$ rectangular lattice. This is to make sure we only need to remove the least number of points from the rectangular toric diagram.

   (b) Draw a brane tiling with m rows and n columns of black nodes and white nodes, namely altogether $2mn$ nodes in the unit cell of torus. Label the nodes as $b_1,...,b_{mn}$ and $w_1,...,w_{mn}$, and label the faces (gauge factors) in the tiling as $f_1,...,f_{2mn}$. Naturally we label the fields in the tilings as $X_{f_if_j}$, where f_i denote the inward face of the field, f_j the outward face.

(c) Construct the *Kasteleyn* matrix K of the rectangular dimer.

(d) Compute the perfect matchings of the rectangular dimer, as $P_i, i = 1, ...\#(\text{perfect matchings})$.

3. Compute the higgsings to reach the target toric diagram.

   (a) List the points to delete from the rectangular toric diagram as $\mathbf{Pts} = \{pt_1, ..., pt_s\}$.

   (b) We know from K that which perfect matchings are mapped to which toric points, hence we write down two lists: the perfect matchings to delete $\mathbf{delPfs} = \{p_{d_1}, ..., p_{d_k}\}$, and the perfect matchings to keep $\mathbf{rePfs} = \{p_{r_1}, ..., p_{r_l}\}$.

   (c) Decide which fields should be removed.

      i. Initialise the one-length choices as $\mathbf{opts} = \{\{X_{f_i f_j}\}\}$, where i, j are ranging the indices of all faces.

      ii. For each element in **opts**, test whether it removes all the perfect matchings in **delPfs** while keeping all perfect matchings in **rePfs**. Delete the unwanted elements from **opts**.

      iii. Insert the fields $X_{f_i f_j}$ into each element of opts, as the new definition of **opts**.

      iv. Repeat the step (ii) until **opts** remains unchanged.

      v. If within the elements of **opts**, one is the subset of another, then remove the subset. This is to make sure we always delete as many fields as possible from the dimer.

4. Check the consistency of the new dimer model. For each higgsing ansatz in **opts**, we remove the edges and re-draw the dimer model, then compute the zig-zag paths. If there is self-intersect in the zig-zag paths, then the model is not consistent. Otherwise we treat the model as a good ansatz of higgsing.

5. Merge the 2-valent vertices. This is because those are massive fields that will be integrated out.

6. Compute the quiver graph and super-potential of the new dimer model. This is straightforward once we re-drew the dimer.

As a remark, the consistency check makes sure that the given higgsing properly assigns R charges to the fields. In fact, not all the bipartite periodic graphs on the two-torus correspond to a geometrically consistent brane tiling and a well behaved four-dimensional $\mathcal{N} = 1$ quiver gauge theory, where by 'well behaved' we mean that the brane tiling could uniquely decide the R-charges, chiral ring and moduli space. Luckily, the in-consistency of a brane tiling is

revealed by the fact that the zig-zag paths of it contains self-intersections. Therefore the most convenient check of the consistency is to compute the zig-zag paths of a brane tiling, which we implemented into our computational package. Though, there could be different angles approaching the consistency, especially under the mathematical context. Interesting readers can check [137–140] for a full story in consistency check. Considering that the method in [137] involves computing zig-zag paths, which is also useful for computing the dual quiver for future work, we hereby followed their notation for zig-zag paths.

5.3.2 Computational Modules

We now introduce the *Mathematica* modules implemented as a computational system of any brane tiling. So far this package is for a standard `Unix` environment, where the default directory of storing the intermediate output is the user's home directory `$HOME`. As introduced in former sections, we always start with rectangular brane tilings, and since its K matrix and perfect matchings are simply following the counting of edges, vertices, unit cell etc., we then organise these calculations into one module called `RecDimerModels[m,n]`, where m and n means the brane tiling is for the geometry $\mathcal{C}/\mathbb{Z}_m \times \mathbb{Z}_n$. In turn the module will print the dimer graph and *Kasteleyn* matrix, where all the objects are labeled, with fields that thread the unit cell highlighted by green dotted lines. Meanwhile the intermediate data, including the decoding of faces, labelling of fields etc., are stored in the file `$HOME.dimer.model.tmp.txt`. Next we want a module which tells us the perfect matchings of the rectangular dimer, which is implemented as `ToricInfo[KM]`, where the only input is the K matrix, with output as perfect matchings and toric diagram. For quickly checking the triangulation of a 2-dim toric diagram, we also provide `TriangDimer[ToricPts]` as a modified version of `DelaunayMesh[]` object by *Mathematica*, where one can view the triangulation and number of areas of a certain toric diagram. For computing the higgsing ansatz, we implemented the module `RemovePoints[KM,Ptsremove]`, which loads the data in `$HOME.dimer.model.tmp.txt`, and returns all the possible partial resolutions for the toric diagram with points we want to delete (`Ptsremove`). This is the most time consuming step, even though we have used parallel computing and an optimised algorithm to enumerate all the pairs of edges. The output will be in the form of a list containing all the higgsing ansatz (`HiggsAntz`). However, once we have all the higgsing ansatz, it is straight-forward to compute the final dimer model by using `HiggsingDimer[RemoveAntz]` to compute the final brane tiling along with the quiver graph, super-potential terms, toric diagram and consistency property. Zig-zag paths are provided for this module. We also provide another version called

`HiggsingDimerNew[RemoveAntz]` to integrate out the 2-valent vertices and re-labelling the indices.

A brief summary of the classification algorithm is listed in Algorithm 1.

Algorithm 1 Algorithm for classifying dimer models of certain triangulation areas

Initialise *Models* as empty set. ▷ used as storing physical models.
Load *PSets* as all the inequivalent toric diagrams with a given area number.
for *polytope* in *PSets* **do**
  Define *Kmatrix* by using `RecDimerModels[m,n]`
    ▷ `m,n` must expand the rectangular lattice which covers *polytope*.
  Define *ptsremove* as the set containing points to be removed from the rectangular toric diagram.
  Compute *HiggsAntz* as all the vev. ansatz by using `RemovePoints[`*Kmatrix*`,`*ptsremove*`]`
  for *higgsantz* in *HiggsAntz* **do**
    ▷ use `HiggsingDimer[]` to check the consistency and compute field contents.
    if `HiggsingDimer[`*Kmatrix*`,`*higgsantz*`]` makes sure the model is consistent. **then**
      Use `HiggsingDimer[`*Kmatrix*`,`*higgsantz*`]` to compute *quiver* and *superpotential* for each *higgsantz*
      Save *quiver* and *superpotential* into *Models*
    end if
  end for
end for
  ▷ Then check the equivalency between models in *Models*.

Given the powerful computing system of all the D3-brane dimers, we could try to enumerate as more dimer models as possible, even work out a complete classification of dimer systems according to the areas of toric diagrams. With the result in paper [141], we have all the convex polytopes with certain triangulation areas. Therefore we can try to firstly generate a rectangular dimer model which covers the expected toric diagram, then calculate the Higgsing models using our dimer system. Finally we could classify all the physical models with certain number of gauge groups.

5.4 A Compendium of Brane Tilings/Dimer Models

5.4.1 Convex toric diagrams

In the paper [141], Folk's formula is applied in order to systematically generate all the inequivalent polytopes, in the sense that the equivalent polytopes are linked via a $SL(2,\mathbb{Z})$

transformation. From toric side we also know that the equivalent toric diagrams give rise to the same moduli space. The natural progression of this classification is to fix the area of the triangulation, then enumerating all the possible shapes. In the paper there are results for toric diagrams of the number of areas as 6 and 7, we further classified the polytopes with area 8.

There are 13 and 11 inequivalent convex polytopes in area 6 and 7 cases, respectively [141]. We implemented Folk's formula and classified the 27 inequivalent polytopes with area as 8. The results are listed into appendix E.4.

5.4.2 New dimer models

Among the 13 shapes of area as 6, most are toric diagrams of $L^{a,b,c}$ type, which are not listed in this thesis. The dP_2 and dP_3 appear with multiple phases. For toric diagrams with area as 7, there are five new dimer models not yet classified. For toric diagrams with area 8, instead of computing the original polygons, we provide the $SL(2,\mathbb{Z})$ equivalent models by shrinking the original toric diagrams into the smaller lattices. The results are listed in appendix E.1.

Chapter 6

Conclusion

We have collected results on String compactification over toric geometry and D-brane gauge theories. We studied heterotic model building on the sixteen families of torically generated Calabi-Yau three-folds with non-trivial fundamental groups and selected the 14 favourable three-folds and we have classified phenomenologically attractive $SU(5)$ and $SO(10)$ line bundle GUT models thereon. For $SU(5)$ we have succeeded in finding all such line bundle models on the 14 base spaces, thereby proving finiteness of the class computationally. The result is a total of 122 $SU(5)$ GUT models. For $SO(10)$ we have obtained a complete classification for all spaces up to Picard number three, resulting in a total of 55 $SO(10)$ GUT models. For the other six manifolds, all with Picard number four, only one was amenable to a complete classification. For the other five manifolds, although the number of models were converging with increasing line bundle entries, they had not quite saturated even at fairly high values of about $k_{\max} = 20$. We expect that we have found the vast majority of models on these manifolds with a small fraction containing some large line bundle entries still missing. Altogether we find 28870 viable $SO(10)$ models.

We also systematically studied the discrete symmetry of Calabi-Yau manifolds over toric four-folds. By setting up an algorithm for classifying symmetries, we undertook first steps to all TCY manifolds with $h^{1,1}(X) \leq 3$, some 350 manifolds. In this way, we find all freely-acting discrete symmetries (which can be embedded into G_A) of these manifolds. We reproduce all symmetries among these manifolds known from the Batyrev Kreuzer classification, as well as those known from the overlap with CICY manifolds. We also find one new, non-toric symmetry group, $\mathbb{Z}_2 \times \mathbb{Z}_2$, on one of the 16 manifolds, where one of the $\mathbb{Z}_2$ sub-groups is the toric symmetry identified by Batyrev Kreuzer. For the resulting five TCY manifolds with $h^{1,1}(X) \leq 3$ and with freely-acting symmetries we also search for additional, non freely-acting symmetries. The method can be applied to larger $h^{1,1}$ geometries in future.

Moving on to quiver gauge theory, we have organized superconformal chiral quiver theories into block structure whilst exploring a unified perspective using the representation theory of quivers. Many of the complicated geometries which ordinarily give rise to many product gauge groups, especially Calabi-Yau manifolds as cones over higher del Pezzo surfaces, now simply belong to the class of 3-, 4- or 5-block models. By incorporating physical conditions of anomaly-cancellation, conformality as well as marginality by enforcing all superpotential terms to have R-charge 2, we have shown how the Diophantine equation arises up to 5-blocks and conjectured a general form. The exponential increase in complexity of our problem as the number of blocks rises, forbids us to further support our results by direct computation, but we find it highly non trivial and suggestive that the first three cases can be attacked in a unified way. The complication of having to enumerate the inequivalent graphs for higher block number is one more computational obstacle. We further draw a connection between the representation theory of quivers, their Tits form and $\mathcal{N} = 1$, 4-d superconformal gauge theories for quivers with odd number of blocks. In the following research we could choose to reverse engineer the subsequent quivers with superpotential. We can do this by finding the explicit moduli space of vacua from the quiver data and find Calabi-Yau geometries, the world-volume theories of the D-branes probing which are not yet known.

Lastly, we aimed at providing a useful catalogue of quiver gauge theories and associated Calabi-Yau geometries, i.e., a database of pairs (Q, D) where Q is a quiver with superpotential expressed as a bipartite graph on the torus and D is the toric diagram of the CY three-fold which is a convex integer polygon. We automated the dimer technology and explored the dimer models for toric diagrams with the number of triangulation areas larger than 6. Many new dimer models have been classified and well prepared for the further phenomenological study. The dimer system we presented is extremely useful for the computation of dimer models of toric type, and is the first computational system ever to have these functionalities on D-brane configurations.

Appendix A

Discrete Symmetries

A.1 Automorphism group of toric variety as ambient space

A.1.1 Zero set and permutation group

We've defined the following permutation groups in sub-section 3.2.2.

$$S = \{\sigma \in S_n \,|\, \sigma(I) = I,\ \forall\, I \in \mathcal{I}\} \subset S_n \ , \tag{A.1}$$

which leaves all sets I in $\mathcal{I}$ invariant individually. Another subgroup of S_n is

$$R = \{\sigma \in S_n \,|\, \sigma(I) \in \mathcal{I},\ \forall I \in \mathcal{I}\} \subset S_n \ , \tag{A.2}$$

the group of permutations which maps the sets $I \in \mathcal{I}$ into each other. Clearly, S is a sub-group of R. It is actually a normal sub-group since for $s \in S$ and $r \in R$ we have $rsr^{-1}(I) = I$ and, hence, $rsr^{-1} \in S$. We can, therefore, define the quotient group

$$P = R/S \ , \tag{A.3}$$

which can be thought of as the group of permutations on $\mathcal{I}$, induced from permutations in S_n. We can write down the short exact group sequence

$$1 \to S \xrightarrow{\imath} R \xrightarrow{[\cdot]} P \to 1 \ . \tag{A.4}$$

where $\imath$ is the inclusion map and $[\cdot]$ denotes taking the equivalence class. We now show that this sequence splits.
We begin with the

Remark Denote by $\mathcal{I}^c = \{\{1, \ldots, n\} \backslash I \,|\, I \in \mathcal{I}\}$ the complementary sets. Then the groups S and R are the same for $\mathcal{I}$ and for $\mathcal{I}^c$. This simply follows from the fact that a set I is invariant

(is mapped to another set I') under a permutation $\sigma \in S_n$ if and only if the complement $\{1,\ldots,n\}\backslash I$ is invariant (is mapped to $\{1,\ldots,n\}\backslash I'$) under σ.

The complication is that the subsets in $\mathcal{I}$ can overlap. It is, therefore, useful to split the set $\{1,\ldots,n\}$ up in a different way. Define an equivalence relation on $\{1,\ldots,n\}$ by

$$i \sim j :\Leftrightarrow i \text{ and } j \text{ are contained in the same sets } I \in \mathcal{I}\,. \tag{A.5}$$

I denote the equivalence classes by $\mathcal{J} = \{1,\ldots,n\}/\sim$ and it follows that

$$\{1,\ldots,n\} = \bigcup_{J\in\mathcal{J}} J \tag{A.6}$$

as a disjoint union. Note that for a $J \in \mathcal{J}$ and $I \in \mathcal{I}$ with $J \cap I \neq \emptyset$ it follows that $J \subset I$. Indeed, if $j \in J \cap I$ and $k \in J$ then $k \sim j$ and, hence, k and j must be contained in the same sets of $\mathcal{I}$. Since $j \in J$ it follow that $k \in J$, so that $J \subset I$. This means every $I \in \mathcal{I}$ can be written as a disjoint union

$$I = \bigcup_{J\in\mathcal{J}, J\cap I\neq\emptyset} J\,. \tag{A.7}$$

Lemma A.1.1 *For $s \in S$ it follows that $s(J) = J$ for all $J \in \mathcal{J}$. Further, for $r \in R$ it follows that $r(J) \in \mathcal{J}$ for all $J \in \mathcal{J}$.*

Proof For the first part consider a set $J \in \mathcal{J}$, a permutation $s \in S$ and any $j \in J$. Assume that i is contained in precisely the sets $I_1,\ldots,I_p \in \mathcal{I}$. Hence, $s(i) \in s(I_k) = I_k$, so that $s(j)$ is also contained in $I_1,\ldots,I_p \in \mathcal{I}$. Also, $s(j)$ cannot be contained in any other $I \in \mathcal{I}$, which is not among $I_1,\ldots,I_p \in \mathcal{I}$, since j would have to be in I in this case. This implies that $i \sim s(j)$, so $s(j) \in J$ and, hence $s(J) \subset J$. Since s is injective and J is a finite set this means $s(J) = J$. For the second part, again focus on a $J \in \mathcal{J}$ and a permutation $r \in R$. Pick a $j \in J$ and call $\tilde{J} \in \mathcal{J}$ the equivalence class of the image $r(j)$. I want to show that $r(J) \subset \tilde{J}$. Let $k \in J$, so that j and k are contained in the same sets $I_1,\ldots,I_p \in \mathcal{I}$. Then, both $r(j)$ and $r(k)$ are contained in $r(I_1),\ldots,r(I_p) \in \mathcal{I}$ and in no further $I \in \mathcal{I}$. This means that $r(k) \sim r(j)$, so $r(k) \in \tilde{J}$ and, hence, $r(J) \subset \tilde{J}$. Further, every $l \in \tilde{J}$ is the image under r of $r^{-1}(l) \in J$, so that $r(J) = \tilde{J}$. □

We can now understand the structure of the stabilizer group S.

Theorem A.1.2 *The stabilizer group S is given by $S = \bigotimes_{J\in\mathcal{J}} S(J)$, where $S(J)$ is the group of permutations on the set J.*

Proof From Lemma (A.1.1) it is clear that $S \subset \bigotimes_{J\in\mathcal{J}} S(J)$. Conversely, let $s \in \bigotimes_{J\in\mathcal{J}} S(J)$, so that $s(J) = J$ for all $J \in \mathcal{J}$. Since, from Eq. (A.7), every $I \in \mathcal{I}$ can be written as a union of certain $J \in \mathcal{J}$ it follows that $s(I) = I$ for all $I \in \mathcal{I}$, so $s \in S$ and, hence, $\bigotimes_{J\in\mathcal{J}} S(J) \subset S$. □

Returning to the general story, we call a permutation $r \in R$ *order-preserving* iff for all $J \in \mathcal{J}$ and all $i, j \in J$ with $i < j$ it follows that $r(i) < r(j)$. In other words, such permutations preserve the natural ordering of the numbers $1, \ldots, n$ but only within each set $J \in \mathcal{J}$. The set of all order-preserving permutations forms a sub-group of R which I denote by P'.

Lemma A.1.3 *Each equivalence class $p \in P$ contains exactly one order-preserving permutation in P'.*

Proof For existence, consider an arbitrary representative $s \in p$ of an equivalence class $p \in P$ and consider the restriction $s|_J : J \to s(J)$ to any $J \in \mathcal{J}$. We can find a permutation $r_J \in S(J)$ of J such that $s|_J \circ r_J$ has the order-preserving property. The maps $r_J : J \to J$ combine into permutation a $r \in S_n$ which, from Theorem A.1.2 is an element of the stabilizer group S. Then, $s \circ r \in p$ and it is order-preserving.
For uniqueness, consider two permutations $s, \tilde{s} \in p$ which are both order-preserving. This means than $r \equiv s \circ \tilde{s}^{-1}$ is in S that is, $r|_J \in S(J)$ is a permutation of J. For $i, j \in J$ with $i < j$ we have $r(i) < r(j)$ which means that $r|_J = \mathrm{id}_J$. This is true for all $J \in \mathcal{J}$ so that $r = \mathrm{id}$ and, hence, $s = \tilde{s}$. $\square$

This result means that we can define a group isomorphism $\tau : P \to P' \subset R$ which assigns to a class $p \in P$ the unique order-preserving permutation $\tau(p) \in p$. Of course, $[\tau(p)] = p$, so τ splits the sequence (A.4). This means that R is a semi-direct product

$$R \cong P \ltimes S \tag{A.8}$$

with the isomorphism $\varphi : P \times S \to R$ defined by $\varphi((p, s)) = \tau(p)s$ and the multiplication in $P \times S$

$$(p, s)(\tilde{p}, \tilde{s}) = (p\tilde{p}, \tilde{p}^{-1} s \tilde{p} \tilde{s}) \ . \tag{A.9}$$

So we can determine $P \cong P'$ by finding the permutations in S_n which map the sets $\mathcal{I}$ into each other (that is, which are elements of R) and are order-preserving. The group R can then be obtained from S and P by forming the semi-direct product (A.8).

A.1.2 Invariance group of $\mathbb{C}^n - Z$

We now discuss the structure of G_B. First note that there is an obvious embedding $S_n \hookrightarrow \mathrm{Gl}(n, \mathbb{C})$ defined by $\sigma(\mathbf{e}_i) = \mathbf{e}_{\sigma(i)}$, with the standard unit vectors $\mathbf{e}_i$. Hence, the above subgroups $S, R, P' \subset S_n$ have isomorphic images in $\mathrm{Gl}(n, \mathbb{C})$ which we denote by S_B, R_B, P_B, respectively. In fact, from the definition of S, R, P it is clear that S_B, R_B, P_B leave the zero set Z invariant and are, hence, sup-groups of G_B. Another obvious sub-group of G_B is

$$H_B = \{g \in G_B \,|\, g(Z(I)) = Z(I), \ \forall I \in \mathcal{I}\} \subset G_B \ , \tag{A.10}$$

that is, the sub-group which leaves the components $Z(I)$ of the zero set invariant individually. Clearly, $S_B \subset H_B$.

Lemma A.1.4 *For $g \in G_B$ we have $g(Z(I)) \in \mathcal{Z}$ for all $I \in \mathcal{I}$, that is, elements of G_B map zero sets $Z(I)$ into other zero sets.*

Proof For $g \in G_B$, the image $g(Z(I))$ is a vector-space of the same dimension as $Z(I)$. But the only vector spaces contained in Z are the $Z(I)$ and their sub-spaces, so $g(Z(I))$ must be contained in some $Z(I')$. Say that $Z(I') = g(Z(I)) \oplus X$, for some vector space X. Then $g^{-1}(Z(I')) = Z(I) \oplus g^{-1}(X)$ which, by the same argument applied to g^{-1}, should be a subset of some $Z(\tilde{I})$. This means that $Z(I) \subset Z(\tilde{I})$ but, since we have dropped trivial zero sets which are already contained in others, it follows that $Z(I) = Z(\tilde{I})$. So we have $Z(I) \oplus g^{-1}(X) \subset Z(\tilde{I}) = Z(I)$ which means that $g^{-1}(X) = 0$ and, hence, $X = 0$. Therefore, $g(Z(I)) = Z(I')$. □

Lemma A.1.5 *The group G_B can be decomposed as $G_B = P_B\, H_B$. Further, H_B is a normal sub-group of G_B and $P_B \cap H_B = 1$.*

Proof For the first part of the statement, consider a $g \in G_B$ and its restriction $g_I : Z(I) \to Z(I') = g(Z(I))$ to the zero set $Z(I)$. We can find a permutation matrix $r_I : Z(I) \to Z(I')$ which maps the standard basis $\{\mathbf{e}_i \,|\, i \notin I\}$ of $Z(I)$ into the basis $\{\mathbf{e}_i \,|\, i \notin I'\}$ of $Z(I')$. Clearly, $\tilde{h}_I \equiv r_I^{-1} \circ g_I : Z(I) \to Z(I)$ and $g_I = r_I \circ \tilde{h}_I$. The maps r_I can be made consistent on intersections of zero sets since $g(Z(I) \cap Z(I')) = g(Z(I)) \cap g(Z(I'))$. Hence, the r_I can be combined to a map $r \in Gl(n, \mathbb{C})$ with $r|_{Z(I)} = r_I$ which permutes the standard basis vectors $\mathbf{e}_i$ and maps zero sets $Z(I)$ into each other, so $r \in R_B$. Further, defining $\tilde{h} = r^{-1} \circ g$ it follows that $\tilde{h} \in H_B$. From the previous section, we know that we can write $r = ps$, where $p \in P_B$ and $s \in S_B$. Finally, with $h \equiv s\tilde{h} \in H_B$ we have $g = ph$, where $p \in P_B$ and $h \in H_B$.
To show that H_B is a normal sub-group of G_B, consider a $\eta \in H_B$ and a $g = ph \in G_B$. Then $g\eta g^{-1} = ph\eta h^{-1}p^{-1} = ph'p^{-1}$, where $h' = h\eta h^{-1} \in H_B$. Hence, $g\eta g^{-1}(Z(I)) = ph'p^{-1}(Z(I)) = Z(I)$, so $g\eta g^{-1} \in H_B$.
Finally, from the definition of R it is clear that $R_B \cap H_B = S_B$. But S_B contains precisely one order-preserving element, the identity. □

The result of the previous Lemma shows that G_B is a semi-direct product $G_B \cong P \ltimes H_B$.
If we denote by $\phi : P \to P_B$ the isomorphism between order-preserving permutations in P and corresponding $Gl(n, \mathbb{C})$ matrices, then a pair $(p, h) \in P \ltimes H_B$ is mapped to $\phi(p)h \in G_B$ and the multiplication in $P \ltimes H_B$ is

$$(p, h)(\tilde{p}, \tilde{h}) = (p\tilde{p}, \phi(\tilde{p})^{-1} h \phi(\tilde{p})\tilde{h}) \,. \tag{A.11}$$

We have already understood the permutation group P and how to compute it from the basic data. I remains to consider H_B. To this end, let me define the group

$$G(\mathcal{J}) = \bigotimes_{J\in\mathcal{J}} \mathrm{Gl}(J,\mathbb{C}) \;, \tag{A.12}$$

where $\mathrm{Gl}(J,\mathbb{C})$ is the general linear group acting in the directions of the coordinates $\mathbf{x}_J \equiv (x_j \,|\, j \in J)$. Recall that the sets $\mathcal{J}$ were defined around Eq. (A.5). The elements of (A.12) can be viewed as block-diagonal $n \times n$ matrices with the blocks corresponding to the coordinates $\mathbf{x}_J$.

Lemma A.1.6 *It follows that $G(\mathcal{J}) \subset H_B$.*

Proof From Eq. (A.7) we know that every set $I \in \mathcal{I}$ can be written as a disjoint union $I = \bigcup J$ of some $J \in \mathcal{J}$. It follows that $Z(I) = Z(\cup J) = \cap Z(J)$. The transformations (A.12) leave all $Z(J)$ and, hence, $Z(I)$ invariant so that $G(\mathcal{J}) \subset H_B$. □

Unfortunately, H_B can be larger than $G(\mathcal{J})$. In general we know that the zero sets $Z(I)$ and their intersections $Z(I_1)\cap\cdots\cap Z(I_p) = Z(I_1\cup\cdots\cup I_p)$ have to be invariant under transformations $h = (h_{ij}) \in H_B$. This implies, for any union $I_1 \cup \cdots \cup I_p$, that

$$h_{ij} = 0 \;\text{ for }\; i \in I_1 \cup \cdots \cup I_p \;,\;\; j \in (I_1 \cup \cdots \cup I_p)^c \;. \tag{A.13}$$

We call a zero set $\mathcal{I}$ and associated set $\mathcal{J}$ *regular* if for every $J \in \mathcal{J}$ and all $i \in J$, $j \in J^c$ there exists an $I \in \mathcal{I}$ with $i \in I$ but $j \notin I$. Then we have:

Theorem A.1.7 *If the zero set $\mathcal{I}$ is regular then $G(\mathcal{J}) = H_B$.*

Proof Focus on a specific $J \in \mathcal{J}$ and fix a $i \in J$ and a $j \in J^c$. From regularity there exists an $I \in \mathcal{I}$ such that $i \in I$ and $j \in I^c$. Applying (A.13) for I and I^c means that $h_{ij} = 0$. Since i and j were arbitrary this means that $h_{ij} = 0$ for all $i \in J$ and all $j \in J^c$.
Now consider an $i \in J^c$ and a $j \in J$. We know that J^c is the disjoint union of the other J, so $i \in \tilde{J} \subset J^c$ for a particular $\tilde{J} \in \mathcal{J}$. Regularity, applied to $\tilde{J}$, means that there exists an $I \in \mathcal{I}$ with $i \in I$ and $j \in I^c$. As before, (A.13) applied to I leads to $h_{ij} = 0$. Since i, j were arbitrary this means that $h_{ij} = 0$ for all $i \in J^c$ and all $j \in J$.
In summary, for all $J \in \mathcal{J}$ we have $h_{ij} = 0$ if $i \in J$ and $j \in J^c$ or if $i \in J^c$ and $j \in J$. This means that $h \in G(\mathcal{J})$, so $H_B \subset G(\mathcal{J})$. The opposite inclusion has already been shown in the previous Lemma, so $G(\mathcal{J}) = H_B$. □

Therefore the complete symmetry group of $B = \mathbb{C}^n - Z$ is

$$G_B \cong P \ltimes G(\mathcal{J}) \tag{A.14}$$

and P and H_B for the examples are given as follows.

A.1.3 Normalizer in $\mathrm{GL}(n,\mathbb{C})$

In order to find the symmetry group G_A of the toric space we need to compute the normalizer of the toric group $\mathcal{G}$ within G_B, the symmetry group of the upstairs space. This is relatively easy if the group elements of $\mathcal{G}$ are proportional to the unit matrix within each block (A.12) of G_B. In order to sort this out it is instructive to first deal with a related - but simpler - problem, namely to compute the normalizer of $\mathcal{G}$ within $\mathrm{Gl}(n,\mathbb{C})$.
To this end it is useful to split the various coordinate directions up into disjoint blocks $\mathcal{K} = \{K \,|\, K \subset \{1,\ldots,n\}\}$, collecting the directions with the same charges $\mathbf{q}_i$, such that

$$\mathcal{G} = \bigotimes_{K\in\mathcal{K}} \mathcal{G}_{\mathbf{q}_K}(K) \tag{A.15}$$

where $\mathcal{G}_{\mathbf{q}_K}(K) = \{\mathbf{s}^{\mathbf{q}_K}\,\mathbf{1}_{|K|} \,|\, \mathbf{s} \in (\mathbb{C}^*)^{n-d}\}$ consists of matrices proportional to the unit matrix and by $\mathbf{q}_K$ I denote the charge in the directions in K. As usual, we think of the symmetric group S_n as being embedded into $\mathrm{GL}(n,\mathbb{C})$ via $\sigma(\mathbf{e}_i) = \mathbf{e}_{\sigma(i)}$ for $\sigma \in S_n$. We would like to work out the normalizer

$$N_{\mathrm{Gl}(n,\mathbb{C})}(\mathcal{G}) = \{g \in \mathrm{Gl}(n,\mathbb{C}) \,|\, g\mathcal{G} = \mathcal{G}g\} = \{g \in \mathrm{Gl}(n,\mathbb{C}) \,|\, \forall\gamma \in \mathcal{G}\ \ \exists\tilde{\gamma} \in \mathcal{G} \,:\, g\gamma = \tilde{\gamma}g\}\ . \tag{A.16}$$

It is also useful to introduce the commutant

$$C_{\mathrm{Gl}(n,\mathbb{C})}(\mathcal{G}) = \{g \in \mathrm{Gl}(n,\mathbb{C}) \,|\, g\gamma = \gamma g\ \forall\gamma \in \mathcal{G}\}\ , \tag{A.17}$$

of $\mathcal{G}$ within $\mathrm{Gl}(n,\mathbb{C})$. We also introduce the sub-groups of S_n defined by

$$\mathcal{R} = S_n \cap N_{\mathrm{Gl}(n,\mathbb{C})}(\mathcal{G})\ , \quad \mathcal{S} = S_n \cap C_{\mathrm{Gl}(n,\mathbb{C})}(\mathcal{G})\ , \tag{A.18}$$

consisting of permutations which normalize or commute $\mathcal{G}$, respectively. I start by characterizing the groups $\mathcal{R}$ and $\mathcal{S}$ in a different way which is more useful for practical calculations.

Lemma A.1.8 *i)* $\mathcal{R} \subset \bar{\mathcal{R}} \equiv \{\sigma \in S_n \,|\, \sigma(K) \in \mathcal{K}\ \ \forall K \in \mathcal{K}\}$, *ii)* $\mathcal{S} = \{\sigma \in S_n \,|\, \sigma(K) = K\ \ \forall K \in \mathcal{K}\}$

Proof i) Consider a permutation $\sigma \in S_n$ which normalizes $\mathcal{G}$ so that for all $\gamma \in \mathcal{G}$ there exists a $\tilde{\gamma} \in \mathcal{G}$ such that $\gamma\sigma = \sigma\tilde{\gamma}$ with $\gamma = \mathrm{diag}(\mathbf{s}^{\mathbf{q}_i})$ and $\tilde{\gamma} = \mathrm{diag}(\tilde{\mathbf{s}}^{\mathbf{q}_i})$. It follows that $\tilde{\mathbf{s}}^{\mathbf{q}_i} = \mathbf{s}^{\mathbf{q}_{\sigma(i)}}$ for all i, so that $\tilde{\gamma} = \mathrm{diag}(\mathbf{s}^{\mathbf{s}_{\sigma(i)}})$. Consider all $i \in K$ for a given block K, so that $\mathbf{q}_i = \mathbf{q}_K$. Then $\mathbf{s}^{\mathbf{q}_{\sigma(i)}} = \tilde{\mathbf{s}}^{\mathbf{q}_K}$ for all $i \in K$. This only works if all $\mathbf{q}_{\sigma(i)} = \mathbf{q}_{K'}$ are equal, so that $\sigma(i) \in K'$ for all $i \in K$. Hence, $\sigma(K) \subset K' \in \mathcal{K}$. Applying the same argument to σ^{-1} and K' leads to $\sigma^{-1}(K') \subset K$, so combined we have $\sigma(K) = K'$.
ii) Clearly, permutations which only act within blocks are in the commutant. Conversely, permutations in the commutant have to be block-diagonal from Schur's Lemma. □

So, $\mathcal{S}$ is the set of permutations of directions within each block and $\bar{\mathcal{R}}$ contains permutations of blocks and within blocks. Unfortunately, the group $\mathcal{R}$ we are actually interested in can be genuinely smaller than $\bar{\mathcal{R}}$. If there are more blocks than variables $\mathbf{s}$ it might happen that a permutation of these blocks cannot be compensated by a choice of $\tilde{\mathbf{s}}$ in the normalizer condition. Clearly, $\mathcal{S} \subset \mathcal{R}$ is a sub-group and indeed a normal sub-group so that we can define the quotient group

$$\mathcal{P} = \mathcal{R}/\mathcal{S} \; . \tag{A.19}$$

There is a monomorphism $\mathcal{P} \to \mathcal{R}$ which involves assigning to an element of $\mathcal{P}$ the element of $\mathcal{R}$ which permutes the blocks in $\mathcal{K}$ in the same way and preserves the natural order in each block $K \in \mathcal{K}$. In this way,

$$\mathcal{R} = \mathcal{P} \ltimes \mathcal{S} \; . \tag{A.20}$$

We are now ready for the following theorem.

Theorem A.1.9 *The normalizer can be expressed in terms of the commutant as* $N_{\mathrm{Gl}(n,\mathbb{C})}(\mathcal{G}) = \mathcal{P}\, C_{\mathrm{Gl}(n,\mathbb{C})}(\mathcal{G})$*,* $C_{\mathrm{Gl}(n,\mathbb{C})}(\mathcal{G})$ *is a normal sub-group of* $N_{\mathrm{Gl}(n,\mathbb{C})}(\mathcal{G})$ *and* $\mathcal{P} \cap C_{\mathrm{Gl}(n,\mathbb{C})}(\mathcal{G}) = 1$*.*

Proof We begin by showing that every matrix $g =\in N_{\mathrm{Gl}(n,\mathbb{C})}(\mathcal{G})$ can be written as a product of a permutation and a matrix in the commutant. First, $g = (g_{ij}) \in N_{\mathrm{Gl}(n,\mathbb{C})}(\mathcal{G})$ means that for all $\gamma \in \mathcal{G}$ there exists a $\tilde{\gamma} \in \mathcal{G}$ such that $g\gamma = \tilde{\gamma} g$. Write $\gamma = \mathrm{diag}(\chi_i)$ and $\tilde{\gamma} = \mathrm{diag}(\tilde{\chi}_i)$ where $\chi_i = \mathbf{s}^{\mathbf{q}_i}$ and $\tilde{\chi}_i = \tilde{\mathbf{s}}^{\mathbf{q}_i}$. Then it follows that $g_{ij}(\tilde{\chi}_i - \chi_j) = 0$ for all i, j. The matrix g is invertible which means that for every row i there exists a column j with $g_{ij} \neq 0$ and, moreover, for each row we can choose a different column. This means there exists a permutation $\sigma \in S_n$ so that $g_{i\sigma^{-1}(i)} \neq 0$ for all i. In order to satisfy the normalized condition we then need that $\tilde{\chi}_i = \chi_{\sigma^{-1}(i)}$. Now define $c = \sigma^{-1} g$ so that $g = \sigma c$. The normalizer condition then reads $c\gamma c^{-1} = \sigma^{-1}\tilde{\gamma}\sigma = \mathrm{diag}(\tilde{\chi}_{\sigma(i)}) = \mathrm{diag}(\chi_i) = \gamma$ and, hence, $c \in C_{\mathrm{Gl}(n,\mathbb{C})}(\mathcal{G})$ is in the commutant. This shows that every g in the normalizer can be written as $g = \sigma c$ with $\sigma \in S_n$ and c in the commutant. With this decomposition, the normalizer condition, $g\gamma = \tilde{\gamma} g$ becomes $\sigma\gamma = \tilde{\gamma}\sigma$ which shows that, in fact, $\sigma \in \mathcal{R}$. Further we know that every $r \in \mathcal{R}$ can be written as $r = ps$, where $p \in \mathcal{P}$ and $s \in \mathcal{S}$, so that $g = rc = psc$. But both s, c and their product sc are in the commutant. This proves the decomposition $N_{\mathrm{Gl}(n,\mathbb{C})}(\mathcal{G}) = \mathcal{P}\, C_{\mathrm{Gl}(n,\mathbb{C})}(\mathcal{G})$.
We now need to show that $C_{\mathrm{Gl}(n,\mathbb{C})}(\mathcal{G})$ is a normal sub-group of $N_{\mathrm{Gl}(n,\mathbb{C})}(\mathcal{G})$. Choose a c in the commutant and $g = pc'$ in the normalizer. Then $gcg^{-1} = p\tilde{c}p^{-1}$ where $\tilde{c} = c'cc'^{-1}$ is in the commutant, so we need to show that $p\tilde{c}p^{-1}$ is also in the commutant, that is $p\tilde{c}p^{-1}\gamma = \gamma p\tilde{c}p^{-1}$ for all $\gamma \in \mathcal{G}$. This is equivalent to $\tilde{c}\tilde{\gamma} = \tilde{\gamma}\tilde{c}$ where $\tilde{\gamma} = p^{-1}\gamma p$. However, $\tilde{\gamma}$ has the same block-structure than elements in $\mathcal{G}$ (as the action of p permutes the blocks) so that $\tilde{c}$ and $\tilde{\gamma}$ indeed commute.

Finally, since the action $p^{-1}\gamma p$ of a $p \in \mathcal{P}$ on $\gamma \in \mathcal{G}$ permutes the blocks of γ, it follows that the only $p \in \mathcal{P}$ for which $p^{-1}\gamma p = \gamma$ is, in fact, $p = 1$, so that $N_{\mathrm{Gl}(n,\mathbb{C})}(\mathcal{G})$ and $\mathcal{P} \cap C_{\mathrm{Gl}(n,\mathbb{C})}(\mathcal{G}) = 1$. □

So, in summary, we have found that the normalizer can be expressed in terms of the commutant as

$$N_{\mathrm{Gl}(n,\mathbb{C})}(\mathcal{G}) = \mathcal{P} \ltimes C_{\mathrm{Gl}(n,\mathbb{C})}(\mathcal{G}) \ , \tag{A.21}$$

and the latter, by means of Schur's Lemma, can be written as

$$C_{\mathrm{Gl}(n,\mathbb{C})}(\mathcal{G}) = \bigotimes_{K \in \mathcal{K}} \mathrm{Gl}(K, \mathbb{C}) \ . \tag{A.22}$$

A.1.4 Invariance group of the toric ambient space A

In order to find the symmetry group G_A of the toric ambient space we have to compute the normalizer $N_{G_B}(\mathcal{G})$. Clearly, this normalizer is given by

$$N_{G_B}(\mathcal{G}) = G_B \cap N_{\mathrm{Gl}(n,\mathbb{C})}(\mathcal{G}) \ . \tag{A.23}$$

The two groups on the right-hand side have been explicitly determined in the previous two sections, so our remaining task is to express their intersection in a useful form. Both groups have a similar structure in that they relate to a block-decomposition of the n coordinates and consist of a semi-direct product of a permutation group which exchanges the blocks times block-diagonal matrices which generate general linear transformations within each block. However, the block-decomposition is in general different for the two cases. The group G_B relates to the block-decomposition $\mathcal{J}$ which follows from the structure of the zero set and is given by

$$G_B = P \ltimes H_B \ , \quad H_B = \bigotimes_{J \in \mathcal{J}} \mathrm{Gl}(J, \mathbb{C}) \ . \tag{A.24}$$

The group $N_{\mathrm{Gl}(n,\mathbb{C})}(\mathcal{G})$, on the other hand, relates to the block-decomposition $\mathcal{K}$ which follows from the toric group $\mathcal{G}$ and is given by

$$N_{\mathrm{Gl}(n,\mathbb{C})}(\mathcal{G}) = \mathcal{P} \ltimes C_{\mathrm{Gl}(n,\mathbb{C})}(\mathcal{G}) \ , \quad C_{\mathrm{Gl}(n,\mathbb{C})}(\mathcal{G}) = \bigotimes_{K \in \mathcal{K}} \mathrm{Gl}(K, \mathbb{C}) \ . \tag{A.25}$$

The complication is that the block-decompositions $\mathcal{J}$ and $\mathcal{K}$ are not necessarily identical. It is, therefore, useful to define the refined block-decomposition given as the intersection of $\mathcal{J}$ and $\mathcal{K}$ defined by

$$\mathcal{L} = \{L = J \cap K \,|\, J \in \mathcal{J} \ , \ K \in \mathcal{K} \ , \ L \neq \emptyset\} \ . \tag{A.26}$$

We introduce the usual collection of groups associated to this block-decomposition. First, there are the block-diagonal matrices in

$$H_A = \bigotimes_{L\in\mathcal{L}} \mathrm{Gl}(L,\mathbb{C}) \ . \tag{A.27}$$

Then we have the stabilizer group, $S_{\mathcal{L}}$, and the block-permutation group, $R_{\mathcal{L}}$, defined by

$$S_{\mathcal{L}} = \{\sigma \in S_n \,|\, \sigma(L) = L \ \ \forall L \in \mathcal{L}\} \ , \quad R_{\mathcal{L}} = \{\sigma \in S_n \,|\, \sigma(L) \in \mathcal{L} \ \ \forall L \in \mathcal{L}\} \ . \tag{A.28}$$

As usual, we can then form the quotient and the semi-direct product

$$P_{\mathcal{L}} = R_{\mathcal{L}}/S_{\mathcal{L}} \ , \quad R_{\mathcal{L}} = P_{\mathcal{L}} \ltimes S_{\mathcal{L}} \ . \tag{A.29}$$

From the definition of the various block structures is it clear that

$$H_A = H_B \cap C_{\mathrm{Gl}(n,\mathbb{C})}(\mathcal{G}) \ , \tag{A.30}$$

and we expect this to be the continuous part of $N_{G_B}(\mathcal{G})$. We also define the intersection of the permutation groups

$$R_A = R \cap \mathcal{R} \ , \quad S_A = S \cap \mathcal{S} \ , \quad P_A = R_A/S_A \ , \quad R_A = P_A \ltimes S_A \ . \tag{A.31}$$

The two sets of discrete groups relate in the following way.

Lemma A.1.10 *i)* $R_A \subset R_{\mathcal{L}}$*, ii)* $S_A = S_{\mathcal{L}}$*, iii)* $P_A \subset P_{\mathcal{L}}$*.*

Proof i) Consider a $r \in R \cap \mathcal{R}$ so that $r(J) \in \mathcal{J}$ for all $J \in \mathcal{J}$ and $r(K) \in \mathcal{K}$ for all $K \in \mathcal{K}$. Then, for any $L = J \cap K \in \mathcal{L}$ we have $r(L) = r(J \cap K) = r(J) \cap r(K)$ so that $r(L) \in \mathcal{L}$. Hence, $R \cap \mathcal{R} \subset R_{\mathcal{L}}$.
ii) "$\subset$": For $s \in S \cap \mathcal{S}$ we have $s(J) = J$ for all $J \in \mathcal{J}$ and $s(K) = K$ for all $K \in \mathcal{K}$. Then, for all $L = J \cap K \in \mathcal{L}$ we have $s(L) = s(J \cap K) = s(J) \cap s(K) = J \cap K = L$, so that $s \in S_{\mathcal{L}}$.
"$\supset$": Let $s \in S_{\mathcal{L}}$, hence $s(L) = L$ for all $L \in \mathcal{L}$. Every $J \in \mathcal{J}$ can be written as a disjoint union $J = \bigcup_{L:L\cap J\neq\emptyset} L$ and likewise every $K \in \mathcal{K}$ as $K = \bigcup_{L:L\cap K\neq\emptyset} L$. Hence, since all L are left invariant by s so are all J and K and it follows that $s \in S \cap \mathcal{S}$.
iii) This follows directly from i) and ii). □

Theorem A.1.11 *The normalizer group* $N_{G_B}(\mathcal{G})$ *can be written as* $N_{G_B}(\mathcal{G}) = R_A H_A$*.*

Proof "$\supset$": Consider a $g = rh \in R_A H_A$, where $r \in R_A = R \cap \mathcal{R}$ and $h \in H_A = H_B \cap C_{\mathrm{Gl}(n,\mathbb{C})}(\mathcal{G})$. It follows that $rh \in RH_B = G_B$ and $rh \in \mathcal{R}C_{\mathrm{Gl}(n,\mathbb{C})} = N_{\mathrm{Gl}(n,\mathbb{C})}(\mathcal{G})$ and, hence, $g = rh \in N_{G_B}(\mathcal{G})$.
"$\subset$": Start with a $g \in N_{G_B}(\mathcal{G}) = G_B \cap N_{\mathrm{Gl}(n,\mathbb{C})}(\mathcal{G})$ which can be written as $g = p\tilde{h} = \pi\tilde{c}$ with

$p \in P$, $\tilde{h} \in H_B$, $\pi \in \mathcal{P}$, $\tilde{c} \in C_{\mathrm{Gl}(n,\mathbb{C})}(\mathcal{G})$. It follows that $\pi^{-1}p = \tilde{c}\tilde{h}^{-1} \in C_{\mathrm{Gl}(n,\mathbb{C})}(\mathcal{G})H_B$. Since $\pi^{-1}p$ is a permutation it follows that $\pi^{-1}p \in \mathcal{S}S$ which is the set of permutations in $C_{\mathrm{Gl}(n,\mathbb{C})}(\mathcal{G})H_B$ (I am not completely sure this conclusion is correct. To be checked!). Write $\pi^{-1}p = \sigma s^{-1}$, where $\sigma \in \mathcal{S}$ and $s \in S$, so that $ps = \sigma\pi \equiv \gamma$. Since $ps \in R$ and $\pi\sigma \in \mathcal{R}$ it follows that $\gamma \in R \cap \mathcal{R} = R_A$. Define $h = s^{-1}\tilde{h} \in H_B$ and $c = \sigma^{-1}\tilde{c} \in C_{\mathrm{Gl}(n,\mathbb{C})}(\mathcal{G}$ so that $g = \gamma h = \gamma c$. It follows that $h = c \in H_B \cap C_{\mathrm{Gl}(n,\mathbb{C})}(\mathcal{G} = H_A$ and, therefore $g = \gamma h \in R_A H_A$. *Box*

It is now clear that we can write $N_{G_B}(\mathcal{G})$ as a semi-direct product

$$N_{G_B}(\mathcal{G}) = P_A \ltimes H_A \tag{A.32}$$

by dividing out the group S_A. To find the invariance group, G_A, of the toric space we have to divide this by $\mathcal{G}$ which results in

$$G_A = P_A \ltimes (H_A/\mathcal{G}) \,. \tag{A.33}$$

This completes the calculation of G_A.

A.1.5 The automorphism group of a toric variety revisited

The toric divisors x_i correspond to elements of $\Sigma'(1)$ and hence lattice points on Δ°. We denote the lattice points by v_i for $i \in \{1, \cdots, n\}$. The toric variety can be presented as

$$\mathbb{P}_{\Sigma'} = (\mathbb{C}^n - Z)/(\mathbb{C}^*)^{n-d} \tag{A.34}$$

Here, Z is the SR-ideal, containing collections $I \in \mathcal{I}$ of v_i not contained in a common cone of Σ'. The $\mathbb{C}^*$ action is described by charge vectors $\mathbf{q}_i$ and acts as

$$x_i \mapsto s_r^{q_i^r} x_i \,. \tag{A.35}$$

for $r = 1 \cdots n - d$ and $s_r \in \mathbb{C}^*$. We also collectively denote $s_r^{q_i^r} = \lambda_i(s_r)$. The components q_i^r of the charge vectors [1] satisfy

$$\sum_i v_i(q_i^r) = 0 \,. \tag{A.36}$$

[1] Our notation is such that a charge vector contains all of the charges under the $(n-d)$ $\mathbb{C}^*$ action on a single homogeneous coordinate x_i.

A.1.5.1 The set $\mathcal{K}$

Let us first consider the set $\mathcal{K}$. Its elements K are sets containing a collection of indices $\{1, .., n\}$ such that $\mathbf{q}_i = \mathbf{q}_j$ for all i, j in a specific K. As we discuss now, this has fairly strong implications for any two i, j in the same K.

Theorem A.1.12 *On a simply connected toric variety, any two lattice points v_i and v_j on Δ° for which $\mathbf{q}_i = \mathbf{q}_j$ are vertices of Δ°. Furthermore, there exist points α_{ij} inside of $\Theta_i^{[3]}$ as well as α_{ji} inside of $\Theta_j^{[3]}$ for which $\alpha_{ij} = -\alpha_{ji}$.*

Proof From the equality of $\mathbf{q}_i$ and $\mathbf{q}_j$ it follows that the corresponding divisors D_i and D_j are linearly equivalent. As all linear equivalences take the form

$$\sum_{k=1}^{n} \langle \alpha_{ij}, v_k \rangle D_k = 0 \tag{A.37}$$

for some vector α_{ij} in $M \otimes \mathbb{R}$, there must be a vector α_{ij} such that

$$\langle \alpha_{ij}, v_i \rangle = -1 \qquad \langle \alpha_{ij}, v_j \rangle = 1 \qquad \langle \alpha_{ij}, v_k \rangle = 0 \ \forall \ k \neq i, j \tag{A.38}$$

For a simply connected toric variety, the set of all vectors v_i generate the lattice N (see e.g. [Fulton, sect 3.2.]). Hence a first consequence of this is that α_{ij} is contained in the dual lattice M. Furthermore, the above implies that it is a lattice point on Δ, as $\langle \alpha_{ij}, v_k \rangle \geq -1$ for all points v_k on Δ°. $\langle \alpha_{ij}, v_k \rangle = 0 \ \forall \ k \neq i, j$ implies that all v_k except v_i and v_j are contained in a three-dimensional hyperplane of $N \otimes \mathbb{R}$ passing through the origin. As Δ° is four-dimensional and the convex hull of all of the v_l, it follows that v_i and v_j must be above and below this hyperplane, so that they must be vertices. In this case (A.38) implies that α_{ij} is inside the dual three-dimensional face of v_i, $\Theta_i^{[3]}$ and $\alpha_{ji} = -\alpha_{ij}$ is inside $\Theta_j^{[3]}$.

The above provides an alternative algorithm for determining the set $\mathcal{K}$: all indices l corresponding to non-vertices v_l form sets $K_l = \{l\}$. For any vertex v_i, we have to find the interior points of the dual face $\Theta_i^{[3]}$. If the negative of such an interior point is also inside of a three-dimensional face $\Theta_j^{[3]}$ (defining a dual vertex v_j of Δ°) there is a set $K \in \mathcal{K}$ containing both i and j. This defines an equivalence relation $\sim_{\mathcal{K}}$ and the equivalence classes are precisely the $K \in \mathcal{K}$.
This way of thinking is supposed to be particularly useful for polytopes Δ° with many integral points, where many points (all non-vertices) can never occur in any non-trivial set $K \in \mathcal{K}$.

A.1.5.2 The set $\mathcal{J}$

The data exploited in the last paragraph only depends on the structure of the polytopes Δ° and Δ. Let us now consider the triangulation data. We collect the generators of the SR ideal into a sets $I \in \mathcal{I}$. Then we construct a refinement $\mathcal{J}$ of $\mathcal{I}$, i.e. every set $J \in \mathcal{J}$ is contained in one $I \in \mathcal{I}$, in the following way: the sets J are the equivalence classes under the equivalence relation

$$j \sim_{\mathcal{J}} i \;\leftrightarrow\; i \text{ and } j \text{ are contained in the same sets } I \in \mathcal{I}\,. \tag{A.39}$$

In other words, $\mathcal{J}$ is obtained by first forming all intersections between sets in $\mathcal{I}$ and then discarding sets which are already containing smaller sets.

Lemma A.1.13 *If all cones in a fan Σ' are symmetrical with respect to exchanging $i \leftrightarrow j$ then $i \sim_{\mathcal{J}} j$.*

Proof To see this, all we have to do is go through the construction of $\mathcal{J}$ from the data of cones. We first find the SR ideal by forming the complement of the set of cones in the power set of $\{1, \cdots, n\}$. By construction this will be symmetrical under $i \leftrightarrow j$. But then also the set of generators $\mathcal{I}$ enjoys the same symmetry so that i and j are in the equivalence class in $\mathcal{J}$ as claimed.

Theorem A.1.14 *If $D_i = D_j$, so that $i \sim_{\mathcal{K}} j$, it follows that $i \sim_{\mathcal{J}} j$.*

Proof Due to the lemma, it is sufficient to show that any triangulation of the polytope Δ° is such that the collection of cones is symmetric under the exchange $i \leftrightarrow j$. First of all, the triangulation $tr(\Delta^\circ)$ is completely fixed in terms of its cones of maximal (i.e. 4) dimension. Every one of these cones is spanned by four linearly independent vectors in N. If such a cone contains both v_i and v_j among its generators, there is nothing to show, as this is symmetric in i and j. A cone which just contains v_i but not v_j is hence spanned by v_i and three vectors $v_{k_1}, v_{k_2}, v_{k_3}$ in the plane orthogonal to α_{ij}. This means the cone in question has a face (which is a three-dimensional cone) spanned only by $v_{k_1}, v_{k_2}, v_{k_3}$. For a fan constructed from a triangulation, every three-dimensional cone is the intersection of precisely two four-dimensional cones. Hence there must be another four-dimensional cone spanned by $v_{k_1}, v_{k_2}, v_{k_3}$ and another vector. The only vector which turns $v_{k_1}, v_{k_2}, v_{k_3}$ into a four-dimensional cone (besides v_i) is v_j. Hence there is a cone $\{1, k_1, k_2, k_3\}$ as well.

As a direct consequence of the above, $\mathcal{J}$ is a refinement of $\mathcal{K}$ (the converse is wrong, i.e. $\mathcal{K} \neq \mathcal{J}$ in general) for any triangulation. This means that the set $\mathcal{L} = \mathcal{K} \cap \mathcal{J} = \mathcal{K}$ is ultimately independent of which triangulation is chosen for Δ° !

A.2 Symmetries of the Calabi-Yau manifolds and Representation Theory

A.2.1 Twisted linear representations

Before considering the more difficult problem of finding all projective π-twisted representations, let us discuss how we can manage to find all π-twisted linear representations of a group G. Such representations can be constructed from appropriate linear representation, see [69] for a discussion in a similar context.

To start the construction, let us assume that we have found a, not necessarily injective, group homomorphism

$$\pi : G \to P_A \tag{A.40}$$

and ask how we can find all compatible π-twisted representations satisfying (3.10). Furthermore, we assume for simplicity that $\pi(\gamma)$ acts transitively on a number of 'blocks' B_i (of course all of these have the same size) and leaves everything else unchanged. We will discuss the general case below.

Labelling the relevant blocks by B_i by $i = 1...k$, we can single out one of the blocks and consider its stabilizer $G_i \subset G$. Note that the restriction of $r(\gamma)$ for $\gamma \in G_i$ to B_i defines a representation of G_i. Let us call these representations $r_i : G_i \to GL(B_i, \mathbb{C})$. An equivalent description is to write the representation $R(\gamma)$ as a product of two matrices

$$R(\gamma) = \pi(\gamma) \cdot \mathrm{diag}(r_1(\gamma), \cdots, r_n(\gamma)\,. \tag{A.41}$$

As we explain in the following, is enough to fix a single of the r_i to recover the whole π-twisted representation (3.10). Let us hence consider G_1, the stabilizer of the first block, and fix the representation $r_1 : G_1 \mapsto GL(B_1, \mathbb{C})$. To reconstruct the whole action of G we pick a set of group elements γ_i such that $\pi(\gamma_i)(1) = i$. We can make the choice $\gamma_1 = 1$ in G. We can then write any group element as

$$\gamma = \gamma_{\pi(\gamma)(i)} h \gamma_i^{-1}\,, \tag{A.42}$$

with h in G_1, for any i. We can hence think of h to depend on γ and i. To see this, note that h is given by

$$h = \gamma^{-1}_{\pi(\gamma)(i)} \gamma \gamma_i\,. \tag{A.43}$$

This is in G_1 as

$$\begin{aligned} \pi(h)(1) &= \pi(\gamma_{\pi(\gamma)(i)})^{-1} \pi(\gamma)\pi(\gamma_i)(1) \\ &= \pi(\gamma_{\pi(\gamma)(i)})^{-1} \pi(\gamma)(i) \\ &= 1 \end{aligned} \tag{A.44}$$

We may hence write

$$R(\gamma) = R(\gamma_{\pi(\gamma)(i)})R(h)R(\gamma_i^{-1}) \tag{A.45}$$

for any i and γ using an appropriate h. Going through the definitions this means that we can write

$$r_i(\gamma) = r_1(h) \tag{A.46}$$

This allows us to recover all of the matrices $r_i(\gamma)$ and hence the entire π-twisted representation. As we may construct h for any γ and i, the above relation holds for any π-twisted representation and we only need to find all group homomorphisms $\pi : G \to P_A$ and all linear representations of $r_i : G_1 \to GL(K, \mathbb{C})$ to construct all π-twisted representations.
In general, it is not true, however, that $\pi : G \to P_A$ acts transitively on the blocks and there may be several orbits. In this case, we can do the above construction separately for each orbit O_k and then combine all of the data to find a linear representation $R : G \to P_A \ltimes H_A$. Here, the representation matrix (A.42) becomes block diagonal with each block acting on the elements $\{B_k\}$ forming the k-th orbit O_k.
Note that neither all of the representations π nor all of the representations $r_1^k : G_1^k \to GL(B_k, \mathbb{C})$ need to be faithful to find a faithful representation R.
If we are given an action of $\pi : G \to P_A$ and want to find all π-twisted representations $r(\gamma)$, we hence need to

- Find all representations $\pi : G \to P_A$, not necessarily faithful.
- Find all orbits of the blocks under this action.
- For each orbit, pick out a block and call it B_1. This defines the group G_1.
- Choose the group elements g_i.
- Study all linear representations r_1 (not necessarily faithful) of G_1 on $GL(B_1, \mathbb{C})$.
- For each such linear representation r_1, we may find the corresponding h for each i and γ using (A.43). Using this h, we can determine all $r_i(\gamma)$ using (A.46). This completely fixes the representation R regarding the orbit under consideration.
- By choosing a linear representation for each orbit, we completely fix the representation R.

Note: as we are led to consider non-faithful representations, not all resulting R will be faithful as well. This means it will be better to start with the largest possible groups G when considering a specific model and exclude subgroup as those will already be dealt with automatically.

A.2.2 Toric representations

Then how do we get the group homomorphisms if we replace $\mathbb{C}^*$ with a correlated blocked $(\mathbb{C}^*)^n$ action? We claim that it is valid to combine different projective representations for each block(free and correlated ones as well), and checking two more conditions to remove the invalid ones.

Assuming we have in total n blocks, with d blocks correlated to the other $(n-d)$ blocks($\mathcal{G} \cong (\mathbb{C}^*)^{n-d}$), then by repeating the standard schur cover trick we have ($\bar{r}_i$,l_i,f_i,ϕ_i,e_i,h_i,$\hat{r}_i$) defined for the i-th block, then by combining the correspondent representations we write out our generalized representation as

$$\bar{r} = \mathrm{Diag}(\bar{r}_1, \bar{r}_2, ..., \bar{r}_n)$$

Firstly our $\bar{r}$ is a group homomorphism from $\Gamma_H \to H_A/\mathcal{G}$: From the above discussion, we know in the upstairs level $\hat{r}(k,\gamma) = \varphi(k)h(\gamma)l(\gamma)$, with each object diagonally blocked. Now $\hat{r}$ is a proper group homomorphism, because

$$\begin{aligned}
\hat{r}((k,\gamma)(\tilde{k},\tilde{\gamma})) &= \hat{r}(e(\gamma,\tilde{\gamma})k\tilde{k}, \gamma\tilde{\gamma}) = \phi(e(\gamma,\tilde{\gamma})k\tilde{k})h(\gamma\tilde{\gamma})l(\gamma\tilde{\gamma}) \\
&= \phi(e(\gamma,\tilde{\gamma}))\phi(k)\phi(\tilde{k})h(\gamma\tilde{\gamma})l(\gamma\tilde{\gamma}) \\
&= f(\gamma,\tilde{\gamma})h(\gamma)h(\gamma\tilde{\gamma})^{-1}h(\gamma)h(\gamma\tilde{\gamma})l(\gamma,\tilde{\gamma})\phi(k)\phi(\tilde{k}) \\
&= f(\gamma,\tilde{\gamma})l(\gamma\tilde{\gamma})h(\gamma)h(\tilde{\gamma})\phi(k)\phi(\tilde{k}) \\
&= \phi(k)\phi(\tilde{k})h(\gamma)h(\tilde{\gamma})l(\gamma)l(\tilde{\gamma})
\end{aligned} \tag{A.47}$$

Notice that this is the same as $\hat{r}(k,\gamma)\hat{r}(\tilde{k},\tilde{\gamma}) = \phi(k)\phi(\tilde{k})h(\gamma)h(\tilde{\gamma})l(\gamma)l(\tilde{\gamma})$, then $\hat{r}$ is a proper group homomorphism. Automatically $\bar{r} = \hat{\pi}(\hat{r})$ is a group homomorphism since both $\hat{\pi}$ and $\hat{r}$ are.

Then we claim that the sufficient condition of the consistency check is the following:

$$\hat{r}(k,\gamma)\hat{r}(\tilde{k},\tilde{\gamma})^{-1} \in \mathcal{G} \tag{A.48}$$

This is because given the same γ, varying k would not change the identification of $\bar{r}(\gamma)$ inside $\hat{r}(k,\gamma)$, namely $\hat{\pi}(k,\gamma) = \hat{\pi}(\tilde{k},\gamma)$ for all $k,\tilde{k} \in K$, then by definition of $\hat{\pi}$ we have $\hat{r}(k,\gamma)\hat{r}(\tilde{k},\tilde{\gamma})^{-1} \in \mathcal{G}$.

The last question is, how do we identify different upstairs linear representation to be the same, when they both are projected down to the correspondent projective representations.

Two projective representations $\bar{r}_1$ and $\bar{r}_2$ are equivalent only when there exist a automorphism $\mathcal{P}$ of the homogeneous coordinate space and a function $\theta : \Gamma_H \to \mathcal{G}$, such that for each $\gamma \in \Gamma_H$, we have $\mathcal{P}(\bar{r}_1(\gamma)) = \theta(\gamma)(\bar{r}_2(\gamma)\mathcal{P})$. Inserting the definition of $\bar{r} = \hat{\pi}(\hat{r}(k, \gamma))$, we would then have

$$\mathcal{P}(\hat{\pi}(\hat{r}(k_1, \gamma)) = \theta(\gamma)(\hat{\pi}(\hat{r}_2(k_2, \gamma))\mathcal{P}) \tag{A.49}$$

We see that choosing different k_1 and k_2 are equivalent to bringing in another factor into θ, namely θ is k_1, k_2 dependent. However in the sense of equivalent representation, we could just make one convenient choice of k_1, k_2 for each γ, checking the formula (A.49). That would be enough to help us removing the redundancies.

A.2.2.1 Surjectivety of δ

In this section we discuss how to recover all projective representations from linear representations in the case of 'correlated blocks'. More specifically, we are interested in maps

$$\Gamma \to \prod GL(d_i, \mathbb{C})/\mathcal{G} \tag{A.50}$$

where $\mathcal{G}$ is $(\mathbb{C}^*)^{n-k} \subset \mathbb{C}^{*n}$
The idea of the proof will be the following: we already know that δ is surjective in the standard case, so we will show that this implies that it also surjective in the more general case we are interested in.

A.2.2.2 Recap of the standard story

In the standard case of projective representations we can lift every

$$\bar{r} : \Gamma \to \prod GL(d, \mathbb{C})/\mathbb{C}^* \,, \tag{A.51}$$

to a linear representation of its Schur cover

$$1 \to K \to \hat{\Gamma} \to \Gamma \to 1 \tag{A.52}$$

i.e.

$$\hat{r} : \hat{\Gamma} \to \prod GL(d, \mathbb{C}) \tag{A.53}$$

by writing

$$\hat{r}(k, \gamma) = \varphi(k)h(\gamma)l(\gamma) \tag{A.54}$$

if δ is surjective.
Here, $l(\gamma)$ is a lift of $\bar{r}$ to $GL(d, \mathbb{C}$ (we can think of these as some matrices) which satisfy

$$l(\gamma)l(\tilde{\gamma}) = f(\gamma, \tilde{\gamma})l(\gamma\tilde{\gamma}) \,, \tag{A.55}$$

for f a factor set $f : \Gamma \times \Gamma \to \mathbb{C}^*$. Note that two such lifts $l, l'$are equivalent if we can find a $h : \Gamma \to \mathbb{C}^*$ such that

$$h(\gamma)l(\gamma) = l'(\gamma) \tag{A.56}$$

By (A.55), in this case the factor sets are related by

$$f'(\gamma, \tilde{\gamma}) = f(\gamma, \tilde{\gamma})h(\gamma)h(\tilde{\gamma})h^{-1}(\gamma\tilde{\gamma}) \tag{A.57}$$

In more abstract language, this is expressed as saying that f and f' define the same class in $H^2(\Gamma, \mathbb{C}^*)$.
The extension (A.52) can be defined by fixing the factor set $e : \Gamma \times \Gamma \to K$ in the multiplication rule

$$(k, \gamma)(\tilde{k}, \tilde{\gamma}) = (k\tilde{k}e(\gamma, \tilde{\gamma}), \gamma\tilde{\gamma})\,. \tag{A.58}$$

The question is no if we can 'undo' the factor set f (which measures the departure of $\bar{r}$ from being a linear representation) by enlarging the group Γ to $\hat{\Gamma}$ and studying linear reps of that. As discussed in the last section, if we can find $\varphi \in Hom(K, \mathbb{C}^*)$ (i.e. φ can be used to map $e(\gamma, \tilde{\gamma}) \to f(\gamma, \tilde{\gamma})$ and we can think of $\varphi(k)$ as a being proportional to the unit matrix) and $h(\gamma)$ such that

$$\varphi(e(\gamma, \tilde{\gamma})) = f(\gamma, \tilde{\gamma})h(\gamma)h(\tilde{\gamma})h^{-1}(\gamma\tilde{\gamma}) \tag{A.59}$$

holds for every factor set $f(\gamma, \tilde{\gamma})$ our choice of $e(\gamma, \tilde{\gamma})$ is good enough. The central statement is now that the Schur cover using the Schur multiplier is precisely such that this holds. Hence using the Schur cover we can lift every projective represetation to the linear one (A.54).
Question: how does that work in practice ?

- We never compile a list of 'all' representations but pick out representatives (sorry for the lack of a better term) corresponding to equivalent representations. How can we be sure the one we choose for $\hat{r}$ are enough to project to all inequivalent representations $\bar{r}$?
- Somewhat related: If we choose an arbitrary linear representation of $\hat{\Gamma}$ and also fix some projection to Γ, are we then guaranteed that elements of the subgroup K are represented by elements of $\mathbb{C}^*$?

A.2.2.3 The case of independent blocks

Let us now discuss the next more complicated cases, representations

$$\bar{r} : \Gamma \to \prod_i GL(d_i, \mathbb{C})/\mathbb{C}^* \tag{A.60}$$

i.e. we have a number of independent blocks. First of all, if we are given such a representation and a lift $l(\gamma)$, (A.55) implies that f is a map $f : \Gamma \times \Gamma \to (\mathbb{C}^*)^n$. We can think of f as a matrix

$$f(\gamma, \tilde{\gamma}) = \oplus \mathbb{I}_{d_i \times d_i} c_i(\gamma, \tilde{\gamma}) \tag{A.61}$$

i.e. it is block diagonal and each block is proportional to the unit matrix. We can of course rewrite

$$f(\gamma, \tilde{\gamma}) = \prod_i f_i(\gamma, \tilde{\gamma}) \tag{A.62}$$

$$f_i(\gamma, \tilde{\gamma}) = \mathbb{I}_{d_i \times d_i} c_i(\gamma, \tilde{\gamma}) \oplus_{j \neq i} \mathbb{I}_{d_j \times d_j} \tag{A.63}$$

where now $f_i : \Gamma \times \Gamma \to \mathbb{C}^*$.
Clearly, equivalent $f(\gamma, \tilde{\gamma})$ are again related by (A.57). This equivalence is derived using the action of $(\mathbb{C}^*)^n$ on the homogeneous coordinates and we may consider each of the n actions in turn and denote the corresponding map $h_i : \Gamma \to \mathbb{C}^*$ $h_i(\gamma)$. This gives rise to a similar decomposition into $h(\gamma) = \prod h_i(\gamma)$ with $h_i : \Gamma \to \mathbb{C}^*$. With this we find that $f(\gamma, \tilde{\gamma}), f'(\gamma, \tilde{\gamma})$ define the same class in $H^2(\Gamma, (\mathbb{C}^*)^n)$ if all of the f_i and f_i' define the same class in $H^2(\Gamma, \mathbb{C}^*)$

$$f_i'(\gamma, \tilde{\gamma}) = f_i(\gamma, \tilde{\gamma}) h_i(\gamma) h_i(\tilde{\gamma}) h_i^{-1}(\gamma\tilde{\gamma}) \tag{A.64}$$

We now use the same Schur cover as before, (i.e. we have the same exact sequence (A.52) and $e : \Gamma \times \Gamma \to K$), and consider maps φ, which now maps $\varphi : \mathbb{K} \to (\mathbb{C}^*)^n$. As is $f(\gamma, \tilde{\gamma})$, $\varphi(k)$ will be a block-diagonal matrix with each block proportional to the unit matrix. We can hence also decompose φ into homomorphisms $\varphi_i : K \to \mathbb{C}^*$,

$$\varphi(k) = \prod_i \varphi_i(k) \tag{A.65}$$

$$\varphi_i(k) = \mathbb{I}_{d_i \times d_i} p_i(k) \oplus_{j \neq i} \mathbb{I}_{d_j \times d_j} \tag{A.66}$$

We are now ready to confront (A.59) for this setup. As we have decomposed φ, h, f in the same way, a solution to the generalization of (A.59) can be found if we can solve

$$\varphi_i(e(\gamma, \tilde{\gamma})) = f_i(\gamma, \tilde{\gamma}) h_i(\gamma) h_i(\tilde{\gamma}) h_i^{-1}(\gamma\tilde{\gamma}) \tag{A.67}$$

The existence of such h_i, φ_i for each $f(\gamma, \tilde{\gamma})$ is already implied if $e(\gamma, \tilde{\gamma})$ originates from the standard Schur cover, so that we are done and the same construction applies here !

A.2.2.4 The case of dependent blocks

We are now ready to confront the real case of interest, i.e. representations

$$\bar{r} : \Gamma \to \left[\prod_i GL(d_i, \mathbb{C})\right] / (\mathbb{C}^*)^{n-k} \tag{A.68}$$

where the j-th $\mathbb{C}^*$s acts as a matrix

$$C_j = \oplus \mathbb{I}_{d_i \times d_i} \lambda_j^{n_{j,i}} \tag{A.69}$$

on the homogeneous coordinates. The integers $n_{j,i}$ are the charges of the corresponding homogeneous coordinates. The decomposition (A.62) used in the last section is the special case where $n_{j,i} = \delta_{ij}$. We can repeat the analysis of the last section, but use the decomposition into matrices C_j instead.
The maps relevant to our problem are now

$$\varphi : K \to (\mathbb{C}^*)^{n-k} \tag{A.70}$$
$$f : \Gamma \times \Gamma \to (\mathbb{C}^*)^{n-k} \tag{A.71}$$
$$h : \Gamma \to (\mathbb{C}^*)^{n-k} \tag{A.72}$$

As before, we may think of these as matrices, which however now must all be of the form

$$\prod_j C_j \tag{A.73}$$

in order to map to $(\mathbb{C}^*)^{n-k} = \mathcal{G}$. As before, we can hence decompose everything into matrices of the form C_j and solve the generalized version of (A.59) by solving

$$\varphi_j(e(\gamma, \tilde{\gamma})) = f_j(\gamma, \tilde{\gamma}) h_j(\gamma) h_j(\tilde{\gamma}) h_j^{-1}(\gamma\tilde{\gamma}) \tag{A.74}$$

Again, all of the maps appearing in the above equation are defined in the same way as for the standard case

$$\varphi_j : K \to \mathbb{C}^* \tag{A.75}$$
$$f_j : \Gamma \times \Gamma \to \mathbb{C}^* \tag{A.76}$$
$$h_j : \Gamma \to \mathbb{C}^* \tag{A.77}$$

there exists a solution by the general theory. Hence any $\mathcal{G}$-projective representation (A.68) can be lifted to a linear representation of $\hat{\Gamma}$ by

$$\hat{r}(k, \gamma) = \varphi(k) h(\gamma) l(\gamma) \tag{A.78}$$

Appendix B

Brane Tilings

B.1 Quiver Gauge Theory

Over the last few decades, the study of quiver theories has occupied a prominent position both in pure mathematics, especially in algebraic geometry and representation theory (cf. e.g., [82–86]), and in theoretical physics, especially in the AdS/CFT correspondence and in the phenomenology of standard-like models (cf. e.g., [42, 44, 87–89]). Quiver gauge groups are characterised by multiple gauge groups and matter contents transforming as 2-index tensor representations. They are usually defined in terms of a directed graph, where the vertices correspond to the gauge groups, and edges correspond to matter fields. In the simplest quiver, all the gauge groups are $U(N)$ or $SU(N)$ groups, assuming the vector spaces of each node are of equal rank. One salient feature is that gauge theories arising as world-volume quantum field theories living on stacks of branes probing Calabi-Yau singularities naturally have a product structure for the gauge group as well as bi-fundamentals.

The computations on quiver gauge theory depends on the quiver diagram and its path algebra. A *Quiver diagram* is defined as a pair $\mathbf{Q} =(\mathbf{Q}_0, \mathbf{Q}_1)$ where $\mathbf{Q}_0$ is a finite set of vertices and $\mathbf{Q}_1$ is a finite set of oriented edges connecting these vertices. For $\rho \in \mathbf{Q}_1$ we let $h(\rho)$ to denote the vertex attached to the head of the arrow and $t(\rho)$ the one attached to the tail. A path in $\mathbf{Q}$ is a sequence $x = \rho_1 \dots \rho_n$ of arrows such that $h(\rho_{i+1}) = t(\rho_i)$. Moreover, for each vertex $i \in \mathbf{Q}_0$ we consider a trivial path e_i which starts and ends at i. The *path algebra* kQ associated with the quiver is the k-algebra whose basis is the collection of paths and with the product rule given by concatenation of the paths and k is some ground number field, usually taken to be $\mathbb{C}$. The rule of multiplication is

$$x \cdot y \equiv \begin{cases} xy, & \text{if} \quad h(y) = t(x) \\ 0, & \text{otherwise} . \end{cases}$$

For example, the path algebra of the Jordan quiver is infinite dimensional, with the basis set being $\{e_1, \rho, \rho^2, \rho^3, \ldots\}$. The algebra is isomorphic to the polynomial ring $k[t]$. An $\hat{A}_2$ quiver has a basis given by the paths $\{e_1, e_2, e_3, \alpha, \beta, \gamma, \beta\alpha, \gamma\beta, \alpha\gamma, \gamma\beta\alpha, \ldots\}$. Note that other combinations of arrows are not allowed, for example $\gamma\alpha = 0$ since $h(\alpha) \neq t(\gamma)$. This quiver has also a superpotential given by the unique cycle $S = \gamma\beta\alpha$. The Jacobian ideal is the one generated by the following relations, which form the zero paths, $\partial_\alpha S = \gamma\beta$, $\partial_\beta S = \alpha\gamma$, $\partial_\gamma S = \beta\alpha$.

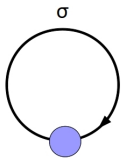

Figure B.1: The Jordan quiver.

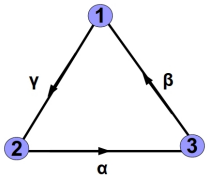

Figure B.2: The $\hat{A}_2$ quiver.

In this work we focus on $\mathcal{N} = 1$ super-symmetry theories. This means the directed edge of the graph denote the $\mathcal{N} = 1$ chiral multiplets: the arrow between two vertices corresponds to a chiral multiplet in the bifundamental representation $(N, \overline{N})$ of the $U(N) \times U(N)$ gauge groups in the endpoints of the arrow, where N is the number of D-branes. The directed edges of the graph specify the $\mathcal{N} = 1$ chiral multiplets: an arrow between two vertices corresponds to a chiral multiple in the bi-fundamental representation $(N, \bar{N})$ of the $U(N) \times U(N)$ gauge groups at the two endpoints of the arrow, and an arrow from a vertex to itself corresponds to a field in the adjoint representation of that single group. In some sense a quiver is usually considered as an abstract graph, not embedded in any particular space, but the topology of it is important.

Now we have a look at the basic properties of $\mathcal{N} = 1$ quivers. The D-terms of the gauge theory can be read off as follows: to each $U(1) \in U(N)$ gauge group factor, there is an associated D-term constraint on the vaccum moduli space, s.t. $\sum_i Q_i^a |X_i|^2 = \zeta^a$, where the sum is over all quiver fields X_i, and Q_i^a is the charge of the field X_i under the a'th gauge group up to the N-th $U(1)$ gauge group. The fields in the fundamental representation of $U(N)$ have charge $+1$, those in the anti-fundamental have -1, and those in the adjoint have charge 0 and do not contribute. ζ^a are Fayet-Iliopolous parameters, which are real numbers. The requirement of a super-symmetric vacuum is $\sum \zeta^a = 0$. In a word, the charge assignment agrees with the incidence matrix of the quiver, which is $Q_i^a = \delta(a, \text{tail}(i)) - \delta(a, \text{head}(i))$, where δ is the Kronecker delta function. Then the exact Novikov-Shifman-Vainshtein-Zakharov (NSVZ) beta function beta function for the gauge couplings g_a of quiver gauge theory is

$$\beta(g_a) = \frac{N}{1 - \frac{g_a^2 N}{8\pi^2}}((3 - \frac{1}{2}\sum_{i \in a}(1 - \gamma_i)) \tag{B.1}$$

where the sum is over all chiral multiplets transforming under the gauge group a, and γ_i is the anomalous dimension of the field X_i, namely the conformal dimension as $\triangle(X_i) = 1 + \frac{1}{2}\gamma_i = \frac{3}{2}R(X_i)$ where $R(X_i)$ is the R-charge of X_i. The statement of the super-conformal invariance is that all β-functions vanish, namely $\sum_{i\in a}(1-\gamma_i) = 6$, which gives us $\sum_a(1-R(X_i)) = 2$. Therefore, the super-potential is then in general the function of gauge-invariant operators which form a closed loop on the quiver graph, due to the gauge invariance, and transform with R-charge two. For the proper quiver graph, the super-potential is fixed by the requirement of invariance under the symmetries of the CY geometry, which consists of interactions invariant under global symmetries on the D3-branes.

The importance of quiver gauge theory is that it represents the D-brane configuration filling transverse spacetime and wrapping cycles of the internal CY space. For now we consider a stack of D3-branes located at a special type of singular point of a toric Calabi-Yau cone. The super-potential is completely fixed by the requirement of invariance under the symmetries on the D3-branes. In a sense, the main reason for studying brane tilings is that any theory admitting a $U(1)^3$ global symmetry falls into this class.

$\mathcal{N} = 1$ quiver gauge theories were first studied in string theory by Douglas and Moore [42], who exploited the toric structure of the quiver gauge theory moduli space by constructing a change of variables parametrizing it as the moduli space of an abelian gauged linear sigma model. Many authors followed up on this work, extending the analysis to more general toric singularities and studying the properties of the resulting models [46–48,94,116,135,137,142,143].

B.2 Brane tilines and dimer models

In this section we exploit two additional structures that appear in toric quiver theories which help us to obtain some highly non-trivial simplifications. We first reformulate the quiver and super-potential as a tiling of a T^2 by polygons (brane tiling), then we introduce the crucial components of a dimer model.

The key idea behind brane tiling is to regard the terms in the super-potential as the terms defining plaquettes, i.e. forming the boundary of polygons. When a field appears in more than one term, the plaquettes are glued together along the corresponding edge. For the most general quiver theories the resulting object does not seem to have interesting structure, but precisely for the toric quiver theories it simplifies dramatically. Thus, the plaquette tiling we form from

a toric quiver theory is a polygonal tiling of a Riemann surface without boundary, called the planar quiver. The dual graph of it is called *brane tiling*. The opposite signs of super-potential terms imply that adjacent faces in the tiling could be labelled by opposite signs. Since the tiling admits an orientation, the Riemann surface is then also orientable. What's more the genus of this Riemann surface should be 2, because super-conformality tells us that $\sum_{e\in V_i}(1-R_e)=2$, where the sum is over edges bounding a plaquette. We then sum it over all the vertices and faces, giving us $N_F-N_E+N_V=2-2g=0$, namely the tiling has genus 1 and is topologically a T^2 space. Therefore we have combined the information of the super-potential and quiver graph into a tiling embedded into a T^2 space. Now each face in the tiling represents a $U(N)$ gauge group. Recall that in the super-potential we have the alternating signs for two terms sharing the same field, this suggest that the tiling is a bipartite graph: each vertex is only connected to vertices of the opposite sign, or we can simply set the convention as referring to positive and negative vertices as black and white nodes.

For example the quiver graph of $\mathbb{C}^3/\mathbb{Z}^2\times\mathbb{Z}^2$ theory is the following:

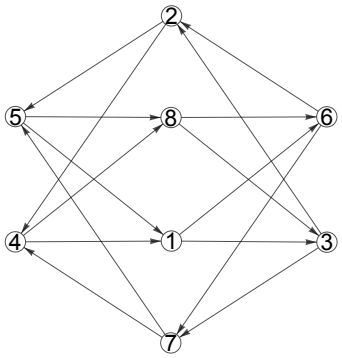

Figure B.3: The $\mathbb{C}^3/\mathbb{Z}^2\times\mathbb{Z}^2$ quiver.

By counting the loops in this quiver, we write down the super-potential as:

$$\begin{aligned}W=&-X_{13}X_{24}X_{32}X_{41}+X_{13}X_{37}X_{51}X_{75}-X_{16}X_{25}X_{51}X_{62}+X_{16}X_{41}X_{67}X_{74}+X_{24}X_{48}X_{62}X_{86}\\&+X_{25}X_{32}X_{58}X_{83}-X_{37}X_{48}X_{74}X_{83}-X_{58}X_{67}X_{75}X_{86}\end{aligned},$$

where X_{ij} means the fundamental representation between the $i-th$ and $j-th$ gauge factor. The brane tiling mapped to the T^2 is presented in fig B.4. The pink square denotes the unit cell of the torus, black and white nodes are evenly distributed and labeled. There are eight areas, which precisely correspondent to the gauge factors in quiver graph. Actually, the brane tiling is simply the dual graph of the planar quiver. We now have the following dictionary summarising the relation between quiver gauge theory, the planar quiver and brane tiling:

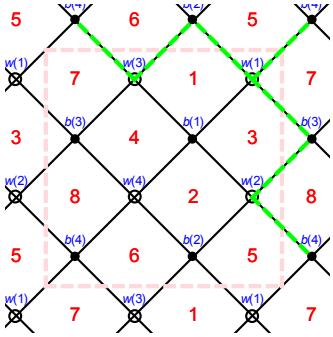

Figure B.4: The $\mathcal{C}^3/\mathbb{Z}^2 \times \mathbb{Z}^2$ dimer model.

Gauge theory	Quiver	Planar quiver	Brane tiling
$SU(N)/U(N)$ gauge group	Node	Vertex	Polygonal face
Chiral multiplet	Arrow	Edge	Edge
Superpotential term	Loops	Polygonal face	Vertex

Table B.1: The quiver/brane tiling dictionary

So far we have developed a quick way of understanding the mathematical structure of quivers and brane tiling. The motivation of a quiver is to represent the chiral multiplets in the field content, but what is the physical meaning of the dimer model? In a word, they are NS5 and D5-brane configurations that are dual to gauge theories on D3-branes. In the type IIB construction, the NS5-brane extends in the 0123 directions and wraps a holomorphic curve embedding in the 4567 direction (the 46 directions are compact). D5-branes span the 012346 directions and stretch inside the holes in the NS5 skeleton. Therefore the D5-branes are bounded by NS5-branes in the 46 directions, leading to a four dimensional low energy theory. This is how the important physics is captured by drawing the brane tilings in the 46 plane: For a $\mathcal{N} = 1$ four dimensional theory, there could be a different number of D5-branes N_I in each stack, which leads to a product gauge group $\prod SU(N_I)$. Strings stretching between D5-branes in a given stack correspond to the gauge bosons, while strings connecting D5-branes in adjacent stacks correspond to states in bifundamental representations, which also appear in quiver gauge theory. We call this whole framework *bipartite field theory*, because the nodes in the dimer model could be equally assigned as white or black. Due to the fact that each bifundamental field appears exactly twice in the superpotential, the underlying geometry must then be an affine toric variety. This is the actual reason for us to systematically classify dimer models via toric geometry.

B.3 Dimer model technology

As analysed in the previous section, we are especially interested in dimers of toric geometry (graphs defined on the torus T^2). Here we develop some powerful computational tools called *dimer technology*.

Given a bipartite graph, one problem of interest is to count the number of perfect matchings of the graph. A *perfect matching* of a bipartite graph is a subset of edges such that every vertex in the graph is an endpoint of precisely one edge in the set. In this manner a dimer model could be understood as the statistical mechanics of a system of random perfect matchings. Under the dictionary in the last section, the vertices are the super-potential terms of the quiver theory, and a perfect matching is to choose one field in each super-potential terms which appears linearly. In this sense the question of finding homogeneous transformations of W is the same as enumerating the perfect matchings of the bipartite graph.

We could also define the *weighted adjacency matrix* A, whose rows and columns index the black and white vertices, with entries as:

$$A_{ij} = \begin{cases} \sum_k a_{ij}^k \text{ for each edge k connecting vertex i to vertex j} \\ 0 \quad \text{otherwise} \end{cases}$$

where $a_{ij}^k \in \mathbb{R}^*$ are formal variables labelling the edges, called edge weights. This matrix A specifies the connectivity of the dimer, which completely determines it as an abstract graph.

Many important properties of the dimer model are governed by the *Kasteleyn matrix* $K(z, w)$, a weighted and signed adjacency matrix of the graph with the rows indexed by the white nodes, and the columns indexed by the black nodes. Now choose a representative of the two primitive winding cycles of the torus, called γ_w and γ_z. One usually choose the paths to be the boundary of the fundamental domain, but in fact any independent choice will suffice and turn out to be physically irrelevant. The Kasteleyn matrix is then defined as:

$$K_{ij} = \sum_k a_{ij}^k z^{<a_{ij}^k, \gamma_z>} w^{<a_{ij}^k, \gamma_w>}$$

where $< a_{ij}^k, \gamma_z >$ is the intersection number of the edge represented by a_{ij}^k and the oriented contour γ, respectively. It takes the value $\pm 1, 0$, depending on whether the edge crosses γ with positive or negative orientation, or does not cross γ. K matrix is the basic object we need to use to recover the D3-brane linear sigma models, which describe the classical and semiclassical moduli space of the quiver gauge theory. The determinant of this matrix $P(z, w) = \det K$ is

a Laurent polynomial called the characteristic polynomial of the dimer model, which provides the link between dimer models and toric geometry. For example, if we denote the conifold as $\mathcal{C}$, the Kasteleyn matrix of $\mathcal{C}/\mathbb{Z}_2 \times \mathbb{Z}_2$ is the following:

$$K = \begin{pmatrix} X_{13} & X_{32} & X_{41} & X_{24} \\ yX_{51} & X_{25} & yX_{16} & X_{62} \\ xX_{37} & xX_{83} & X_{74} & X_{48} \\ xyX_{75} & xX_{58} & yX_{67} & X_{86} \end{pmatrix} \tag{B.2}$$

Given the Kasteleyn matrix, it is very easy to calculate the perfect matchings and toric diagram: simply take the determinant of K matrix as the characteristic polynomial, then each coefficient is a perfect matching and the powers of x and y are mapped to points in toric diagram.

All the perfect matchings of $\mathcal{C}/\mathbb{Z}_2 \times \mathbb{Z}_2$:

X/P	P_1	P_2	P_3	P_4	P_5	P_6	P_7	P_8	P_9	P_{10}	P_{11}	P_{12}	P_{13}	P_{14}	P_{15}	P_{16}	P_{17}	P_{18}	P_{19}	P_{20}	P_{21}	P_{22}	P_{23}	P_{24}
X_{13}	0	0	0	0	0	0	0	1	1	0	1	0	1	0	0	0	0	0	0	0	1	0	1	0
X_{16}	0	0	1	1	0	1	0	0	0	0	0	0	1	0	0	0	0	0	0	0	0	1	1	0
X_{24}	0	0	1	0	1	1	0	0	0	0	0	0	0	0	1	0	1	0	1	0	0	0	0	0
X_{25}	0	0	0	0	0	0	0	1	0	1	1	0	0	0	1	0	0	1	1	0	0	0	0	0
X_{32}	0	1	0	1	0	0	0	0	0	0	0	1	0	0	0	1	0	0	0	1	0	1	0	0
X_{37}	1	0	0	0	0	1	0	0	0	1	0	0	0	0	1	1	0	0	0	0	0	1	0	0
X_{41}	1	0	0	0	0	0	1	0	0	1	0	0	0	1	0	0	0	1	0	0	0	0	0	1
X_{48}	0	1	0	1	0	0	0	0	0	0	1	0	1	1	0	0	0	1	0	0	0	0	0	0
X_{51}	0	1	0	0	1	0	0	0	0	0	0	1	0	1	0	0	1	0	0	0	0	0	0	1
X_{58}	1	0	0	0	0	1	0	0	1	0	0	0	1	1	0	0	1	0	0	0	0	0	0	0
X_{62}	1	0	0	0	0	0	1	0	1	0	0	0	0	0	0	1	0	0	0	1	1	0	0	0
X_{67}	0	1	0	0	1	0	0	0	0	0	1	0	0	0	1	1	0	0	0	0	1	0	0	0
X_{74}	0	0	0	0	0	0	0	1	1	0	0	1	0	0	0	0	1	0	1	1	0	0	0	0
X_{75}	0	0	1	1	0	0	1	0	0	0	0	0	0	0	0	0	0	1	1	1	0	0	0	0
X_{83}	0	0	1	0	1	0	1	0	0	0	0	0	0	0	0	0	0	0	0	0	1	0	1	1
X_{86}	0	0	0	0	0	0	0	1	0	1	0	1	0	0	0	0	0	0	0	0	0	1	1	1

(B.3)

The perfect matchings are named as P_i. We can also work out the correspondence between each toric points and perfect matchings:

$$\begin{gathered} \{2,2\} \to P_3, \{2,1\} \to -P_6 - P_7, \{2,0\} \to P_1, \{1,2\} \to -P_4 - P_5, \\ \{1,1\} \to P_{13} - P_{14} + P_{15} - P_{16} + P_{17} + P_{18} - P_{19} + P_{20} + P_{21} + P_{22} - P_{23} + P_{24} \\ \{1,0\} \to -P_9 - P_{10}, \{0,2\} \to P_2, \{0,1\} \to -P_{11} - P_{12}, \{0,0\} \to P_8 \end{gathered} \tag{B.4}$$

This gives us the two by two square toric diagram for as the lattice defining $\mathcal{C}/\mathbb{Z}_2 \times \mathbb{Z}_2$.

Appendix C

Appendices to Chapter 2

C.1 Toric Data

i	Vertices of $\widetilde{\Delta_i}$	Vertices of Δ_i
1	$\begin{pmatrix} \tilde{x}_1 & \tilde{x}_2 & \tilde{x}_3 & \tilde{x}_4 & \tilde{x}_5 \\ \hline 4 & -1 & -1 & -1 & -1 \\ -1 & 0 & 1 & 0 & 0 \\ -1 & 1 & 0 & 0 & 0 \\ -1 & 0 & 0 & 1 & 0 \end{pmatrix}$	$\begin{pmatrix} x_1 & x_2 & x_3 & x_4 & x_5 \\ \hline 0 & -5 & 0 & 0 & 5 \\ -4 & 1 & 0 & 3 & 0 \\ -2 & 0 & 1 & 1 & 0 \\ 1 & -1 & 0 & -1 & 1 \end{pmatrix}$
2	$\begin{pmatrix} \tilde{x}_1 & \tilde{x}_2 & \tilde{x}_3 & \tilde{x}_4 & \tilde{x}_5 & \tilde{x}_6 \\ \hline 2 & -1 & -1 & -1 & -1 & 2 \\ 0 & 1 & 0 & 0 & 0 & -1 \\ 0 & 0 & 1 & 0 & 0 & -1 \\ -1 & 0 & 0 & 1 & 0 & 0 \end{pmatrix}$	$\begin{pmatrix} x_1 & x_2 & x_3 & x_4 & x_5 & x_6 \\ \hline 3 & 0 & 0 & 3 & 0 & 0 \\ -1 & 0 & 0 & 2 & -1 & 0 \\ 0 & 1 & 0 & 1 & -1 & -1 \\ 1 & 0 & 1 & 0 & -1 & -1 \end{pmatrix}$
3	$\begin{pmatrix} \tilde{x}_1 & \tilde{x}_2 & \tilde{x}_3 & \tilde{x}_4 & \tilde{x}_5 & \tilde{x}_6 & \tilde{x}_7 & \tilde{x}_8 \\ \hline 1 & -1 & -1 & -1 & 1 & 1 & 1 & -1 \\ 0 & 1 & 0 & 0 & 0 & 0 & -1 & 0 \\ 0 & 0 & 1 & 0 & 0 & -1 & 0 & 0 \\ 0 & 0 & 0 & 1 & -1 & 0 & 0 & 0 \end{pmatrix}$	$\begin{pmatrix} x_1 & x_2 & x_3 & x_4 & x_5 & x_6 & x_7 & x_8 \\ \hline 2 & 0 & 0 & 0 & 0 & 0 & 0 & -2 \\ 0 & -1 & 0 & 1 & -1 & 0 & 1 & 0 \\ 0 & 0 & -1 & 1 & -1 & 1 & 0 & 0 \\ 1 & 0 & 0 & 1 & -1 & 0 & 0 & -1 \end{pmatrix}$
4	$\begin{pmatrix} \tilde{x}_1 & \tilde{x}_2 & \tilde{x}_3 & \tilde{x}_4 & \tilde{x}_5 & \tilde{x}_6 \\ \hline -1 & 2 & -1 & -1 & -1 & -1 \\ 0 & -1 & 1 & 0 & 0 & 0 \\ 3 & -1 & 0 & 0 & 0 & 1 \\ -1 & 0 & 0 & 1 & 0 & 0 \end{pmatrix}$	$\begin{pmatrix} x_1 & x_2 & x_3 & x_4 & x_5 & x_6 \\ \hline 3 & 0 & 0 & 0 & -3 & 0 \\ -2 & 0 & 1 & 0 & -1 & -1 \\ -1 & 1 & 0 & 0 & -2 & -1 \\ -2 & 0 & 0 & 1 & 1 & 0 \end{pmatrix}$
5	$\begin{pmatrix} \tilde{x}_1 & \tilde{x}_2 & \tilde{x}_3 & \tilde{x}_4 & \tilde{x}_5 & \tilde{x}_6 & \tilde{x}_7 \\ \hline -1 & -1 & 1 & -1 & -1 & -1 & -1 \\ 4 & 0 & -1 & 0 & 0 & 0 & 2 \\ -2 & 2 & 0 & 0 & 0 & 1 & -1 \\ -1 & 0 & 0 & 1 & 0 & 0 & 0 \end{pmatrix}$	$\begin{pmatrix} x_1 & x_2 & x_3 & x_4 & x_5 & x_6 & x_7 \\ \hline -4 & 0 & 4 & 0 & 0 & 2 & -2 \\ -1 & 0 & 2 & -1 & 0 & 1 & -1 \\ 0 & 1 & 1 & -2 & 0 & 1 & -1 \\ -3 & 0 & 0 & -1 & 1 & 0 & -2 \end{pmatrix}$
6	$\begin{pmatrix} \tilde{x}_1 & \tilde{x}_2 & \tilde{x}_3 & \tilde{x}_4 & \tilde{x}_5 & \tilde{x}_6 & \tilde{x}_7 \\ \hline -1 & 1 & -1 & -1 & -1 & -1 & -1 \\ 2 & -1 & 0 & 2 & 0 & 0 & 0 \\ 0 & 0 & 0 & -1 & 0 & 1 & 0 \\ -1 & 0 & 0 & -1 & 2 & 1 & 1 \end{pmatrix}$	$\begin{pmatrix} x_1 & x_2 & x_3 & x_4 & x_5 & x_6 & x_7 \\ \hline -4 & 0 & 0 & 0 & 2 & 0 & -2 \\ -3 & 1 & 0 & -1 & 0 & -2 & -2 \\ 1 & 0 & 1 & -1 & 0 & -1 & 0 \\ -1 & 0 & 0 & -1 & 1 & 0 & -1 \end{pmatrix}$
7	$\begin{pmatrix} \tilde{x}_1 & \tilde{x}_2 & \tilde{x}_3 & \tilde{x}_4 & \tilde{x}_5 & \tilde{x}_6 & \tilde{x}_7 \\ \hline -1 & -1 & 1 & -1 & -1 & -1 & -1 \\ 0 & 2 & -1 & 0 & 0 & 0 & 0 \\ 2 & -1 & 0 & 0 & 0 & 0 & 1 \\ -1 & 0 & 0 & 0 & 2 & 1 & 0 \end{pmatrix}$	$\begin{pmatrix} x_1 & x_2 & x_3 & x_4 & x_5 & x_6 & x_7 \\ \hline -4 & 0 & 0 & 0 & 2 & -2 & 0 \\ -3 & 0 & 1 & -1 & 0 & -2 & -1 \\ -7 & 1 & 0 & -1 & 0 & -4 & 2 \\ -1 & 0 & 0 & -1 & 1 & -1 & 0 \end{pmatrix}$

continued in the next page

i	Vertices of $\widetilde{\Delta_i}$	Vertices of Δ_i
8	$\begin{pmatrix} \tilde{x}_1 & \tilde{x}_2 & \tilde{x}_3 & \tilde{x}_4 & \tilde{x}_5 & \tilde{x}_6 & \tilde{x}_7 \\ -1 & 1 & -1 & -1 & -1 & -1 & -1 \\ 2 & -1 & 0 & 0 & 0 & 0 & 0 \\ -1 & 0 & 2 & 0 & 2 & 0 & 1 \\ 0 & 0 & 0 & 1 & -1 & 0 & 0 \end{pmatrix}$	$\begin{pmatrix} x_1 & x_2 & x_3 & x_4 & x_5 & x_6 & x_7 \\ -2 & 0 & 0 & 4 & 0 & 4 & 2 \\ -2 & 1 & 0 & 1 & -1 & 0 & 0 \\ -1 & 0 & 0 & 3 & -1 & 2 & 1 \\ -1 & 0 & 1 & 2 & 0 & 1 & 1 \end{pmatrix}$
9	$\begin{pmatrix} \tilde{x}_1 & \tilde{x}_2 & \tilde{x}_3 & \tilde{x}_4 & \tilde{x}_5 & \tilde{x}_6 & \tilde{x}_7 & \tilde{x}_8 \\ 3 & -1 & -1 & -1 & 1 & -1 & -1 & 1 \\ 0 & 0 & 0 & 1 & -1 & 0 & 0 & 0 \\ -2 & 2 & 0 & 0 & 0 & 0 & 1 & -1 \\ -1 & 0 & 1 & 0 & 0 & 0 & 0 & 0 \end{pmatrix}$	$\begin{pmatrix} x_1 & x_2 & x_3 & x_4 & x_5 & x_6 & x_7 & x_8 \\ -4 & 4 & 0 & 0 & 0 & 0 & 2 & -2 \\ -1 & 2 & 0 & 0 & 0 & -1 & 1 & -1 \\ 0 & 1 & 1 & 0 & 0 & -2 & 1 & -1 \\ 1 & 0 & 0 & 1 & -1 & -1 & 0 & 0 \end{pmatrix}$
10	$\begin{pmatrix} \tilde{x}_1 & \tilde{x}_2 & \tilde{x}_3 & \tilde{x}_4 & \tilde{x}_5 & \tilde{x}_6 & \tilde{x}_7 & \tilde{x}_8 \\ -1 & 1 & -1 & -1 & 1 & -1 & -1 & -1 \\ 0 & -1 & 2 & 0 & 0 & 0 & 0 & 1 \\ 2 & 0 & 0 & 0 & -1 & 0 & 1 & 0 \\ -1 & 0 & 0 & 1 & 0 & 0 & 0 & 0 \end{pmatrix}$	$\begin{pmatrix} x_1 & x_2 & x_3 & x_4 & x_5 & x_6 & x_7 & x_8 \\ 0 & -4 & 0 & 0 & 2 & 0 & 0 & -2 \\ -1 & 1 & 2 & -1 & 0 & 0 & 1 & 0 \\ 0 & -1 & 0 & -1 & 1 & 0 & 0 & -1 \\ -1 & 0 & 1 & 0 & 0 & 1 & 1 & 0 \end{pmatrix}$
11	$\begin{pmatrix} \tilde{x}_1 & \tilde{x}_2 & \tilde{x}_3 & \tilde{x}_4 & \tilde{x}_5 & \tilde{x}_6 & \tilde{x}_7 & \tilde{x}_8 \\ 1 & 1 & 1 & -1 & -1 & -1 & -1 & -1 \\ 0 & 0 & -1 & 0 & 0 & 1 & 0 & 0 \\ 0 & -1 & 0 & 0 & 0 & 0 & 1 & 0 \\ -1 & 0 & 0 & 0 & 2 & 0 & 0 & 1 \end{pmatrix}$	$\begin{pmatrix} x_1 & x_2 & x_3 & x_4 & x_5 & x_6 & x_7 & x_8 \\ 0 & 0 & 0 & 2 & -2 & 0 & 0 & 0 \\ 1 & -1 & 0 & 0 & 0 & 0 & -1 & -1 \\ 0 & 1 & -1 & 0 & 0 & 1 & -1 & 0 \\ 0 & 1 & 0 & 1 & -1 & 0 & -1 & 0 \end{pmatrix}$
12	$\begin{pmatrix} \tilde{x}_1 & \tilde{x}_2 & \tilde{x}_3 & \tilde{x}_4 & \tilde{x}_5 & \tilde{x}_6 & \tilde{x}_7 & \tilde{x}_8 \\ -1 & 1 & 1 & -1 & -1 & -1 & -1 & -1 \\ 0 & 0 & -1 & 0 & 0 & 1 & 0 & 0 \\ 2 & -1 & 0 & 0 & 0 & 0 & 0 & 1 \\ -1 & 0 & 0 & 0 & 2 & 0 & 1 & 0 \end{pmatrix}$	$\begin{pmatrix} x_1 & x_2 & x_3 & x_4 & x_5 & x_6 & x_7 & x_8 \\ 0 & 0 & -2 & 0 & 0 & 2 & 0 & 0 \\ 0 & 1 & 0 & -1 & -3 & 0 & -2 & -1 \\ 1 & 0 & 0 & -1 & -1 & 0 & -1 & 0 \\ 0 & 0 & -1 & -1 & 1 & 1 & 0 & 0 \end{pmatrix}$
13	$\begin{pmatrix} \tilde{x}_1 & \tilde{x}_2 & \tilde{x}_3 & \tilde{x}_4 & \tilde{x}_5 & \tilde{x}_6 & \tilde{x}_7 & \tilde{x}_8 \\ 1 & -1 & -1 & -1 & -1 & 1 & -1 & -1 \\ 0 & 0 & 0 & 1 & 0 & -1 & 0 & 0 \\ -1 & 2 & 0 & 0 & 2 & 0 & 0 & 1 \\ 0 & 0 & 1 & 0 & -1 & 0 & 0 & 0 \end{pmatrix}$	$\begin{pmatrix} x_1 & x_2 & x_3 & x_4 & x_5 & x_6 & x_7 & x_8 \\ 0 & 0 & 0 & -2 & 2 & 0 & 0 & 0 \\ -1 & -1 & 2 & 0 & 0 & 0 & 3 & 1 \\ 0 & -1 & 0 & -1 & 1 & 0 & 1 & 0 \\ -1 & 0 & 1 & 0 & 0 & 1 & 2 & 1 \end{pmatrix}$
14	$\begin{pmatrix} \tilde{x}_1 & \tilde{x}_2 & \tilde{x}_3 & \tilde{x}_4 & \tilde{x}_5 & \tilde{x}_6 & \tilde{x}_7 \\ 1 & -1 & -1 & -1 & -1 & -1 & -1 \\ -1 & 2 & 0 & 2 & 0 & 2 & 0 \\ 0 & -1 & 1 & 0 & 0 & -1 & 1 \\ 0 & 0 & 1 & 0 & 0 & -1 & 0 \end{pmatrix}$	$\begin{pmatrix} x_1 & x_2 & x_3 & x_4 & x_5 & x_6 & x_7 \\ 0 & 0 & 0 & -2 & 2 & 0 & 0 \\ -1 & -1 & 2 & 2 & 0 & 0 & 3 \\ 0 & -1 & 0 & -1 & 1 & 0 & 1 \\ -1 & 0 & 1 & 2 & 0 & 1 & 2 \end{pmatrix}$
15	$\begin{pmatrix} \tilde{x}_1 & \tilde{x}_2 & \tilde{x}_3 & \tilde{x}_4 & \tilde{x}_5 & \tilde{x}_6 & \tilde{x}_7 & \tilde{x}_8 \\ -1 & 3 & -1 & -1 & -1 & -1 & -1 & 1 \\ 2 & -2 & 0 & 0 & 0 & 0 & 1 & -1 \\ 0 & -1 & 1 & 0 & 0 & 0 & 0 & 0 \\ -1 & 0 & 0 & 0 & 2 & 1 & 0 & 0 \end{pmatrix}$	$\begin{pmatrix} x_1 & x_2 & x_3 & x_4 & x_5 & x_6 & x_7 & x_8 \\ -4 & 0 & 4 & -4 & 0 & -4 & -2 & 2 \\ -1 & 0 & 2 & -3 & 0 & -2 & -1 & 1 \\ -2 & 1 & 1 & -2 & 0 & -2 & -1 & 1 \\ -1 & 0 & 0 & -1 & 1 & -1 & 0 & 0 \end{pmatrix}$
16	$\begin{pmatrix} \tilde{x}_1 & \tilde{x}_2 & \tilde{x}_3 & \tilde{x}_4 & \tilde{x}_5 & \tilde{x}_6 & \tilde{x}_7 & \tilde{x}_8 \\ -3 & -1 & -1 & -1 & -1 & -1 & -1 & 1 \\ -1 & 1 & 0 & 0 & 0 & 0 & 0 & 0 \\ -2 & 0 & 0 & 2 & 0 & 2 & 1 & -1 \\ 0 & 0 & 1 & 0 & 0 & -1 & 0 & 0 \end{pmatrix}$	$\begin{pmatrix} x_1 & x_2 & x_3 & x_4 & x_5 & x_6 & x_7 & x_8 \\ 4 & 0 & 0 & 0 & -4 & -4 & 2 & -2 \\ 2 & 0 & 0 & 1 & -3 & -2 & 1 & -1 \\ 1 & 1 & 0 & 0 & -2 & -2 & 1 & -1 \\ 0 & 0 & 1 & 1 & -1 & -1 & 0 & 0 \end{pmatrix}$

Table C.1: *The sixteen pairs $(\widetilde{\Delta_i}, \Delta_i)$ of reflexive four-polytopes, for $i = 1, \cdots, 16$, each pair leading to the upstairs Calabi-Yau geometry $\widetilde{X_i} \subset \widetilde{\mathcal{A}_i}$ and the downstairs geometry $X_i \subset \mathcal{A}_i$ with $\pi_1(X_i) \neq \emptyset$. The polytopes are described in terms of their integral vertices.*

C.2 Base Geometries: Upstairs and Downstairs

In this Appendix, we analyse the quotient relationship between the 16 upstairs manifolds $\widetilde{X_i} \subset \widetilde{\mathcal{A}_i}$ and the corresponding 16 downstairs manifolds $X_i \subset \mathcal{A}_i$ whose defining polytopes were given in the previous Appendix. In addition, some geometrical properties of these manifolds relevant

to model building will also be discussed.

C.2.1 An Illustrative Example: the Quintic three-fold

Amongst the sixteen pairs is the quintic manifold $\widetilde{X_1}$ and its $\mathbb{Z}_5$ quotient X_1, which we take as an illustrative example. The corresponding two polytopes $\widetilde{\Delta_1}$ and Δ_1 have 5 vertices each. Firstly, the vertices of $\widetilde{\Delta_1}$ for the quintic three-fold $\widetilde{X_1}$ can be read off from Table C.1:

$$\begin{pmatrix} \tilde{x}_1 & \tilde{x}_2 & \tilde{x}_3 & \tilde{x}_4 & \tilde{x}_5 \\ \hline 4 & -1 & -1 & -1 & -1 \\ -1 & 0 & 1 & 0 & 0 \\ -1 & 1 & 0 & 0 & 0 \\ -1 & 0 & 0 & 1 & 0 \end{pmatrix} , \tag{C.1}$$

where $\tilde{x}_{\rho=1,\cdots,5}$ are the homogeneous coordinates on the ambient space $\mathbb{P}^4$. The polytope $\widetilde{\Delta_1}$ naturally leads to the usual 126 quintic monomials in $\tilde{x}_\rho$; these generate the defining polynomial of the quintic Calabi-Yau three-fold $\widetilde{X_1}$.
Similarly, the vertices of Δ_1 for the quotiented quintic $X_1 = \widetilde{X_1}/\mathbb{Z}_5$ are given as follows:

$$\begin{pmatrix} x_1 & x_2 & x_3 & x_4 & x_5 \\ \hline 0 & -5 & 0 & 0 & 5 \\ -4 & 1 & 0 & 3 & 0 \\ -2 & 0 & 1 & 1 & 0 \\ 1 & -1 & 0 & -1 & 1 \end{pmatrix} , \tag{C.2}$$

where $x_{\rho=1,\cdots,5}$ are again the homogeneous coordinates on the corresponding toric ambient space. As for the generators of the defining polynomial, the polytope Δ_1 leads to the following 26 monomials in x_ρ:

$$\begin{gathered} x_2^5\ ,\ \ x_1x_2^3x_3\ ,\ \ x_2^2x_3^2x_5\ ,\ \ x_2^3x_4x_5\ ,\ \ x_1x_2^2x_5^2\ ,\ \ x_2x_3x_5^3\ ,\ \ x_5^5\ ,\ \ x_3^5\ ,\ \ x_1^2x_2x_3^2\ , \\ x_2x_3^3x_4\ ,\ \ x_1x_3^3x_5\ ,\ \ x_1^2x_2^2x_4\ ,\ \ x_1^3x_2x_5\ ,\ \ x_2^2x_3x_4^2\ ,\ \ x_1x_2x_3x_4x_5\ ,\ \ x_1^2x_3x_5^2\ ,\ \ x_3^2x_4x_5^2\ , \\ x_2x_4^2x_5^2\ ,\ \ x_1x_4x_5^3\ ,\ \ x_1^5\ ,\ \ x_1^3x_3x_4\ ,\ \ x_1x_3^2x_4^2\ ,\ \ x_1x_2x_4^3\ ,\ \ x_1^2x_4^2x_5\ ,\ \ x_3x_4^3x_5\ ,\ \ x_4^5\ . \end{gathered} \tag{C.3}$$

Now, by demanding that the 26 monomials be invariant, we find the following phase rotation rule

$$\{\tilde{x}_1 \to x_1,\ \tilde{x}_2 \to e^{\frac{2i\pi}{5}}x_2,\ \tilde{x}_3 \to e^{\frac{4i\pi}{5}}x_3,\ \tilde{x}_4 \to e^{\frac{6i\pi}{5}}x_4,\ \tilde{x}_5 \to e^{\frac{8i\pi}{5}}x_5\}\ , \tag{C.4}$$

which links the two sets of homogeneous coordinates.
This phase rotation relates the two manifolds $\widetilde{X_1}$ and X_1 tightly. Not only the Laurant polynomials are explicitly connected, it turns out that the integral cohomology groups are also very much similar under the phase rotation.
As an example illustrating the precise relation between upstairs and downstairs space, consider one of the 126 monomials, $\widetilde{x}_1\widetilde{x}_2^3\widetilde{x}_3$, defining the upstairs ambient space of the quintic $\widetilde{X_1}$. If we

transform this monomial using the rules in Eq. (C.4) we obtain $\widetilde{x}_1\widetilde{x}_2^3\widetilde{x}_3 \to x_1(e^{\frac{2i\pi}{5}}x_2)^3e^{\frac{4i\pi}{5}}x_3 = x_1x_2^3x_3$. The phase independence of the result means that this is one of the 26 monomials which define the downstairs manifold $X_1 = \widetilde{X_1}/\mathbb{Z}_5$. The remaining 25 downstairs monomials can be obtained by applying this procedure systematically to all upstairs monomials [1].

We next turn to some relevant base geometries, most of which can be easily extracted from PALP [71]. Let us start from upstairs. Firstly, the Picard group of $\widetilde{X_1}$ is generated by a single element $\tilde{J}_1$ and all the toric divisors are rationally equivalent to $\tilde{J}_1$:

$$\tilde{D}_1 = \tilde{J}_1,\ \tilde{D}_2 = \tilde{J}_1,\ \tilde{D}_3 = \tilde{J}_1,\ \tilde{D}_4 = \tilde{J}_1,\ \tilde{D}_5 = \tilde{J}_1\ .$$

Note that we do not carefully distinguish harmonic $(1,1)$-forms from divisors unless ambiguities arise. The intersection polynomial is:

$$5\tilde{J}_1^3\ ,$$

which means that $d_{111}(\widetilde{X_1}) = 5$. In general, the coefficient of the monomial term $\tilde{J}_r\tilde{J}_s\tilde{J}_t$ in the intersection polynomial is the value of $d_{rst}(\widetilde{X})$, without any symmetry factors. Finally, the Hodge numbers are:

$$h^{1,1}(\widetilde{X_1}) = 1,\quad h^{1,2}(\widetilde{X_1}) = 101\ ,$$

leading to the Euler character $\chi(\widetilde{X_1}) = -200$.

As for the downstairs manifold X_1, the $\mathbb{Z}_5$-quotient of the quintic $\widetilde{X_1}$, the Picard group is again spanned by a single element J_1 and the toric divisors are all equivalent:

$$D_1 = J_1,\ D_2 = J_1,\ D_3 = J_1,\ D_4 = J_1,\ D_5 = J_1\ .$$

The intersection polynomial is given as:

$$J_1^3\ ,$$

and hence, $d_{111}(X_1) = 1$. Finally, the Hodge numbers are:

$$h^{1,1}(X_1) = 1,\quad h^{1,2}(X_1) = 21$$

and the Euler character $\chi(X_1) = -40$.

Note that the intersection polynomial of X_1 is equal to that of $\widetilde{X_1}$ divided by 5, the order of the discrete group $\mathbb{Z}_5$. This remains true for all the fourteen favorable manifolds $X_{i=1,\cdots,14}$ in an appropriate basis of $H^{1,1}$.

[1] In some cases, an additional permutation of the downstairs homogeneous coordinate has to be included, as in some of the examples in Table. C.2. This is to ensure that the linear relationships between divisors and integral basis are literally the same for both the upstairs and the downstairs manifolds.

C.2.2 Summary of the Base Geometries

For the remaining fifteen cases, the phase rotations of the homogeneous coordinates are not as straight-forward as in the quintic example. One needs to make use of some combinatorial tricks to figure out the explicit results. In some cases, permutations are also required to make the upstairs and the downstairs intersection polynomials proportional to each other. In Table C.2, we summarise the complete results for all the sixteen pairs of geometries. For each pair, we first present the phase rotation map between upstairs and downstairs coordinates (and the permutation of the coordinates if required). The base geometries of $\widetilde{X_i}$ and X_i then follow in order: number of generating monomials,[2] toric divisors in terms of the $(1,1)$-form basis elements, intersection polynomial. The Hodge numbers $h^{1,1}$ and $h^{2,1}$, as well as the Euler character χ of the manifold X are presented using the notation $[X]^{h^{1,1},h^{2,1}}_{\chi}$. In addition, the second Chern class $c_2(TX)$ and Kähler cone matrix K for the downstairs manifolds are also being listed. The Kähler cone is then given by all Kähler parameters satisfying $K_{rs}t^s \geq 0$ for all r.

Base Geometries: Upstairs and Downstairs

Pair 1: $\{\tilde{x}_1 \to x_1,\ \tilde{x}_2 \to e^{\frac{2i\pi}{5}}x_2,\ \tilde{x}_3 \to e^{\frac{4i\pi}{5}}x_3,\ \tilde{x}_4 \to e^{\frac{6i\pi}{5}}x_4,\ \tilde{x}_5 \to e^{\frac{8i\pi}{5}}x_5\}$

$[\widetilde{X_1}]^{1,101}_{-200}$	#(monomials) = 126
$\tilde{D}_1 = \tilde{J}_1,\ \tilde{D}_2 = \tilde{J}_1,\ \tilde{D}_3 = \tilde{J}_1,\ \tilde{D}_4 = \tilde{J}_1,\ \tilde{D}_5 = \tilde{J}_1$	
$5\tilde{J}_1^3$	
$[X_1]^{1,21}_{-40}$	#(monomials) = 26
$D_1 = J_1, D_2 = J_2, D_3 = J_2, D_4 = J_1, D_5 = J_1, D_6 = J_2$	
${J_1}^3$	
$c_2(TX) = (10)$	$K = (1)$

Pair 2: $\{\tilde{x}_1 \to x_1,\ \tilde{x}_4 \to e^{\frac{2i\pi}{3}}x_4,\ \tilde{x}_5 \to e^{\frac{4i\pi}{3}}x_5,\ \tilde{x}_2 \to x_2,\ \tilde{x}_3 \to e^{\frac{2i\pi}{3}}x_3,\ \tilde{x}_6 \to e^{\frac{4i\pi}{3}}x_6\}$

$[\widetilde{X_2}]^{2,83}_{-162}$	#(monomials) = 100
$\tilde{D}_1 = \tilde{J}_1, \tilde{D}_2 = \tilde{J}_2, \tilde{D}_3 = \tilde{J}_2, \tilde{D}_4 = \tilde{J}_1, \tilde{D}_5 = \tilde{J}_1, \tilde{D}_6 = \tilde{J}_2$	
$3\,\tilde{J}_1^2\,\tilde{J}_2 + 3\,\tilde{J}_1\,\tilde{J}_2^2$	
$[X_2]^{2,29}_{-54}$	#(monomials) = 34
$D_1 = J_1,\ D_2 = J_1,\ D_3 = J_1,\ D_4 = J_1,\ D_5 = J_1$	
$J_1^2\,J_2 + J_1\,J_2^2$	
$c_2(TX) = (12, 12)$	$K = \begin{pmatrix} 0 & 1 \\ 1 & 0 \end{pmatrix}$

[2]For simplicity, we do not attempt to explicitly show the generating monomials and only give the number of viable terms. However, the idea should be clear from the quintic example in section C.2.1.

Pair 3: $\{\tilde{x}_1 \to e^{i\pi}x_1,\ \tilde{x}_2 \to e^{i\pi}x_2,\ \tilde{x}_3 \to e^{i\pi}x_3,\ \tilde{x}_4 \to e^{i\pi}x_4,\ \tilde{x}_5 \to x_5,\ \tilde{x}_6 \to x_6,\ \tilde{x}_7 \to x_7,\ \tilde{x}_8 \to x_8\}$

$[\widetilde{X_3}]^{4,68}_{-128}$	#(monomials) = 81
$\tilde{D}_1 = \tilde{J}_4, \tilde{D}_2 = \tilde{J}_3, \tilde{D}_3 = \tilde{J}_2, \tilde{D}_4 = \tilde{J}_1, \tilde{D}_5 = \tilde{J}_1, \tilde{D}_6 = \tilde{J}_2, \tilde{D}_7 = \tilde{J}_3, \tilde{D}_8 = \tilde{J}_4$	
$2\,\tilde{J}_1\,\tilde{J}_2\,\tilde{J}_3 + 2\,\tilde{J}_1\,\tilde{J}_2\,\tilde{J}_4 + 2\,\tilde{J}_1\,\tilde{J}_3\,\tilde{J}_4 + 2\,\tilde{J}_2\,\tilde{J}_3\,\tilde{J}_4$	
$[X_3]^{4,36}_{-64}$	#(monomials) = 26
$D_1 = J_4, D_2 = J_3, D_3 = J_2, D_4 = J_1, D_5 = J_1, D_6 = J_2, D_7 = J_3, D_8 = J_4$	
$J_1\,J_2\,J_3 + J_1\,J_2\,J_4 + J_1\,J_3\,J_4 + J_2\,J_3\,J_4$	
$c_2(TX) = (12, 12, 12, 12)$	$K = \begin{pmatrix} 1 & 0 & 0 & 0 \\ 0 & 0 & 0 & 1 \\ 0 & 1 & 0 & 0 \\ 0 & 0 & 1 & 0 \end{pmatrix}$

Pair 4: $\{\tilde{x}_1 \to x_1,\ \tilde{x}_2 \to e^{\frac{2i\pi}{3}}x_2,\ \tilde{x}_4 \to e^{\frac{4i\pi}{3}}x_4,\ \tilde{x}_3 \to x_3,\ \tilde{x}_5 \to e^{\frac{2i\pi}{3}}x_5,\ \tilde{x}_6 \to e^{\frac{4i\pi}{3}}x_6\}$

$[\widetilde{X_4}]^{4,112}_{-216}$	#(monomials) = 145
$\tilde{D}_1 = \tilde{J}_1, \tilde{D}_2 = 3\,\tilde{J}_1 + \tilde{J}_2, \tilde{D}_3 = 3\,\tilde{J}_1 + \tilde{J}_2, \tilde{D}_4 = \tilde{J}_1, \tilde{D}_5 = \tilde{J}_1, \tilde{D}_6 = \tilde{J}_2$	
$3\,\tilde{J}_1^2\,\tilde{J}_2 - 9\,\tilde{J}_1\,\tilde{J}_2^2 + 27\,\tilde{J}_2^3$	
$[X_4]^{2,38}_{-72}$	#(monomials) = 49
$D_1 = J_1, D_2 = 3\,J1 + J2, d3 = 3\,J1 + J2, D_4 = J_1, D_5 = J_1, D_6 = J_2$	
$J_1^2\,J_2 - 3\,J_1\,J_2^2 + 9\,J_2^3$	
$c_2(TX) = (12, -6)$	$K = \begin{pmatrix} 0 & 1 \\ 1 & -3 \end{pmatrix}$

Pair 5: $\{\tilde{x}_1 \to e^{i\pi}x_1,\ \tilde{x}_2 \to e^{i\pi}x_2,\ \tilde{x}_3 \to e^{i\pi}x_3,\ \tilde{x}_6 \to e^{i\pi}x_6,\ \tilde{x}_4 \to x_4, \tilde{x}_5 \to x_5\}$
$\{x_3 \to x_5,\ x_5 \to x_3\}$

$[\widetilde{X_5}]^{3,83}_{-160}$	#(monomials) = 105
$\tilde{D}_1 = \tilde{J}_1, \tilde{D}_2 = \tilde{J}_2, \tilde{D}_3 = 4\,\tilde{J}_1 + 2\,\tilde{J}_3, \tilde{D}_4 = \tilde{J}_1, \tilde{D}_5 = \tilde{J}_2, \tilde{D}_6 = 2\,\tilde{J}_1 - 2\,\tilde{J}_2 + \tilde{J}_3, \tilde{D}_7 = \tilde{J}_3$	
$2\,\tilde{J}_1\,\tilde{J}_2\,\tilde{J}_3 + 4\,\tilde{J}_1\,\tilde{J}_3^2 - 4\,\tilde{J}_2\,\tilde{J}_3^2 - 16\,\tilde{J}_3^3$	
$[X_5]^{3,43}_{-80}$	#(monomials) = 53
$D_1 = J_2, D_2 = J_1, D_3 = J_1, D_4 = J_2, D_5 = 4\,J_2 + 2\,J_3, D_6 = -2\,J_1 + 2\,J_2 + J_3, D_7 = J_3$	
$J_1\,J_2\,J_3 - 2\,J_1\,J_3^2 + 2\,J_2\,J_3^2 - 8\,J_3^3$	
$c_2(TX) = (12, 12, 4)$	$K = \begin{pmatrix} 0 & 1 & -2 \\ 1 & 0 & 0 \\ 0 & 0 & 1 \end{pmatrix}$

Pair 6: $\{\tilde{x}_1 \to e^{i\pi}x_1,\ \tilde{x}_2 \to e^{i\pi}x_2,\ \tilde{x}_3 \to e^{i\pi}x_3,\ \tilde{x}_4 \to e^{i\pi}x_4,\ \tilde{x}_5 \to x_5,\ \tilde{x}_6 \to x_6\}$
$\{x_1 \to x_5, x_5 \to x_1, x_3 \to x_4, x_4 \to x_3\}$

$[\widetilde{X_6}]^{3,115}_{-224}$	#(monomials) = 153

$\tilde{D}_1 = 2\,\tilde{J}_1 + \tilde{J}_3, \tilde{D}_2 = 4\,\tilde{J}_1 + 2\,\tilde{J}_2 + 2\,\tilde{J}_3, \tilde{D}_3 = \tilde{J}_1, \tilde{D}_4 = \tilde{J}_2, \tilde{D}_5 = \tilde{J}_1, \tilde{D}_6 = \tilde{J}_2, \tilde{D}_7 = \tilde{J}_3$
$2\,\tilde{J}_1\,\tilde{J}_2\,\tilde{J}_3 - 4\,\tilde{J}_2\,\tilde{J}_3^2$

$[X_6]^{3,59}_{-112}$	#(monomials) = 77

$D_1 = J_1, D_2 = 4\,J_1 + 2\,J_2 + 2\,J_3, D_3 = J_2, D_4 = J_1, D_5 = 2\,J_1 + J_3, D_6 = J_2, D_7 = J_3$
$J_1\,J_2\,J_3 - 2\,J_2\,J_3^2$
$c_2(TX) = (12, 12, 0)$
$K_1 = \begin{pmatrix} 0 & 1 & -2 \\ 1 & 0 & 0 \\ 0 & 0 & 1 \end{pmatrix}$, $K_2 = \begin{pmatrix} 0 & 0 & 1 \\ 1 & 0 & -2 \\ 0 & 1 & -1 \end{pmatrix}$, $K_{join} = \begin{pmatrix} 1 & 0 & 0 \\ 0 & 1 & 0 \\ 0 & 0 & 1 \end{pmatrix}$

Pair 7: $\{\tilde{x}_1 \to e^{i\pi}x_1,\ \tilde{x}_2 \to e^{i\pi}x_2,\ \tilde{x}_3 \to e^{i\pi}x_3,\ \tilde{x}_4 \to e^{i\pi}x_4\}$
$\{x_1 \to x_5, x_5 \to x_1, x_2 \to x_3, x_3 \to x_2\}$

$[\widetilde{X_7}]^{4,148}_{-288}$	#(monomials) = 126

$\tilde{D}_1 = 2\,\tilde{J}_1 + \tilde{J}_2, \tilde{D}_2 = 4\,\tilde{J}_1 + 2\,\tilde{J}_2 + \tilde{J}_3, \tilde{D}_3 = 8\,\tilde{J}_1 + 4\,\tilde{J}_2 + 2\,\tilde{J}_3, \tilde{D}_4 = \tilde{J}_1, \tilde{D}_5 = \tilde{J}_1, \tilde{D}_6 = \tilde{J}_2, \tilde{D}_7 = \tilde{J}_3$
$2\,\tilde{J}_1\,\tilde{J}_2\,\tilde{J}_3 - 4\,\tilde{J}_2^2\,\tilde{J}_3 - 4\,\tilde{J}_1\,\tilde{J}_3^2 + 16\,\tilde{J}_3^3$

$[X_7]^{3,75}_{-144}$	#(monomials) = 26

$D_1 = J_1, D_2 = 8\,J_1 + 4\,J_2 + 2\,J_3, D_3 = 4\,J_1 + 2\,J_2 + J_3, D_4 = J_1, D_5 = 2\,J_1 + J_2, D_6 = J_2, D_7 = J_3$	
$J_1\,J_2\,J_3 - 2\,J_2^2\,J_3 - 2\,J_1\,J_3^2 + 8\,J_3^3$	
$c_2(TX) = (12, 0, -4)$	$K = \begin{pmatrix} 1 & -2 & 0 \\ 0 & 0 & 1 \\ 0 & 1 & -2 \end{pmatrix}$

Pair 8: $\{\tilde{x}_1 \to e^{i\pi}x_1,\ \tilde{x}_2 \to e^{i\pi}x_2,\ \tilde{x}_3 \to e^{i\pi}x_3,\ \tilde{x}_4 \to e^{i\pi}x_4\}$

$[\widetilde{X_8}]^{4,148}_{-288}$	#(monomials) = 201

$\tilde{D}_1 = 2\,\tilde{J}_1 + 2\,\tilde{J}_2 + \tilde{J}_3, \tilde{D}_2 = 4\,\tilde{J}_1 + 4\,\tilde{J}_2 + 2\,\tilde{J}_3, \tilde{D}_3 = \tilde{J}_2, \tilde{D}_4 = \tilde{J}_1, \tilde{D}_5 = \tilde{J}_1, \tilde{D}_6 = \tilde{J}_2, \tilde{D}_7 = \tilde{J}_3$
$2\,\tilde{J}_1\,\tilde{J}_2\,\tilde{J}_3 - 4\,\tilde{J}_1\,\tilde{J}_3^2 - 4\,\tilde{J}_2\,\tilde{J}_3^2 + 16\,\tilde{J}_3^3$

$[X_8]^{3,75}_{-144}$	#(monomials) = 101

$D_1 = 2\,J_1 + 2\,J_2 + J_3, D_2 = 4\,J_1 + 4\,J_2 + 2\,J_3, D_3 = J_2, D_4 = J_1, D_5 = J_1, D_6 = J_2, D_7 = J_3$	
$J_1\,J_2\,J_3 - 2\,J_1\,J_3^2 - 2\,J_2\,J_3^2 + 8\,J_3^3$	
$c_2(TX) = (12, 12, -4)$	$K = \begin{pmatrix} 0 & 0 & 1 \\ 1 & 0 & -2 \\ 0 & 1 & -2 \end{pmatrix}$

Pair 9: $\{\tilde{x}_1 \to e^{i\pi}x_1,\ \tilde{x}_2 \to e^{i\pi}x_2,\ \tilde{x}_4 \to e^{i\pi}x_4,\ \tilde{x}_7 \to e^{i\pi}x_7\}$
$\{x_3 \to x_6,\ x_6 \to x_3\}$

$[\widetilde{X_9}]^{4,52}_{-96}$	#(monomials) = 57

$\tilde{D}_1 = \tilde{J}_1, \tilde{D}_2 = \tilde{J}_3, \tilde{D}_3 = \tilde{J}_1, \tilde{D}_4 = \tilde{J}_2, \tilde{D}_5 = \tilde{J}_2, \tilde{D}_6 = \tilde{J}_3, \tilde{D}_7 = 2\,\tilde{J}_1 - 2\,\tilde{J}_3 + \tilde{J}_4, \tilde{D}_8 = \tilde{J}_4$
$2\,\tilde{J}_1\,\tilde{J}_2\,\tilde{J}_3 + 4\,\tilde{J}_1\,\tilde{J}_2\,\tilde{J}_4 + 2\,\tilde{J}_1\,\tilde{J}_3\,\tilde{J}_4 + 4\,\tilde{J}_1\,\tilde{J}_4^2 - 8\,\tilde{J}_2\,\tilde{J}_4^2 - 4\,\tilde{J}_3\,\tilde{J}_4^2 - 16\,\tilde{J}_4^3$

$[X_9]^{4,28}_{-48}$	#(monomials) = 29
$D_1 = J_3, D_2 = J_1, D_3 = J_1, D_4 = J_2, D_5 = J_2, D_6 = J_3, D_7 = -2\,J_1 + 2\,J_3 + J_4, D_8 = J_4$	
$J_1\,J_2\,J_3 + J_1\,J_3\,J_4 + 2\,J_2\,J_3\,J_4 - 2\,J_1\,J_4^2 - 4\,J_2\,J_4^2 + 2\,J_3\,J_4^2 - 8\,J_4^3$	
$c_2(TX) = (12, 12, 12, 4)$	$K = \begin{pmatrix} 1 & 0 & 0 & 0 \\ 0 & 0 & 0 & 1 \\ 0 & 0 & 1 & -2 \\ 0 & 1 & 0 & 0 \end{pmatrix}$

Pair 10: $\{\tilde{x}_1 \to e^{i\pi}x_1,\ \tilde{x}_2 \to e^{i\pi}x_2,\ \tilde{x}_3 \to e^{i\pi}x_3,\ \tilde{x}_5 \to e^{i\pi}x_5\}$
$\{x_1 \to x_2,\ x_2 \to x_1,\ x_7 \to x_8,\ x_8 \to x_7\}$

$[\widetilde{X_{10}}]^{4,68}_{-128}$	#(monomials) = 81
$\tilde{D}_1 = \tilde{J}_1, \tilde{D}_2 = 2\,\tilde{J}_2 + \tilde{J}_4, \tilde{D}_3 = \tilde{J}_2, \tilde{D}_4 = \tilde{J}_1, \tilde{D}_5 = 2\,\tilde{J}_1 + \tilde{J}_3, \tilde{D}_6 = \tilde{J}_2, \tilde{D}_7 = \tilde{J}_3, \tilde{D}_8 = \tilde{J}_4$	
$2\,\tilde{J}_1\,\tilde{J}_2\,\tilde{J}_3 - 4\,\tilde{J}_2\,\tilde{J}_3^2 + 2\,\tilde{J}_1\,\tilde{J}_2\,\tilde{J}_4 - 4\,\tilde{J}_1\,\tilde{J}_4^2$	
$[X_{10}]^{4,36}_{-64}$	#(monomials) = 41
$D_1 = 2\,J_2 + J_3, D_2 = J_1, D_3 = J_2, D_4 = J_1, D_5 = 2\,J_1 + J_4, D_6 = J_2, D_7 = J_3, D_8 = J_4$	
$J_1\,J_2\,J_3 - 2\,J_1\,J_3^2 + J_1\,J_2\,J_4 - 2\,J_2\,J_4^2$	
$c_2(TX) = (12, 12, 0, 0)$	$K = \begin{pmatrix} 0 & 0 & 1 & 0 \\ 0 & 1 & -2 & 0 \\ 0 & 0 & 0 & 1 \\ 1 & 0 & 0 & -2 \end{pmatrix}$

Pair 11: $\{\tilde{x}_1 \to e^{i\pi}x_1,\ \tilde{x}_2 \to e^{i\pi}x_2,\ \tilde{x}_3 \to e^{i\pi}x_3,\ \tilde{x}_4 \to e^{i\pi}x_4\}$
$\{x_2 \to x_4,\ x_4 \to x_2,\ x_5 \to x_7,\ x_7 \to x_5\}$

$[\widetilde{X_{11}}]^{4,68}_{-128}$	#(monomials) = 81
$\tilde{D}_1 = 2\,\tilde{J}_1 + \tilde{J}_4, \tilde{D}_2 = \tilde{J}_3, \tilde{D}_3 = \tilde{J}_2, \tilde{D}_4 = \tilde{J}_1, \tilde{D}_5 = \tilde{J}_1, \tilde{D}_6 = \tilde{J}_2, \tilde{D}_7 = \tilde{J}_3, \tilde{D}_8 = \tilde{J}_4$	
$2\,\tilde{J}_1\,\tilde{J}_2\,\tilde{J}_3 + 2\,\tilde{J}_1\,\tilde{J}_2\,\tilde{J}_4 + 2\,\tilde{J}_1\,\tilde{J}_3\,\tilde{J}_4 - 4\,\tilde{J}_2\,\tilde{J}_4^2 - 4\,\tilde{J}_3\,\tilde{J}_4^2$	
$[X_{11}]^{4,36}_{-64}$	#(monomials) = 41
$D_1 = 2\,J_3 + J_4, D_2 = J_3, D_3 = J_2, D_4 = J_1, D_5 = J_1, D_6 = J_2, D_7 = J_3, D_8 = J_4$	
$J_1\,J_2\,J_3 + J_1\,J_3\,J_4 + J_2\,J_3\,J_4 - 2\,J_1\,J_4^2 - 2\,J_2\,J_4^2$	
$c_2(TX) = (12, 12, 12, 0)$	$K = \begin{pmatrix} 1 & 0 & 0 & 0 \\ 0 & 1 & 0 & 0 \\ 0 & 0 & 0 & 1 \\ 0 & 0 & 1 & -2 \end{pmatrix}$

Pair 12: $\{\tilde{x}_1 \to e^{i\pi}x_1,\ \tilde{x}_2 \to e^{i\pi}x_2,\ \tilde{x}_3 \to e^{i\pi}x_3,\ \tilde{x}_4 \to e^{i\pi}x_4\}$

$[\widetilde{X_{12}}]^{5,85}_{-160}$	#(monomials) = 105
$\tilde{D}_1 = 2\,\tilde{J}_1 + \tilde{J}_3, \tilde{D}_2 = 4\,\tilde{J}_1 + 2\,\tilde{J}_3 + \tilde{J}_4, \tilde{D}_3 = \tilde{J}_2, \tilde{D}_4 = \tilde{J}_1, \tilde{D}_5 = \tilde{J}_1, \tilde{D}_6 = \tilde{J}_2, \tilde{D}_7 = \tilde{J}_3, \tilde{D}_8 = \tilde{J}_4$	
$2\,\tilde{J}_1\,\tilde{J}_2\,\tilde{J}_3 - 4\,\tilde{J}_2\,\tilde{J}_3^2 + 2\,\tilde{J}_1\,\tilde{J}_3\,\tilde{J}_4 - 4\,\tilde{J}_3^2\,\tilde{J}_4 - 4\,\tilde{J}_1\,\tilde{J}_4^2 + 16\,\tilde{J}_4^3$	
$[X_{12}]^{4,44}_{-80}$	#(monomials) = 53

$D_1 = 2\,J_1 + J_3, D_2 = 4\,J_1 + 2\,J_3 + J_4, D_3 = J_2, D_4 = J_1, D_5 = J_1, D_6 = J_2, D_7 = J_3, D_8 = J_4$
$J_1\,J_2\,J_3 - 2\,J_2\,J_3^2 + J_1\,J_3\,J_4 - 2\,J_3^2\,J_4 - 2\,J_1\,J_4^2 + 8\,J_4^3$
$c_2(TX) = (12, 12, 0, -4)$ $\quad$ $K = \begin{pmatrix} 0 & 1 & 0 & 0 \\ 1 & 0 & -2 & 0 \\ 0 & 0 & 0 & 1 \\ 0 & 0 & 1 & -2 \end{pmatrix}$

Pair 13: $\{\tilde{x}_1 \to e^{i\pi}x_1,\ \tilde{x}_2 \to e^{i\pi}x_2,\ \tilde{x}_3 \to e^{i\pi}x_3,\ \tilde{x}_4 \to e^{i\pi}x_4\}$
$\{x_5 \to x_6,\ x_6 \to x_5\}$

$[\widetilde{X_{13}}]^{5,85}_{-160}$	#(monomials) = 105
$\tilde{D}_1 = 2\,\tilde{J}_1 + 2\,\tilde{J}_3 + \tilde{J}_4, \tilde{D}_2 = \tilde{J}_3, \tilde{D}_3 = \tilde{J}_1, \tilde{D}_4 = \tilde{J}_2, \tilde{D}_5 = \tilde{J}_1, \tilde{D}_6 = \tilde{J}_2, \tilde{D}_7 = \tilde{J}_3, \tilde{D}_8 = \tilde{J}_4$	
$2\,\tilde{J}_1\,\tilde{J}_2\,\tilde{J}_3 + 2\,\tilde{J}_1\,\tilde{J}_3\,\tilde{J}_4 - 4\,\tilde{J}_1\,\tilde{J}_4^2 - 4\,\tilde{J}_3\,\tilde{J}_4^2 + 16\,\tilde{J}_4^3$	
$[X_{13}]^{4,44}_{-80}$	#(monomials) = 53
$D_1 = 2\,J_2 + 2\,J_3 + J_4, D_2 = J_3, D_3 = J_2, D_4 = J_1, D_5 = J_1, D_6 = J_2, D_7 = J_3, D_8 = J_4$	
$J_1\,J_2\,J_3 + J_2\,J_3\,J_4 - 2\,J_2\,J_4^2 - 2\,J_3\,J_4^2 + 8\,J_4^3$	
$c_2(TX) = (12, 12, 12, -4)$	$K = \begin{pmatrix} 1 & 0 & 0 & 0 \\ 0 & 0 & 0 & 1 \\ 0 & 1 & 0 & -2 \\ 0 & 0 & 1 & -2 \end{pmatrix}$

Pair 14: $\{\tilde{x}_1 \to e^{i\pi}x_1,\ \tilde{x}_2 \to e^{i\pi}x_2,\ \tilde{x}_3 \to e^{i\pi}x_3,\ \tilde{x}_4 \to e^{i\pi}x_4\}$

$[\widetilde{X_{14}}]^{3,115}_{-224}$	#(monomials) = 153
$\tilde{D}_1 = 2\,\tilde{J}_1 + 2\,\tilde{J}_2 + 2\,\tilde{J}_3, \tilde{D}_2 = \tilde{J}_3, \tilde{D}_3 = \tilde{J}_2, \tilde{D}_4 = \tilde{J}_1, \tilde{D}_5 = \tilde{J}_1, \tilde{D}_6 = \tilde{J}_2, \tilde{D}_7 = \tilde{J}_3$	
$2\,\tilde{J}_1\,\tilde{J}_2\,\tilde{J}_3$	
$[X_{14}]^{3,59}_{-112}$	#(monomials) = 77
$D_1 = 2\,J_1 + 2\,J_2 + 2\,J_3, D_2 = J_3, D_3 = J_2, D_4 = J_1, D_5 = J_1, D_6 = J_2, D_7 = J_3$	
$J_1\,J_2\,J_3$	
$c_2(TX) = (12, 12, 12)$	
$K_1 = \begin{pmatrix} 0 & 1 & 0 \\ 1 & -1 & 0 \\ 0 & -1 & 1 \end{pmatrix}$, $K_2 = \begin{pmatrix} 0 & 0 & 1 \\ 0 & 1 & -1 \\ 1 & 0 & -1 \end{pmatrix}$, $K_3 = \begin{pmatrix} 1 & 0 & 0 \\ -1 & 0 & 1 \\ -1 & 1 & 0 \end{pmatrix}$, $K_{join} = \begin{pmatrix} 1 & 0 & 0 \\ 0 & 1 & 0 \\ 0 & 0 & 1 \end{pmatrix}$	

Table C.2: *Summary of the Calabi-Yau three-fold geometries, for both upstairs manifolds $\widetilde{X_i}$ and downstairs manifolds X_i. The phase rotation rule (together with the permutation if needed) is specified at the start of each geometry pair. The Hodge numbers $h^{1,1}$ and $h^{2,1}$, as well as the Euler Character χ of the manifold X are presented as $[X_i]^{h^{1,1},h^{2,1}}_{\chi}$. Further geometrical properties follow in order: number of generating monomials, Picard group structure and intersection polynomial, as well as $c_2(TX_i)$ and Kähler cone matrix for the downstairs spaces.*

C.3 GUT Models

Downstairs Rank-5 GUT Models

$[X_3]^{4,36}_{-64}$	$\pi_1(X_3) = \mathbb{Z}_2$
{(-1, 2, 2, 0),(0, -1, 1, 0),(0, -1, 1, 0),(0, 0, -3, 1),(1, 0, -1, -1)}	{(-1, 1, 3, 0),(0, 1, -1, 0),(0, 1, -1, 0),(0, 1, -1, 0),(1, -4, 0, 0)}
{(-1, 1, 3, 0),(0, 1, -1, 0),(0, 1, -1, 0),(0, -4, 0, 1),(1, 1, -1, -1)}	{(-1, 1, 2, 0),(0, 1, -1, 0),(0, 1, -1, 0),(0, -4, 0, 1),(1, 1, 0, -1)}
{(-1, 1, 1, 0),(0, 1, 1, -2),(0, -1, 0, 1),(0, -1, 0, 1),(1, 0, -2, 0)}	{(-1, 0, 1, 0),(-1, 1, 0, -1),(-1, 0, 1, 0),(1, 0, 0, -1),(2, -1, -2, 2)}
{(-1, 0, 1, 0),(-1, 0, 1, 0),(-1, 0, 1, 0),(1, 1, -1, -2),(2, -1, -2, 2)}	{(-1, 0, 1, 0),(-1, 1, -1, 0),(0, 1, 2, -2),(1, -1, -1, 1),(1, -1, -1, 1)}
{(-1, 1, 1, -1),(-2, -1, 1, 1),(-1, 1, 1, -1),(2, 1, -2, 0),(2, -2, -1, 1)}	{(-1, 1, 1, -1),(-1, 1, 1, -1),(-1, 1, 1, -1),(1, -3, -1, 2),(2, 0, -2, 1)}
$[X_6]^{3,59}_{-112}$	$\pi_1(X_6) = \mathbb{Z}_2$
{(-3, 0, 1), (0, 3, -1), (1, -1, 0), (1, -1, 0), (1, -1, 0)}	{(-1, 1, 0), (-1, 1, 0), (-1, 1, 0), (1, -4, 1), (2, 1, -1)}
$[X_9]^{4,28}_{-48}$	$\pi_1(X_9) = \mathbb{Z}_2$
{(-4, 0, 1, 1),(1, 3, -1, -1),(1, -1, 0, 0),(1, -1, 0, 0),(1, -1, 0, 0)}	{(-3, 1, -1, 1),(0, 2, 1, -1),(1, -1, 0, 0),(1, -1, 0, 0),(1, -1, 0, 0)}
{(-3, 1, 0, 1),(0, 2, 0, -1),(1, -1, 0, 0),(1, -1, 0, 0),(1, -1, 0, 0)}	{(-2, 3, 0, -1),(-1, 0, 0, 1),(1, -1, 0, 0),(1, -1, 0, 0),(1, -1, 0, 0)}
{(-2, 1, 1, 0),(-1, -2, 2, 1),(1, 1, -1, -1),(1, 0, -1, 0),(1, 0, -1, 0)}	{(-2, 0, 0, 1),(-1, 3, 0, -1),(1, -1, 0, 0),(1, -1, 0, 0),(1, -1, 0, 0)}
{(-2, 1, 0, 1),(-1, 2, 0, -1),(1, -1, 0, 0),(1, -1, 0, 0),(1, -1, 0, 0)}	{(-2, 0, 1, 2),(-1, 3, -1, -2),(1, -1, 0, 0),(1, -1, 0, 0),(1, -1, 0, 0)}
{(-1, 1, 0, 0),(-1, 1, 0, 0),(-1, 1, 0, 0),(-1, -1, -1, 1),(4, -2, 1, -1)}	{(-1, 1, 0, 0),(-1, 1, 0, 0),(-1, 1, 0, 0),(0, -4, 1, 1),(3, 1, -1, -1)}
{(-1, 1, 3, 0),(0, 1, -1, 0),(0, 1, -1, 0),(0, 1, -1, 0),(1, -4, 0, 0)}	{(-1, -4, 2, 1),(0, 1, -1, 0),(0, 1, -1, 0),(0, 1, -1, 0),(1, 1, 1, -1)}
$[X_{10}]^{4,36}_{-64}$	$\pi_1(X_{10}) = \mathbb{Z}_2$
{(-3, 4, 2, -1),(1, -1, -1, 0),(1, -1, -1, 0),(1, -1, -1, 0),(0, -1, 1, 1)}	{(-3, 4, 2, -2),(1, -1, -1, 1),(1, -1, -1, 1),(1, -1, -1, 1),(0, -1, 1, -1)}
{(-4, 3, 2, -1),(2, -2, -1, 1),(2, -2, -1, 1),(2, -2, -1, 1),(-2, 3, 1, -2)}	{(-2, 1, 2, 1),(5, -4, -2, 2),(-1, 1, 0, -1),(-1, 1, 0, -1),(-1, 1, 0, -1)}
{(0, 1, 2, -2),(1, -1, -1, 1),(1, -1, -1, 1),(1, -1, -1, 1),(-3, 2, 1, -1)}	{(-1, 1, 1, 0),(1, 0, -2, -1),(2, -3, -1, 1),(-1, 1, 1, 0),(-1, 1, 1, 0)}
{(-3, 1, 1, 0),(0, -1, -1, 1),(1, -1, 0, 0),(1, -1, 0, 0),(1, 2, 0, -1)}	{(-4, 1, 1, 0),(2, -2, -1, 1),(1, -1, 0, 0),(1, -1, 0, 0),(0, 3, 0, -1)}
{(-4, 1, 1, 0),(2, -1, -1, 1),(1, -1, 0, 0),(1, -1, 0, 0),(0, 2, 0, -1)}	{(-4, 1, 1, 0),(1, 2, -1, 0),(1, -1, 0, 0),(1, -1, 0, 0),(1, -1, 0, 0)}
{(-2, 1, 1, -1),(2, 1, -1, 0),(1, -1, 0, 0),(1, -1, 0, 0),(-2, 0, 0, 1)}	{(-1, 0, 1, 1),(2, -1, -2, 0),(3, -3, -1, 1),(-2, 2, 1, -1),(-2, 2, 1, -1)}
{(-1, 0, 1, 0),(0, 0, -1, 1),(0, 0, -1, 1),(1, -1, 0, 0),(0, 1, 1, -2)}	{(0, -1, 1, 1),(1, 0, -2, 0),(-1, 1, -1, 1),(0, 0, 1, -1),(0, 0, 1, -1)}
{(0, -3, 1, 0),(3, 0, -1, 0),(-1, 1, 0, 0),(-1, 1, 0, 0),(-1, 1, 0, 0)}	{(0, -3, 1, 0),(1, 0, -1, 1),(1, 1, 0, -1),(-1, 1, 0, 0),(-1, 1, 0, 0)}
{(-1, 2, 0, 1),(1, -2, -3, 2),(0, 0, 1, -1),(0, 0, 1, -1),(0, 0, 1, -1)}	{(-1, 1, 0, 0),(1, 0, -2, 1),(0, -1, 0, 1),(0, 0, 1, -1),(0, 0, 1, -1)}
{(-1, 1, 0, 0),(2, 1, -1, 0),(1, -3, 0, 1),(-1, 1, 0, 0),(-1, 0, 1, -1)}	{(-3, 0, 0, 1),(1, 1, -1, 0),(1, -1, 0, 0),(1, -1, 0, 0),(0, 1, 1, -1)}
{(-3, 0, 0, 1),(1, 2, -1, 0),(1, -1, 0, 0),(1, -1, 0, 0),(0, 0, 1, -1)}	{(0, -1, 0, 1),(3, -2, -2, 1),(1, -1, 0, 0),(-2, 2, 1, -1),(-2, 2, 1, -1)}
{(-1, 0, -1, 2),(1, 0, -2, 1),(0, 0, 1, -1),(0, 0, 1, -1),(0, 0, 1, -1)}	{(-1, 0, -1, 1),(4, -3, -2, 2),(-1, 1, 1, -1),(-1, 1, 1, -1),(-1, 1, 1, -1)}
{(1, 0, -2, 2),(2, -3, -1, 1),(-1, 1, 1, -1),(-1, 1, 1, -1),(-1, 1, 1, -1)}	
$[X_{11}]^{4,36}_{-64}$	$\pi_1(X_{11}) = \mathbb{Z}_2$
{(2, 2, -1, -1), (-3, 0, 1, 0), (-1, 0, 0, 1), (1, -1, 0, 0), (1, -1, 0, 0)}	{(2, 2, -3, -1), (-2, 1, 0, 1), (0, -1, 1, 0), (0, -1, 1, 0), (0, -1, 1, 0)}
{(2, 2, -3, -1), (-1, -1, 1, 1), (-1, 0, 1, 0), (-1, 0, 1, 0), (1, -1, 0, 0)}	{(2, 2, -3, -2), (-2, 1, 0, -1), (0, -1, 1, 1), (0, -1, 1, 1), (0, -1, 1, 1)}
{(1, 3, -1, 0), (-4, 0, 1, 0), (1, -1, 0, 0), (1, -1, 0, 0), (1, -1, 0, 0)}	{(1, 3, -1, -1), (-4, 0, 1, 1), (1, -1, 0, 0), (1, -1, 0, 0), (1, -1, 0, 0)}
{(1, 2, -1, 0), (-4, 0, 1, 1), (1, -1, 0, 0), (1, -1, 0, 0), (1, 0, 0, -1)}	{(1, 2, -3, -1), (-1, -1, 2, 1), (-1, -1, 2, 1), (0, 2, -1, -2), (1, -2, 0, 1)}
{(1, 2, -4, -1), (-1, -1, 2, 1), (-1, -1, 2, 1), (-1, -1, 2, 1), (2, 1, -2, -2)}	{(1, 2, -2, -2), (-1, -1, 2, 1), (-1, -1, 2, 1), (0, 1, -1, 0), (1, -1, -1, 0)}
{(1, 1, -2, 0), (-2, 0, 1, 1), (0, -1, 1, 0), (0, -1, 1, 0), (1, 1, -1, -1)}	{(1, 1, -1, -1), (-4, 0, 1, 1), (1, -1, 2, 0), (1, 0, -1, 0), (1, 0, -1, 0)}
{(1, 1, -2, -1), (-4, 0, 1, 1), (1, -1, 3, 0), (1, 0, -1, 0), (1, 0, -1, 0)}	{(1, 1, -2, -1), (-3, -1, 3, 1), (0, -2, 3, 2), (1, 1, -2, -1), (1, 1, -2, -1)}

continued in the next page

Downstairs Rank-5 GUT Models	
{(1, 1, -2, -1), (-3, -1, 3, 2), (0, -2, 3, 1), (1, 1, -2, -1), (1, 1, -2, -1)}	{(1, 1, -2, -1), (-2, -1, 3, 1), (-1, 1, -1, 1), (1, -2, 2, 0), (1, 1, -2, -1)}
{(1, 1, -2, -1), (-2, 0, 3, 1), (0, -1, 1, 0), (0, -1, 0, 1), (1, 1, -2, -1)}	{(1, 1, -3, -1), (-1, 0, 1, 1), (-1, 0, 1, 1), (-1, 0, 1, 1), (2, -1, 0, -2)}
{(1, 1, -3, -2), (-1, 0, 1, 0), (-1, 0, 1, 0), (-1, 0, 1, 0), (2, -1, 0, 2)}	{(0, 3, 0, -1), (-1, -1, 2, 1), (0, -1, 1, 0), (0, -1, 1, 0), (1, 0, -4, 0)}
{(0, 3, 0, -1), (0, -1, 1, 0), (0, -1, 1, 0), (0, -1, 1, 0), (0, 0, -3, 1)}	{(0, 2, -1, 1), (-3, 1, 1, 2), (1, -1, 0, -1), (1, -1, 0, -1), (1, -1, 0, -1)}
{(0, 2, 1, -1), (-1, -1, 1, 1), (0, 1, -1, 0), (0, 1, -1, 0), (1, -3, 0, 0)}	{(0, 2, 1, -1), (-1, 0, 0, 1), (0, -1, 1, 0), (0, -1, 1, 0), (1, 0, -3, 0)}
{(0, 2, 0, -1), (-1, 0, 2, 1), (0, -1, 1, 0), (0, -1, 1, 0), (1, 0, -4, 0)}	{(0, 2, -1, -2), (-3, 1, 1, -1), (1, -1, 0, 1), (1, -1, 0, 1), (1, -1, 0, 1)}
{(0, 1, -1, 0), (-2, -1, 2, 1), (0, 1, -1, 0), (0, 1, -1, 0), (2, -2, 1, -1)}	{(0, 1, -1, 0), (-2, 0, 1, 1), (0, 1, -1, 0), (1, -2, 1, 0), (1, 0, 0, -1)}
{(0, 1, -1, 0), (-2, 2, 1, -1), (0, -1, 0, 1), (1, -1, 0, 0), (1, -1, 0, 0)}	{(0, 1, -1, 0), (-2, 2, 1, 1), (0, -1, 0, 1), (1, -1, 0, -1), (1, -1, 0, -1)}
{(0, 1, -1, 0), (-1, -2, 4, 2), (0, 1, -1, 0), (0, 1, -1, 0), (1, -1, -1, -2)}	{(0, 1, -1, 0), (-1, 0, 1, 0), (-1, 0, 0, 1), (0, 1, -1, 0), (2, -2, 1, -1)}
{(0, 1, -1, 0), (-1, 1, 3, 0), (0, 1, -1, 0), (0, 1, -1, 0), (1, -4, 0, 0)}	{(0, 1, -1, 0), (-1, 1, 0, 1), (0, 1, 2, -1), (0, 1, -1, 0), (1, -4, 0, 0)}
{(0, 1, -1, 0), (-1, 1, 1, 1), (0, 1, 1, -1), (0, 1, -1, 0), (1, -4, 0, 0)}	{(0, 1, -1, 0), (-1, 2, 2, 0), (0, -3, 1, 1), (0, 1, -1, 0), (1, -1, -1, -1)}
{(0, 1, -1, 0), (0, -4, 1, 1), (0, 1, 2, -1), (0, 1, -1, 0), (0, 1, -1, 0)}	{(0, 1, -4, 0), (-1, 0, 1, 0), (-1, 0, 1, 0), (-1, 0, 1, 0), (3, -1, 1, 0)}
{(0, 1, 0, -1), (-2, 1, 1, 0), (0, 0, -1, 1), (1, -1, 0, 0), (1, -1, 0, 0)}	{(0, 1, 0, -1), (-1, 0, 1, 0), (-1, 0, 1, 0), (0, 0, -3, 1), (2, -1, 1, 0)}
{(0, 1, -1, -1), (-3, -1, 3, 1), (0, 1, -1, -1), (0, 1, -1, -1), (3, -2, 0, 2)}	{(0, 1, -1, -1), (-2, -2, 5, 2), (0, 1, -1, -1), (0, 1, -1, -1), (2, -1, -2, 1)}
{(0, 1, -1, -1), (-2, -1, 2, 1), (0, 1, -1, -1), (0, 1, -1, -1), (2, -2, 1, 2)}	{(0, 1, -1, -1), (-1, -2, 4, 2), (0, 1, -1, -1), (0, 1, -1, -1), (1, -1, -1, 1)}
{(0, 1, -2, -1), (-1, 0, 1, 0), (-1, 0, 1, 0), (0, 0, -2, 1), (2, -1, 2, 0)}	{(0, 1, 0, -2), (-3, 2, 0, -1), (1, -1, 0, 1), (1, -1, 0, 1), (1, -1, 0, 1)}
{(0, 1, 0, -2), (-1, 0, 1, 0), (-1, 1, -1, 0), (1, -1, 0, 1), (1, -1, 0, 1)}	{(0, 1, 0, -2), (-1, 1, 0, 1), (-1, 1, 0, 1), (1, -2, 1, -1), (1, -1, -1, 1)}
{(0, 0, -3, 1), (-1, 0, 1, 0), (-1, 0, 1, 0), (-1, 1, 0, -1), (3, -1, 1, 0)}	{(-1, 2, -1, 1), (-2, 2, 1, 0), (1, -2, 0, 1), (1, -1, 0, -1), (1, -1, 0, -1)}
{(-1, 2, -2, 1), (-2, 1, 2, 2), (1, -1, 0, -1), (1, -1, 0, -1), (1, -1, 0, -1)}	{(-1, 2, -2, -3), (-2, 1, 2, 0), (1, -1, 0, 1), (1, -1, 0, 1), (1, -1, 0, 1)}
{(-1, 1, -1, 2), (-2, 2, 1, 1), (1, -1, 0, -1), (1, -1, 0, -1), (1, -1, 0, -1)}	{(-1, 1, -1, 1), (-2, 2, 1, -1), (1, -1, 0, 0), (1, -1, 0, 0), (1, -1, 0, 0)}
$[X_{12}]^{4,44}_{-80}$	$\pi_1(X_{12}) = \mathbb{Z}_2$
{(1, -4, 1, 0),(-1, 1, 0, 0),(-1, 1, 0, 0),(-1, 1, 0, 0),(2, 1, -1, 0)}	
$[X_{13}]^{4,44}_{-80}$	$\pi_1(X_{13}) = \mathbb{Z}_2$
{(3, 1, -1, 0),(-1, 1, 0, 0),(-1, 1, 0, 0),(-1, 1, 0, 0),(0, -4, 1, 0)}	{(3, -1, 1, 0),(-1, 0, 1, 0),(-1, 0, 1, 0),(-1, 0, 1, 0),(0, 1, -4, 0)}
{(3, 1, -1, -1),(-1, 1, 0, 0),(-1, 1, 0, 0),(-1, 1, 0, 0),(0, -4, 1, 1)}	{(3, -1, 1, -1),(-1, 0, 1, 0),(-1, 0, 1, 0),(-1, 0, 1, 0),(0, 1, -4, 1)}
{(2, 1, -4, -1),(-1, 0, 1, 0),(-1, 0, 1, 0),(-1, 0, 1, 0),(1, -1, 1, 1)}	{(2, -4, 1, -1),(-1, 1, 0, 0),(-1, 1, 0, 0),(-1, 1, 0, 0),(1, 1, -1, 1)}
{(1, 3, -1, 0),(-4, 0, 1, 0),(1, -1, 0, 0),(1, -1, 0, 0),(1, -1, 0, 0)}	{(1, 0, -1, 0),(-4, 1, 0, 0),(1, -1, 3, 0),(1, 0, -1, 0),(1, 0, -1, 0)}
{(1, 0, -1, 0),(-4, 1, 0, 1),(1, -1, 3, -1),(1, 0, -1, 0),(1, 0, -1, 0)}	{(1, 0, -1, 0),(-2, 1, 0, -1),(-1, -1, 3, 1),(1, 0, -1, 0),(1, 0, -1, 0)}
{(1, 0, -3, 0),(-1, 1, 1, 1),(0, 1, 0, -1),(0, -1, 1, 0),(0, -1, 1, 0)}	{(1, 0, -4, 0),(-1, 3, 1, 0),(0, -1, 1, 0),(0, -1, 1, 0),(0, -1, 1, 0)}
{(1, -1, 0, 0),(-4, 0, 1, 1),(1, 3, -1, -1),(1, -1, 0, 0),(1, -1, 0, 0)}	{(1, -1, 0, 0),(-3, 5, -1, 2),(0, -2, 1, -2),(1, -1, 0, 0),(1, -1, 0, 0)}
{(1, -1, 0, 0),(-2, 0, 1, -1),(-1, 3, -1, 1),(1, -1, 0, 0),(1, -1, 0, 0)}	{(1, -3, 0, 0),(-1, 1, 1, 1),(0, 0, 1, -1),(0, 1, -1, 0),(0, 1, -1, 0)}
{(1, -4, 0, 0),(-1, 1, 3, 0),(0, 1, -1, 0),(0, 1, -1, 0),(0, 1, -1, 0)}	
$[X_{14}]^{3,59}_{-112}$	$\pi_1(X_{14}) = \mathbb{Z}_2$
{(-1, 1, 3), (0, 1, -1), (0, 1, -1), (0, 1, -1), (1, -4, 0)}	

Table C.3: *Heterotic $SU(5)$-GUT models on the downstairs Calabi-Yau three-folds $[X_i]^{h^{1,1},h^{2,1}}_{\chi}$ with $\pi_1 \neq \phi$. The superscripts and the subscript denote, respectively, Hodge numbers and Euler character of the Calabi-Yau base. The gauge bundle of each model is a Whitney sum of five line bundles.*

Downstairs Rank-4 GUT Models	
$[X_5]^{3,43}_{-80}$	$\pi_1(X_5) = \mathbb{Z}_2$
{(3, 3, -1), (-2, 2, 0), (1, -1, 0), (-2, -4, 1)}	{(3, 3, -1), (1, -1, 0), (2, -2, 0), (-6, 0, 1)}
{(5, 1, -1), (-2, 2, 0), (-1, 1, 0), (-2, -4, 1)}	{(5, 1, -1), (-2, 2, 0), (3, -3, 0), (-6, 0, 1)}
{(5, 1, -1), (-1, 1, 0), (2, -2, 0), (-6, 0, 1}	
$[X_6]^{3,59}_{-112}$	$\pi_1(X_6) = \mathbb{Z}_2$
{(2, 1, -1), (-1, 1, 0), (-2, 2, 0), (1, -4, 1)}	{(6, 1, -1), (-2, 1, 0), (-4, 2, 0), (0, -4, 1)}
{(3, 2, -1), (3, -3, 0), (-2, 2, 0), (-4, -1, 1)}	{(3, 2, -1), (2, -2, 0), (-1, 1, 0), (-4, -1, 1)}
{(3, 2, -1), (1, -1, 0), (-4, 4, 0), (0, -5, 1)}	{(3, 2, -1), (-1, 1, 0), (-2, 2, 0), (0, -5, 1)}
{(0, 3, -1), (2, -2, 0), (1, -1, 0), (-3, 0, 1)}	{(0, 3, -1), (1, -1, 0), (-2, 2, 0), (1, -4, 1)}
{(1, 4, -1), (4, -4, 0), (-1, 1, 0), (-4, -1, 1)}	{(1, 4, -1), (2, -2, 0), (1, -1, 0), (-4, -1, 1)}
{(1, 4, -1), (2, -2, 0), (-3, 3, 0), (0, -5, 1)}	{(1, 4, -1), (1, -1, 0), (-2, 2, 0), (0, -5, 1)}
{(0, 7, -1), (2, -4, 0), (1, -2, 0), (-3, -1, 1}	
$[X_8]^{3,75}_{-144}$	$\pi_1(X_8) = \mathbb{Z}_2$
{(1, -3, 1), (2, -2, 0), (-3, 3, 0), (0, 2, -1)}	{(1, -3, 1), (1, -1, 0), (-2, 2, 0), (0, 2, -1)}
{(1, -3, 1), (1, -1, 0), (2, 0, -1), (-4, 4, 0)}	{(1, -3, 1), (-1, 1, 0), (-2, 2, 0), (2, 0, -1)}
{(4, -4, 0), (-3, 1, 1), (-1, 1, 0), (0, 2, -1)}	{(4, -4, 0), (-3, 1, 1), (2, 0, -1), (-3, 3, 0)}
{(3, -3, 0), (-3, 1, 1), (-2, 2, 0), (2, 0, -1)}	{(2, -2, 0), (-3, 1, 1), (1, -1, 0), (0, 2, -1)}
{(2, -2, 0), (-3, 1, 1), (-1, 1, 0), (2, 0, -1}	
$[X_{14}]^{3,59}_{-112}$	$\pi_1(X_{14}) = \mathbb{Z}_2$
{(1, -1, -5), (0, 2, -2), (0, -3, 3), (-1, 2, 4)}	{(1, -1, -5), (0, 1, -1), (0, -2, 2), (-1, 2, 4)}
{(1, -1, -5), (0, 1, -1), (-1, 4, 2), (0, -4, 4)}	{(1, -1, -5), (0, -1, 1), (0, -2, 2), (-1, 4, 2)}
{(-1, 1, -5), (2, 0, -2), (-3, 0, 3), (2, -1, 4)}	{(-1, 1, -5), (1, 0, -1), (4, -1, 2), (-4, 0, 4)}
{(-1, 1, -5), (1, 0, -1), (-2, 0, 2), (2, -1, 4)}	{(-1, 1, -5), (-1, 0, 1), (4, -1, 2), (-2, 0, 2)}
{(1, -1, -4), (0, -2, 1), (-1, 7, 1), (0, -4, 2)}	{(1, 0, -4), (0, 2, -2), (0, -3, 3), (-1, 1, 3)}
{(1, 0, -4), (0, 1, -1), (0, -2, 2), (-1, 1, 3)}	{(1, 0, -4), (0, -1, 1), (-1, 3, 1), (0, -2, 2)}
{(2, 0, -4), (1, 0, -2), (-4, 1, -1), (1, -1, 7)}	{(4, 0, -4), (-5, 1, -1), (-1, 0, 1), (2, -1, 4)}
{(-1, 1, -4), (7, -1, 1), (-2, 0, 1), (-4, 0, 2)}	{(0, 1, -4), (2, 0, -2), (1, -1, 3), (-3, 0, 3)}
{(0, 1, -4), (1, 0, -1), (-2, 0, 2), (1, -1, 3)}	{(0, 1, -4), (3, -1, 1), (-1, 0, 1), (-2, 0, 2)}
{(0, 2, -4), (0, 1, -2), (1, -4, -1), (-1, 1, 7)}	{(0, 4, -4), (1, -5, -1), (0, -1, 1), (-1, 2, 4)}
{(3, 0, -3), (-5, 1, -1), (4, -1, 2), (-2, 0, 2)}	{(3, 0, -3), (-4, 1, 0), (3, -1, 1), (-2, 0, 2)}
{(0, 3, -3), (1, -5, -1), (0, -2, 2), (-1, 4, 2)}	{(0, 3, -3), (1, -4, 0), (-1, 3, 1), (0, -2, 2)}
{(2, 0, -2), (1, 0, -1), (-5, 1, -1), (2, -1, 4)}	{(2, 0, -2), (1, 0, -1), (-4, 1, 0), (1, -1, 3)}
{(2, 0, -2), (-5, 1, -1), (-1, 0, 1), (4, -1, 2)}	{(2, 0, -2), (-4, 1, 0), (3, -1, 1), (-1, 0, 1}

Table C.4: *Heterotic $SO(10)$-GUT models on the Calabi-Yau three-folds $[X_i]^{h^{1,1},h^{2,1}}_{\chi}$ with $h^{1,1} = 3$ and $\pi_1 \neq \phi$. The superscripts and the subscript denote, respectively, Hodge numbers and Euler character of the Calabi-Yau base. The gauge bundle of each model is a Whitney sum of four line bundles.*

Appendix D

Appendices to Chapter 4

D.1 Quivers, an Algebraic Interlude

In this appendix, we give, in an as self-contained fashion as possible, some rudiments on the representation theory of quiver. The interested reader is referred to [82–85] for a more in depth presentation of this material and to [88] for considerations in the gauge-theoretic context.
A quiver diagram is defined as a pair $\mathbf{Q} = (\mathbf{Q}_0, \mathbf{Q}_1)$ where $\mathbf{Q}_0$ is a finite set of vertices and $\mathbf{Q}_1$ is a finite set of oriented edges connecting these vertices. For $\rho \in \mathbf{Q}_1$ we let $h(\rho)$ to denote the vertex attached to the head of the arrow and $t(\rho)$ the one to the tail. A path in $\mathbf{Q}$ is a sequence $x = \rho_1 \dots \rho_n$ of arrows such that $h(\rho_{i+1}) = t(\rho_i)$. Moreover, for each vertex $i \in \mathbf{Q}_0$ we consider a trivial path e_i which starts and ends in i. The *path algebra* kQ associated with the quiver is the k-algebra whose basis is the collection of paths and with the product rule given by concatenation of the paths and k is some ground number field, usually taken to be $\mathbb{C}$. That is, the multiplication is

$$x \cdot y \equiv \begin{cases} xy, & \text{if} \quad h(y) = t(x) \\ 0, & \text{otherwise} . \end{cases} \tag{D.1}$$

An important class of quivers consists of the ones that are endowed with a *superpotential*. The superpotential is the set of all cyclic paths in the quiver diagram. One can formally define a derivative with respect to arrows, acting on these cyclic paths. The set of derivatives of all cyclic paths with respect to all their constituent arrows forms an ideal called the *Jacobian ideal*. The quotient of the path algebra by the Jacobian ideal is referred to as the *Jacobian algebra*. We call such a quiver with superpotential a *bounded* quiver since it is bounded by zero-relations, while in the absence of a superpotential we refer to the quiver as *unbounded*.
Let us illustrate these definitions with two simple examples.

The Jordan quiver. The path algebra of the Jordan quiver is infinite dimensional, with the basis set being $\{e_1, \rho, \rho^2, \rho^3, \dots\}$. The algebra is isomorphic to the polynomial ring $k[t]$.

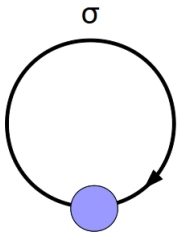

Figure D.1: The Jordan quiver.

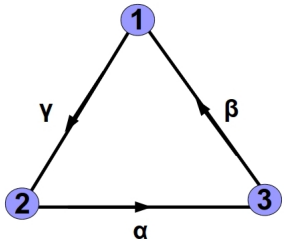

Figure D.2: The oriented $\hat{A}_2$ quiver.

A quiver with relations. The path algebra of the quiver depicted in Fig. D.2 has a basis given by the paths $\{e_1, e_2, e_3, \alpha, \beta, \gamma, \beta\alpha, \gamma\beta, \alpha\gamma, \gamma\beta\alpha, \ldots\}$. Note that other combinations of arrows are not allowed, for example $\gamma\alpha = 0$ since $h(\alpha) \neq t(\gamma)$. This quiver has also a superpotential given by the unique cycle $S = \gamma\beta\alpha$. The Jacobian ideal is the one generated by the following relations, which form the zero paths,

$$\partial_\alpha S = \gamma\beta \ , \quad \partial_\beta S = \alpha\gamma \ , \quad \partial_\gamma S = \beta\alpha$$

D.1.1 Quiver Representations

A representation of a quiver is the assignment of a vector space V_i to each vertex $i \in \mathbf{Q}_0$ and a linear map $V_\rho : \ V_{t_{(\rho)}} \mapsto V_{h_{(\rho)}}$ to each edge $\rho \in \mathbf{Q}_1$. Different representations of a given quiver are different sets of vector spaces and morphisms that one can assign to each vertex or edge respectively. The dimension vector is defined as follows,

$$d_V = (\dim V_1, \ldots, \dim V_n) \in \mathbb{Z}^{\mathbf{Q}_0} \tag{D.2}$$

where n is the number of vector spaces. This is just the vector labelling the ranks.
Clearly, there are infinite representations, since there are infinite dimension vectors, but one does not need to classify them. A key notion is that of indecomposable representations of a given quiver. Let $V \equiv (V_i, V_\rho)$, $W \equiv (W_i, W_\rho)$ be two representations of a quiver $\mathbf{Q}$, where

Latin indices denote vertices and Greek, edges. Define a direct sum of two representations as

$$V \oplus W \equiv \Big\{(V \oplus W)_i, (V \oplus W)_\rho\Big\}$$

where the resulting vector space set is

$$(V \oplus W)_i = V_i \oplus W_i \tag{D.3}$$

and the resulting map set $(V \oplus W)_\rho : (V \oplus W)_{t(\rho)} \mapsto (V \oplus W)_{h(\rho)}$

$$(V \oplus W)_\rho\big((v,w)\big) = \Big(V_\rho(u), W_\rho(w)\Big), \quad v \in V_{t(\rho)}, w \in W_{t(\rho)}. \tag{D.4}$$

A representation V is *trivial* if $V_i = 0,\ \forall\ i \in \mathbf{Q}_0$ and *simple* if its only subrepresentation is the trivial and itself in complete analogy with the group theoretical definitions. In addition, a representation V is *decomposable* if it is isomorphic to $W \oplus U$ for some $W, U \in \mathrm{Rep}_k(\mathbf{Q})$, and *indecomposable* otherwise. It is an important fact that *every representation of a quiver diagram has a unique, up to isomorphism, decomposition into indecomposable representations.*
Thus, one needs only classify the indecomposable representations of a quiver diagram.
Let us once more illustrate the above notions with two simple examples:

An unbounded linear quiver.

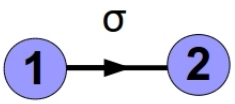

This diagram has the following indecomposable representations U, V, W, where

$$\{U_1 \cong k,\ U_2 = 0,\ U_\sigma = 0\}\ , \{V_1 = 0,\ V_2 \cong k,\ V_\sigma = 0\}\ , \{W_1 \cong k,\ W_2 \cong k,\ W_\sigma = 1\}\ . \tag{D.5}$$

Therefore, any representation $Z = \{Z_1, Z_2; Z_\sigma\}$ of $\mathbf{Q}$ is isomorphic to

$$Z \cong U^\alpha \oplus V^\beta \oplus W^\gamma \tag{D.6}$$

with $U^\alpha \equiv \underbrace{U \oplus \ldots \oplus U}_{\alpha}$. The positive integers α, β, γ are related to the rank of the morphism Z_σ and the dimensions of the vector spaces Z_1 and Z_2 as follows. Since the spaces on the LHS are isomorphic to the direct sum on the RHS for each value of the index i, the dimension vectors must be the same. Denoting the dimension of a vector space A_i as $\dim(A_i) \equiv d_i$, where A runs over all four representations, namely U, V, Z, W, we have

$$d_1 = \alpha + \gamma \quad \text{and} \quad d_2 = \beta + \gamma.$$

The exponent γ is the rank σ of the morphism Z_σ. Solving the above equations we find $a = d_1 - \sigma,\ \beta = d_2 - \sigma$. Thus, the decomposition of any representation Z of this quiver, with dimension vector $d_Z = (d_1, d_2)$, is

$$Z \cong U^{d_1-\sigma} \oplus V^{d_2-\sigma} \oplus W^\sigma \ . \tag{D.7}$$

Note how d_Z governs the decomposition.

The bounded $\hat{A}_2$ quiver. The quiver with relations depicted in Fig. D.2 falls under the category of *gentle* algebras [86,144]. A gentle algebra is defined as the one that has the following properties:

(C1) At each point of $\mathbf{Q}$ start at most two arrows and stop at most two arrows.

(C2) The ideal of zero relations I is generated by paths of length 2.

(C3) For each arrow β there is at most one arrow α and at most one arrow γ such that $\alpha\beta \in I$ and $\beta\gamma \in I$.

(C4) For each arrow β there is at most one arrow α and at most one arrow γ such that $\alpha\beta \notin I$ and $\beta\gamma \notin I$.

The representation theory of these quivers is well studied. Their indecomposable representations fall under two categories, the *string modules* and the *band modules*. Denoting by A the Jacobian algebra, a string is by definition a reduced walk w in A avoiding the zero-relations. A string is cyclic if the first and the last vertex coincide. A band is defined to be a cyclic string b such that each power b^n is a string, but b itself is not a proper power of some string c. The string module $M(w)$ is obtained from the string w by replacing each vertex that belongs to the walk by a copy of the field k. The dimension vector $\dim M(w)$ of $M(w)$ is obtained by counting how often the string w passes through each vertex x of the quiver $\mathbf{Q}$. Similarly, each band b in A gives rise to a family of band modules $M(b)$. All string and band modules are indecomposable, and in fact every indecomposable $A-$module is either a string module $M(w)$ or a band module $M(b)$. For the $\hat{A}_2$ quiver we have the following string modules: $\{e_1, e_2, e_3\}$ of zero length giving rise to dimension vectors $\{(1,0,0)\ ,\ (0,1,0)\ ,\ (0,0,1)\}$ and $\{\alpha, \beta, \gamma\}$ of unit length giving rise to dimension vectors $\{(0,1,1)\ ,\ (1,0,1)\ ,\ (1,1,0)\}$ respectively. Note that there are no band modules since any walk of length greater than one contains the zero relations.
Let us close this section by stating two important theorems on quiver representations:
Gabriel's Theorem.

- *A quiver is of finite type if and only if the underlying graph is a union of Dynkin graphs of type A,D or E.*

- *A quiver is of tame type if and only if the underlying graph is a union of Dynkin graphs of type A,D or E and extended Dynkin diagrams of type $\hat{A}, \hat{D}$ or $\hat{E}$.*

- *The isomorphism classes of indecomposable representations of a quiver* $\mathbf{Q}$ *of finite type are in one-to-one correspondence with the positive roots of the root system associated to the underlying graph of* $\mathbf{Q}$ *. The correspondence is given by*

$$V \mapsto \sum_{i \in \mathbb{Q}_0} d_V(i)\alpha_i$$

where a_i is the i-th positive root and by graph is meant the set of edges and vertices without considering the orientations in each case.

Kac's Theorem. *Let* $\mathbf{Q}$ *be an arbitrary quiver. The dimension vectors of indecomposable representations of* $\mathbf{Q}$ *correspond to positive roots of the root system of the underlying graph of* $\mathbf{Q}$ *. Real roots correspond to dimension vectors for which there is exactly one indecomposable representation, while imaginary roots correspond to dimension vectors for which there are families of indecomposable representations. If a positive root α is real, then $q(\alpha) = 1$. If it is imaginary, then $q(\alpha) \leq 0$.*

D.2 Complementary Results

In this Appendix, we list the results obtained for the rest of the quivers. We list the cycle structure of each Type as well as all the possible consistent subsets of choices which could satisfy the constraints of the sum of R-charges of each cycle equalling to 2, for Types I, IV and VI of the five-block quiver. Each set is given as a reference to the equation number in the text and consists of 6 members because, as explained, we need a rank six linear space.

D.2.1 Subsets of Marginal Operators for Type I

There are 33 possible choices:

$_1\{(4.44),(4.50),(4.51),(4.52),(4.53),(4.54)\}$, $_2\{(4.44),(4.45),(4.47),(4.48),(4.50),(4.51)\}$
$_3\{(4.44),(4.45),(4.47),(4.48),(4.49),(4.50)\}$, $_4\{(4.44),(4.45),(4.47),(4.49),(4.50),(4.54)\}$
$_5\{(4.44),(4.45),(4.48),(4.49),(4.50),(4.51)\}$, $_6\{(4.44),(4.45),(4.46),(4.47),(4.51),(4.52)\}$
$_7\{(4.44),(4.45),(4.46),(4.47),(4.48),(4.51)\}$, $_8\{(4.44),(4.45),(4.46),(4.47),(4.48),(4.49)\}$
$_9\{(4.44),(4.45),(4.46),(4.47),(4.49),(4.52)\}$, $_{10}\{(4.44),(4.45),(4.46),(4.48),(4.53),(4.54)\}$
$_{11}\{(4.44),(4.45),(4.46),(4.48),(4.49),(4.51)\}$, $_{12}\{(4.44),(4.45),(4.46),(4.49),(4.51),(4.52)\}$
$_{13}\{(4.44),(4.47),(4.48),(4.49),(4.52),(4.53)\}$, $_{14}\{(4.44),(4.46),(4.47),(4.48),(4.50),(4.51)\}$
$_{15}\{(4.44),(4.46),(4.47),(4.48),(4.49),(4.50)\}$, $_{16}\{(4.44),(4.46),(4.47),(4.49),(4.50),(4.52)\}$
$_{17}\{(4.44),(4.46),(4.48),(4.49),(4.50),(4.51)\}$, $_{18}\{(4.43),(4.44),(4.50),(4.51),(4.53),(4.54)\}$
$_{19}\{(4.43),(4.44),(4.50),(4.51),(4.52),(4.53)\}$, $_{20}\{(4.43),(4.44),(4.50),(4.51),(4.52),(4.54)\}$
$_{21}\{(4.43),(4.44),(4.50),(4.52),(4.53),(4.54)\}$, $_{22}\{(4.43),(4.44),(4.45),(4.47),(4.48),(4.49)\}$
$_{23}\{(4.43),(4.44),(4.45),(4.49),(4.52),(4.54)\}$, $_{24}\{(4.43),(4.44),(4.45),(4.46),(4.51),(4.54)\}$
$_{25}\{(4.43),(4.44),(4.45),(4.46),(4.47),(4.48)\}$, $_{26}\{(4.43),(4.44),(4.45),(4.46),(4.47),(4.49)\}$
$_{27}\{(4.43),(4.44),(4.45),(4.46),(4.48),(4.49)\}$, $_{28}\{(4.43),(4.44),(4.51),(4.52),(4.53),(4.54)\}$
$_{29}\{(4.43),(4.44),(4.47),(4.48),(4.50),(4.53)\}$, $_{30}\{(4.43),(4.44),(4.47),(4.49),(4.50),(4.52)\}$
$_{31}\{(4.43),(4.44),(4.46),(4.47),(4.48),(4.49)\}$, $_{32}\{(4.43),(4.44),(4.46),(4.48),(4.51),(4.53)\}$
$_{33}\{(4.43),(4.45),(4.46),(4.47),(4.48),(4.49)\}$

D.2.2 Equivalence Classes for Type I Quivers.

Here we list the the Diophantine equations which represent each class within Type I. Recall that we consider two equations equivalent if they are equivalent as quadratic forms. The six equivalence classes are

Class 1: $Dio_1(4), Dio_1(10), Dio_1(12), Dio_1(13), Dio_1(14), Dio_1(22), Dio_1(25),$
$Dio_1(26), Dio_1(27), Dio_1(31)$

Class 2: $Dio_1(18), Dio_1(19), Dio_1(20), Dio_1(21), Dio_1(28)$

Class 3: $Dio_1(23), Dio_1(24), Dio_1(29), Dio_1(30), Dio_1(32)$

Class 4: $Dio_1(1), Dio_1(2), Dio_1(5), Dio_1(6), Dio_1(16), Dio_1(17), Dio_1(33)$

Class 5: $Dio_1(3), Dio_1(7), Dio_1(9), Dio_1(11), Dio_1(15)$

Class 6: $Dio_1(8)$

where n in $Dio_1(n)$ refers to the n-th set of R-charge relations according to the numbering of (D.8). Writing the diagonal part of the quadratic form as $Q_n^I = \frac{A_1^2}{\alpha_1} + \frac{A_2^2}{\alpha_2} + \frac{A_3^2}{\alpha_3} + \frac{A_4^2}{\alpha_4} + \frac{A_5^2}{\alpha_5}$, the representative Diophantine equations are as follows:

Class 1 : Set 10

$$Q^I_{10} = \frac{1}{2}\mathbf{A}^T \begin{pmatrix} \frac{2}{\alpha_1} & a_{12} & 2a_{13} & a_{41} & 0 \\ a_{12} & \frac{2}{\alpha_2} & 0 & a_{42} & 0 \\ 2a_{13} & 0 & \frac{2}{\alpha_3} & 0 & a_{35} \\ a_{41} & a_{42} & 0 & \frac{2}{\alpha_4} & 0 \\ 0 & 0 & a_{35} & 0 & \frac{2}{\alpha_5} \end{pmatrix} \mathbf{A} \tag{D.8}$$

Class 2 : Set 28

$$Q^I_{28} = \frac{1}{2}\mathbf{A}^T \begin{pmatrix} \frac{2}{\alpha_1} & 0 & a_{13} & 0 & 3a_{51} \\ 0 & \frac{2}{\alpha_2} & 0 & a_{24} & 0 \\ a_{13} & 0 & \frac{2}{\alpha_3} & 0 & a_{35} \\ 0 & a_{24} & 0 & \frac{2}{\alpha_4} & 0 \\ 3a_{51} & 0 & a_{35} & 0 & \frac{2}{\alpha_5} \end{pmatrix} \mathbf{A} \tag{D.9}$$

Class 3 : Set 32

$$Q^I_{32} = \frac{1}{2}\mathbf{A}^T \begin{pmatrix} \frac{2}{\alpha_1} & 2a_{12} & a_{13} & 0 & a_{51} \\ 2a_{12} & \frac{2}{\alpha_2} & 0 & a_{24} & 0 \\ a_{13} & 0 & \frac{2}{\alpha_3} & 0 & a_{35} \\ 0 & a_{24} & 0 & \frac{2}{\alpha_4} & 0 \\ a_{51} & 0 & a_{35} & 0 & \frac{2}{\alpha_5} \end{pmatrix} \mathbf{A} \tag{D.10}$$

Class 4 : Set 1

$$Q^I_{1} = \frac{1}{2}\mathbf{A}^T \begin{pmatrix} \frac{2}{\alpha_1} & a_{21} & 0 & a_{41} & 0 \\ a_{21} & \frac{2}{\alpha_2} & 0 & a_{24} & 0 \\ 0 & 0 & \frac{2}{\alpha_3} & 0 & a_{35} \\ a_{41} & a_{24} & 0 & \frac{2}{\alpha_4} & 0 \\ 0 & 0 & a_{35} & 0 & \frac{2}{\alpha_5} \end{pmatrix} \mathbf{A} \tag{D.11}$$

Class 5 : Set 11

$$Q_{11}^I = \frac{1}{2}\mathbf{A}^T \begin{pmatrix} \frac{2}{\alpha_1} & 0 & 2a_{13} & 0 & 0 \\ 0 & \frac{2}{\alpha_2} & 2a_{23} & a_{24} & 0 \\ 2a_{13} & 2a_{23} & \frac{2}{\alpha_3} & 0 & 0 \\ 0 & a_{24} & 0 & \frac{2}{\alpha_4} & 0 \\ 0 & 0 & 0 & 0 & \frac{2}{\alpha_5} \end{pmatrix} \mathbf{A} \tag{D.12}$$

Class 6 : Set 8

$$Q_8^I = \frac{1}{2}\mathbf{A}^T \begin{pmatrix} \frac{6}{\alpha_1} & 0 & a_{31} & 0 & a_{51} \\ 0 & \frac{6}{\alpha_2} & 0 & 5a_{24} & 0 \\ a_{31} & 0 & \frac{6}{\alpha_3} & 6a_{34} & 5a_{35} \\ 0 & 5a_{24} & 6a_{34} & \frac{6}{\alpha_4} & 0 \\ a_{51} & 0 & 5a_{35} & 0 & \frac{6}{\alpha_5} \end{pmatrix} \mathbf{A} \tag{D.13}$$

where $\mathbf{A}$ is the column vector with entries $A_1, \ldots, A_5$ defined in (4.40).

With respect to the above classes, we tabulate below the couplings that have to be set to zero for each set of R-charge relations so that it admits a solution to the marginality condition:

Class 1 In the first class of Diophantine equations one has to set the couplings of the operators depicted in Fig. D.3 to zero together with the quintic operator formed by the outer pentagon of the quiver. The setting of this figure corresponds to the set 22 of (D.8). Then by rotating four times according to the rotational symmetries of the dihedral group on the pentagon, one gets the zero couplings corresponding to sets $25, 26, 27, 31$ respectively.

For the rest five sets of class 1 the couplings to be set to zero are depicted in Fig. D.4. This figure corresponds to set 4 and by rotating four times one gets the couplings of sets $10, 12, 13, 14$.

Class 2 The five equations of class 2 are described by setting to zero the five quadratic operators and one out of five cubics each time.

Class 3 For class 3 the initial set of zero couplings, corresponding to set 23, is depicted in Fig. D.5. The rest can be found by rotating as previously.

Class 4 For class 4 and set 1 we set to zero the coupling of the quintic operator formed by external lines as well as all the quadratic operators, while for set 33 we set to zero only the other

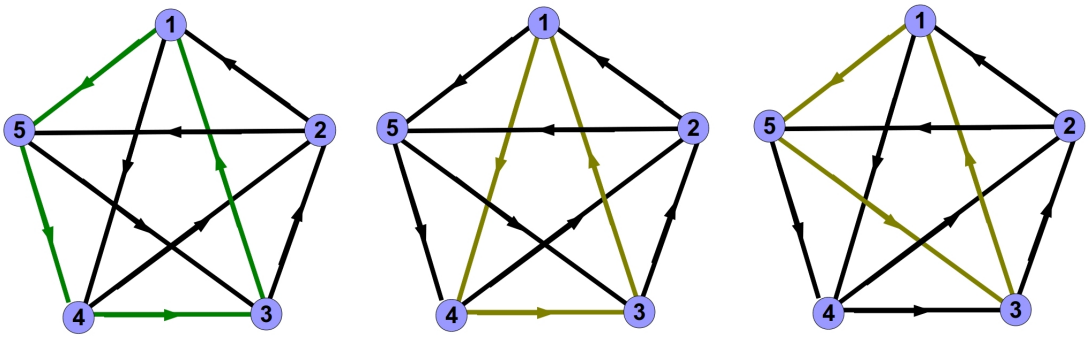

Figure D.3: A sketch of the operators whose couplings are set to zero. The configuration given by the superposition of the three images corresponds to the set 22 of class 1. Sets $25, 26, 27, 31$ can be found by four consecutive rotations.

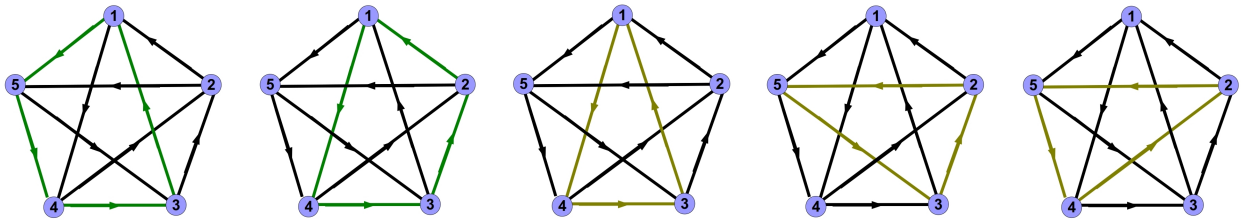

Figure D.4: Set 4 of class 1. Sets 10,12,13,14 can be found by rotations.

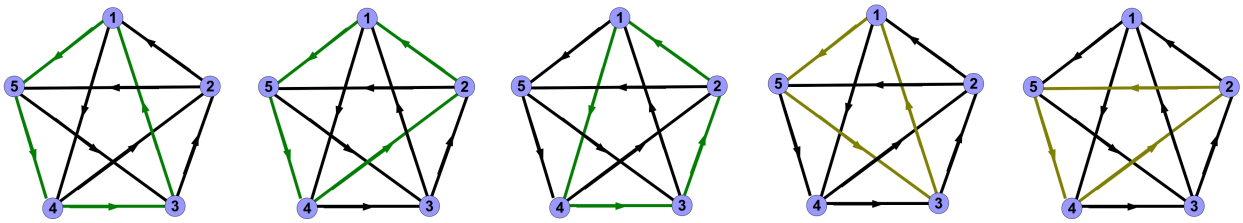

Figure D.5: Set 23 of class 3. Sets 24,29,30,32 can be found by rotating.

quintic operator formed by the internal lines of the quiver diagram. Note that this set is the unique one with maximal cardinality. For the rest five sets of class 4 we start by the configuration of Fig. D.6 corresponding to set 2 and rotate consecutively.

Class 5 For class 5 the initial configuration to be rotated is depicted in Fig. D.7 and corresponds to set 3.

Class 6 Finally, class 6 contains only one set of simultaneously marginal operators. It corresponds to setting the coupling of the "outer" quintic operator as well as all the cubic operators to zero.

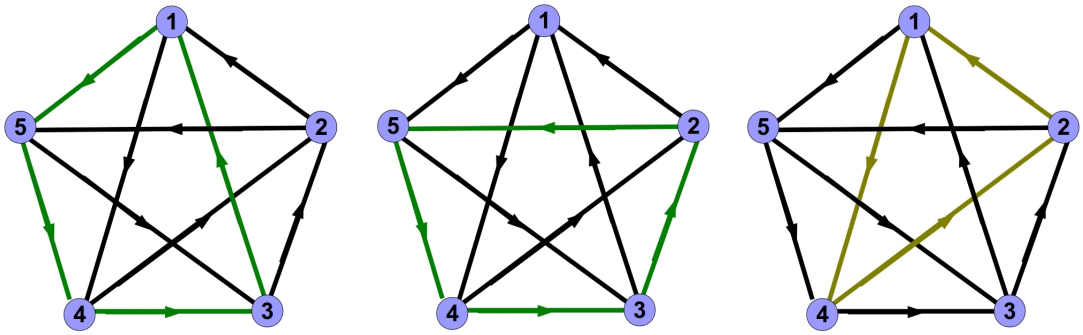

Figure D.6: Set 2 of class 4. Sets 5,6,16,17 can be found by rotating this configuration.

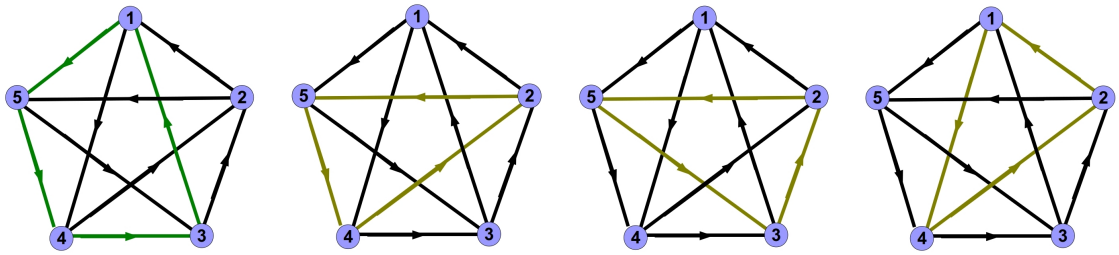

Figure D.7: Set 3 of class 5. Sets 7,9,11,15 can be found by rotating this configuration.

D.2.3 Properties of Other Types

Here we present the structure of the superpotential through the R-charge relations for rest of the five-block quivers.

Type II, III and V The R-charge relations for Type II are:

$$\begin{aligned} r_{43}+r_{54}+r_{15}+r_{21}+r_{32} &= 2 \\ r_{15}+r_{53}+r_{32}+r_{21} &= 2 \\ r_{43}+r_{54}+r_{15}+r_{31} &= 2 \\ r_{43}+r_{21}+r_{32}+r_{14} &= 2 \\ r_{43}+r_{54}+r_{32}+r_{25} &= 2 \\ r_{43}+r_{32}+r_{24} &= 2 \\ r_{15}+r_{53}+r_{31} &= 2 \\ r_{25}+r_{32}+r_{53} &= 2 \\ r_{43}+r_{31}+r_{14} &= 2 \end{aligned} \tag{D.14}$$

For Type III we have:

$$
\begin{aligned}
r_{43}+r_{54}+r_{15}+r_{12}+r_{23} &= 2\\
r_{15}+r_{45}+r_{43}+r_{13} &= 2\\
r_{34}+r_{23}+r_{12}+r_{14} &= 2\\
r_{34}+r_{45}+r_{23}+r_{25} &= 2\\
r_{45}+r_{43}+r_{35} &= 2\\
r_{43}+r_{23}+r_{24} &= 2\\
r_{43}+r_{14}+r_{13} &= 2
\end{aligned}
\tag{D.15}
$$

and for Type V:

$$
\begin{aligned}
r_{34}+r_{45}+r_{15}+r_{12}+r_{23} &= 2\\
r_{15}+r_{45}+r_{34}+r_{13} &= 2\\
r_{34}+r_{45}+r_{23}+r_{25} &= 2\\
r_{45}+r_{34}+r_{35} &= 2\\
r_{34}+r_{23}+r_{24} &= 2\\
r_{15}+r_{14}+r_{45} &= 2
\end{aligned}
\tag{D.16}
$$

These relations when more than 6 they are linearly dependent, leading to unique Diophantine equations related to the Type I special subset (33) discussed in detail in the main part of the paper.

Type IV The R-charge relations for this type are:

$$r_{34}+r_{45}+r_{15}+r_{12}+r_{23} = 2 \tag{D.17}$$
$$r_{34}+r_{15}+r_{13}+r_{24}+r_{25} = 2 \tag{D.18}$$
$$r_{34}+r_{12}+r_{14}+r_{35}+r_{25} = 2 \tag{D.19}$$
$$r_{34}+r_{35}+r_{24}+r_{25} = 2 \tag{D.20}$$
$$r_{34}+r_{45}+r_{15}+r_{13} = 2 \tag{D.21}$$
$$r_{34}+r_{12}+r_{23}+r_{14} = 2 \tag{D.22}$$
$$r_{15}+r_{25}+r_{12} = 2 \tag{D.23}$$
$$r_{34}+r_{45}+r_{35} = 2 \tag{D.24}$$
$$r_{34}+r_{23}+r_{24} = 2 \tag{D.25}$$
$$r_{34}+r_{13}+r_{14} = 2 \tag{D.26}$$

Out of these 10 R-charge equations one can choose 22 sets of six linearly independent which lead to 22 Diophantine equations.
These are:

$_1\{(D.19),(D.20),(D.22),(D.23),(D.24),(D.26)\}$, $_2\{(D.18),(D.20),(D.21),(D.23),(D.26),(D.25)\}$
$_3\{(D.18),(D.19),(D.23),(D.24),(D.26),(D.25)\}$, $_4\{(D.18),(D.19),(D.20),(D.21),(D.22),(D.23)\}$
$_5\{(D.18),(D.19),(D.22),(D.23),(D.24),(D.26)\}$, $_6\{(D.18),(D.19),(D.21),(D.23),(D.26),(D.25)\}$
$_7\{(D.17),(D.19),(D.23),(D.24),(D.26),(D.25)\}$, $_8\{(D.17),(D.19),(D.20),(D.23),(D.24),(D.26)\}$
$_9\{(D.17),(D.19),(D.20),(D.21),(D.22),(D.23)\}$, $_{10}\{(D.17),(D.19),(D.21),(D.23),(D.24),(D.25)\}$
$_{11}\{(D.17),(D.18),(D.23),(D.24),(D.26),(D.25)\}$, $_{12}\{(D.17),(D.18),(D.20),(D.23),(D.26),(D.25)\}$
$_{13}\{(D.17),(D.18),(D.20),(D.21),(D.22),(D.23)\}$, $_{14}\{(D.17),(D.18),(D.19),(D.23),(D.26),(D.25)\}$
$_{15}\{(D.17),(D.18),(D.19),(D.23),(D.24),(D.26)\}$, $_{16}\{(D.17),(D.18),(D.19),(D.23),(D.24),(D.25)\}$
$_{17}\{(D.17),(D.18),(D.19),(D.20),(D.22),(D.23)\}$, $_{18}\{(D.17),(D.18),(D.19),(D.20),(D.21),(D.23)\}$
$_{19}\{(D.17),(D.18),(D.19),(D.20),(D.21),(D.22)\}$, $_{20}\{(D.17),(D.18),(D.19),(D.21),(D.22),(D.23)\}$
$_{21}\{(D.17),(D.18),(D.22),(D.23),(D.24),(D.25)\}$, $_{22}\{(D.17),(D.21),(D.22),(D.23),(D.24),(D.25)\}$

All subsets are related to the Type I equivalence classes.

Type VI The R-charge relations for the last type are

$$r_{34}+r_{45}+r_{15}+r_{12}+r_{23} = 2 \quad (D.27)$$
$$r_{12}+r_{13}+r_{35}+r_{45}+r_{24} = 2 \quad (D.28)$$
$$r_{15}+r_{45}+r_{24}+r_{12} = 2 \quad (D.29)$$
$$r_{25}+r_{35}+r_{12}+r_{13} = 2 \quad (D.30)$$
$$r_{13}+r_{35}+r_{45}+r_{14} = 2 \quad (D.31)$$
$$r_{34}+r_{45}+r_{35} = 2 \quad (D.32)$$
$$r_{12}+r_{23}+r_{13} = 2 \quad (D.33)$$
$$r_{15}+r_{45}+r_{14} = 2 \quad (D.34)$$
$$r_{15}+r_{25}+r_{12} = 2 \quad (D.35)$$

Out of these equations one can pick 11 sets of 6 linearly independent, which lead to 11 Diophantine equations. All subsets are again related to the Type I equivalence classes. These are:

$_1\{(D.28),(D.29),(D.30),(D.31),(D.32),(D.33)\}$, $_2\{(D.27),(D.28),(D.30),(D.31),(D.32),(D.33)\}$
$_3\{(D.27),(D.28),(D.30),(D.32),(D.33),(D.34)\}$, $_4\{(D.27),(D.28),(D.31),(D.32),(D.33),(D.35)\}$
$_5\{(D.27),(D.28),(D.29),(D.30),(D.31),(D.33)\}$, $_6\{(D.27),(D.28),(D.29),(D.30),(D.31),(D.32)\}$
$_7\{(D.27),(D.28),(D.32),(D.33),(D.34),(D.35)\}$, $_8\{(D.27),(D.29),(D.30),(D.31),(D.32),(D.33)\}$
$_9\{(D.27),(D.29),(D.30),(D.32),(D.33),(D.34)\}$, $_{10}\{(D.27),(D.29),(D.31),(D.32),(D.33),(D.35)\}$
$_{11}\{(D.27),(D.29),(D.32),(D.33),(D.34),(D.35)\}$

Appendix E

Appendices to Chapter 5

E.1 Area 6 Dimer Models

i	Quiver	Toric Diagram	Toric Points
3	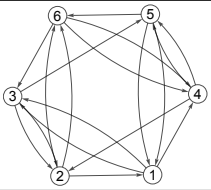	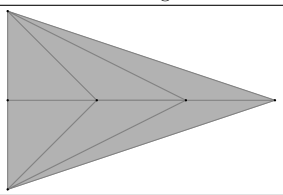	$\begin{pmatrix} 3 & 1 \\ 2 & 1 \\ 1 & 1 \\ 0 & 2 \\ 0 & 1 \\ 0 & 0 \end{pmatrix}$
type	W terms	Dimer Model	
	$-X_{13}X_{21}X_{32}$ $-X_{26}X_{32}X_{63}$ $X_{13}X_{35}X_{51}$ $X_{13}X_{21}X_{32}$ $-X_{14}X_{45}X_{51}$ $-X_{13}X_{35}X_{51}$ $X_{45}X_{56}X_{64}$ $X_{14}X_{45}X_{51}$ $-X_{26}X_{42}X_{64}$ $-X_{45}X_{56}X_{64}$ $X_{26}X_{32}X_{63}$ $X_{26}X_{42}X_{64}$	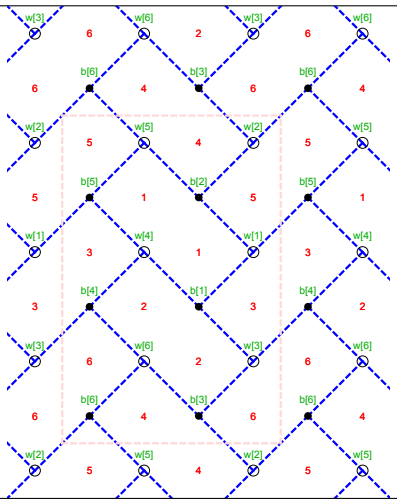	

i	Quiver	Toric Diagram	Toric Points
3	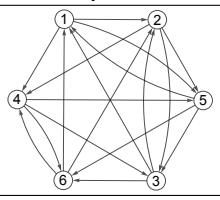	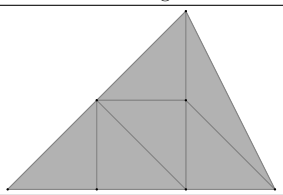	$\begin{pmatrix} 3 & 0 \\ 2 & 2 \\ 2 & 1 \\ 2 & 0 \\ 1 & 1 \\ 1 & 0 \\ 0 & 0 \end{pmatrix}$
type	W terms	Dimer Model	
	$-X_{12}X_{23}X_{31}$ $-X_{14}X_{45}X_{51}$ $-X_{24}X_{46}X_{62}$ $-X_{25}X_{32}X_{53}$ $-X_{15}X_{56}X_{61}$ $-X_{36}X_{43}X_{64}$ $X_{12}X_{25}X_{51}$ $X_{45}X_{56}X_{64}$ $X_{24}X_{32}X_{43}$ $X_{15}X_{31}X_{53}$ $X_{14}X_{46}X_{61}$ $X_{23}X_{36}X_{62}$	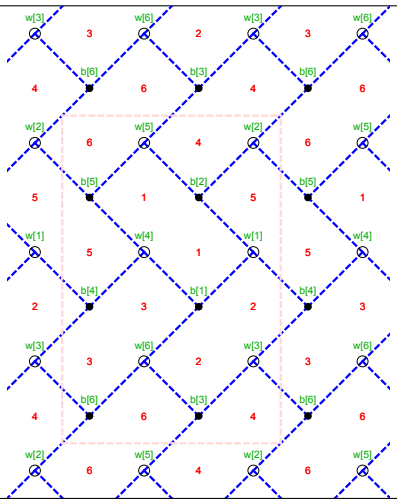	

E.2 Area 7 Dimer Models

i	Quiver	Toric Diagram	Toric Points
7	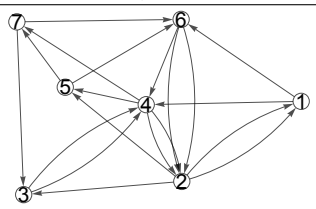	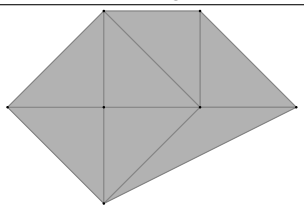	$\begin{pmatrix} 3 & 1 \\ 2 & 2 \\ 2 & 1 \\ 1 & 2 \\ 1 & 1 \\ 1 & 0 \\ 0 & 1 \end{pmatrix}$
type	W terms	Dimer Model	
	$-X_{23}X_{34}X_{42}$ $-X_{25}X_{56}X_{62}$ $-X_{34}X_{45}X_{57}X_{73}$ $-X_{14}X_{21}X_{42}$ $-X_{16}X_{21}X_{62}$ $-X_{47}X_{64}X_{76}$ $X_{16}X_{21}X_{62}$ $X_{45}X_{56}X_{64}$ $X_{23}X_{34}X_{42}$ $X_{14}X_{21}X_{42}$ $X_{25}X_{57}X_{62}X_{76}$ $X_{34}X_{47}X_{73}$	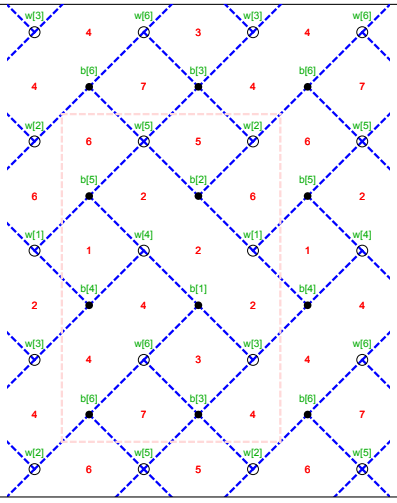	

i	Quiver	Toric Diagram	Toric Points
8	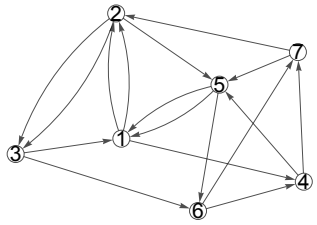	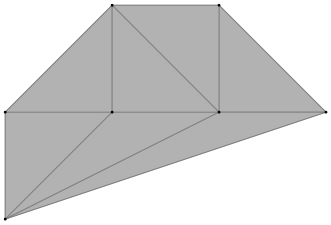	$\begin{pmatrix} 3 & 1 \\ 2 & 2 \\ 2 & 1 \\ 1 & 2 \\ 1 & 1 \\ 0 & 1 \\ 0 & 0 \end{pmatrix}$
type	W terms	Dimer Model	
	$-X_{12}X_{23}X_{31}$ $-X_{14}X_{45}X_{51}$ $-X_{23}X_{36}X_{47}X_{64}X_{72}$ $-X_{12}X_{25}X_{51}$ $-X_{56}X_{67}X_{75}$ $X_{12}X_{25}X_{51}$ $X_{45}X_{56}X_{64}$ $X_{12}X_{23}X_{31}$ $X_{14}X_{47}X_{51}X_{75}$ $X_{23}X_{36}X_{67}X_{72}$	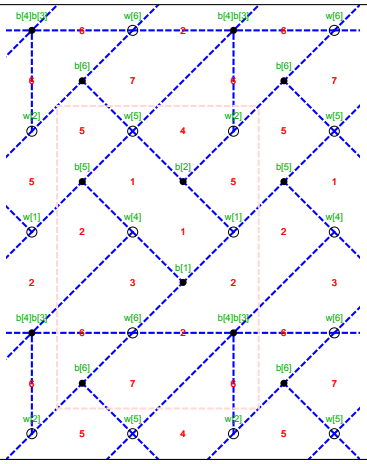	

i	Quiver	Toric Diagram	Toric Points
9	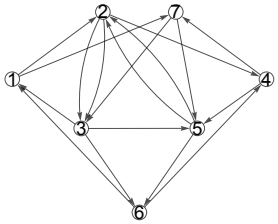	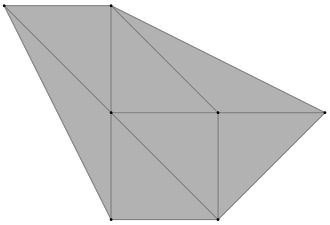	$\begin{pmatrix} 3 & 1 \\ 2 & 1 \\ 2 & 0 \\ 1 & 2 \\ 1 & 1 \\ 1 & 0 \\ 0 & 2 \end{pmatrix}$
type	W terms	Dimer Model	
	$-X_{24}X_{45}X_{52}$ $-X_{36}X_{47}X_{64}X_{73}$ $-X_{12}X_{23}X_{31}$ $-X_{23}X_{35}X_{52}$ $-X_{17}X_{56}X_{61}X_{75}$ $X_{23}X_{35}X_{52}$ $X_{45}X_{56}X_{64}$ $X_{12}X_{23}X_{36}X_{61}$ $X_{24}X_{47}X_{52}X_{75}$ $X_{17}X_{31}X_{73}$	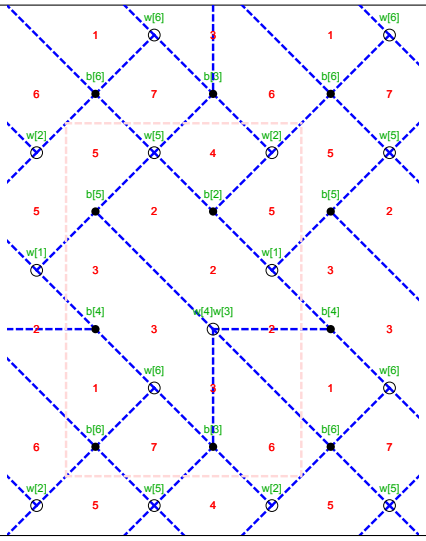	

E.3 Area 8 Dimer Models

i	Quiver	Toric Diagram	Toric Points
10	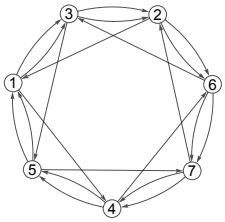	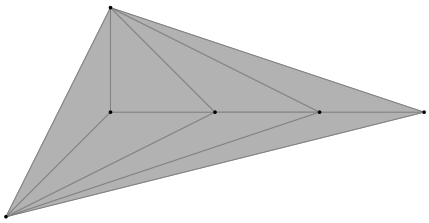	$\begin{pmatrix} 4 & 1 \\ 3 & 1 \\ 2 & 1 \\ 1 & 2 \\ 1 & 1 \\ 0 & 0 \end{pmatrix}$
type	W terms	Dimer Model	
	$-X_{13}X_{21}X_{32}$ $-X_{14}X_{45}X_{51}$ $-X_{46}X_{67}X_{74}$ $-X_{26}X_{67}X_{72}$ $-X_{26}X_{32}X_{63}$ $-X_{13}X_{35}X_{51}$ $-X_{45}X_{57}X_{74}$ $X_{13}X_{35}X_{51}$ $X_{45}X_{57}X_{74}$ $X_{26}X_{67}X_{72}$ $X_{26}X_{32}X_{63}$ $X_{13}X_{21}X_{32}$ $X_{14}X_{45}X_{51}$ $X_{46}X_{67}X_{74}$	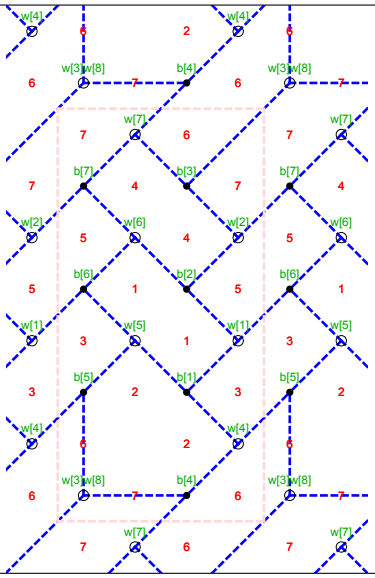	

i	Quiver	Toric Diagram	Toric Points
11	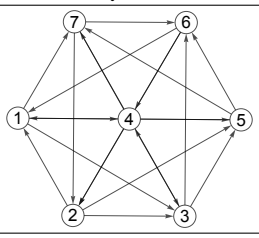	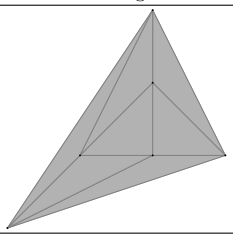	$\begin{pmatrix} 3 & 1 \\ 2 & 3 \\ 2 & 2 \\ 2 & 1 \\ 1 & 1 \\ 0 & 0 \end{pmatrix}$
type	W terms	Dimer Model	
	$-X_{23}X_{34}X_{42}$ $-X_{25}X_{56}X_{62}$ $-X_{35}X_{57}X_{73}$ $-X_{13}X_{36}X_{61}$ $-X_{14}X_{45}X_{51}$ $-X_{17}X_{21}X_{72}$ $-X_{47}X_{64}X_{76}$ $X_{23}X_{36}X_{62}$ $X_{45}X_{56}X_{64}$ $X_{13}X_{35}X_{51}$ $X_{17}X_{61}X_{76}$ $X_{14}X_{21}X_{42}$ $X_{25}X_{57}X_{72}$ $X_{34}X_{47}X_{73}$	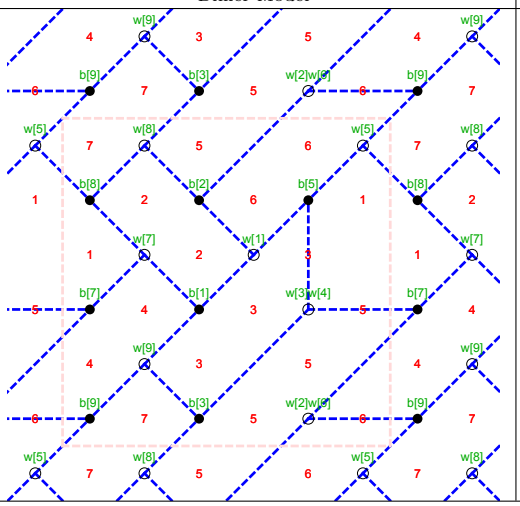	

i	Quiver	Toric Diagram	Toric Points
1	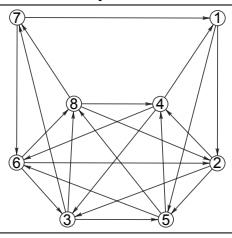	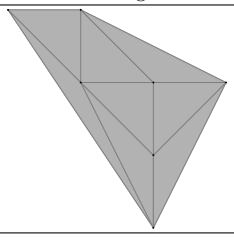	$\begin{pmatrix} 3 & 2 \\ 2 & 2 \\ 2 & 1 \\ 2 & 0 \\ 1 & 3 \\ 1 & 2 \\ 0 & 3 \end{pmatrix}$
type	W terms	Dimer Model	
	$-X_{35}X_{43}X_{54}$ $-X_{37}X_{63}X_{76}$ $-X_{46}X_{68}X_{84}$ $-X_{15}X_{58}X_{71}X_{87}$ $-X_{25}X_{56}X_{62}$ $-X_{12}X_{24}X_{41}$ $-X_{23}X_{38}X_{82}$ $X_{35}X_{56}X_{63}$ $X_{24}X_{46}X_{62}$ $X_{15}X_{41}X_{54}$ $X_{25}X_{58}X_{82}$ $X_{12}X_{23}X_{37}X_{71}$ $X_{68}X_{76}X_{87}$ $X_{38}X_{43}X_{84}$	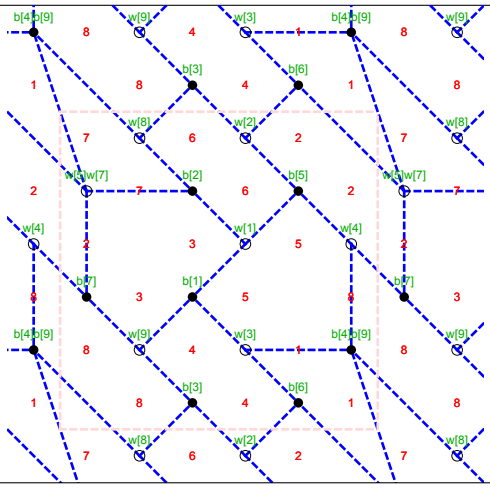	

i	Quiver	Toric Diagram	Toric Points
3	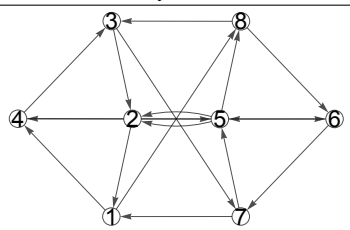	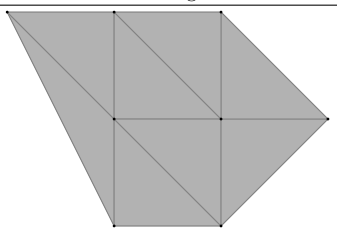	$\begin{pmatrix} 3 & 1 \\ 2 & 2 \\ 2 & 1 \\ 2 & 0 \\ 1 & 2 \\ 1 & 1 \\ 1 & 0 \\ 0 & 2 \end{pmatrix}$
type	W terms	Dimer Model	
	$-X_{24}X_{32}X_{43}$ $-X_{26}X_{52}X_{65}$ $-X_{37}X_{58}X_{75}X_{83}$ $-X_{14}X_{21}X_{45}X_{52}$ $-X_{18}X_{67}X_{71}X_{86}$ $X_{24}X_{45}X_{52}$ $X_{26}X_{52}X_{67}X_{75}$ $X_{14}X_{37}X_{43}X_{71}$ $X_{58}X_{65}X_{86}$ $X_{18}X_{21}X_{32}X_{83}$	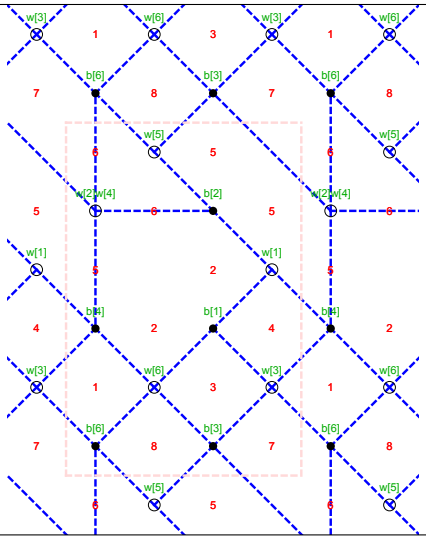	

i	Quiver	Toric Diagram	Toric Points
4	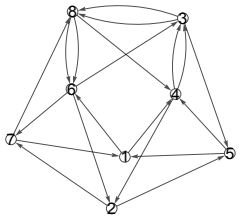	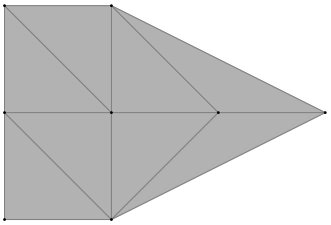	$\begin{pmatrix} 3 & 1 \\ 2 & 1 \\ 1 & 2 \\ 1 & 1 \\ 1 & 0 \\ 0 & 2 \\ 0 & 1 \\ 0 & 0 \end{pmatrix}$
type	W terms	Dimer Model	
	$-X_{14}X_{35}X_{43}X_{51}$ $-X_{16}X_{67}X_{71}$ $-X_{38}X_{63}X_{86}$ $-X_{25}X_{42}X_{54}$ $-X_{27}X_{62}X_{78}X_{86}$ $-X_{38}X_{43}X_{84}$ $X_{14}X_{27}X_{42}X_{71}$ $X_{67}X_{78}X_{86}$ $X_{38}X_{43}X_{84}$ $X_{16}X_{25}X_{51}X_{62}$ $X_{38}X_{63}X_{86}$ $X_{35}X_{43}X_{54}$	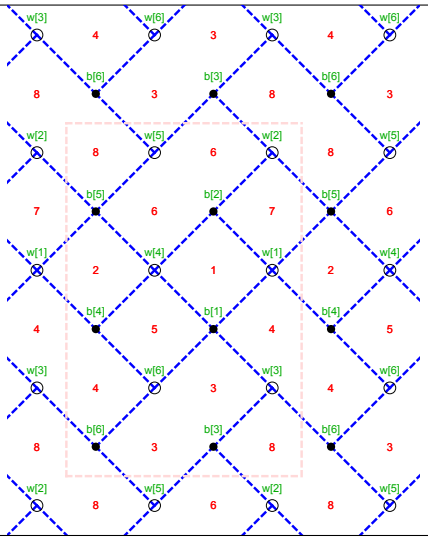	

i	Quiver	Toric Diagram	Toric Points
5	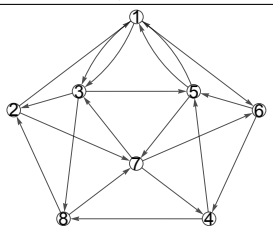	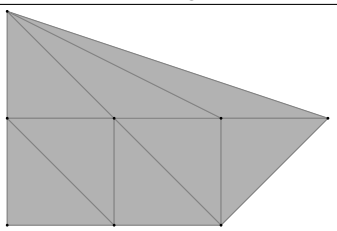	$\begin{pmatrix} 3 & 1 \\ 2 & 1 \\ 2 & 0 \\ 1 & 1 \\ 1 & 0 \\ 0 & 2 \\ 0 & 1 \\ 0 & 0 \end{pmatrix}$
type	W terms	Dimer Model	
	$-X_{13}X_{21}X_{32}$ $-X_{16}X_{45}X_{51}X_{64}$ $-X_{27}X_{48}X_{74}X_{82}$ $-X_{13}X_{35}X_{51}$ $-X_{57}X_{65}X_{76}$ $-X_{38}X_{73}X_{87}$ $X_{13}X_{35}X_{51}$ $X_{45}X_{57}X_{74}$ $X_{27}X_{32}X_{73}$ $X_{16}X_{51}X_{65}$ $X_{48}X_{64}X_{76}X_{87}$ $X_{13}X_{21}X_{38}X_{82}$	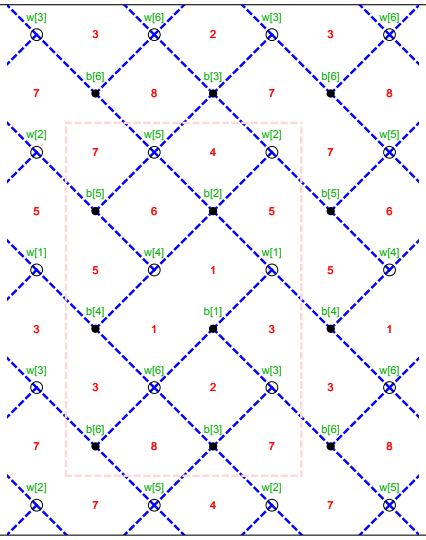	

i	Quiver	Toric Diagram	Toric Points
6	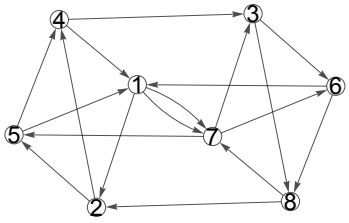	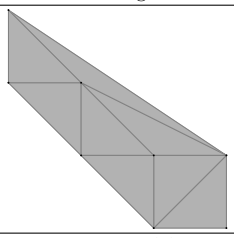	$\begin{pmatrix} 3 & 1 \\ 3 & 0 \\ 2 & 1 \\ 2 & 0 \\ 1 & 2 \\ 1 & 1 \\ 0 & 3 \\ 0 & 2 \end{pmatrix}$
type	W terms	Dimer Model	
	$-X_{68}X_{76}X_{87}$ $-X_{17}X_{36}X_{61}X_{73}$ $-X_{17}X_{51}X_{75}$ $X_{38}X_{73}X_{87}$ $X_{12}X_{25}X_{51}$ $-X_{12}X_{24}X_{41}$ $-X_{25}X_{38}X_{43}X_{54}X_{82}$ $X_{17}X_{41}X_{54}X_{75}$ $X_{24}X_{36}X_{43}X_{68}X_{82}$ $X_{17}X_{61}X_{76}$	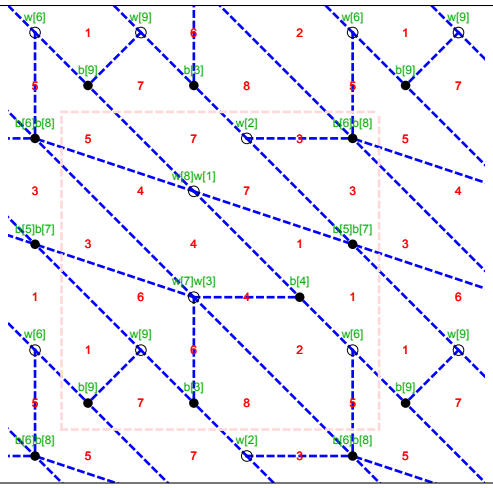	

i	Quiver	Toric Diagram	Toric Points
7	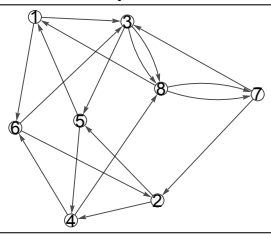	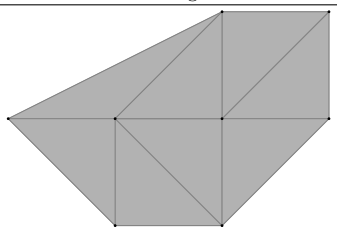	$\begin{pmatrix} 3 & 2 \\ 3 & 1 \\ 2 & 2 \\ 2 & 1 \\ 2 & 0 \\ 1 & 1 \\ 1 & 0 \\ 0 & 1 \end{pmatrix}$
type	W terms	Dimer Model	
	$-X_{35}X_{46}X_{54}X_{63}$ $-X_{16}X_{25}X_{51}X_{62}$ $-X_{24}X_{48}X_{72}X_{87}$ $X_{38}X_{73}X_{87}$ $X_{16}X_{38}X_{63}X_{81}$ $-X_{38}X_{73}X_{87}$ $-X_{13}X_{38}X_{81}$ $X_{13}X_{35}X_{51}$ $X_{25}X_{48}X_{54}X_{72}X_{87}$ $X_{24}X_{46}X_{62}$	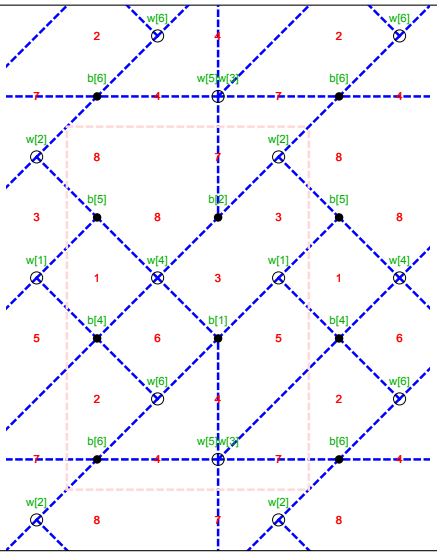	

i	Quiver	Toric Diagram	Toric Points
8	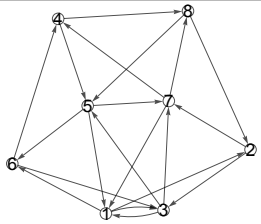	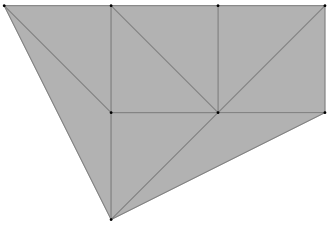	$\begin{pmatrix} 3 & 2 \\ 3 & 1 \\ 2 & 2 \\ 2 & 1 \\ 1 & 2 \\ 1 & 1 \\ 1 & 0 \\ 0 & 2 \end{pmatrix}$
type	W terms	Dimer Model	
	$-X_{12}X_{23}X_{31}$ $-X_{16}X_{45}X_{51}X_{64}$ $-X_{27}X_{48}X_{74}X_{82}$ $-X_{13}X_{37}X_{71}$ $-X_{35}X_{56}X_{63}$ $-X_{57}X_{78}X_{85}$ $X_{13}X_{35}X_{51}$ $X_{45}X_{57}X_{74}$ $X_{12}X_{27}X_{71}$ $X_{16}X_{31}X_{63}$ $X_{48}X_{56}X_{64}X_{85}$ $X_{23}X_{37}X_{78}X_{82}$	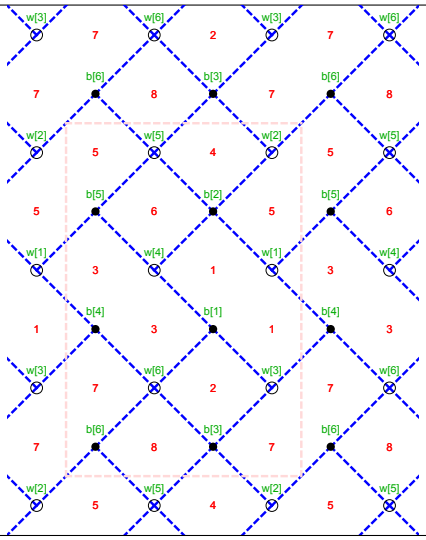	

i	Quiver	Toric Diagram	Toric Points
9	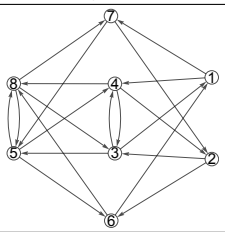	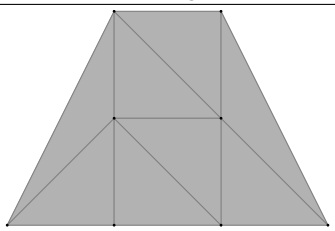	$\begin{pmatrix} 3 & 0 \\ 2 & 2 \\ 2 & 1 \\ 2 & 0 \\ 1 & 2 \\ 1 & 1 \\ 1 & 0 \\ 0 & 0 \end{pmatrix}$
type	W terms	Dimer Model	
	$-X_{14}X_{31}X_{43}$ $-X_{17}X_{56}X_{61}X_{75}$ $-X_{35}X_{58}X_{83}$ $-X_{23}X_{34}X_{42}$ $-X_{26}X_{68}X_{72}X_{87}$ $-X_{48}X_{54}X_{85}$ $X_{14}X_{26}X_{42}X_{61}$ $X_{56}X_{68}X_{85}$ $X_{35}X_{43}X_{54}$ $X_{17}X_{23}X_{31}X_{72}$ $X_{58}X_{75}X_{87}$ $X_{34}X_{48}X_{83}$	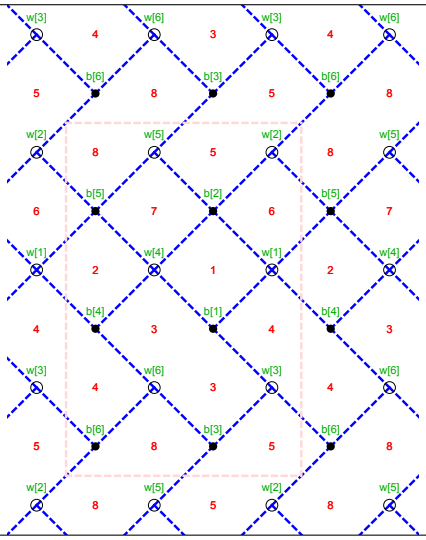	

i	Quiver	Toric Diagram	Toric Points
10	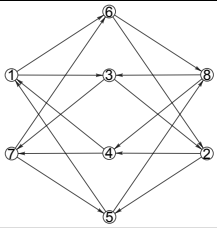	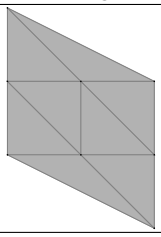	$\begin{pmatrix} 2 & 2 \\ 2 & 1 \\ 2 & 0 \\ 1 & 2 \\ 1 & 1 \\ 0 & 3 \\ 0 & 2 \\ 0 & 1 \end{pmatrix}$
type	W terms	Dimer Model	
	$-X_{13}X_{24}X_{32}X_{41}$ $-X_{16}X_{25}X_{51}X_{62}$ $-X_{37}X_{68}X_{76}X_{83}$ $-X_{47}X_{58}X_{75}X_{84}$ $X_{13}X_{37}X_{51}X_{75}$ $X_{25}X_{32}X_{58}X_{83}$ $X_{24}X_{47}X_{62}X_{76}$ $X_{16}X_{41}X_{68}X_{84}$	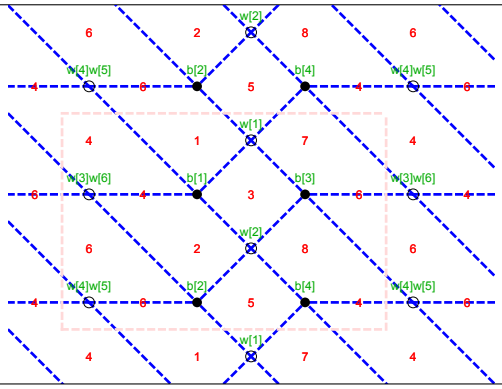	

i	Quiver	Toric Diagram	Toric Points
11	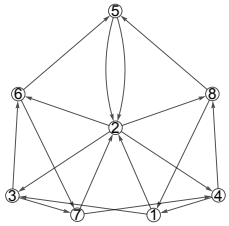	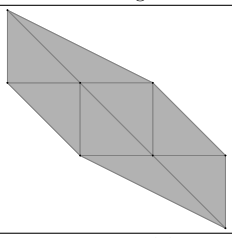	$\begin{pmatrix} 3 & 1 \\ 3 & 0 \\ 2 & 2 \\ 2 & 1 \\ 1 & 2 \\ 1 & 1 \\ 0 & 3 \\ 0 & 2 \end{pmatrix}$
type	W terms	Dimer Model	
	$-X_{26}X_{67}X_{72}$ $-X_{12}X_{28}X_{81}$ $-X_{13}X_{37}X_{41}X_{74}$ $-X_{23}X_{36}X_{52}X_{65}$ $-X_{24}X_{48}X_{52}X_{85}$ $X_{28}X_{52}X_{85}$ $X_{13}X_{36}X_{48}X_{67}X_{74}X_{81}$ $X_{26}X_{52}X_{65}$ $X_{12}X_{24}X_{41}$ $X_{23}X_{37}X_{72}$	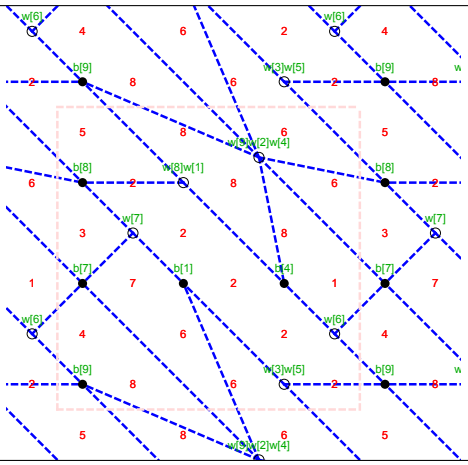	

i	Quiver	Toric Diagram	Toric Points
12	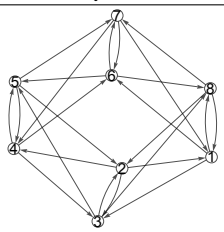	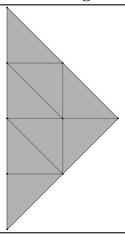	$\begin{pmatrix} 2 & 2 \\ 1 & 3 \\ 1 & 2 \\ 1 & 1 \\ 0 & 4 \\ 0 & 3 \\ 0 & 2 \\ 0 & 1 \\ 0 & 0 \end{pmatrix}$
type	W terms	Dimer Model	
	$-X_{46}X_{54}X_{65}$ $-X_{45}X_{57}X_{74}$ $-X_{68}X_{76}X_{87}$ $-X_{16}X_{67}X_{71}$ $-X_{18}X_{21}X_{82}$ $-X_{13}X_{38}X_{81}$ $-X_{23}X_{35}X_{52}$ $-X_{24}X_{32}X_{43}$ $X_{46}X_{67}X_{74}$ $X_{57}X_{65}X_{76}$ $X_{16}X_{68}X_{81}$ $X_{18}X_{71}X_{87}$ $X_{23}X_{38}X_{82}$ $X_{13}X_{21}X_{32}$ $X_{35}X_{43}X_{54}$ $X_{24}X_{45}X_{52}$	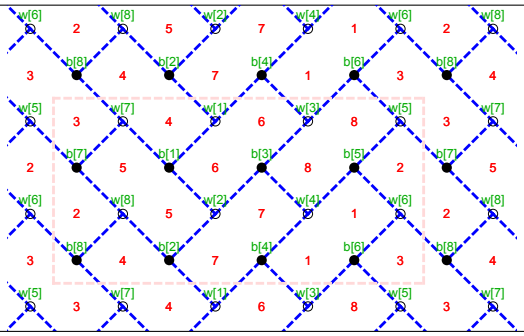	

i	Quiver	Toric Diagram	Toric Points
13	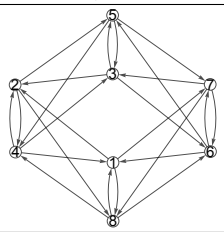	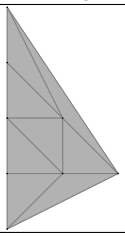	$\begin{pmatrix} 2 & 1 \\ 1 & 2 \\ 1 & 1 \\ 0 & 4 \\ 0 & 3 \\ 0 & 2 \\ 0 & 1 \\ 0 & 0 \end{pmatrix}$
type	W terms	Dimer Model	
	$-X_{36}X_{53}X_{65}$ $-X_{35}X_{57}X_{73}$ $-X_{67}X_{78}X_{86}$ $-X_{17}X_{61}X_{76}$ $-X_{12}X_{28}X_{81}$ $-X_{18}X_{41}X_{84}$ $-X_{24}X_{32}X_{43}$ $-X_{25}X_{42}X_{54}$ $X_{36}X_{67}X_{73}$ $X_{57}X_{65}X_{76}$ $X_{17}X_{78}X_{81}$ $X_{18}X_{61}X_{86}$ $X_{12}X_{24}X_{41}$ $X_{28}X_{42}X_{84}$ $X_{35}X_{43}X_{54}$ $X_{25}X_{32}X_{53}$	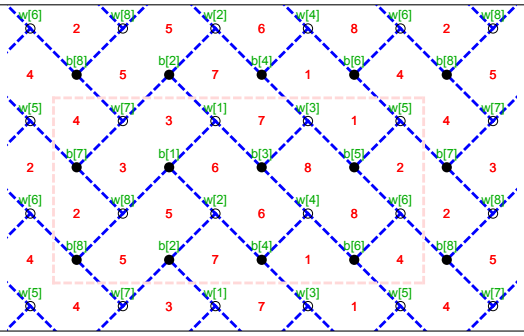	

E.4 Inequivalent Convex Polytopes of area 8

i	Shape	Toric Points	i	Shape	Toric Points
1	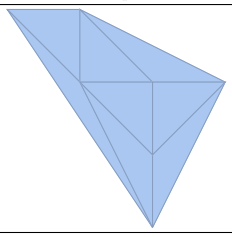	$\begin{pmatrix} 0 & 3 \\ 1 & 3 \\ 2 & 1 \\ 2 & 0 \\ 1 & 2 \\ 2 & 2 \\ 3 & 2 \end{pmatrix}$	2	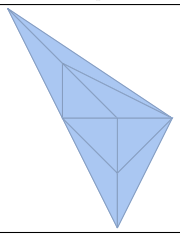	$\begin{pmatrix} -1 & 1 \\ -2 & 2 \\ 0 & -1 \\ 0 & -2 \\ -1 & 0 \\ 0 & 0 \\ 1 & 0 \end{pmatrix}$
3	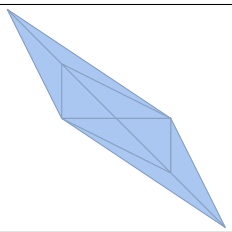	$\begin{pmatrix} -1 & 1 \\ -2 & 2 \\ 1 & -1 \\ 2 & -2 \\ -1 & 0 \\ 0 & 0 \\ 1 & 0 \end{pmatrix}$	4	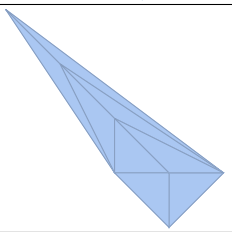	$\begin{pmatrix} -1 & 1 \\ -2 & 2 \\ -3 & 3 \\ 0 & -1 \\ -1 & 0 \\ 0 & 0 \\ 1 & 0 \end{pmatrix}$
5	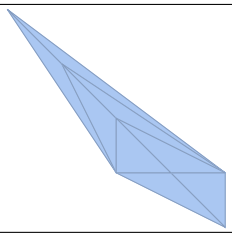	$\begin{pmatrix} -1 & 1 \\ -2 & 2 \\ -3 & 3 \\ 1 & -1 \\ -1 & 0 \\ 0 & 0 \\ 1 & 0 \end{pmatrix}$	6	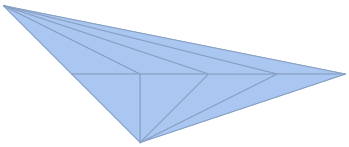	$\begin{pmatrix} -3 & 1 \\ -1 & -1 \\ -2 & 0 \\ -1 & 0 \\ 0 & 0 \\ 1 & 0 \\ 2 & 0 \end{pmatrix}$
7	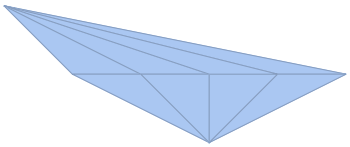	$\begin{pmatrix} -3 & 1 \\ 0 & -1 \\ -2 & 0 \\ -1 & 0 \\ 0 & 0 \\ 1 & 0 \\ 2 & 0 \end{pmatrix}$	8	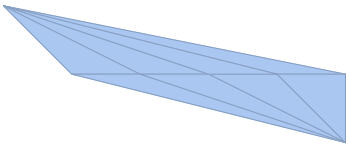	$\begin{pmatrix} -3 & 1 \\ 2 & -1 \\ -2 & 0 \\ -1 & 0 \\ 0 & 0 \\ 1 & 0 \\ 2 & 0 \end{pmatrix}$
9	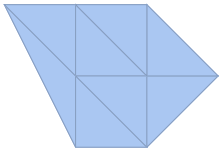	$\begin{pmatrix} -2 & 1 \\ -1 & 1 \\ 0 & 1 \\ -1 & -1 \\ 0 & -1 \\ -1 & 0 \\ 0 & 0 \\ 1 & 0 \end{pmatrix}$	10	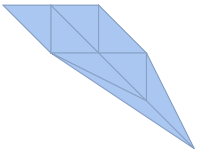	$\begin{pmatrix} -2 & 1 \\ -1 & 1 \\ 0 & 1 \\ 1 & -1 \\ 2 & -2 \\ -1 & 0 \\ 0 & 0 \\ 1 & 0 \end{pmatrix}$
11	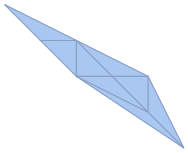	$\begin{pmatrix} -2 & 1 \\ -1 & 1 \\ -3 & 2 \\ 1 & -1 \\ 2 & -2 \\ -1 & 0 \\ 0 & 0 \\ 1 & 0 \end{pmatrix}$	12	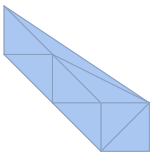	$\begin{pmatrix} -2 & 1 \\ -1 & 1 \\ -2 & 2 \\ 0 & -1 \\ 1 & -1 \\ -1 & 0 \\ 0 & 0 \\ 1 & 0 \end{pmatrix}$
13	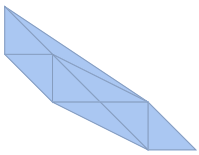	$\begin{pmatrix} -2 & 1 \\ -1 & 1 \\ -2 & 2 \\ 1 & -1 \\ 2 & -1 \\ -1 & 0 \\ 0 & 0 \\ 1 & 0 \end{pmatrix}$	14	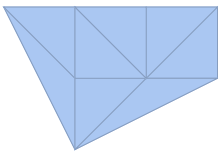	$\begin{pmatrix} -2 & 1 \\ -1 & 1 \\ 0 & 1 \\ 1 & 1 \\ -1 & -1 \\ -1 & 0 \\ 0 & 0 \\ 1 & 0 \end{pmatrix}$
15	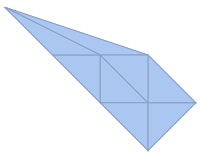	$\begin{pmatrix} -2 & 1 \\ -1 & 1 \\ 0 & 1 \\ -3 & 2 \\ 0 & -1 \\ -1 & 0 \\ 0 & 0 \\ 1 & 0 \end{pmatrix}$	16	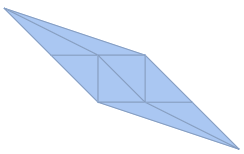	$\begin{pmatrix} -2 & 1 \\ -1 & 1 \\ 0 & 1 \\ -3 & 2 \\ 2 & -1 \\ -1 & 0 \\ 0 & 0 \\ 1 & 0 \end{pmatrix}$

i	Shape	Toric Points	i	Shape	Toric Points
17	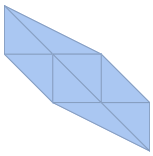	$\begin{pmatrix} -2 & 1 \\ -1 & 1 \\ 0 & 1 \\ -2 & 2 \\ 1 & -1 \\ -1 & 0 \\ 0 & 0 \\ 1 & 0 \end{pmatrix}$	18	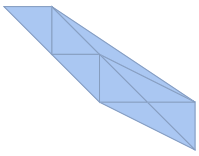	$\begin{pmatrix} -2 & 1 \\ -1 & 1 \\ -3 & 2 \\ -2 & 2 \\ 1 & -1 \\ -1 & 0 \\ 0 & 0 \\ 1 & 0 \end{pmatrix}$
19	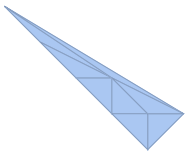	$\begin{pmatrix} -2 & 1 \\ -1 & 1 \\ -3 & 2 \\ -4 & 3 \\ 0 & -1 \\ -1 & 0 \\ 0 & 0 \\ 1 & 0 \end{pmatrix}$	20	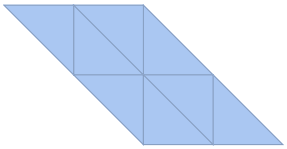	$\begin{pmatrix} -2 & 1 \\ -1 & 1 \\ 0 & 1 \\ 0 & -1 \\ 1 & -1 \\ 2 & -1 \\ -1 & 0 \\ 0 & 0 \\ 1 & 0 \end{pmatrix}$
21	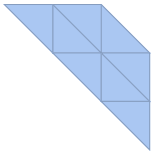	$\begin{pmatrix} -2 & 1 \\ -1 & 1 \\ 0 & 1 \\ 0 & -1 \\ 1 & -1 \\ 1 & -2 \\ -1 & 0 \\ 0 & 0 \\ 1 & 0 \end{pmatrix}$	22	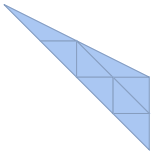	$\begin{pmatrix} -2 & 1 \\ -1 & 1 \\ -3 & 2 \\ 0 & -1 \\ 1 & -1 \\ 1 & -2 \\ -1 & 0 \\ 0 & 0 \\ 1 & 0 \end{pmatrix}$
23	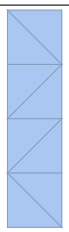	$\begin{pmatrix} -2 & 1 \\ -1 & 1 \\ 0 & 1 \\ 1 & 1 \\ 2 & 1 \\ -2 & 0 \\ -1 & 0 \\ 0 & 0 \\ 1 & 0 \\ 2 & 0 \end{pmatrix}$	24	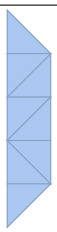	$\begin{pmatrix} -1 & 1 \\ 0 & 1 \\ 1 & 1 \\ 2 & 1 \\ -2 & 0 \\ -1 & 0 \\ 0 & 0 \\ 1 & 0 \\ 2 & 0 \\ 3 & 0 \end{pmatrix}$
25		$\begin{pmatrix} -1 & 1 \\ 0 & 1 \\ 1 & 1 \\ -3 & 0 \\ -2 & 0 \\ -1 & 0 \\ 0 & 0 \\ 1 & 0 \\ 2 & 0 \\ 3 & 0 \end{pmatrix}$	26		$\begin{pmatrix} 0 & 1 \\ 1 & 1 \\ -3 & 0 \\ -2 & 0 \\ -1 & 0 \\ 0 & 0 \\ 1 & 0 \\ 2 & 0 \\ 3 & 0 \\ 4 & 0 \end{pmatrix}$
			27	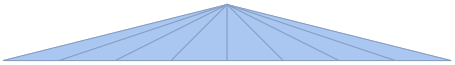	$\begin{pmatrix} 0 & 1 \\ -4 & 0 \\ -3 & 0 \\ -2 & 0 \\ -1 & 0 \\ 0 & 0 \\ 1 & 0 \\ 2 & 0 \\ 3 & 0 \\ 4 & 0 \end{pmatrix}$

Bibliography

[1] JE Paton and Chan Hong-Mo. Generalized veneziano model with isospin. *Nuclear Physics B*, 10(3):516–520, 1969.

[2] F Gliozzi, J Scherk, and D Olive. Supergravity and the spinor dual model. *Physics Letters B*, 65(3):282–286, 1976.

[3] Edward Witten. String theory dynamics in various dimensions. *Nuclear Physics B*, 443(1):85–126, 1995.

[4] Michael J Duff. *The world in eleven dimensions: supergravity, supermembranes and M-theory*. Taylor & Francis, 1999.

[5] Philip Candelas, Gary T Horowitz, Andrew Strominger, and Edward Witten. Vacuum configurations for superstrings. *Nuclear Physics B*, 258:46–74, 1985.

[6] Maximilian Kreuzer and Harald Skarke. Complete classification of reflexive polyhedra in four dimensions. *arXiv preprint hep-th/0002240*, 2000.

[7] Peter B Kronheimer. The construction of ale spaces as hyper-kähler quotients. *Journal of differential geometry*, 29(3):665–683, 1989.

[8] George Whitelaw Mackey. Graphs, singularities, and finite groups. *Uspekhi Matematicheskikh Nauk*, 38(3):159–162, 1983.

[9] Amihay Hanany and Edward Witten. Type iib superstrings, bps monopoles, and three-dimensional gauge dynamics. *Nuclear Physics B*, 492(1):152–190, 1997.

[10] Yukari Ito and Miles Reid. The mckay correspondence for finite subgroups of sl (3, c). In *Higher Dimensional Complex Varieties: Proceedings of the International Conference held in Trento, Italy, June 15-24, 1994*, page 221. Walter de Gruyter, 1996.

[11] Amihay Hanany and Yang-Hui He. Non-abelian finite gauge theories. *Journal of High Energy Physics*, 1999(02):013, 1999.

[12] Suresh Govindarajan and T Jayaraman. D-branes, exceptional sheaves and quivers on calabi–yau manifolds: from mukai to mckay. *Nuclear Physics B*, 600(3):457–486, 2001.

[13] Alessandro Tomasiello. D-branes on calabi-yau manifolds and helices. *Journal of High Energy Physics*, 2001(02):008, 2001.

[14] Theodor Kaluza. On the problem of unity in physics. In *Unified Field Theories of¿ 4 Dimensions*, volume 1, page 427, 1983.

[15] Oskar Klein. Quantum theory and five dimensional theory of relativity (1926). *Modern Kaluza-Klein Theories. Addison-Wesley Publishing Company*, 1987.

[16] Eugene Cremmer, Bernard Julia, and Joel Scherk. Supergravity in theory in 11 dimensions. *Physics Letters B*, 76(4):409–412, 1978.

[17] Michael B Green, John H Schwarz, and Edward Witten. *Superstring theory: volume 2, Loop amplitudes, anomalies and phenomenology*. Cambridge university press, 2012.

[18] Es Calabi. Algebraic geometry and topology: A symposium in honor of s lefschetz. *Princeton UP, Princeton, NJ*, 1957.

[19] Shing-Tung Yau. Calabi's conjecture and some new results in algebraic geometry. *Proceedings of the National Academy of Sciences*, 74(5):1798–1799, 1977.

[20] Lara Anderson, Yang-Hui He, and André Lukas. Monad bundles in heterotic string compactifications. *Journal of High Energy Physics*, 2008(07):104, 2008.

[21] Lara B Anderson, James Gray, Dan Grayson, Yang-Hui He, and André Lukas. Yukawa couplings in heterotic compactification. *Communications in Mathematical Physics*, 297(1):95–127, 2010.

[22] Lara B Anderson, James Gray, Andre Lukas, and Eran Palti. Two hundred heterotic standard models on smooth calabi-yau threefolds. *Physical Review D*, 84(10):106005, 2011.

[23] Lara B Anderson, James Gray, Andre Lukas, and Eran Palti. Heterotic line bundle standard models. *Journal of High Energy Physics*, 2012(6):1–57, 2012.

[24] Lara B Anderson, James Gray, Andre Lukas, and Eran Palti. Heterotic standard models from smooth calabi-yau three-folds. *PoS (CORFU2011)*, 96, 2011.

[25] Lara B Anderson, James Gray, Andre Lukas, and Burt Ovrut. Vacuum varieties, holomorphic bundles and complex structure stabilization in heterotic theories. *arXiv preprint arXiv:1304.2704*, 2013.

[26] Maxime Gabella, Yang-Hui He, and Andre Lukas. An abundance of heterotic vacua. *Journal of High Energy Physics*, 2008(12):027, 2008.

[27] Ron Donagi, Yang-Hui He, Burt A Ovrut, and René Reinbacher. The particle spectrum of heterotic compactifications. *Journal of High Energy Physics*, 2004(12):054, 2005.

[28] Yang-Hui He, Seung-Joo Lee, and André Lukas. Heterotic models from vector bundles on toric calabi-yau manifolds. *Journal of High Energy Physics*, 2010(5):1–38, 2010.

[29] Yang-Hui He, Maximilian Kreuzer, Seung-Joo Lee, and Andre Lukas. Heterotic bundles on calabi-yau manifolds with small picard number. *Journal of High Energy Physics*, 2011(12):1–24, 2011.

[30] Victor Batyrev and Maximilian Kreuzer. Integral cohomology and mirror symmetry for calabi-yau 3-folds. *arXiv preprint math/0505432*, 2005.

[31] David A Cox, John B Little, and Henry K Schenck. *Toric varieties*. American Mathematical Soc., 2011.

[32] Kentaro Hori and Cumrun Vafa. Mirror symmetry. *arXiv preprint hep-th/0002222*, 2000.

[33] William Fulton. *Introduction to toric varieties*. Number 131. Princeton University Press, 1993.

[34] Philip Candelas, Anders Martin Dale, CA Lütken, and Rolf Schimmrigk. Complete intersection calabi-yau manifolds. *Nuclear Physics B*, 298(3):493–525, 1988.

[35] Robert Friedman, John Morgan, and Edward Witten. Vector bundles and f theory. *Communications in Mathematical Physics*, 187(3):679–743, 1997.

[36] Victor V Batyrev and Lev A Borisov. On calabi-yau complete intersections in toric varieties. *Higher-dimensional complex varieties (Trento, 1994)*, pages 39–65, 1996.

[37] Victor V Batyrev and Lev A Borisov. Dual cones and mirror symmetry for generalized calabi-yau manifolds. *arXiv preprint alg-geom/9402002*, 1994.

[38] Juan Martin Maldacena. The large n limit of superconformal field theories and supergravity. *Adv.Theor.Math.Phys.*, 2:231–252, 1998.

[39] Sergey Fomin and Andrei Zelevinsky. Cluster algebras i: foundations. *Journal of the American Mathematical Society*, 15(2):497–529, 2002.

[40] Sergey Fomin and Andrei Zelevinsky. Cluster algebras ii: Finite type classification. *Inventiones Mathematicae*, 154(1):63–121, 2003.

[41] Michael R. Douglas, Brian R. Greene, and David R. Morrison. Orbifold resolution by D-branes. *Nucl.Phys.*, B506:84–106, 1997. 26 pages, 2 figures (TeX, harvmac big, epsf) Report-no: RU-97-12, CU-TP-823, IASSNS-HEP-97/24.

[42] Michael R. Douglas and Gregory W. Moore. D-branes, quivers, and ale instantons. 1996.

[43] Clifford V. Johnson and Robert C. Myers. Aspects of type IIB theory on ALE spaces. *Phys.Rev.*, D55:6382–6393, 1997.

[44] Amihay Hanany and Yang-Hui He. NonAbelian finite gauge theories. *JHEP*, 9902:013, 1999.

[45] Chris Beasley, Brian R. Greene, C.I. Lazaroiu, and M.R. Plesser. D3-branes on partial resolutions of Abelian quotient singularities of Calabi-Yau threefolds. *Nucl.Phys.*, B566:599–640, 2000.

[46] Bo Feng, Amihay Hanany, and Yang-Hui He. D-brane gauge theories from toric singularities and toric duality. *Nucl.Phys.*, B595:165–200, 2001.

[47] Bo Feng, Amihay Hanany, Yang-Hui He, and Angel M. Uranga. Toric duality as Seiberg duality and brane diamonds. *JHEP*, 0112:035, 2001.

[48] Amihay Hanany and Kristian D Kennaway. Dimer models and toric diagrams. *arXiv preprint hep-th/0503149*, 2005.

[49] Sebastian Franco, Amihay Hanany, Kristian D. Kennaway, David Vegh, and Brian Wecht. Brane dimers and quiver gauge theories. *JHEP*, 0601:096, 2006.

[50] Sebastian Franco, Amihay Hanany, Dario Martelli, James Sparks, David Vegh, et al. Gauge theories from toric geometry and brane tilings. *JHEP*, 0601:128, 2006.

[51] Bo Feng, Yang-Hui He, Kristian D. Kennaway, and Cumrun Vafa. Dimer models from mirror symmetry and quivering amoebae. *Adv.Theor.Math.Phys.*, 12:3, 2008.

[52] Amihay Hanany and Rak-Kyeong Seong. Brane tilings and reflexive polygons. 2012.

[53] B. V. Karpov and D. Y. Nogin. Three-block exceptional collections over del pezzo surfaces. *Izv. Ross. Nauk Ser. Mat*, 62:429–463, 1998.

[54] Christopher P. Herzog. Exceptional collections and del pezzo gauge theories. *JHEP*, 0404:069, 2004.

[55] Christopher P. Herzog. Seiberg duality is an exceptional mutation. *JHEP*, 0408:064, 2004.

[56] Bo Feng, Amihay Hanany, Yang Hui He, and Amer Iqbal. Quiver theories, soliton spectra and Picard-Lefschetz transformations. *JHEP*, 0302:056, 2003.

[57] Paul S. Aspinwall and Ilarion V. Melnikov. D-branes on vanishing del Pezzo surfaces. *JHEP*, 12:042, 2004.

[58] Lara B Anderson, Yang-Hui He, and André Lukas. Heterotic compactification, an algorithmic approach. *Journal of High Energy Physics*, 2007(07):049, 2007.

[59] Lara B Anderson, Andrei Constantin, James Gray, Andre Lukas, and Eran Palti. A comprehensive scan for heterotic su (5) gut models. *arXiv preprint arXiv:1307.4787*, 2013.

[60] Yang-Hui He, Philip Candelas, Amihay Hanany, Andre Lukas, and Burt Ovrut. Computational algebraic geometry in string and gauge theory. *Advances in High Energy Physics*, 2012, 2012.

[61] Ralph Blumenhagen and Thorsten Rahn. Landscape study of target space duality of (0, 2) heterotic string models. *Journal of High Energy Physics*, 2011(9):1–34, 2011.

[62] Ralph Blumenhagen, Benjamin Jurke, Thorsten Rahn, and Helmut Roschy. Cohomology of line bundles: applications. *Journal of Mathematical Physics*, 53(1):012302, 2012.

[63] Xin Gao and Pramod Shukla. On classifying the divisor involutions in calabi-yau threefolds. *arXiv preprint arXiv:1307.1139*, 2013.

[64] Ron Donagi, Yang-Hui He, Burt A Ovrut, and René Reinbacher. Higgs doublets, split multiplets and heterotic. *arXiv preprint hep-th/0409291*, 2005.

[65] Volker Braun, Yang-Hui He, Burt A Ovrut, and Tony Pantev. The exact mssm spectrum from string theory. *Journal of High Energy Physics*, 2006(05):043, 2006.

[66] Vincent Bouchard and Ron Donagi. An su (5) heterotic standard model. *Physics Letters B*, 633(6):783–791, 2006.

[67] Lara B Anderson, James Gray, Yang-Hui He, and Andre Lukas. Exploring positive monad bundles and a new heterotic standard model. *Journal of High Energy Physics*, 2010(2):1–49, 2010.

[68] Yang-Hui He. Calabi–yau geometries: Algorithms, databases and physics. *International Journal of Modern Physics A*, 28(21):1330032, 2013.

[69] Volker Braun. On free quotients of complete intersection calabi-yau manifolds. *Journal of High Energy Physics*, 2011(4):1–32, 2011.

[70] Maximilian Kreuzer. Toric geometry and calabi-yau compactifications. *arXiv preprint hep-th/0612307*, 2006.

[71] Maximilian Kreuzer and Harald Skarke. Palp: a package for analysing lattice polytopes with applications to toric geometry. *Computer Physics Communications*, 157(1):87–106, 2004.

[72] Philip Candelas, Andrei Constantin, and Harald Skarke. An abundance of k3 fibrations from polyhedra with interchangeable parts. *Communications in Mathematical Physics*, 324(3):937–959, 2013.

[73] The database of rank four and five line bundle models on the 16 toric spaces. `http://www-thphys.physics.ox.ac.uk/projects/CalabiYau/toricdata/index.html`.

[74] Kenneth G Wilson. Confinement of quarks. *Physical Review D*, 10(8):2445, 1974.

[75] Anton Kapustin and Edward Witten. Electric-magnetic duality and the geometric langlands program. *arXiv preprint hep-th/0604151*, 2006.

[76] Alexander M Polyakov. Quark confinement and topology of gauge theories. *Nuclear Physics B*, 120(3):429–458, 1977.

[77] Ross Altman, James Gray, Yang-Hui He, Vishnu Jejjala, and Brent D Nelson. A calabi-yau database: threefolds constructed from the kreuzer-skarke list. *arXiv preprint arXiv:1411.1418*, 2014.

[78] Brian R Greene, Kelley H Kirklin, Paul J Miron, and Graham G Ross. A three-generation superstring model:(i). compactification and discrete symmetries. *Nuclear Physics B*, 278(3):667–693, 1986.

[79] Brian R Greene, Kelley H Kirklin, Paul J Miron, and Graham G Ross. A three-generation superstring model:(ii). symmetry breaking and the low-energy theory. *Nuclear Physics B*, 292:606–652, 1987.

[80] The GAP Group. *GAP – Groups, Algorithms, and Programming, Version 4.8.4*, 2016.

[81] Yang-Hui He, Seung-Joo Lee, Andre Lukas, and Chuang Sun. Heterotic model building: 16 special manifolds. *arXiv preprint arXiv:1309.0223*, 2013.

[82] W. Crawley-Boevey. Lectures on representations of quivers. *available at www.maths.leeds.ac.uk/ pmtwc/quivlecs.pdf*.

[83] H. Derksen and J. Weyman. Quiver representations. *Notices Amer. Math. Soc*, 52:200–206, 2005.

[84] Alistair Savage. Finite dimensional algebras and quivers. *Francoise, J.-P.; Naber, G. L.; Tsou, S.T., Encyclopedia of Mathematical Physics*, 2:313–320, 2005.

[85] Michel Brion. Representations of quivers. *Notes de lcole dt Geometric Methods in Representation Theory*, 2008.

[86] Ibrahim Assem, Andrzej Skowronski, and Daniel Simson. Elements of Representation Theory of Associative Algebras, Vol. 1. *Cambridge University Press*, 2006.

[87] Sergio Benvenuti and Amihay Hanany. New results on superconformal quivers. *JHEP*, 0604:032, 2006.

[88] Yang-Hui He. Some remarks on the finitude of quiver theories. *In.J.Math.Math.Sci.*, 1999.

[89] David Berenstein and Samuel Pinansky. The Minimal Quiver Standard Model. *Phys.Rev.*, D75:095009, 2007.

[90] F. Cachazo, S. Katz, and C. Vafa. Geometric transitions and N=1 quiver theories. 2001.

[91] Martijn Wijnholt. Large volume perspective on branes at singularities. *Adv.Theor.Math.Phys.*, 7:1117–1153, 2004.

[92] Bo Feng, Amihay Hanany, and Yang-Hui He. Counting gauge invariants: The Plethystic program. *JHEP*, 0703:090, 2007.

[93] Joseph Hewlett and Yang-Hui He. Probing the Space of Toric Quiver Theories. *JHEP*, 1003:007, 2010.

[94] John Davey, Amihay Hanany, and Jurgis Pasukonis. On the Classification of Brane Tilings. *JHEP*, 1001:078, 2010.

[95] Amihay Hanany, Domenico Orlando, and Susanne Reffert. Sublattice counting and orbifolds. *Journal of High Energy Physics*, 2010(6):1–24, 2010.

[96] Amihay Hanany and Rak-Kyeong Seong. Symmetries of abelian orbifolds. *Journal of High Energy Physics*, 2011(1):1–64, 2011.

[97] Chris E. Beasley and M. Ronen Plesser. Toric duality is Seiberg duality. *JHEP*, 0112:001, 2001.

[98] F. Cachazo, B. Fiol, Kenneth A. Intriligator, S. Katz, and C. Vafa. A Geometric unification of dualities. *Nucl.Phys.*, B628:3–78, 2002.

[99] Bartomeu Fiol. Duality cascades and duality walls. *JHEP*, 0207:058, 2002.

[100] David Berenstein and Michael R. Douglas. Seiberg duality for quiver gauge theories. 2002.

[101] Volker Braun. On Berenstein-Douglas-Seiberg duality. *JHEP*, 0301:082, 2003.

[102] Sebastian Franco, Amihay Hanany, Yang-Hui He, and Pavlos Kazakopoulos. Duality walls, duality trees and fractional branes. 2003.

[103] V.A. Novikov, Mikhail A. Shifman, A.I. Vainshtein, and Valentin I. Zakharov. Exact Gell-Mann-Low Function of Supersymmetric Yang-Mills Theories from Instanton Calculus. *Nucl.Phys.*, B229:381, 1983.

[104] M. Henningson and K. Skenderis. The holographic weyl anomaly. *JHEP*, 07:023, 1998.

[105] Sergio Cecotti and Cumrun Vafa. Classification of complete n=2 supersymmetric theories in 4 dimensions. 2011.

[106] Murad Alim, Sergio Cecotti, Clay Cordova, Sam Espahbodi, Ashwin Rastogi, and Cumrun Vafa. N=2 quantum field theories and their bps quivers. 2011. 93 Pages, 18 Figures.

[107] Sergio Cecotti and Cumrun Vafa. On classification of N=2 supersymmetric theories. *Commun.Math.Phys.*, 158:569–644, 1993.

[108] Bangming Deng. *Finite dimensional algebras and quantum groups*. Number 150. American Mathematical Soc., 2008.

[109] Sergio Cecotti. Categorical Tinkertoys for N=2 Gauge Theories. 2012.

[110] Richard Eager and Sebastián Franco. Colored bps pyramid partition functions, quivers and cluster transformations. *Journal of High Energy Physics*, 2012(9):1–44, 2012.

[111] Vishnu Jejjala, Sanjaye Ramgoolam, and Diego Rodriguez-Gomez. Toric cfts, permutation triples, and belyi pairs. *Journal of High Energy Physics*, 2011(3):1–60, 2011.

[112] Amihay Hanany, Yang-Hui He, Vishnu Jejjala, Jurgis Pasukonis, Sanjaye Ramgoolam, and Diego Rodriguez-Gomez. The beta ansatz: a tale of two complex structures. *Journal of High Energy Physics*, 2011(6):1–32, 2011.

[113] Amihay Hanany, Yang-Hui He, Vishnu Jejjala, Jurgis Pasukonis, Sanjaye Ramgoolam, and Diego Rodriguez-Gomez. Invariants of toric seiberg duality. *International Journal of Modern Physics A*, 27(01):1250002, 2012.

[114] Amihay Hanany and Rak-Kyeong Seong. Brane tilings and specular duality. *Journal of High Energy Physics*, 2012(8):1–36, 2012.

[115] Sebastián Franco, Daniele Galloni, and Alberto Mariotti. Bipartite field theories, cluster algebras and the grassmannian. *Journal of Physics A: Mathematical and Theoretical*, 47(47):474004, 2014.

[116] Sebastian Franco, Daniele Galloni, and Rak-Kyeong Seong. New directions in bipartite field theories. *arXiv preprint arXiv:1211.5139*, 2012.

[117] Jonathan J Heckman, Cumrun Vafa, Dan Xie, and Masahito Yamazaki. String theory origin of bipartite scfts. *arXiv preprint arXiv:1211.4587*, 2012.

[118] Victor Ginzburg. Calabi-yau algebras. *arXiv preprint math/0612139*, 2006.

[119] Raf Bocklandt. Graded calabi yau algebras of dimension 3. *Journal of pure and applied algebra*, 212(1):14–32, 2008.

[120] Karin Baur, Alastair King, and Robert J Marsh. Dimer models and cluster categories of grassmannians. *arXiv preprint arXiv:1309.6524*, 2013.

[121] Nathan Broomhead. Dimer models and calabi-yau algebras. *arXiv preprint arXiv:0901.4662*, 2009.

[122] Harm Derksen, Jerzy Weyman, and Andrei Zelevinsky. Quivers with potentials and their representations i: Mutations. *Selecta Mathematica*, 14(1):59–119, 2008.

[123] Harm Derksen, Jerzy Weyman, and Andrei Zelevinsky. Quivers with potentials and their representations ii: applications to cluster algebras. *Journal of the American Mathematical Society*, 23(3):749–790, 2010.

[124] Akira Ishii and Kazushi Ueda. On moduli spaces of quiver representations associated with dimer models. *arXiv preprint arXiv:0710.1898*, 2007.

[125] Raf Bocklandt. Generating toric noncommutative crepant resolutions. *Journal of Algebra*, 364:119–147, 2012.

[126] Raf Bocklandt. Generating toric noncommutative crepant resolutions. *Journal of Algebra*, 364:119–147, 2012.

[127] Sergey Mozgovoy and Markus Reineke. On the noncommutative donaldson–thomas invariants arising from brane tilings. *Advances in mathematics*, 223(5):1521–1544, 2010.

[128] Charlie Beil. The geometry of noncommutative singularity resolutions. *arXiv preprint arXiv:1102.5741*, 2011.

[129] Raf Bocklandt, Alastair Craw, and Alexander Quintero Vélez. Geometric reids recipe for dimer models. *Mathematische Annalen*, 361(3-4):689–723, 2015.

[130] Gregg Musiker, Ralf Schiffler, and Lauren Williams. Bases for cluster algebras from surfaces. *Compositio Mathematica*, 149(02):217–263, 2013.

[131] Tri Lai and Gregg Musiker. Beyond aztec castles: Toric cascades in the dp_3 quiver. *arXiv preprint arXiv:1512.00507*, 2015.

[132] Alexander B Goncharov and Richard Kenyon. Dimers and cluster integrable systems. In *Annales scientifiques de l'École Normale Supérieure*, volume 46, pages 747–813. Société mathématique de France, 2013.

[133] Daniel R Gulotta. Properly ordered dimers, r-charges, and an efficient inverse algorithm. *Journal of High Energy Physics*, 2008(10):014, 2008.

[134] Yang-Hui He, Philip Candelas, Amihay Hanany, Andre Lukas, and Burt Ovrut. Computational algebraic geometry in string and gauge theory. *Advances in High Energy Physics*, 2012, 2012.

[135] Bo Feng, Sebastián Franco, Amihay Hanany, and Yang-Hui He. Unhiggsing the del pezzo. *Journal of high energy physics*, 2003(08):058, 2003.

[136] Amihay Hanany, Pavlos Kazakopoulos, and Brian Wecht. A new infinite class of quiver gauge theories. *Journal of High Energy Physics*, 2005(08):054, 2005.

[137] Amihay Hanany, Vishnu Jejjala, Sanjaye Ramgoolam, and Rak-Kyeong Seong. Consistency and derangements in brane tilings. *arXiv preprint arXiv:1512.09013*, 2015.

[138] Raf Bocklandt. Consistency conditions for dimer models. *Glasgow Mathematical Journal*, 54(02):429–447, 2012.

[139] Ben Davison. Consistency conditions for brane tilings. *Journal of Algebra*, 338(1):1–23, 2011.

[140] Akira Ishii and Kazushi Ueda. A note on consistency conditions on dimer models. *arXiv preprint arXiv:1012.5449*, 2010.

[141] Heling Liu and Chuanming Zong. On the classification of convex lattice polytopes. *Advances in Geometry*, 11(4):711–729, 2011.

[142] Matthew J Dolan, Sven Krippendorf, and Fernando Quevedo. Towards a systematic construction of realistic d-brane models on a del pezzo singularity. *Journal of High Energy Physics*, 2011(10):1–41, 2011.

[143] Bo Feng, Yang-Hui He, and Francis Lam. On correspondences between toric singularities and (p, q)-webs. *Nuclear Physics B*, 701(1):334–356, 2004.

[144] Ibrahim Assem, Thomas Brustle, Gabrielle Charbonneau-Jodoin, and Pierre-Guy Plamondon. Gentle Algebras Arising From Surface Triangulations. 2009.